

The effect of cooling and non-uniform fires on structural behaviour

Charlotte Röben

Doctor of Philosophy



The University of Edinburgh

December 2009

Declaration

The work in this thesis was completed solely by Charlotte Röben, under the supervision of Dr. Martin Gillie and Professor Jose Torero. Where other sources were used, references are given.

Declaration

The work in this thesis was completed solely by Charlotte Röben, under the supervision of Dr. Martin Gillie and Professor Jose Torero. Where other sources were used, references are given.

Charlotte Röben

December 2009

Abstract

As the application of structural fire engineering principles is extended to increasingly complex structures, the need for accurate predictions of structural behaviour in fire becomes more crucial. Such predictions require structures to be analysed when subject to temperatures that are representative of those that will occur in real fires. Although international standards provide design fires, these have inherent limitations and shortcomings which mean they often do not accurately describe the fire evolution in real structures.

For example, observations of real fires have shown large forces may develop during cooling leading to connection failure. Yet some design fires completely ignore the cooling phase and consider the peak temperature of the fire the most critical part of the analysis, whilst those that do include it rely on very limited research done on the structural behaviour during cooling. Design fires also assume a uniform temperature across compartments; whereas many real fires and experiments have shown large variations in temperature may occur, even in very small compartments.

This research aims to provide an insight into the global behaviour of structures during cooling and non-uniform fires. A range of structures (1D, 2D and 3D) is considered and are firstly analysed during various cooling regimes. Behaviour during travelling fires is then analysed and compared with uniform fire scenarios. Horizontally travelling fires are investigated on 1D and 3D structures, whilst 2D models of multi-storey buildings are subjected to vertically travelling fires. It is shown that structural behaviour in cooling and during travelling fires may be very different to that expected from currently used design fires. It is concluded that

more realistic fires scenarios must be used to ensure that the structural fire design is appropriate.

Publications

Journal Papers

Röben, C., Gillie, M., Torero, J. Structural Behaviour during Vertically Travelling Fires, *Journal for Constructional Steel Research*, Volume 66(2) 2010, pp 191-197.

Usmani, A., C. Röben, and A. Al-Remal, *A Very Simple Method for Assessing Tall Building Safety in Major Fires*. *International Journal of Steel Structures*, 2009(9): p. 17-28.

Conference Papers

Martin Gillie, Charlotte Röben, Adam Ervine, Sandy Kirkpatrick, The Effects on Non-Uniform Fires on Structural Behaviour, *Proceedings of the Fifth International Conference on Structures in Fire*, Singapore, 28-30 May 2008

C. Röben, M. Gillie, Fundamental Mechanics of Structures Cooling after Fire Loading, *Proceedings of the 5th International Conference on Advances in Steel Structures*, Singapore, December 2007.

C. Röben, M Gillie, J. Torero, Structural Behaviour during a vertically travelling fire, *Proceedings of the 5th International Conference on Advances in Steel Structures*, Singapore, December 2007.

C. Röben, M. Gillie, J. Torero, Behaviour of composite structures during the cooling phase of a fire, *Proceeding of the 3rd International Conference on Structural Engineering, Mechanics and Computation*, Cape Town, South Africa, September 2007

Röben, C., Gillie, M., Usmani, A., Torero, J, Collapse scenarios for tall buildings in fire during cooling, Proceedings of the 5th International Seminar on Fire and Explosion Hazards, Edinburgh, UK, April 2007.

Asif Usmani, Charlotte Röben, Louise Johnston, Graeme Flint and Allan Jowsey, Tall building collapse mechanisms initiated by fire, Proceeding of the 4th Workshop on Structures in Fire (SiF'06), Aveiro, Portugal.

Usmani, A., Flint, G. , Jowsey, A. , Röben, C. , Torero, J., Collapse scenarios of WTC 1 & 2 with extension to generic tall buildings, Proceedings of the Fire Safety in Tall Buildings conference, Santander, Spain, October 2006.

Acknowledgements

I would like to thank my supervisor Dr. Martin Gillie, for his support, enthusiasm and advice. I would like to thank Professor Jose Torero and Dr. Guillermo Rein for their input.

I would also like to thank my family and friends for their support. In particular I would like to thank Rupert for his encouragement and support.

Further thanks to all the members of the BRE Centre for Fire Engineering at the University of Edinburgh.

My thanks also goes to those at Arup Fire for their advice throughout this research.

Thanks to EPSRC and Corus for funding this research.

Contents

1. Introduction.....	1-1
1.1. Background to the Research	1-2
1.2. Research aims	1-4
1.3. Outline of chapters.....	1-4
2. Background	2-1
2.1. Introduction	2-2
2.2. Fire Behaviour	2-2
2.2.1. Standard Fires.....	2-2
2.2.2. Parametric Fires.....	2-5
2.2.3. Travelling Fires	2-9
2.3. Structural Behaviour in Fire	2-16
2.3.1. Cardington Tests	2-17
2.3.2. WTC.....	2-19
2.3.3. Cooling and Travelling Fires.....	2-20
2.4. Material behaviour.....	2-23
2.5. Why this research is needed	2-24
3. Behaviour of simplified 1D beams during cooling	3-1
3.1. Introduction	3-2
3.2. Results 1D Beams.....	3-3
3.2.1. An Idealised Case.....	3-3
3.2.2. Linear temperature gradients.....	3-4
3.2.3. Linear temperature gradients with pinned ends	3-8
3.2.4. Varying Boundary Stiffness	3-11
3.2.5. Realistic Material Behaviour.....	3-18
3.2.6. I-sections with imposed loading.....	3-21
3.3. 3D Validation	3-23
3.4. Cardington Test 1	3-33

3.5. Conclusions	3-39
4. Behaviour of simplified 1D beams during travelling fires.....	4-1
4.1. Introduction	4-2
4.2. Modelling	4-3
4.2.1. Structural Models	4-3
4.2.2. Fire definition.....	4-4
4.3. Results	4-5
4.3.1. Linear temperatures gradients with fixed supports	4-6
4.3.2. Temperature gradients with fixed supports	4-9
4.3.3. Temperature gradients with pinned supports	4-16
4.3.4. Loading	4-19
4.4. Conclusions	4-35
5. Structural Behaviour of Tall Buildings in Cooling.....	5-1
5.1. Introduction	5-2
5.1.1. Background	5-2
5.2. The Structure	5-5
5.2.1. Structural variables.....	5-6
5.3. Structural Modelling.....	5-7
5.3.1. Material properties	5-10
5.4. Fire scenarios.....	5-13
5.4.1. Gas Temperatures.....	5-13
5.5. Structural Temperatures	5-18
5.5.1. Linear Temperatures	5-19
5.5.2. Heat Transfer Temperatures.....	5-20
5.6. Behaviour during Cooling	5-25
5.6.1. Case 1: Linear cooling vs. heat transfer analysis	5-26
5.6.2. Case 2: Varying cooling times	5-37
5.7. Cardington Test 1	5-42

5.8. Conclusions	5-45
6. Structural Behaviour of Tall Buildings during Vertically Travelling Fires	6-1
6.1. Introduction	6-2
6.1.1. Background	6-2
6.2. Travelling Fires Scenarios	6-3
6.2.1. Rapid vertically travelling fire scenario for WB model	6-5
6.2.2. Rapid travelling fire scenario for SB model	6-7
6.2.3. Slow travelling fire scenarios	6-9
6.3. Conclusions	6-11
7. Behaviour of 3D structures during travelling fires	7-1
7.1. Introduction	7-2
7.2. Structure	7-2
7.3. Fires	7-4
7.3.1. Travelling Fires	7-4
7.3.2. Uniform Fires	7-11
7.4. Modelling	7-12
7.4.1. Structure	7-12
7.4.2. Structural Temperatures	7-14
7.5. Results	7-24
7.5.1. Uniform Fires	7-24
7.5.2. Travelling Fires	7-28
7.5.3. Comparison	7-45
7.5.4. Cooling	7-53
7.6. Alternative direction of travel	7-57
7.7. Conclusions	7-62
8. Conclusions and Further Work	1
8.1. Conclusions	2
8.1.1. General observations	2

8.1.2. General conclusions	3
8.1.3. Specific conclusions	5
8.2. Further Work	10
References	15
Appendices.....	24
Appendix A.....	25
Appendix B1	31
Appendix B2	32
Appendix C.....	36
Appendix D.....	38

List of Figures

Figure 2-1 – The course of a well-ventilated compartment fire expressed as the rate of heat release as a function of time [8]	2-4
Figure 2-2 – Standard fire temperature-time curve and a typical parametric fire curve.....	2-8
Figure 2-3 – Compartment with near and far field temperatures.....	2-11
Figure 2-4 – Time-temperature curve at a general location of the ceiling for a travelling fire as represented by Stern-Gottfried [26]	2-12
Figure 2-5 – Time-temperature curve for a family of fires based on a range of burning floor areas [26].....	2-12
Figure 2-6 – Fire spread through cavities [27].....	2-14
Figure 2-7 – Fire break out with slow and rapid propagation [27]	2-15
Figure 3-1- An idealized fixed-ended beam subject to a heating-cooling cycle. a) The support conditions; b) Simplified, elastic-plastic material behaviour; c) Linear heating-cooling cycle; d) The stress-strain response	3-4
Figure 3-2 - Axial forces and bending moments in a fixed-ended beam subject to a heating- cooling cycle with various thermal gradients.....	3-6
Figure 3-3 - Plastic strains in a fixed-ended beam subject to a heating-cooling cycle with various thermal gradients.....	3-8
Figure 3-4 - Axial forces, bending moments and vertical displacements in a pinned beam subject to a heating-cooling cycle with various thermal gradients.....	3-9
Figure 3-5 – Representation of bending during fire.....	3-10
Figure 3-6 – Representation of the boundary conditions varied with (a) rotational boundary springs and (b) horizontal boundary springs	3-11
Figure 3-7 - Comparison of the section forces when the stiffness of the rotational boundary conditions is varied. Gradients corresponding to lower surface temperatures of 200 °C and 800 °C are shown.	3-12

Figure 3-8 - Comparison of mid-span vertical deflections when rotational boundary conditions are varied. Gradients corresponding to lower surface temperatures of 200°C and 800°C are shown.....	3-13
Figure 3-9 - Mid-span vertical deflections when the axial boundary conditions are varied. Gradients corresponding to lower surface temperatures of 200°C and 800°C are shown.....	3-15
Figure 3-10 - Identical to Figure 3-9 without the fixed beam which provides a better view of the displacements at lower stiffnesses.....	3-16
Figure 3-11 - Axial forces when the axial boundary conditions are varied. Gradients corresponding to lower surface temperatures of 200°C and 800°C are shown.	3-17
Figure 3-12 – Stress-strain relationship for steel	3-18
Figure 3-13 - Axial forces and bending moments developed in a fixed-ended beam subjected to a heating -cooling cycle with temperature dependant material properties.....	3-19
Figure 3-14 - Comparison of the section forces encountered in a fixed-ended I-beam (top) and rectangular section (bottom)	3-21
Figure 3-15 – Axial force, bending moments and vertical displacements with real material behaviour and gravity loading incorporated for the I-beam.....	3-22
Figure 3-16 - A 3D model with fixed ends. Vertical deflections at the end of the heating and cooling phase for 800°C maximum temperature.....	3-24
Figure 3-17 - Comparison of axial forces predicted by a beam element model and a 3D shell element model for maximum temperatures of 200°C and 800°C. Fixed end conditions.	3-26
Figure 3-18 - Section forces in an I-beam comparing the simple beam model with the 3D model for a maximum of 200°C degrees with pinned end conditions.	3-27

Figure 3-19 – A 3D model with pinned ends. Deflected shape at 750°C when significant buckling of the top flange occurs.	3-28
Figure 3-20 – Section forces in an I-beam comparing the simple beam model with the 3D model for a maximum of 800°C degrees with pinned end conditions.	3-29
Figure 3-21 - Section forces in an I-beam comparing the simple beam model with the 3D model for a maximum 600°C degrees with pinned end conditions.	3-29
Figure 3-22 - A 3D model with pinned ends. Horizontal deflections at the end of the heating phase for 800°C maximum temperature. Magnification factor of 5	3-30
Figure 3-23 - Comparison of axial forces predicted by a beam element model and a 3D shell element model for maximum temperatures of 200°C and 800°C. Fixed end conditions.	3-31
Figure 3-24 - Section forces in an I-beam comparing the simple beam model with the 3D model for a maximum of 200°C and 800°C degrees respectively with pinned end conditions.	3-32
Figure 3-25 – Geometry of the structure and section dimensions [64].....	3-34
Figure 3-26 – Vertical displacement plotted against temperature [64].....	3-35
Figure 3-27 – 3D Representation of 1D and 3D model	3-36
Figure 3-28 – Temperature evolution in steel and concrete.....	3-36
Figure 3-29 – Axial force comparison of 1D and 3D model	3-38
Figure 3-30 – Vertical displacement comparison of 1D and 3D model.....	3-38
Figure 3-31 – Bending moment comparison of 1D and 3D model.....	3-39
Figure 4-1 – Model geometry	4-3
Figure 4-2 – Definition of patch loading showing the movement of the temperature along the length of the beam with the length, d , and peak temperature, T , indicated	4-5

Figure 4-3 – Axial force evolution for peak temperatures of 800°C and varying patch lengths.....	4-6
Figure 4-4 – Axial force evolution for 20% patch length and varying peak temperatures	4-9
Figure 4-5 – Axial force evolution for peak temperatures of 800°C with gradients and varying patch lengths and uniform fire.....	4-11
Figure 4-6 – Axial force evolution for 50% patch length and varying peak temperatures	4-12
Figure 4-7 – Bending moments at mid-span for 50% patch length and varying peak temperatures	4-13
Figure 4-8 – Mid span displacement for 50% patch length and 1000°C peak temperature at various points along the beam length.....	4-13
Figure 4-9 – Representation of the beam deflection for different fire patch positions	4-14
Figure 4-10 – Mid span displacement for 50% patch length and varying peak temperatures	4-15
Figure 4-11 – Axial force evolution for 800°C temperature and varying patch length. Uniform fire case included.....	4-16
Figure 4-12 – Bending moments at mid-span for 800°C temperature and varying patch length.....	4-17
Figure 4-13 – Mid-span deflection for varying patch lengths and a peak temperature of 800°C	4-18
Figure 4-14 – Deflection at mid-span for 50% patch length and 800°C peak temperatures, plotted at various points along its length.....	4-19
Figure 4-15 – Assumed simplified stress-strain relationship.....	4-21
Figure 4-16 – Axial force evolution for 1000°C temperature and varying patch length.....	4-21

Figure 4-17 – Vertical displacements for 1000°C peak temperature and varying patch length	4-22
Figure 4-18 – Representation of the beam deflection for different fire patch positions	4-23
Figure 4-19 – Axial force evolution for 1000°C temperature and varying patch length compared with uniform heating and cooling.....	4-23
Figure 4-20 – Temperature dependant plastic stress-strain relationship.....	4-24
Figure 4-21 –Axial force evolution for 1000°C temperature and varying patch length.....	4-25
Figure 4-22 – Axial force plotted for part of the analysis duration with the four distinct phases indicated.....	4-26
Figure 4-23 – Representation of the beam with locations of fire at 0.25 and 0.35 (total time) corresponding to the start of phase 3 and 4, respectively	4-26
Figure 4-24 – Total strains plotted along the length of the beam for load step and partial heating (1000°C peak temperature and 100% patch length)	4-28
Figure 4-25 – Strain evolution at the bottom surface at mid span of the beam plotted for part of the analysis (1000°C peak temperature and 100% patch length)	4-28
Figure 4-26 – Bending moment evolution for several locations in the first half of the beam plotted for part of the analysis. The location given in the beam means for example that 0.25 at a quarter of the length and 0.5 at mid-span (1000°C peak temperature and 100% patch length)	4-29
Figure 4-27 – Vertical Displacements at mid-span plotted for part of the analysis (1000°C peak temperature and 100% patch length).....	4-30
Figure 4-28 – Capacity of an I-section – relationship between axial force P and bending moment M, dependant on temperature.....	4-31
Figure 4-29 – Plastic strain evolution at the bottom surface at different locations along the beam (1000°C peak temperature and 100% patch length).....	4-32

Figure 4-30 – Axial force evolution for 1000°C peak temperature and varying patch lengths compared with uniform heating and cooling	4-33
Figure 4-31 – Bending moments for 1000°C peak temperature and varying patch length, including for a uniform fire.....	4-34
Figure 4-32 – Vertical displacements for 1000°C peak temperature and varying patch length, including for a uniform fire	4-34
Figure 5-1 Suggested Collapse mechanisms for WTC towers structure in fire [68]	5-4
Figure 5-2 – Plan view and 2D representation of the structure considered. The three fire floors (Section 5.4) are indicated as are the differences between weak and strong beam versions of the structure.....	5-6
Figure 5-3 – 2D representation of the structure as modelled with Abaqus. The three fire floors are indicated together with selected floor numbers	5-9
Figure 5-4 – Stress-strain relationship for concrete in both compression and tension respectively	5-11
Figure 5-5 – Comparison of temperature evolution in the concrete slab for a typical fire scenario with varying moisture contents.....	5-12
Figure 5-6 – Range of fires with ‘800’ heating for Case 2. This heating curve also applies to Case 1.....	5-17
Figure 5-7 – Range of fires with ‘SF’ heating for Case 2.....	5-17
Figure 5-8 – Linear temperature input for Case 1.....	5-19
Figure 5-9 – Temperatures through the section predicted by heat transfer analysis, (a) when gas temperature is at a maximum, (b) when gas temperature has returned to ambient. The steel section pictured does not form part of the heat transfer analysis.....	5-21
Figure 5-10 – Temperature distribution through the concrete slab as given by the heat transfer analysis	5-22

Figure 5-11– Temperature output points through the concrete slab from the heat transfer analysis and the linear approximation at three points used for the input into the structural model	5-23
Figure 5-12 – Temperatures as given by the heat transfer analysis and linear Abaqus input	5-24
Figure 5-13 – Concrete temperatures with ‘SF’ fire for Case 2.....	5-24
Figure 5-14 – Concrete temperatures with ‘800’ fire for Case 2.....	5-25
Figure 5-15 – Final deformed shape of two models regardless of linear or HT heating regime. SB on left, WB on right.....	5-26
Figure 5-16 – Section forces for whole floors at the connection with the core, WB model with linear temperature analysis.....	5-28
Figure 5-17 – Section forces for whole floors at the connection with the core, WB model with HT analysis.....	5-28
Figure 5-18 – Displaced shape of the weak beam structure during phase 1 and 2 respectively for either heating-cooling regime.....	5-29
Figure 5-19 – Diagram of compression (C) and tension (T) forces for the WB model at the early stage of heating, the end of the heating phase and the end of the cooling phase of the linear temperature profile analysis.....	5-30
Figure 5-20 – Diagram of compression (C) and tension (T) forces for the WB model at the early stage of heating, the end of the heating phase and the end of the cooling phase of the HT profile analysis.....	5-30
Figure 5-21 – Horizontal displacement of the column at the connection with the floors, WB model with Linear and HT analysis.....	5-32
Figure 5-22 – Section forces for whole floors at the connection with the core, SB model with linear temperature analysis.....	5-33
Figure 5-23 – Section forces for whole floors at the connection with the core, SB model with HT analysis.....	5-34

Figure 5-24 – Horizontal displacement of the column for the Strong Beam scenario	5-34
Figure 5-25 – Section forces for the steel beams in the SB model for the HT analysis.....	5-35
Figure 5-26 – Horizontal displacement of the column at the three fire floors for the WB ‘800’ scenario	5-37
Figure 5-27 – Horizontal displacement of the column at the three fire floors for the WB ‘800’ scenario, focussed on the first part of cooling.....	5-38
Figure 5-28 – Horizontal displacement of the column at the three fire floors for the SB ‘800’ scenario.....	5-39
Figure 5-29 – Horizontal displacement of the column at the three fire floors for the WB ‘SF’ scenario.....	5-40
Figure 5-30 – Comparison of horizontal displacements for both the ‘800’ and ‘SF’ fires with the 1400s cooling phase.....	5-41
Figure 5-31 – Axial force in steel beams for both heating scenarios and two cooling phases.....	5-42
Figure 5-32 – Axial force comparison for various cooling rates	5-43
Figure 5-33 – Vertical displacement comparison for various cooling rates	5-44
Figure 5-34 – Bending moment comparison for various cooling rates.....	5-44
Figure 6-1 – Plot of the time temperature profile of the concrete slabs and steel beams for rapid fire spread between floors.	6-4
Figure 6-2 – Plot of the time temperature profile of the concrete slabs and steel beams for slow fire spread between floors.....	6-4
Figure 6-3 – Total axial forces in floors for the WB model with rapid fire spread for the whole fire duration.....	6-5
Figure 6-4 – Total axial forces in floors for the WB model with rapid fire spread, shown for the magnification of the heating phase on the right	6-6

Figure 6-5 – Horizontal displacements of the column at each floor level, WB model.....	6-7
Figure 6-6 – Total axial forces in floors for the SB model with rapid fire spread, whole heating-cooling cycle.....	6-8
Figure 6-7 – Total axial forces in floors for the SB model with rapid fire spread, magnification of the heating phase.....	6-8
Figure 6-8 – Horizontal displacements for the column at the SB floors for the 500s time interval	6-9
Figure 6-9 – Horizontal displacements for the column at the SB floors for the 1500s time interval.....	6-10
Figure 7-1 – Plan layout of the composite structure	7-3
Figure 7-2 – Dimensions of Structural Sections in mm.....	7-4
Figure 7-3 – Alpert curve and T^4 average comparison a typical case.....	7-7
Figure 7-4 – Family of fires (far field temperatures) for the considered fire compartment.....	7-8
Figure 7-5 – Definition of fire loading	7-9
Figure 7-6 – Path of travelling fire	7-10
Figure 7-7 – Temperature evolution of three uniform fires	7-11
Figure 7-8 – Abaqus view of primary and secondary beam layout	7-13
Figure 7-9 – Tensile stress-strain relationship of concrete	7-13
Figure 7-10 – Numbering of primary and secondary beams.....	7-14
Figure 7-11 – I-beam cross-section with temperature points and gradients indicated.....	7-15
Figure 7-12 – Temperature in the slab for 25% travelling fire scenario at times 500s, 2000s and 4500s respectively	7-16
Figure 7-13 – Steel temperature in primary beam 2 for two travelling fire scenarios at points shown in Figure 7-11	7-17

Figure 7-14 – Steel temperature in primary beam 2 for various travelling fire scenarios with respect to normalised time at points shown in Figure 7-11 7-18	
Figure 7-15 – Plan view of the compartment with heated area in lighter colour. Locations of slab temperature output points indicated.....	7-19
Figure 7-16 – Location of temperature points through the depth of the slab.....	7-19
Figure 7-17 – Concrete temperature in the slab for 25% travelling fire case	7-20
Figure 7-18 – Concrete temperature in the slab for 25% and 50% travelling fire case, bottom slab temperatures only	7-21
Figure 7-19 – Concrete temperature evolution based on the standard fire (SF) and constant temperature fire cases	7-22
Figure 7-20 – Concrete temperature evolution based on Parametric fire case....	7-23
Figure 7-21 – Gas and steel temperature for the parametric fire	7-23
Figure 7-22 – Location of path across the slab along which results are plotted .	7-24
Figure 7-23 – Peak vertical displacement during uniform fires.....	7-26
Figure 7-24 – Vertical displacement of steel beams in the parametric fire.....	7-27
Figure 7-25 – Section force in primary and secondary beams for uniform fires	7-27
Figure 7-26 – Displacements along the slab for the 33% travelling fire case at various normalised times.....	7-31
Figure 7-27 – Selected displacements along the slab for 33% travelling fire case at selected normalised times.....	7-31
Figure 7-28 – Displacements along path for all travelling fires at various normalised times	7-32
Figure 7-29 – Vertical displacement at mid-span for all travelling fire scenarios..	7-34
Figure 7-30 – Axial forces in the steel beams for the 25% travelling fire scenario	7-35
Figure 7-31 – Force and temperature plot for Primary Beam 1 in 25% scenario	7-36

Figure 7-32 – Plastic strain in the lower flange in each of the secondary beams for the 25% fire scenario.....	7-36
Figure 7-33 – Strain and displacements for 1D beam example	7-37
Figure 7-34 – Stress-strain plot (a) idealised and (b) for 1D beam.....	7-39
Figure 7-35 – Total, Elastic, Plastic and thermal strains in secondary beam 4 in the 25% fire scenario.....	7-41
Figure 7-36 – Stress-strain plot for secondary beam 4	7-42
Figure 7-37 – Plastic strain and bending moment in secondary beam 4 for the 25% travelling fire scenario.....	7-43
Figure 7-38 – Bending moments in the secondary beams for the 33% scenario	7-44
Figure 7-39 – Section forces in Primary Beam 1 for all travelling fire scenarios against normalised time.....	7-45
Figure 7-40 – Section forces in Primary Beam 1 and 2 for travelling fire scenarios 25, 33 and 50 plotted against real time.....	7-46
Figure 7-41 – Bending moments in secondary beam 1 for the travelling fire scenarios	7-47
Figure 7-42 – Bending moments for secondary beam 3 and 4 for travelling fire cases 25, 33 and 50%	7-48
Figure 7-43 – Maximum vertical displacements for all fire scenarios with uniform fires reduced to 90 minutes in normalised time	7-49
Figure 7-44 – Maximum vertical displacements for all fire scenarios with uniform fires reduced to 90 minutes in real time	7-50
Figure 7-45 – Plastic strains in the rebar for (a) 33% travelling fire at the end of heating at 4560s and (b) standard fire after 90 minutes of heating	7-52
Figure 7-46 – Plastic strains (where strain of 1 relates to 100%) at three locations in the slab compared for travelling and uniform fires	7-52
Figure 7-47 – Axial force comparison of primary beams for 33% travelling fire scenario and the parametric fire	7-54

Figure 7-48 – Axial force comparison of secondary beams for 33% travelling fire scenario and the parametric fire	7-55
Figure 7-49 – Bending moment comparison of secondary beam 2 for range of travelling fire scenarios and the parametric fire	7-56
Figure 7-50 – Bending moment comparison of primary beam 1 for range of travelling fire scenarios and the parametric fire	7-56
Figure 7-51 – Path of travelling fire along y-axis with the width of the fire, d, indicated as well as the naming convention for the bays	7-58
Figure 7-52 – Vertical displacements along the path for both the x-direction and y-direction fires	7-59
Figure 7-53 – Axial forces in the secondary beams at comparable locations for both the x and y-axis travelling fires	7-60
Figure 7-54 – Plastic strains and bending moments plotted in secondary beam 1 at mid-span of bay 1 and bay 2	7-61
Figure A-0-1 – Displacements with spring = 43750000 (0.7) and peak 800°C and 1000°C respectively	26
Figure A-0-2 – Displacements with spring = 37500000 (0.5) and peak with 800°C and 1000°C respectively	27
Figure A-0-3 – Displacements at mid-span against step increments for all four cases considered individually	28
Figure A-0-4 – Displacements at mid-span against step increments for all four cases considered combined	29
Figure A-0-5 – Displacements at mid-span with step increment reduced to obtain accurate results	30
Figure A-0-6 - Displacements at mid-span for step increments for I beam	30

Nomenclature

- α 'Rate of heating' parameter
- A_f Floor area of the fire compartment
- A_t Total area of enclosure (walls, ceiling and floor, including openings)
- A_v Total area of vertical openings on all walls ($A_v = \sum_i A_{v,i}$)
- A_w Area of the opening (m^2)
- b Thermal absorptivity for the total enclosure ($b = \sqrt{\rho c \lambda}$)
- c Specific heat
- d Patch length P force
- δ Displacement
- ϵ Strain or emissivity
- E Young's Modulus
- h Heat transfer coefficient
- H Height of the opening (m)
- H_{eq} Weighted average of window heights on all walls
- $(H_{eq} = \left(\sum_i A_{v,i} h_i \right) / A_v)$
- λ Thermal conductivity
- Γ Time factor function of the opening factor O and thermal absorptivity b
- \dot{m} Rate of burning
- M Moment
- O Opening factor of the fire compartment ($O = A_v \sqrt{H_{eq}} / A_t$)
- q''_c Convective heat flux
- q_f Fire load per unit area related to the floor area A_f

q''_r	Radiative heat flux
\dot{Q}''	Heat release rate per unit area
ρ	Density
σ	Stress or Stefan-Boltzmann constant ($5.67E^{-8} \text{ W/m}^2\text{K}^4$)
σ_y	Yield stress
t	Time
t^*	Factored time
t_b	Burning time (s)
T	Temperature
T_0	Initial ambient temperature
T_g	Gas temperature (K)
T_{\max}	Maximum temperature
T_s	Temperature of the solid surface

Chapter 1

1. Introduction

1.1. Background to the Research

The widespread introduction of performance-based design codes for fire engineering (e.g. EN1994 [1]) has given engineers much greater freedom to use innovative solutions to fire safety. Whereas for prescriptive-based design a structure may be deemed safe on the basis of empirical tabular data and construction details such as material properties or member sizes, in performance-based design the engineer must be able to demonstrate the safety of a structure. This approach has been adopted in many areas of structural design in the previous decades but has only recently been introduced in the field of structural fire engineering.

The advantages of performance-based design are well documented (e.g. Lamont *et al* [2]) and include a more rational consideration of fire loading and the possibility to find innovative solutions for structures not covered by prescriptive-based codes. However, to be used with confidence, performance-based design requires engineers to be able to predict accurately how a structure will respond to fire under a given load case.

Research into the behaviour of steel-concrete composite structures during heating over the last ten years has been successfully translated into more efficient solutions to fire safety by designers and structural behaviour in these conditions can be predicted with some accuracy, for example [3-5]. However, to date much of this work has been limited to understanding how structures behave in a fire up to the point at which peak gas temperatures are reached. The response of structures

to the cooling phase of a fire is not yet well understood. Behaviour on cooling may be important as large forces can develop in a structure as it cools from the highly plastified state that will typically arise due to restraint to thermal expansion during heating. It is known, for example, that the connection failures seen in the Cardington [6] tests of a steel-concrete composite structure occurred during cooling. The need for research into the behaviour of buildings during the cooling stage of the fire also results from the design-codes, which explicitly require engineers to consider the structural effects of fire during the full cycle of heating and cooling for performance based designs.

Currently there is also a general assumption that temperatures within a fire compartment are uniform at any level. Recent experimental results and observations from real buildings fires, together with computer simulations, show that this assumption is not valid and that even in relatively small fire compartments there will be significant variations in both gas temperature and heat flux at different locations. It has also been noted that the location of peak gas temperatures does not remain constant with time but moves, depending on the fuel location and oxygen supply. It is thus entirely possible that in a large compartment, the structure will be heating at one location and cooling at another. To date the effects of such of a situation on structural behaviour have not been considered.

This thesis attempts to understand the structural mechanics of cooling structures as well as the global structural behaviour of structures subject to non-uniform fires, where heating and cooling will take place simultaneously.

1.2. Research aims

This research provides an initial insight into the global behaviour of structures during cooling and non-uniform fires.

The aims of this research are to:

- Investigate the mechanics of structural behaviour of 1D, 2D and 3D structures when subjected to cooling.
- Investigate the global response of structures to non-uniform fires.
- Assess whether the currently assumed uniform fire conditions are conservative compared to cooling and travelling fire scenarios.

1.3. Outline of chapters

Chapter 2: Structural Fire Engineering – State of the Art

This chapter gives an overview of the current state of the art in structural fire engineering with respect to cooling and non-uniform fires. The importance of understanding structural behaviour when these alternative fire scenarios are considered is discussed as well as the current design practices and their limitations.

Chapter 3: Behaviour of 1D beams in cooling

This chapter explores fundamental structural behaviour during cooling by investigating the behaviour of a beam subject to uniform heating and cooling. The effects of thermal gradients, temperature dependent material properties and boundary conditions are established by using simple 1D finite element models.

The results are validated through 3D finite shell element models which show that beam behaviour is accurately represented by 1D beam element models during both the heating and cooling. A model of Cardington Test 1 is used to compare the results for simplified beams to those for composite sections.

Chapter 4: Behaviour of 1D Beams in horizontally travelling fires

This chapter examines the fundamental mechanics of beams subject to horizontally travelling fires. Finite element analysis is used to determine the likely response of a heated beam to a simplified version of the sort of temperature loading that experimental results and theoretical predictions suggest will occur in structural members in real compartment fires.

Chapter 5: Behaviour of 2D frames in cooling

In this chapter 2D frames representing a multi-storey building are subjected to a variety of fire scenarios to investigate global behaviour in cooling. Two structural models are used for this purpose. The results are compared to the simple beam analysis undertaken in Chapter 3, which again is shown to accurately represent the behaviour seen in these more complex 2D models. The 3D Cardington Test 1 model is also subjected to a range of cooling phases and the global behaviour observed is compared with that in the 2D structures.

Chapter 6: Behaviour of 2D frames in vertically travelling fires

The 2D frames modelled in the previous chapter are now investigated when subject to travelling fires. In design, multi-storey fires are considered where appropriate, i.e. when large atria are present. However, there is no guideline on

whether these fires should be designed to occur simultaneously or with some delay representing fire spread. Real fires suggest a range of fire spread rates. The effects of these are analysed and compared, with the aim of understanding the effect on structural behaviour.

Chapter 7: Behaviour of 3D frames in travelling fires

3D frames are modelled and structural behaviour during horizontally travelling fires is investigated. A range of fires are considered, including a variety of travelling fires and a standard and parametric fire. The fires are modelled according to the latest theory on travelling fire behaviour within real compartments. The structural behaviour is compared to ascertain whether the current assumption of a uniform fire across a compartment is sufficiently conservative.

Chapter 8: Conclusions and Further Work

The conclusions are presented and suggestions for further work are outlined.

Chapter 2

2. Background

2.1. Introduction

Structural fire engineering requires two main considerations to complete the design process fully. Firstly the definition of the fire must be chosen which is followed by the heat transfer to the structural elements based on the assumed gas temperatures. Secondly the structural behaviour must be assessed when subjected to the resulting thermal profile. This chapter gives an overview of the range of fire definitions commonly used for design as well as recent developments in improving this definition. Subsequently it discusses the current understanding of the response of structures to such fire assumptions whilst highlighting the shortcomings in the research to date.

2.2. Fire Behaviour

This section gives an overview of the existing approaches to fire definition used in design and research and the shortcomings are highlighted.

2.2.1. Standard Fires

A large number of variables may affect compartment fire behaviour; consequently there are a wide range of possible design fires. However, for the purpose of structural fire engineering, the main interest lies with the response of the structure to the compartment fire. It has therefore been suggested that for the objective of calculating fire resistance it is necessary only to find a fire temperature-time curve

'whose effect, with reasonable probability, will not be exceeded during the use of the building.' [7]

All temperature-time curves incorporate aspects of the idealised compartment fire description. Real compartment fires can be divided into three periods [8];

- I. growth or pre-flashover stage in which the average compartment temperature is relatively low and the fire is localised in the vicinity of its origin;
- II. the fully developed or post-flashover fire, during which all combustible items in the compartment are involved and flames appear to fill the volume;
- III. the decay period, often identified as the stage of the fire after the average temperature has fallen to 80% of its peak value.

Figure 2-1 illustrates these three periods with respect to the heat release rate of the fire. When the average temperature during phase 1 is low, high local temperatures exist in and around the burning zone. During the transition to stage 2 the interaction between the fire and the compartment boundaries becomes significant. This transition is known as 'flashover' and involves a rapid spread of the fire from the area of localised burning to all combustible surfaces within the room. Following flashover, the exposed surfaces of combustible items in the fire compartment are assumed to be burning and the rate of heat release will develop to a maximum, producing high temperatures. Post-flashover fires are assumed to consume all combustible materials in the compartment [8].

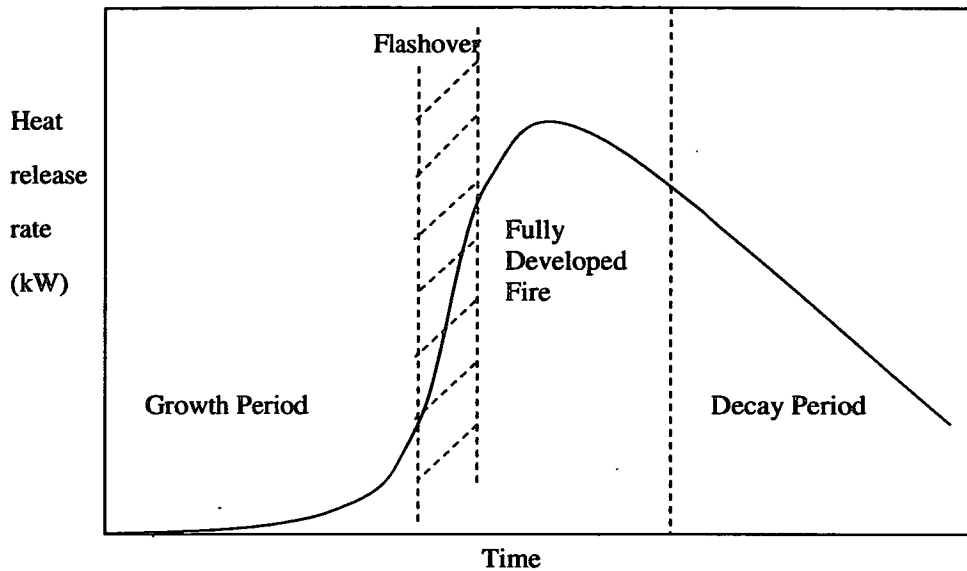


Figure 2-1 – The course of a well-ventilated compartment fire expressed as the rate of heat release as a function of time [8]

It is generally assumed that the fully developed fire poses the greatest threat to structural elements as this is when temperatures are at their highest and structural failure leading to full or partial collapse is most likely. Structural fire analyses often neglect the decay phase altogether as this is deemed to be of limited risk due to the relatively low temperatures in the compartment. It is therefore assumed that the effect of these temperatures on the structure will be minimal and thus need not be included in the analysis. The pre-flashover stage of a fire is also ignored during structural analysis for the same reasons.

The temperature-time curve often used for this purpose is the 'standard fire' or 'nominal fire', where the pre-flashover and cooling phases are not included. This fire curve is described by an arbitrary temperature-time relationship, which is completely independent of ventilation and boundary conditions. The Eurocodes [9] describe the standard curve, or ISO-834 [10], on which many other national

standards are based. The curve specifies the temperature-time correlation as follows:

$$T_g = 20 + 345 \log_{10}(8t + 1) \quad (2.1)$$

where t is the time in minutes.

This standard fire curve was initially created for use in fire resistance furnace tests. Single element testing, whereby an isolated structural element is placed within a furnace, uses the standard fire to classify and verify the fire resistance of structural elements mostly for regulatory purposes. Although perhaps suitable for fire rating and prescriptive design, using structural temperatures derived from a Standard Fire Test in a performance-based design is difficult to justify. The cooling phase should not be ignored as critical behaviour may occur during this stage of a compartment fire. As a consequence, when using performance-based design, it is currently common to use some form of "Natural Fire" to estimate structural temperatures. The Eurocodes introduced such a 'natural' time-temperature curve which does include a cooling phase; the parametric fire curve.

2.2.2. Parametric Fires

Parametric fires are used as an alternative to the Standard Fire to approximate post-flashover compartment temperatures. They take into account the compartment size, fuel load, ventilation conditions and the thermal properties of compartment boundaries. Although this provides a much better estimate of the temperature evolution for a given compartment than the Standard Fire, the assumption of a uniformly distributed fire remains.

Both the ISO-834 (Standard Fire) and the parametric curves have been used extensively for both research and industry purposes [11-14].

The parametric fire definition was based on extended research on the behaviour of a fully-developed fire within small compartments. Many experimental studies were done over an extended period of time. Initially compartments were burned using wood cribs as the fuel bed. The rate of burning was found to be highly dependent on ventilation as well as the size and shape of the opening. Research by Kawagoe [15] led to the relationship shown in Equation 2.2.

$$\dot{m} = 0.9A_w H^{1/2} \text{ (kg/s)} \quad (2.2)$$

where A_w is the area (m^2) and H is the height (m) of the opening. This in turn led to the semi-empirical deduction of the commonly used ventilation factor $A_w H^{1/2}$ the full deduction of which can be found in Drysdale [8].

The maximum heat release rate of a fire and thus the associated temperature distribution in the compartment are highly dependent on this ventilation factor. Many attempts have been made to develop a characteristic temperature-time curve for a compartment, some of which are currently being used in structural fire engineering as design fires.

Pettersson [16], Kawagoe and Sekine [17] and Brabauskas and Williamson [18] have all developed time-temperature curves each including a different range of variables such as fuel distribution, ventilation factors, burning rates and compartment details.

Eurocode 1 [9] developed Petterson's approach by introducing an explicit equation for estimating gas temperatures in fire compartments shown in Equation 2.3.

$$T_g = 20 + 1325 \left(1 - 0.324e^{-0.2t} - 0.204e^{-1.7t} - 0.472e^{-19t} \right) \quad (2.3)$$

where $t^* = t\Gamma$ representing a fictitious time (in hours) and $\Gamma = (O/b)^2(0.04/1160)^2$ which provides a factor for the fire duration based on the compartment properties. The opening factor is given by $O = A_v\sqrt{H_{eq}}/A_t$, with A_v giving the area of the window opening (m^2), H_{eq} is the height of the window openings (m) and A_t is the total internal area of the bounding surfaces (including openings) (m^2). The thermal properties of the compartment linings are incorporated by $b = (\lambda\rho c)^{1/2}$, where λ , ρ and c represent the thermal conductivity, density and specific heat of the compartment lining respectively. This exponential equation describes the first part of the curve, until the maximum and pre-determined temperature is reached after which linear decay of temperature occurs until ambient is reached. This decay rate is based on a reference rate from Eurocode factored by the fictitious time t^* .

An example of a typical parametric fire curve with respect to the standard fire curve is given in Figure 2-2.

The main shortcoming of the parametric temperature-time curves is that their applicability is limited to compartments with floor areas of up to $500m^2$ and a maximum height of 4m. These limitations were established based on the range of test data which were used to calibrate the design equations [19].

Clearly many current structures will not fall within this category as open plan offices, multi-storey atria and highly irregular layouts become more and more common. As there is no accepted suitable alternative, parametric curves are often used for compartments which are outside the scope of their applicability [14].

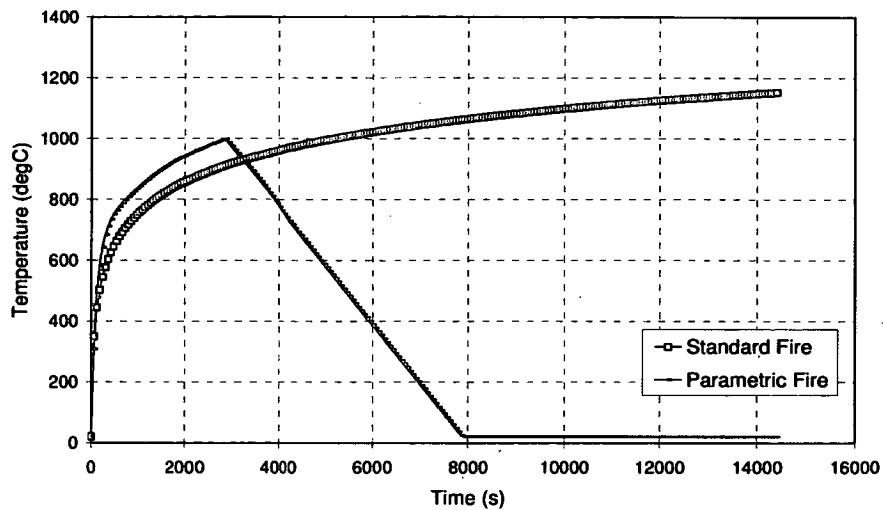


Figure 2-2 – Standard fire temperature-time curve and a typical parametric fire curve

Underlying both the Pettersson and Eurocode approaches to calculating gas temperatures is an assumption that the gases are well mixed and consequently that compartment temperatures are uniform. This has previously been assumed to be reasonable for small fire compartments. Experimental evidence increasingly suggests that even in these situations the assumption of uniform heating is not valid. Cooke [20] undertook a number of fire tests with uniform fire loads and showed there was a clear progression of peak temperature through compartments as the seat of the fire moved according to the available ventilation. The effect of non-uniform gas temperatures on structural temperatures has been shown to be significant in recent work by Gillie and Stratford [21] who reported on temperatures in a concrete slab above a fire compartment. Lower surface concrete temperatures varied by as much as 400°C despite a compartment size of only 3.5m by 4.5m.

2.2.3. Travelling Fires

Although both the Standard Fires and Parametric Fires definitions are important methods in the field of structural fire engineering, the inherent shortcomings listed in the sections above often result in inappropriate use of these methods. The most obvious issue is that the methods are not applicable to large and irregular spaces due to the assumption of uniform fires across such compartments. Although the design codes limit the use to spaces up to 500m²; in reality the fire description of three distinct phases given in section 2.2.1 is only valid for very small compartments, well below this area limit. In larger fire compartments the seat of a fire will move in a manner governed by the available ventilation and fuel. The extrapolation of these simplified fire models is therefore unsatisfactory, even for most compartments within the design guidelines.

Despite the fact that large variations in temperature will occur within a compartment, to date almost all work on structural behaviour in fire has assumed that temperatures within a compartment are uniform at any level. In turn this implies that structural elements are assumed to be heated uniformly along their lengths, or over their areas. In several recent real fires, such as the World Trade Center, the Windsor Tower in Madrid and the TU Delft University building in the Netherlands [22-24], fires were observed to travel across compartments and even travel vertically between different floor levels – quite the opposite of uniform burning. These observations together with recent experimental results [20, 21] and computer simulations of real fires confirm that the uniform fire assumption is not valid and that even in relatively small fire compartments there will be significant variations in both gas temperature and heat flux at different locations. It has also

been noted that the location of peak gas temperatures does not remain constant with time but moves, depending on the fuel location and oxygen supply. It is thus entirely possible that in a large compartment, the structure will be heating at one location and cooling at another. To date the effects of such of a situation on structural behaviour have not received much attention.

As a more realistic alternative to Standard and Parametric Fires, Rein [25] proposed a model consisting of "near-field" and "far-field" temperatures. In this model the far-field temperatures result from hot gases and near-field temperatures from direct impingement of a flame.

By choosing a percentage of the compartment area assumed to be impinged by flame (near field), a range or family of fires can be created. When considering an area of 100%, a uniform fire which burns out quickly is assumed, whereas an assumed burning area of 1% would result in a slow travelling fire. Any other chosen areas of burning represent travelling fires of different sizes and durations. This percentage fire area is governed by ventilation in real compartments.

It was proposed that the duration of exposure to near-field temperatures in a well-ventilated fire is governed by the available fuel load. Equation 2.4 calculates the burning time based on a uniform fuel load across the fire path and a constant heat release rate per unit area.

$$t_{b=} \equiv \frac{q_f}{\dot{Q}''} \quad (2.4)$$

Where t_b is the burning time in seconds, q_f is the fuel density in MJ/m² and \dot{Q}'' is the heat release rate per unit area in MW/m².

It can be seen that the burning time is independent of the burning area [25]. This implies that the burning time of any one area is constant, regardless of the total

size of the compartment. However, when considering a travelling fire, only a part of the total compartment is burning at any one time as is represented in Figure 2-3. For the purpose of determining a burning time, the generally accepted values for fuel load density and heat release rate per unit area for office spaces are taken as 570MJ/m^2 and 500kW/m^2 respectively [26]. This therefore leads to a constant characteristic burning time of 19 minutes. The total fire duration may therefore differ substantially depending on the percentage area of burning assumed.

When a section of the compartment is burning, that area is subjected to near field gas temperatures. These are taken as the flame temperature and assumed to be more or less constant at 1200°C for a typical office fire [8]. However, the area of the compartment which is not burning will also be subjected to increased gas temperatures, referred to as the far field. Although this temperature distribution varies as a function away from the fire and thus non-uniformly, Rein has simplified this to a constant temperature to simplify the analysis. How to obtain the single far field temperature value is explained by Stern-Gottfried [26].

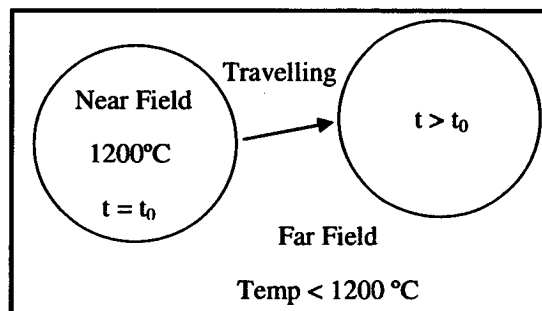


Figure 2-3 – Compartment with near and far field temperatures

Exposure to far field temperatures may be for a significant time, depending on the assumed fire size. When the fire size is taken as small (for example 5%) the

overall fire duration will be long, but the average far field temperatures will be low. Figure 2-4 shows the temperature evolution at a single point in a compartment.

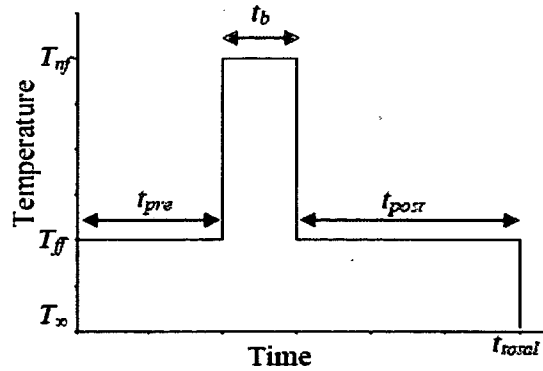


Figure 2-4 – Time-temperature curve at a general location of the ceiling for a travelling fire as represented by Stern-Gottfried [26]

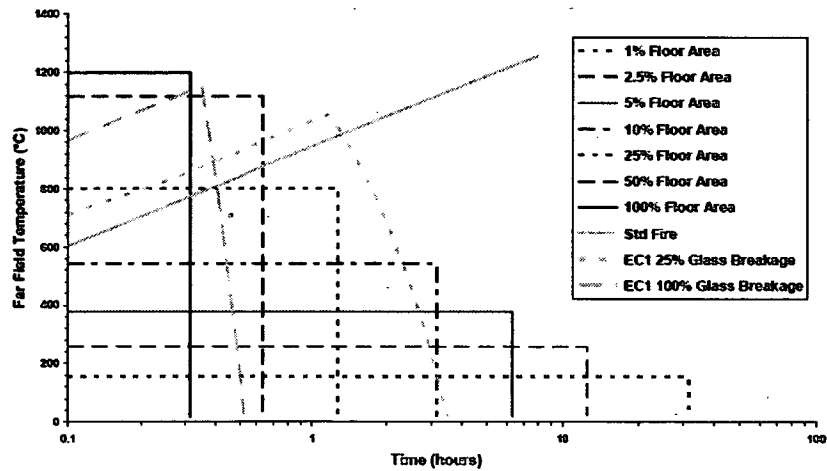


Figure 2-5 – Time-temperature curve for a family of fires based on a range of burning floor areas [26]

Figure 2-5 shows how the far field temperature changes depending on the burning area chosen, thus creating a family of fires. A family of fires such as this can be

created for any fire compartment considered in design. To date the implications of this for structural behaviour have not been considered in a systematic manner. In Chapter 7 however, this method is applied to a composite compartment and details on the fires specific to the structure are given.

Vertical Fire Spread

All of the notes on fire definitions thus far are based on the assumption that the fire is contained within a single compartment. However, fire spread can occur between compartments as compartmentation is breached. This refers to both horizontal and vertical fire spread, either of which may occur. As previously mentioned, fire spread has been observed in real fires and can lead to multiple floor fires [22-24]. Vertically travelling fires are considered in Chapter 6. Horizontal fire spread between compartments is not considered in this work.

Fires may spread vertically through a building, either internally or externally, and by several possible means. If the fire develops to flashover it may break out from the room of origin through a window-opening or doorway causing external flaming. Flames breaking out of a building from a post-flashover fire will typically extend 2m above the top of the opening irrespective of the material used to construct the outer face of the building envelope [27] thus reaching the floor level above externally, where ignition may occur as a result.

Depending on the external cladding system and the presence of any fire barriers, in some cases the fire will be limited to the floor of origin whilst in other cases the cladding will contribute to the fire spread. Propagation of the fire can occur along the surface of the external wall depending on the materials used or the fire may

propagate through cavities in the cladding, either existing or as a result of the fire. For example, there may be flame and smoke propagation through unprotected service shafts or thermal expansion may push out part of the external structure thus failing connections to the floor system and façade and creating new openings to the upper floors.

Propagation through cavities poses a particular problem as this type of fire spread is not visible until the subsequent floors are involved. This process can be very rapid as once the fire is within a cavity the flames may extend to five to ten times of the original length in search of oxygen and fuel. This phenomenon is represented in Figure 2-6.

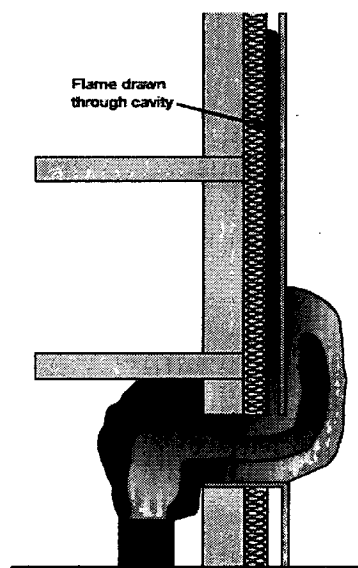


Figure 2-6 – Fire spread through cavities [27]

Depending on the contribution from the external cladding, the fire may spread to other floors rapidly or slowly as is shown in Figure 2-7. This figure does not show

the risk of internal fire spread which may add to the speed at which fire propagation occurs. Although downward fire spread is not observed as often in real fires as upward spread, liquefied burning plastic materials and falling burning materials through service shafts could result in downward spread. In the Delft University fire [24] downward spread did occur although there are some doubts about the level of compartmentation in place.

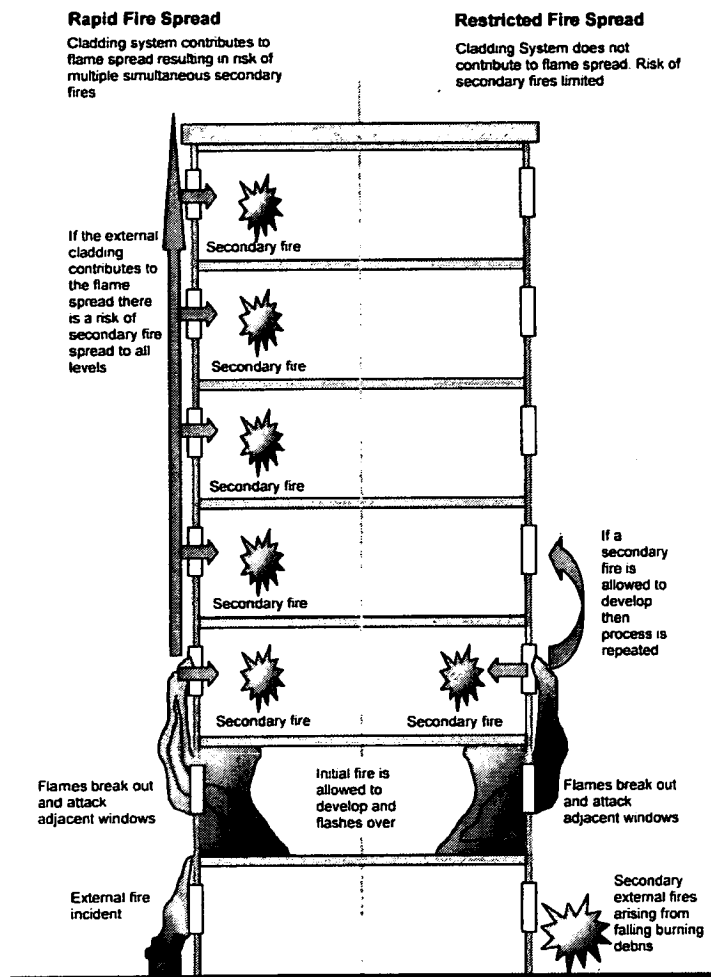


Figure 2-7 – Fire break out with slow and rapid propagation [27]

As is clear from the above, many factors determine the exact method in which fire spread takes place. In a recent real fire, the Windsor Tower fire in Madrid, vertical fire spread was observed. In the aftermath several sources reported on the rate at which this fire spread took place.

However, each of the sources gives substantially different estimates of the time it took for each floor to be affected by the fire. The range varied from 3min/floor to 20min/floor [28]. Some of this variation may be due to the unclear definition of fire spread, i.e. does flashover have to have occurred on the floor for it to be counted or as soon as the first signs of a fuel burning are observed. From observations at the Windsor tower; initial upward spread seems to have been fastest on the east face, above the room where the fire initial broke out, suggesting that floor-to-floor spread was predominantly occurring in the region of the façade, rather than internally [28].

For this particular case fire spread was likely due to the lack of fire stops between floors as reported in the NCE magazine [29]. Additional gaps created by the thermal expansion of the façade, significant external flaming and ongoing refurbishment (compromising compartmentation as some vertical openings were not yet fire proofed) are all likely to have added to the very rapid spread.

2.3. Structural Behaviour in Fire

Once the suitable gas temperature-time curve has been determined, the next stage in a performance-based structural fire design is to examine the resulting structural behaviour. The approach taken to analysing structural response to fire can range from simple hand calculations to complex finite element analyses using computer

modelling. Prescriptive-based design is based on the strength of individual elements which are tested to code requirements. These standard fire tests were used to quantify the fire resistance of single elements under prescribed fire conditions. One of the many shortcomings of this method is the lack of consideration of structural interactions, which could potentially lead to partial or progressive collapse of the entire structure. For this reason it is necessary to take a performance-based approach which requires an understanding of the structural behaviour in full. To further this understanding, significant amounts of research were and continue to be done.

2.3.1. Cardington Tests

Between 1995 and 1997, British Steel's Swindon Technology Centre carried out a fire research programme on a purpose built, eight storey composite steel-framed structure built within the BRE large scale test facility at Cardington. The main aim of the research programme was to understand and develop calculation procedures which are capable of predicting the structural behaviour in fire, in particular in composite frames similar to the Cardington test set up. For this purpose, a number of major tests were carried out, each in different parts of the frame to study a variety of aspects of structural behaviour.

These experiments produced a huge amount of experimental data subsequently used by a number of research groups to further analyse the effects of fire on the behaviour of the structure. The experimental data allowed for many numerical models to be verified and benchmarked. The research team at Sheffield University produced a series of numerical results [30-32] using the finite element analysis

program Vulcan [33], whilst at Imperial research on the Cardington results was done using ADAPTIC [4, 34]. Similarly work by the research group at Edinburgh University used the finite element package, ABAQUS [35] to model aspects of the Cardington tests [36-39].

There were some distinct findings of the tests which are now generally accepted within the fire engineering discipline. It was found that the behaviour of composite structures in fire is dominated by thermal effects, both material and geometric. Although the material effects such as loss of strength were always seen as the main factor for large deformations, geometric effects such as thermal expansion and thermal bowing were discovered to be dominating the response, especially in the early stages. However, the way in which these geometric and material effects interact depends on the details of the structure and the specific fire loading present. The interaction of structural members is also of great importance to the behaviour, thus reinforcing the fact that standard fire tests cannot capture structural behaviour in fire accurately.

As a result of the tests and the subsequent analyses guidance on performance based design progressed and several simple techniques were developed [40-42]. Although these methods have been applied in many recent structural fire designs, real fires have showed that the Cardington tests were limited in that the tests did not consider whole floors or multiple floors which may be involved in real fires. However, using the experimental results to validate the modelling techniques can leave the researchers confident that the assumptions made and methods used are appropriate for a particular analysis.

2.3.2. WTC

On September 11, 2001 when the World Trade Centre Towers collapsed it became clear that there are significant areas of limited knowledge in structural fire engineering. The twin towers and WTC 7 were the first large composite structures to collapse due to fire. Although WTC 1 and 2 incurred structural damage due to the impact of the planes, WTC 7 did not have any such damage and collapsed solely due to fire loading. Flint [43] modelled the structure of a World Trade Centre Tower to investigate the effect the multiple floor fire had on the long span trusses. This showed collapse through a conventional plastic hinge failure mechanism was possible. All structural damage was ignored for this model and thus Flint showed that failure could have occurred due to fire related behaviour alone. For a similar frame, where the trusses were replaced by more commonly used universal beam sections, both a plastic mechanism and a second, buckling failure mechanism were shown to induce collapse [44, 45]. This is described in a little more detail in Chapter 5. This detailed research into the different failure mechanisms also concludes that the behaviour of composite structures in fire is dominated by thermal expansion effects, as did the Cardington results.

The Cardington results and those found for the WTC collapse have significantly increased the knowledge of structural behaviour in fire. However, research thus far has by no means covered all aspects of structural behaviour in fire and significant research is needed to further the knowledge.

2.3.3. Cooling and Travelling Fires

Clearly a substantial amount of research has been done on the behaviour of structures during fire. However, as described in Section 2.2 many researchers have limited their research to the heating phase of a fire as this was deemed the most critical part of the structural fire design process.

Only a very small amount of work on cooling structures has been undertaken. El-Rimawi *et al* [46] discussed the behaviour of structural steel during cooling and provided some simple examples of the behaviour of structural elements after a fire and Bailey [47] built upon this work. Both researchers showed that high tensile forces are generated in restrained steel beams as they cool from an inelastic state. Wang [48] investigated cooling behaviour of structures using the example of a truss and compared predictions made using non-linear elastic and fully-plastic material models. There have also been a number of studies that considered the behaviour of fires that travel within a structure and thus have heating and cooling occurring simultaneously, notably Franssen [49] who considered car-park fires and Bailey [47] who analysed the behaviour of 2-d steel frames subject to travelling fires. In each case the fire scenarios were highly simplified. Although all this initial research provided a significant insight into the structural behaviour of steel members during cooling, the work was limited in that the behaviour of the steel members acting with the composite floor slab was ignored.

Similarly to the previous theoretical work, past experimental work on structures in fire has also tended to concentrate on the behaviour during the heating phase of a fire. Liu *et al* [50] performed experiments on heated steel beams with axial restraint and recorded beam temperatures during the cooling phase of the tests.

Other test data on the behaviour of cooling structures is available; however, for the purposes of this research, it tends to have two important shortcomings. Firstly, fire tests are typically conducted on single, simply supported structural members and so the effects of thermal restraint are not captured. Secondly, mechanical loading is often removed during the cooling phase of experiments and so the results do not accurately represent the likely structural behaviour of the real structure. Additionally, many fire tests heat the tested element uniformly, which is not representative of a real fire.

The lack of consideration of cooling is somewhat surprising considering that the observations from the full-scale fire tests at Cardington suggested that connections showed signs of failure during the cooling stage of the fire [6]. High axial tensile forces which develop during cooling appear to be the reason for this. It is failure during the cooling stage that is significantly dangerous to fire-fighters who may obtain a false sense of security when the peak of the fire has passed. Similar failure of connections in cooling was observed after the Broadgate Phase 8 fire [51] and so it is a matter of urgency that the cooling behaviour of structures be addressed so that the benefits of performance based fire design can be more fully and confidently exploited by designers. Not only does structural integrity become questionable upon cooling, residual forces may affect the reparability of the structure post-fire.

The main objective of fire engineering is life safety and evacuation is a crucial consideration in design. For high rise buildings in particular evacuation may not always be possible, mostly when the fire occurs at a level below where the persons are. Limiting fire spread and maintaining compartmentation therefore becomes even more critical. Additionally, access for fire fighters in high-rise structures also

tends to be difficult or impossible thus making fires harder to tackle. This potentially can lead to full burn-out on one or more floors while evacuation or fire-fighting on other floors is still taking place. Normally it is assumed that full evacuation has taken place when burn out occurs and therefore even when structural stability is affected, life safety is no longer a major issue. For high-rise buildings however this is not the case and it is imperative that overall structural stability is maintained throughout the fire duration.

Several recent high-rise building fires have shown that very large, multiple-floor fires are possible in such buildings and that the structural response will involve a similarly large portion of the structure. The Windsor Tower fire in Madrid is one such recent multi-storey fire. The fire started at a paper bin in an office on the 21st floor and after a few hours encompassed almost all of the 28 levels above ground. The fire spread was very rapid and the damage to the structure was substantial after partial collapse of the façade [23]. Another major fire at the University of Delft left the majority of the structure completely burnt out after fire spread in all directions, including downward. Again, partial collapse of the façade occurred [24].

In both these examples fires spread rapidly across the structure which results in burning at different stages on several floors. This leads to a requirement to understand the behaviour of structures subject to fires that travel between floors, perhaps with some floors cooling after burning-out while other floors are in the early stages of heating.

2.4. Material behaviour

The following section considers aspects of behaviour relevant to this thesis only. Others have described general material behaviour of steel and concrete in significant detail. [28, 52-54].

It is generally accepted that the behaviour of steel in fire is well understood and that the existing material models include all of the critical behavioural aspects. For concrete however this is not as straightforward as there is still limited understanding about important characteristics of the behaviour such as cracking and spalling. It is therefore necessary to make certain assumptions to simplify the material behaviour for modelling input purposes.

The principal influences of high temperature in concrete are loss of compressive strength and spalling [28]. Loss of material due to spalling has two main effects on structural reinforced concrete members; it reduces the total area of concrete in the member and it reduces the amount of protective cover provided to the reinforcement bars, allowing the rebar to heat up faster. All of this will reduce the capacity of the concrete section. The extent of the permanent weakening of concrete is still unknown in detail [28, 55-57].

The behaviour of steel during heating is fairly well understood and no major phenomena are omitted in the current modelling practices. The main issue which arises during cooling is the residual strength which can be difficult to quantify. The Young's Modulus is generally assumed to follow the same path for increasing and decreasing temperature. Both Bailey [47] and El-Rimawi [46] have used a constitutive relationship based on a Ramberg-Osgood equation [58] to describe the strain reversal upon cooling. This research uses non-linear elasticity with an added

hysteresis loop for the unloading path. This unloading is non-linear but no plastic deformations are included and the material returns to zero strain when at ambient temperatures. The material models in this thesis use a plasticity model for the definition of the stress-strain relationship. Although this is a linear unloading path (which will run parallel to the loading path), it allows for permanent plastic deformations, thus leading to residual strains and stresses as a result of heating and cooling. This is also valid for the concrete material model where unloading also uses the same stiffness as the elastic loading path.

Appendix D provides details of the material properties used in this thesis.

2.5. Why this research is needed

It can be argued that the prescriptive methods currently used for design work. Although structural damage from fires is not uncommon, apart from the World Trade Center, full progressive collapse has never occurred in a multi-storey composite frame and the design standards have therefore performed as expected.

It is however essential to realise this method works due to its extremely conservative approach. This results in structures which are over-designed and not cost effective. To truly understand the risks involved when designing for fire loading, a more thorough understanding is required of both the real fire actions as well as the structural response. Risks can not be quantified properly using the prescriptive design method as it clearly does not reflect the actual behaviour of a structure.

As is clear from many real fires and fire tests [13, 59-61] structural behaviour during fires is far more complex than can be understood from considering single

elements only. This is why understanding the structural behaviour of buildings during fires is accepted as being essential to make full use of performance-based design codes.

However, there are limitations in the current definitions of a fire with the standard and parametric fires curves as described in section 2.2. The recent research into more realistic fires by Rein and Stern-Gottfried [26] suggests that fires travel across a compartment and that temperatures may vary significantly with time and location. Heating and cooling may therefore occur simultaneously. It has been discussed that the limited available research on structures behaviour during cooling shows significant stresses and strains may develop upon cooling.

Structural behaviour as a result of travelling fires within a compartment has yet to be researched, even though this is shown to be a more realistic fire load. This thesis is a first attempt at understanding this response. To correctly model and predict the full structural response to real fire scenarios, the underlying mechanics of cooling need to be understood properly as this forms the basis for the response. The basic mechanics of cooling and moving fires as well as the effect of cooling and vertically travelling fires on tall buildings have been investigated. Finally a 3D model of a compartment, based on a real structure, is subjected to several realistic fire scenarios (i.e. travelling fires) and these are compared to the behaviour based on the current standard and parametric fire curves.

3.1. Introduction

This chapter describes the fundamental mechanics of cooling structural elements. An understanding of this area of structural mechanics is important as it will underpin the descriptions and understanding of the behaviour of more complex, real structures that will be analysed under fire conditions in later chapters.

The behaviour of beams with varying temperature distributions, end conditions and material properties during a heating-cooling cycle are considered in this chapter. A combination of theoretical descriptions and numerical modelling using the commercially available Abaqus software [35] is used. Initially a very simplified “thought experiment” of a fully restrained, uniformly heated beam is studied. The remainder the chapter then considers more realistic scenarios of heating and cooling and determines the extent to which the stresses developed in the idealized case will in fact occur. In order to be able to separate the contributions of material non-linearity and structural effects on the overall behaviour of cooling beams, the earlier parts of the chapter will consider examples where a simplified material behaviour that does not depend on temperature is used. Later, examples with full, temperature-dependent material behaviour are examined. All these numerical models use beam type finite elements. Such elements cannot capture local buckling phenomena and so, to ensure that the behaviour obtained from simplified models is accurate, a set of results compares the behaviour of beam element based models to 3D models that use shell finite elements. Finally, a full structure modelled on Cardington Test 1, is analysed to identify how the phenomena identified in the simplified cases compare to the behaviour of real composite buildings.

3.2. Results 1D Beams

3.2.1. An Idealised Case

To appreciate why the cooling behaviour of structures is of interest it is helpful to consider a built-in beam made of an idealized elastic-plastic material subject to uniform heating followed by uniform cooling (Figure 3-1a-c). Assuming no buckling occurs, elastic compressive stresses will develop in the beam upon heating as a result of thermal expansion being restrained by the supports. Point A in Figure 3-1d represents the point at which the yield stress of the beam is reached and if heating is continued beyond this point all the material in the beam will plastify and mechanical strains will develop at a constant stress until heating is stopped at point B. It is noteworthy that point A is reached at only a little over 100°C temperature change for typical structural steel. At point B cooling commences. Initially the beam will unload elastically due to thermal contraction. A point of zero stress will be reached and then tensile forces will develop in the beam. Providing the plateau A-B is of sufficient length, these tensile forces will grow until point C, which represents tensile yield of the beam, is reached. If cooling continues then ambient temperature will be reached at point D. After this heating-cooling cycle the beam will be entirely yielded in tension and would therefore have zero bending resistance for small rotations.

Assuming point A is reached at 100°C, it is only necessary to heat the beam to 300°C for full tensile yield to be reached on cooling. Such a temperature is well below what is likely to be experienced in a fire, even in protected steelwork.

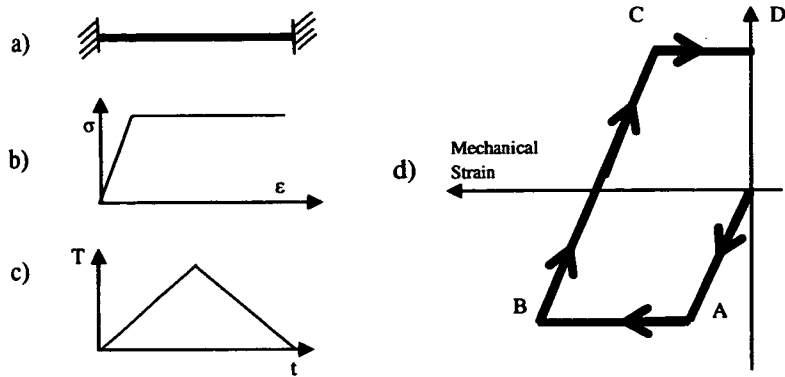


Figure 3-1- An idealized fixed-ended beam subject to a heating-cooling cycle. a) The support conditions; b) Simplified, elastic-plastic material behaviour; c) Linear heating-cooling cycle; d) The stress-strain response

The idealized example considered in Figure 3-1 thus offers a likely explanation of why connection failure was seen in cooling during the Cardington tests and also suggests that the forces developed in cooling may be as large as those produced by heating, although of opposite sign. However, the idealisations adopted in this example are significant; the following sections will determine whether the conclusions hold in more realistic scenarios.

3.2.2. Linear temperature gradients

In a fire beams will typically develop a thermal gradient because they are heated only from below and because floor slabs on their upper flanges act as heat-sinks. To consider the effect of this form of heating, a built-in 2m span beam with a square 0.1m×0.1m cross-section was modelled in Abaqus with various linear

thermal gradients applied. The dimensions of this beam were taken arbitrarily at this stage; what is of interest here is the form and relative magnitude of the stress-resultants produced by cooling. Loading is taken into consideration from section 3.2.6 and here the dimensions will be reconsidered. The uniaxial yield stress of the beam was taken as 250 MPa, Young's modulus as 207 GPa and the coefficient of thermal expansion as $1.25 \times 10^{-5} \text{ }^\circ\text{C}^{-1}$, all independent of temperature. The section was taken to be initially unstressed. Various temperature-time profiles of the form shown in Figure 3-1c were applied to the bottom of the section whilst the top was assumed to remain at ambient temperature, which was taken as 0°C . The peak temperature reached by the bottom of the section is thus a measure of the temperature gradient through the beam. Because of the assumed perfect geometry of the beam and the lack of vertical displacements, Euler buckling is not captured in this model. This is physically reasonable as steel beams will often be restrained by floor systems in building structures.

Figure 3-2 shows the axial forces in the beam plotted against the temperature of the bottom of the section for various gradients over a heating-cooling cycle. Upon heating elastic compressive stress builds up in the section as it expands against the fixed supports. The plateau described for the idealized case does not occur as the gradient through the section prevents all the material from reaching yield simultaneously and therefore the axial force rises during the entire heating phase. Upon cooling, thermal contraction results in tensile forces developing in the beam. At each level within the beam stresses are initially elastic and then, for levels exposed to temperatures above around 100°C , plastic. As a result, at the end of the heating-cooling cycle, the beam is partially yielded in tension. For larger gradients a greater proportion of the cross-section yields in tension and so the residual axial

force in the beam is higher. However, the residual axial force does not vary linearly with the peak temperature in the beam; the difference in residual force gets relatively smaller with an increase in peak temperature.

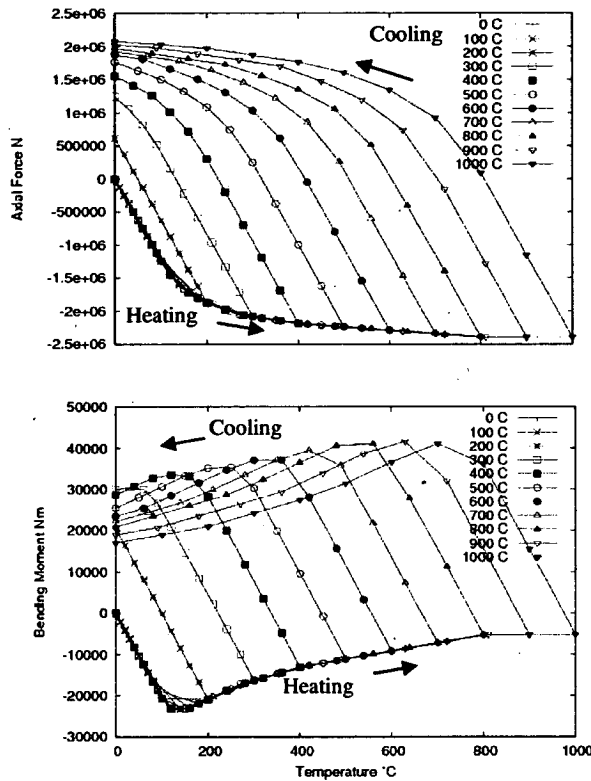


Figure 3-2 - Axial forces and bending moments in a fixed-ended beam subject to a heating- cooling cycle with various thermal gradients.

The bending moments in the beam are also shown in Figure 3-2. On heating, a positive moment is induced by restrained thermal expansion of the lower part of the beam against its fixed supports. For larger thermal gradients this moment then reduces gradually as the material above the mid-surface of the section starts to yield. On cooling this process is reversed with negative moments being produced

as the beam yields in tension from the bottom surface up. The residual bending moment is highest when only relatively low gradients are present (300°C peak temperature) whilst more recovery is achieved when higher temperatures occur within the section. This is a consequence of the upper parts of the beam remaining elastic for lower gradients. It should be noted that the peak residual moments occur when the magnitude of thermal gradient that might typically be experienced by a beam exposed to fire is applied. Effectively, the residual bending moments within the beam act as an additional load on the structure. This demonstrates that following a heating-cooling cycle, a beam's capacity at small displacements will not be as great as prior to heating because of locked-in stresses.

The plastic strains developed through the depth of the beam for various gradients can be seen in Figure 3-3 where the strains in both the heating and cooling phases of the fire are shown. The bottom of the section experiences the highest plastic strains, as a result of being exposed to the highest temperatures. Initially the plastic strains are zero as the material remains in the elastic range.

As yielding occurs progressively through the section the plastic strains increase accordingly. When cooling begins the forces are initially unloaded elastically, thus keeping the plastic strains constant. Further cooling reduces the strains until ambient temperature is reached and a small, permanent plastic strain remains. Deflections are zero for this scenario as the thermally induced moment in the beam is uniform along its length and exactly countered by a mechanical couple provided by the end supports [61]. Total strains are also zero as mechanical and thermal strains balance.

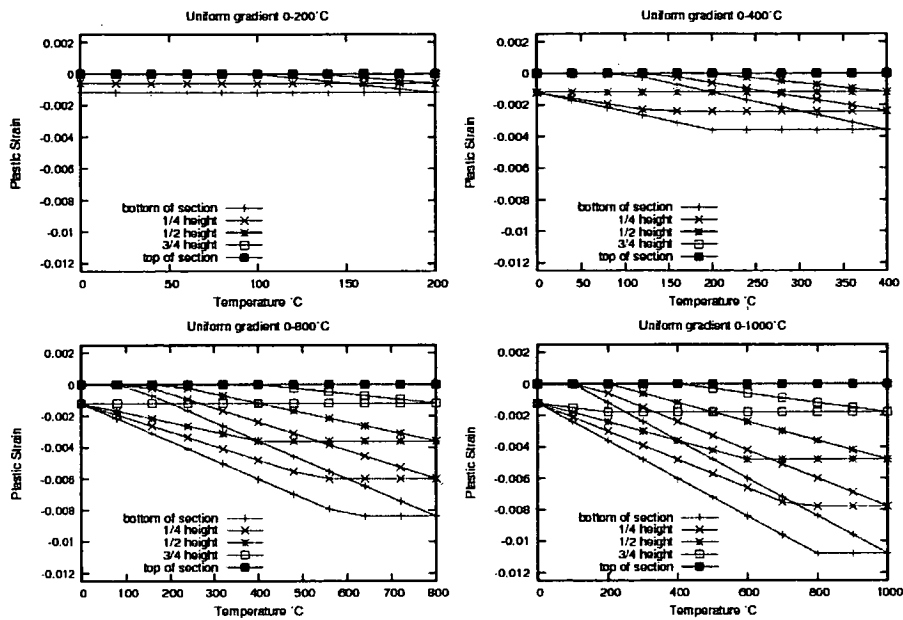


Figure 3-3 - Plastic strains in a fixed-ended beam subject to a heating-cooling cycle with various thermal gradients.

3.2.3. Linear temperature gradients with pinned ends

This case is identical to the previous one apart from the beam end conditions which now allow free rotation with pins at the centroid of the section. Due to these pinned ends, the beam now deflects when heated which allows for Euler buckling to occur. This deflection results in quite different behaviour than in the previous example. Mechanical strains can now be relieved by the increase in length of the beam which occurs as a result of deflection and so the total strains will no longer equal zero. Figure 3-4 shows the axial forces and bending moments in the beam as well as the mid-span vertical displacements. On heating the beam takes an increasing axial force until it buckles. The displacements are caused by the thermal gradients inducing thermal bowing which is no longer restrained by the supports.

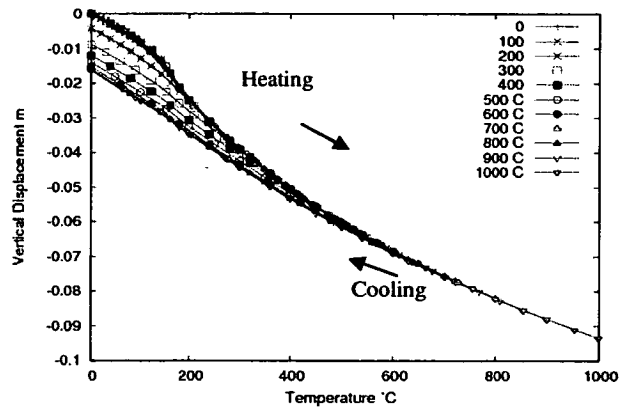
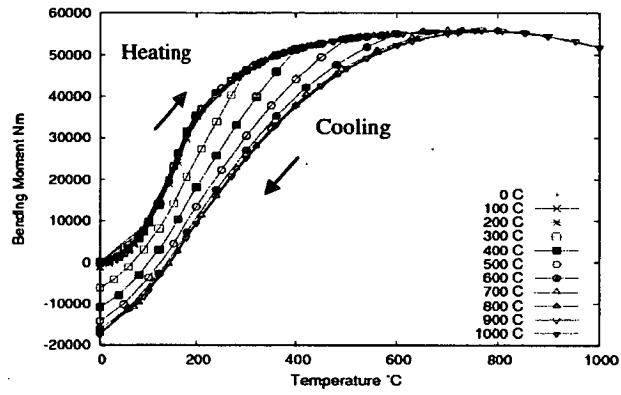
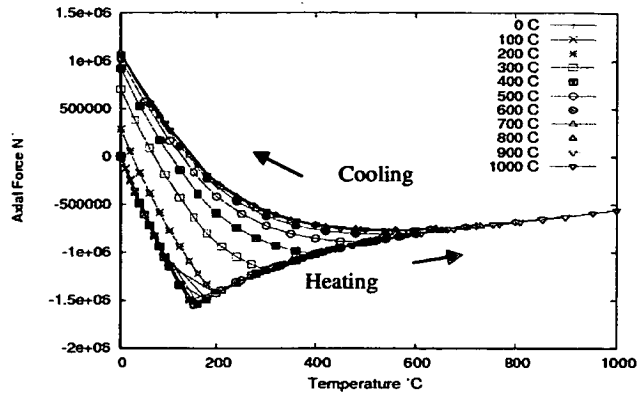


Figure 3-4 - Axial forces, bending moments and vertical displacements in a pinned beam subject to a heating-cooling cycle with various thermal gradients

Depending on the peak temperature, this buckling occurs from about 175°C; this moment can also be identified on the vertical displacement graph as the point where the rate of deflection increases. From this point onwards the deflections continue to increase and so the axial forces in the section reduce. Figure 3-4 shows the bending moments at mid-span where they initially increase as the temperature rises through the cross section.

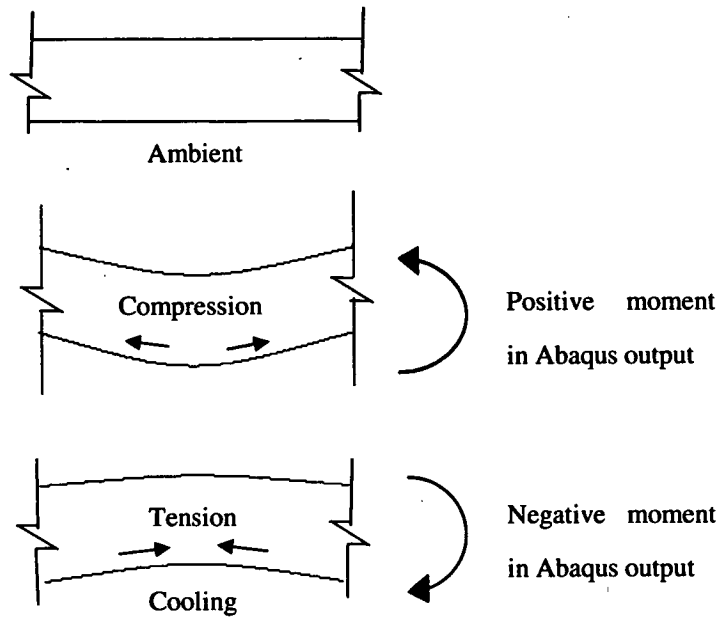


Figure 3-5 – Representation of bending during fire

This temperature increase leads to vertical displacements which add a P- δ effect and the bending moments increase. As the temperature increases further parts of the cross section yield which reduces the bending moments. On cooling, the bottom surface of the section contracts thus resulting in a decrease in bending moment. On cooling, the deflections recover a significant amount until ambient

temperature is reached and only a small deflection remains. The beam yields in tension and has residual forces, though these are much smaller than those encountered in the fixed-ended beam scenario. Figure 3-5 shows a representation of bending during the fire, which shows more clearly how the beam starts with a positive bending moment and finishes with negative residual bending.

3.2.4. Varying Boundary Capacity

The previous sections have shown that boundary conditions have a strong effect on behaviour in cooling. To explore the behaviour of realistic end conditions, which will always be somewhere between fully-fixed and pinned, springs were introduced to the models to represent boundary conditions of finite rotational and axial capacity. The capacity of these springs was given as a proportion of the ambient temperature axial or rotational capacity of the beam cross-section.

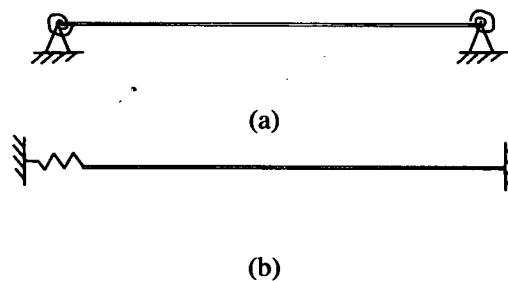


Figure 3-6 – Representation of the boundary conditions varied with (a) rotational boundary springs and (b) horizontal boundary springs

Rotational capacities studied range from zero, representing in the case of rotational supports, a pinned beam, to ten times the bending stiffness (where the bending stiffness is taken as $4EI/L$) of the section, representing a beam with more or less

fixed supports. In each of the figures the range is therefore indicated from pinned to 10. Allowing some rotational flexibility simulates a connection type which does not allow for axial deformations but has some capacity in rotation. This can be compared to real connection types such as a double angle web cleat [62]. Figure 3-7 shows the section forces encountered in a beam with varying degrees of rotational support capacity when subject to gradients giving maximum temperatures of 200°C and 800°C respectively.

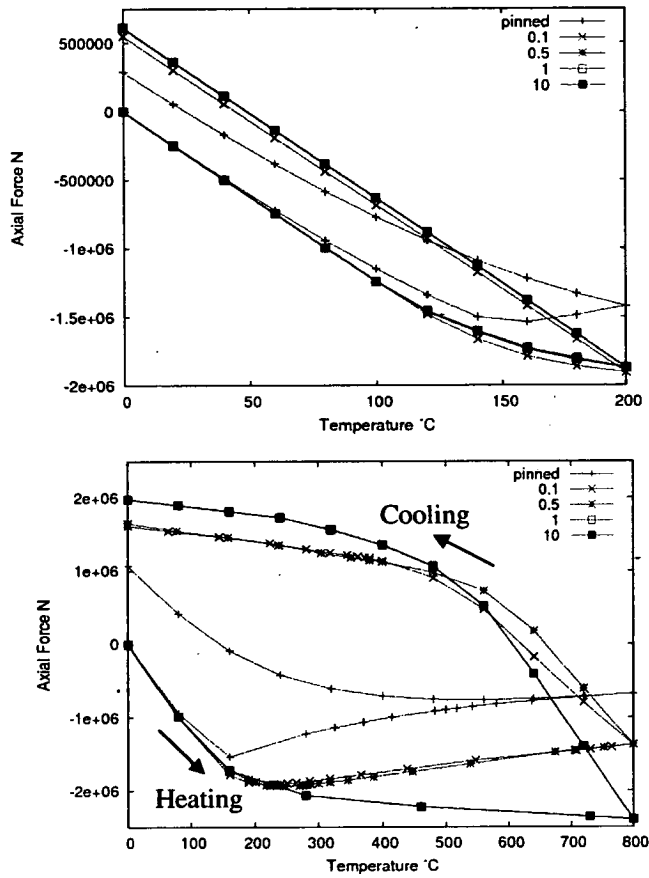


Figure 3-7 - Comparison of the section forces when the rotational capacity of the boundary conditions is varied. Gradients corresponding to lower surface temperatures of 200 °C and 800 °C are shown.

The translational supports were fixed in these analyses. The pinned and '10' results show the outer limits of the behaviour and roughly correspond to the curves seen in previous graphs. For intermediate rotational support capacities and a peak temperature of 200°C, the change in behaviour with varying boundary conditions is very small and the residual force is similar for all models. However, when higher gradients are imposed the behaviour varies quite substantially as the rotational boundary capacity is changed.

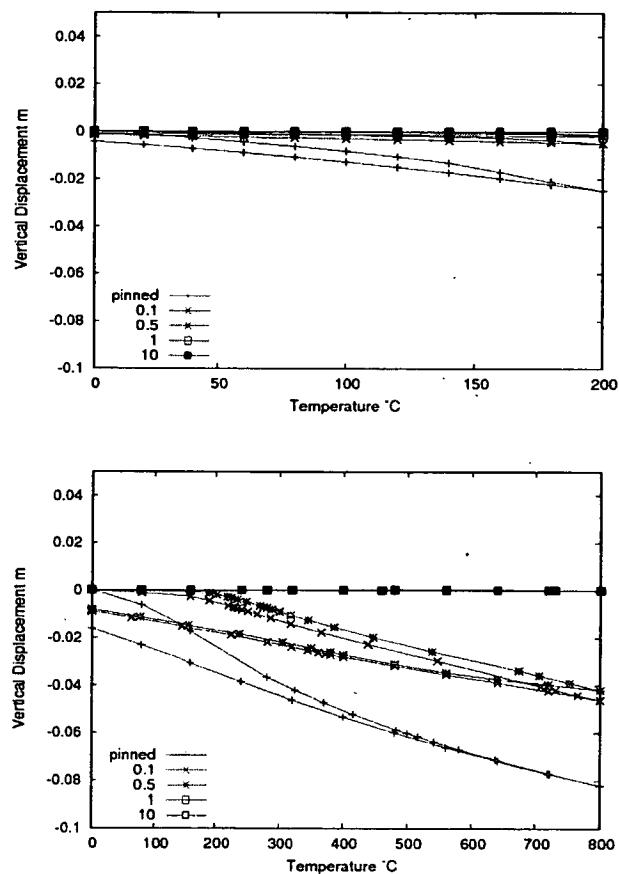


Figure 3-8 - Comparison of mid-span vertical deflections when rotational boundary conditions are varied. Gradients corresponding to lower surface temperatures of 200°C and 800°C are shown.

For a rotation capacity of 1, the behaviour is almost identical to that of the '10' case, which in turn is close to fixed. When the rotation capacity is between pinned and '1', the behaviour is more similar to the fixed scenario than to the pinned, with substantial residual forces.

The peak axial forces which occur during heating are similar for both the 200°C and 800°C cases. However, as little yielding takes place at lower temperatures, almost full recovery takes place after a peak temperature of 200°C and hence only small residual forces remain. The vertical displacements at the midpoint of the beam are shown in Figure 3-8. From this plot it is clear deflections also vary with support conditions and thermal gradients. Only marginal deflections are seen for the beams heated to 200°C, apart from the fully pinned case which does deflect somewhat. When the beam is heated to higher temperatures more pronounced movement occurs. At 800°C due to the larger amount of thermal expansion combined with the steeper gradient through the beam, deflections occur with all degrees of bending capacity other than full fixity. This behaviour is expected as the higher temperatures induce higher axial forces, larger thermal gradients and thus larger deflections against identical boundaries.

During the modelling of the varying rotational capacity, some inconsistent results were observed. Upward buckling occurred for some of the models. This was shown to be a numerical problem, further detailed in Appendix A.

Varying the degree of axial capacity was considered next. For these cases no rotation was permitted but lateral restraints were varied, thus allowing for some movement in the horizontal direction. The axial restraint is defined as a multiple of EA/L , which defines the axial stiffness of the section. Figure 3-9 shows the

vertical displacement in beams with peak lower surface temperatures of 200°C and 800°C and varying axial support capacities. The rotational boundaries are fixed for this scenario. As heating begins, thermal expansion causes the beam to push against the supports. Since these supports provide limited resistance against lateral movement, the expansion is not fully restrained resulting in only very small vertical displacements.

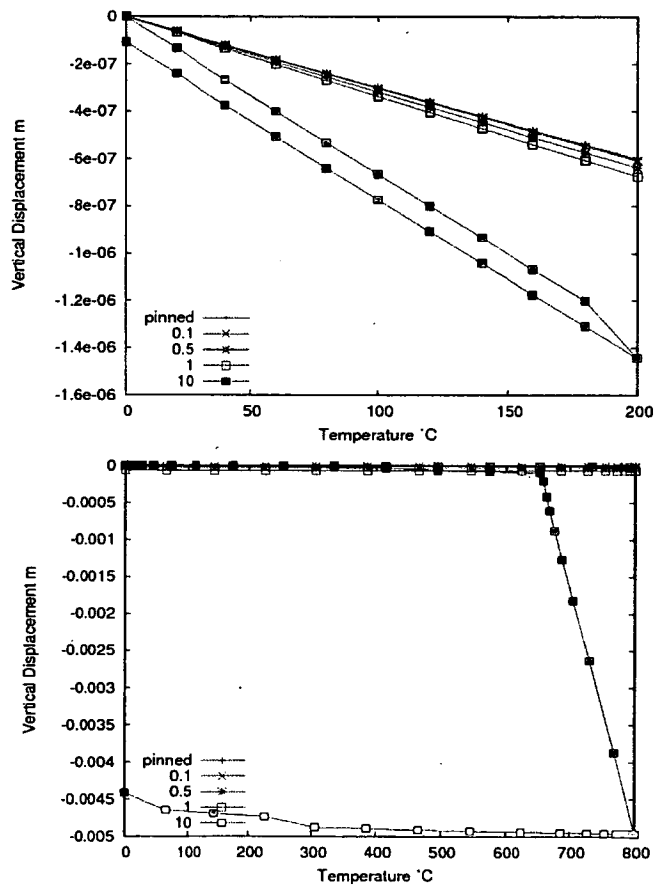


Figure 3-9 - Mid-span vertical deflections when the axial boundary conditions are varied. Gradients corresponding to lower surface temperatures of 200°C and 800°C are shown.

Upon cooling, thermal contraction reverses this effect. No displacements are expected as rotation is restrained; it may be that the complex definition of the boundary conditions results in some numerical inconsistency allowing very small vertical displacements.

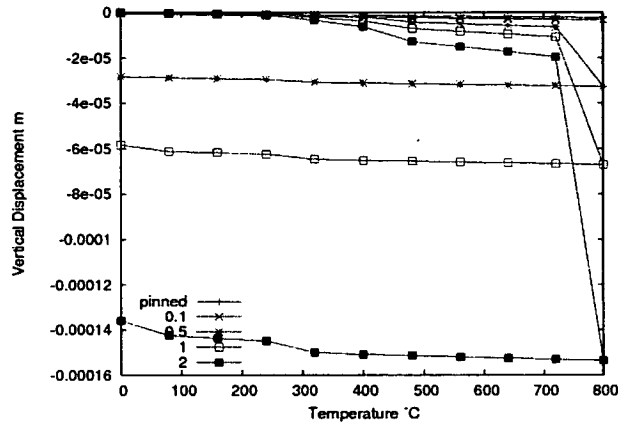


Figure 3-10 - Identical to Figure 3-9 without the fixed beam which provides a better view of the displacements at lower capacities

When the boundary capacity is sufficiently high (i.e. fixed) the beam is forced to deflect downwards more to continue its expansion as the supports are providing some restraint. Once cooling commences this effect partially reverses, but some residual displacement remains. The displacement of the 800°C beam with a fixed boundary is significantly larger than the others as buckling occurs towards the end of the heating phase; hence the other displacements appear to be zero when in fact they are still greater than those seen for the 200°C beam models.

Figure 3-11 shows the section forces for the beams heated to 200°C and 800°C respectively. When no axial restraint is provided, the section forces in the beam

will be zero. As the restraint increases, so does the axial force in the beam as is clear from the figures. When relatively low temperatures are reached, the thermal expansion causes small vertical deflections at all of the capacity variations considered. The rotational boundary is completely restrained.

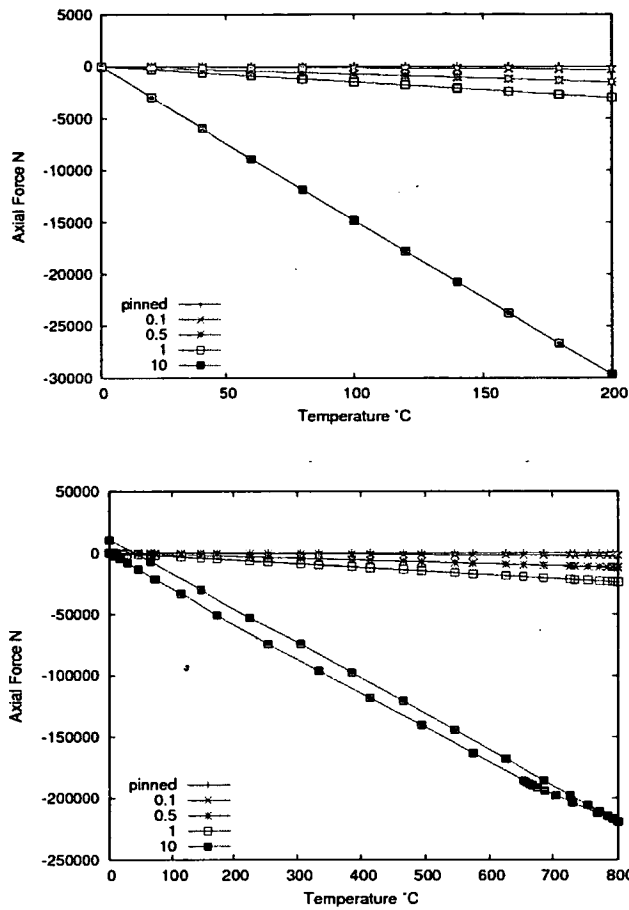


Figure 3-11 - Axial forces when the axial boundary conditions are varied.

Gradients corresponding to lower surface temperatures of 200°C and 800°C are shown.

It is clear that the amount of restraint has a significant impact on the behaviour of beams in fire. It should be noted that the restraint may vary during a fire as this is

provided by the surrounding structure which may be affected by the fire. Again, varying the boundary condition (axial capacity) can be related to a connection type. In this case the connection does not have significant rotational capacity but has reasonable ductility in the lateral direction, which may be compared to a fin plate.

3.2.5. Realistic Material Behaviour

To explore the influence of material degradation, the fixed-ended beam with linear gradients was remodelled with a non-linear, temperature dependent modulus, yield stress and coefficient of thermal expansion all appropriate for typical structural steel. Values for these quantities were taken from Eurocode 3 [54] and used with a von Mises yield criterion together with isotropic hardening. It was assumed that ambient temperature values were the same as in the previous examples and that full recovery of properties occurred on cooling. The stress-strain relationship, which is dependent on temperature, is shown in Figure 3-12. Detailed input of the material model is given in Appendix D.

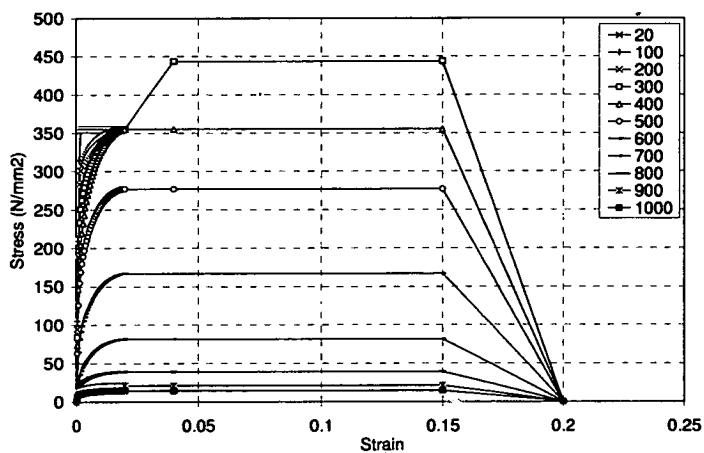


Figure 3-12 – Stress-strain relationship for steel

Comparing the axial forces and bending moments in Figure 3-13, with those obtained from the simplified case (Figure 3-2), we see the overall behaviour is very similar.

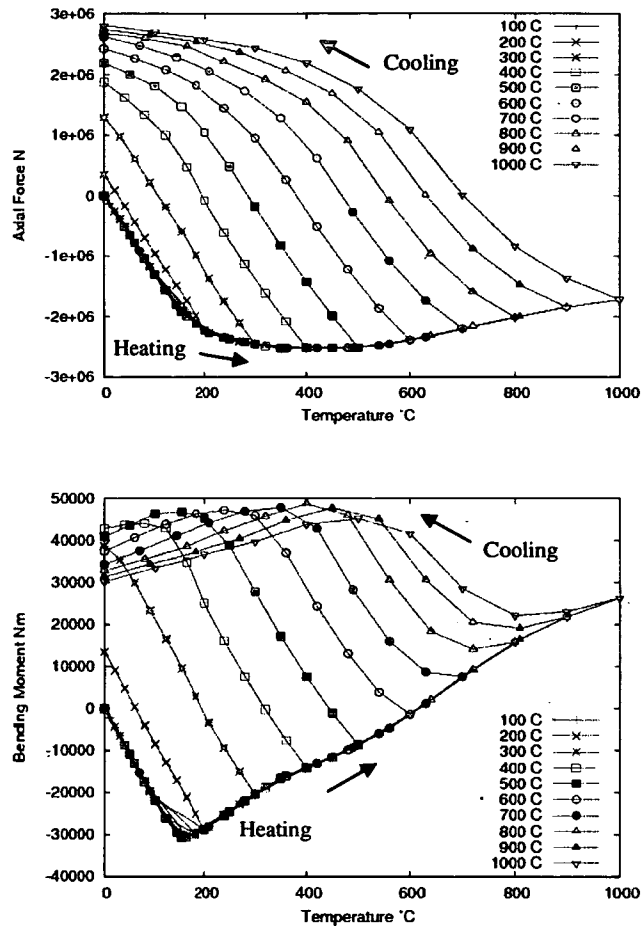


Figure 3-13 - Axial forces and bending moments developed in a fixed-ended beam subjected to a heating -cooling cycle with temperature dependent material properties.

As in the previous analyses, the axial forces increase with a rise in temperature. However, with temperature dependent material properties considered, a loss of

strength occurs as the temperature through the section increases. This loss of strength reduces the capacity of the section which results in a reducing axial force after a temperature of 400°C is reached. The bending moments are also initially similar to the simplified case; however they quickly reduce as the temperatures increase. With the simplified material behaviour this reduction was solely due to the increasing area of yielded material above the midpoint of the section as the temperature rose; an effect that is still present in this scenario. With temperature dependent material properties a reduction in strength also takes place. This combination of partial yielding and reducing strength leads to more complex behaviour than in the earlier case but the trends are similar. It should be noted that the residual forces and bending moments for this scenario are larger than those seen previously. The largest residual forces are still obtained when the section is subjected to the highest gradients, however, the largest residual bending moments now occur when the lower surface temperature peaks at 400°C, slightly higher than previously.

The section considered up to this point was a solid square section of 0.1x0.1m. Although this simplified analyses, in real structures beams are likely to be made up of beams with complex cross-sections such as I-sections. The force development for I-beams as well as the original square section is shown in Figure 3-14 which shows that the behaviour is qualitatively similar. The I-beam considered has a different total area to the square section but the figure shows that cross-section shape does not influence the behaviour in principle; only the associated values differ. This allows for use of the results obtained thus far when understanding the behaviour of I-beams during cooling.

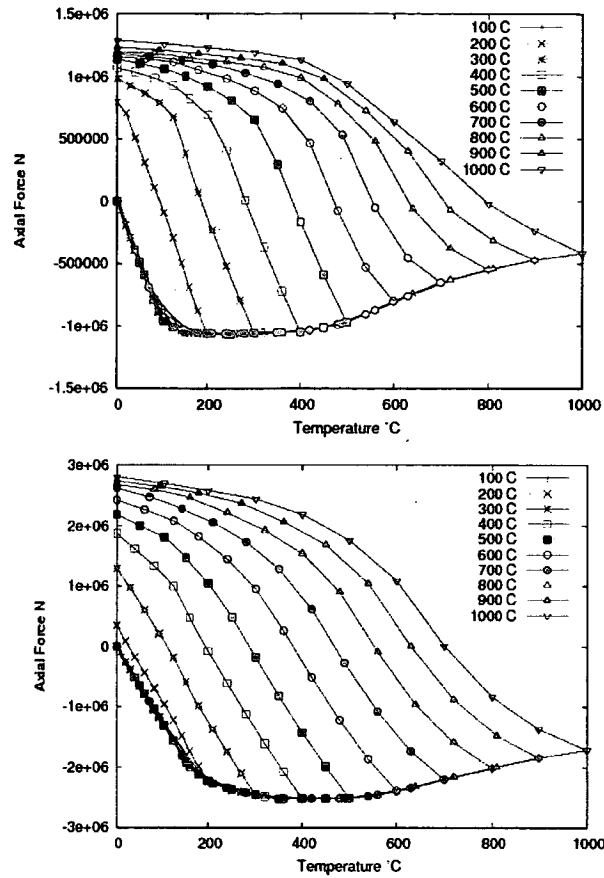


Figure 3-14 - Comparison of the section forces encountered in a fixed-ended I-beam (top) and rectangular section (bottom)

3.2.6. I-sections with imposed loading

To further increase the applicability of these results, several changes have to be made. For this example, a beam designed in accordance to EC3-1993 [54] has been modelled. The I-beam of UB 356x127x33, over a span of 6m has been considered. Gravity and dead loads based on this Eurocode are incorporated,

representing the self-weight of the section and the load imposed by a concrete slab.

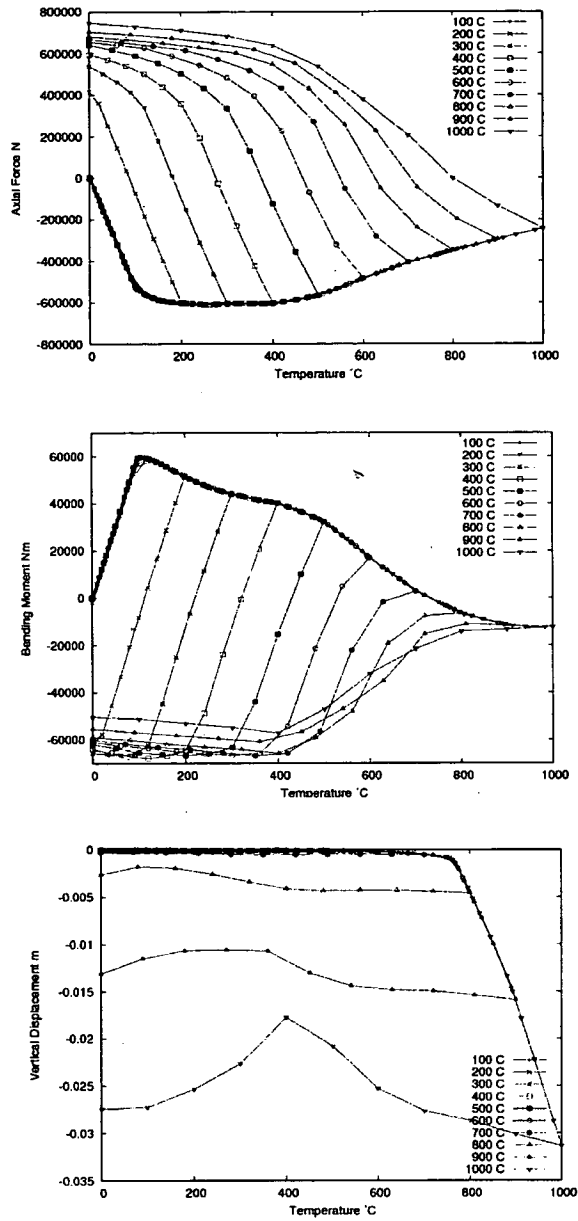


Figure 3-15 – Axial force, bending moments and vertical displacements with real material behaviour and gravity loading incorporated for the I-beam

The overall pattern of force and bending moment evolution remains very similar to the previous examples without loading. However, the loading does result in deflections more substantial than those caused by thermal gradients alone. The displacements remain extremely small as the example shown here is a fixed beam. The residual bending moments remain larger than when no loading is considered as less recovery is possible. Both fixed and pinned scenarios were considered and these may be compared with detailed 3D models described in Section 3.3.

3.3. 3D Validation

All the previous discussion has been based on the assumption that the behaviour of beams modelled using 1-d finite elements is representative of real behaviour. This is reasonable for a square section beam but I-sections may be prone to local buckling that could affect their response in a manner not captured by 1-d elements. To investigate the influence of local buckling and to validate the simpler beam models two I beams of different sizes were considered.

Scenario 1

A 3D analysis of the I-section from section 3.2.6 was undertaken, again using UB 356x127x33. The beam was modelled with Abaqus, using a dense mesh of 4-noded shell elements as shown in Figure 3-16. The top flange was restrained in the horizontal direction to prevent lateral-torsional buckling occurring; such restraint would in reality be provided by the presence of a floor slab above the beam. However, the slab would not necessarily restrict the vertical movement and so this was left unrestrained in the model. Several mesh densities were tested to ensure all

buckling phenomena were observed and the optimum mesh was chosen. Two types of end conditions were modelled; fixed and pinned. To model the pinned condition correctly distributing constraints were used. Distributing constraints tie several nodes or elements to a single reference node in translation and rotation and allow nodal output (such as the lateral reaction force) representing the whole beam to be obtained. For each boundary condition two linear temperature gradients were considered – a low gradient where the lower flange reached 200°C and a high gradient where the lower flange reached 800°C. These two temperature gradients were also considered with 1-d beam analyses and thus allow for a direct comparison with the 3-D beam model.

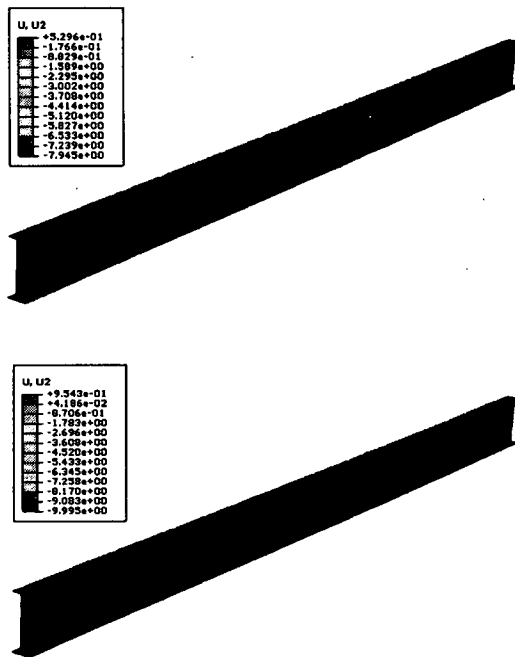


Figure 3-16 - A 3D model with fixed ends. Vertical deflections at the end of the heating and cooling phase for 800°C maximum temperature

Local buckling of steel beams has been observed in real fires [63] and it was thought that this could have an effect on the total section forces. However, when considering the fully-fixed beams, no significant local buckling was observed in the models studied. The displaced shape of the fully fixed beam subjected to a peak temperature of 800°C is shown in Figure 3-16 where it can be seen that almost no vertical displacement takes place.

This is also in accordance with the results from the 1-D beams where no displacement occurred. Figure 3-17 compares the axial forces predicted for a beam with fixed-end conditions when modelled using beam elements and shell elements. Gradients producing peak temperatures of 200°C and 800°C are shown and in both cases there is a very close match between the two modelling approaches.

For the case of a pinned I-section significant buckling occurred and some of the beams failed during the heating phase. Figure 3-18 shows a comparison of axial force evolution for the pinned-end condition reaching a peak temperature of 200°C. The comparison is initially quite close, but shortly before the end of the heating phase the axial force in the 3D model suddenly reduces a little, whilst the beam element axial force continues to increase until the end of the heating. At this point, yielding occurs in the top flange which reduces the overall capacity of the beam and thus the total axial force. In part due to these differences during heating, the behaviour in cooling is not completely similar. The predicted force in the 3D beam becomes tensile at a slower rate than the 1D beam which leads to a smaller residual axial force than the 1D beam calculates. Although the 1D model does not fully capture the behaviour, the residual forces are overestimated thus giving a conservative output.

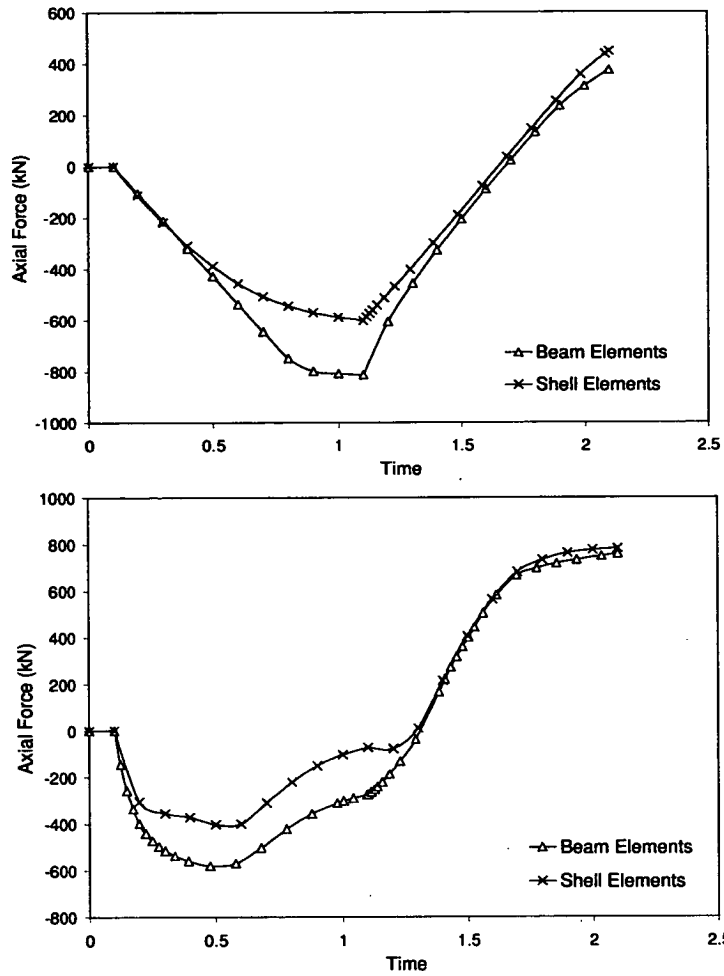


Figure 3-17 - Comparison of axial forces predicted by a beam element model and a 3D shell element model for maximum temperatures of 200°C and 800°C. Fixed end conditions.

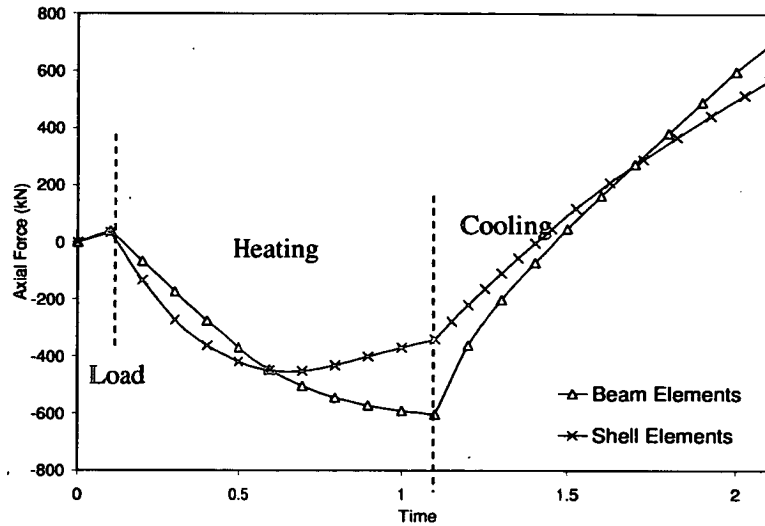


Figure 3-18 - Section forces in an I-beam comparing the simple beam model with the 3D model for a maximum of 200°C degrees with pinned end conditions.

As the peak temperature reached increases, the vertical deflections also increase (larger thermal gradient and lower material strength) which in turn results in a larger compressive force in the top flange.

In some cases this leads to local buckling failure of the beam during the heating phase, which results in numerical failure of the model, thus preventing a full comparison with the 1D models. For the specific beam considered here, (numerical) failure occurs when a peak temperature of 800°C is applied. Figure 3-19 shows the displaced shape of the pinned beam subjected to a peak temperature of 800°C. The beam deflects substantially during the heating phase, which results in a local buckle at mid-span large enough to discontinue the numerical analysis. Reducing the design load does not stop this buckling failure occurring, which indicates this failure is predominately caused by the thermal gradient inducing thermal bowing. The thermal bowing is larger when a higher

peak temperature is applied and at the same time a reduction of material strength affects a larger part of the cross-section. This combination results in a top flange buckle.

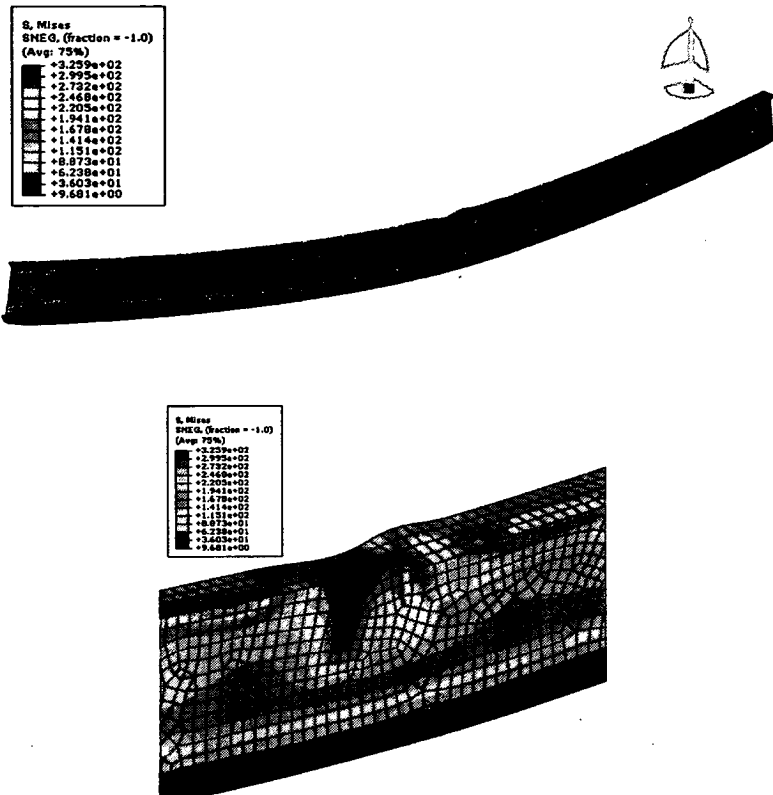


Figure 3-19 – A 3D model with pinned ends. Deflected shape at 750°C when significant buckling of the top flange occurs.

In Figure 3-20 the axial force for the 3D and 1D beams are plotted, which clearly shows the point at which buckling occurs in the 3D beam and when the analysis is discontinued. Applying a peak temperature of 600°C to the beam also results in some buckling at mid-span but does not result in a numerical failure.

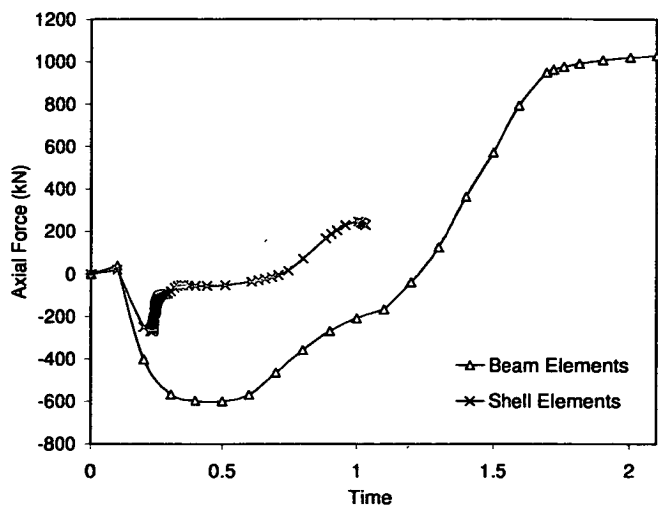


Figure 3-20 – Section forces in an I-beam comparing the simple beam model with the 3D model for a maximum of 800°C degrees with pinned end conditions.

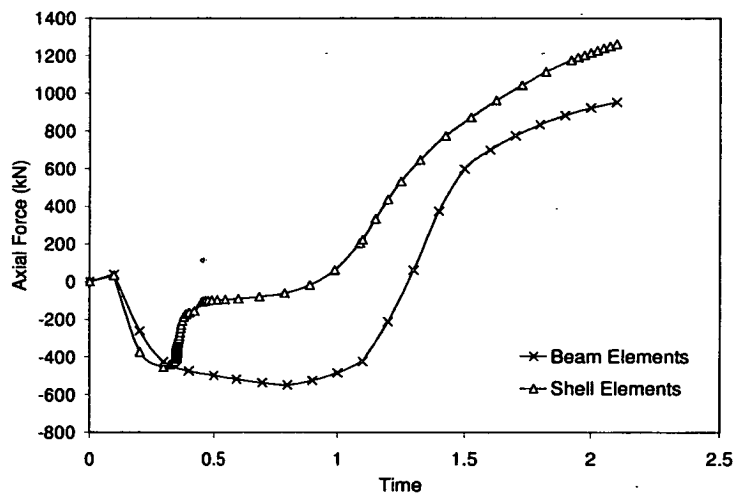


Figure 3-21 - Section forces in an I-beam comparing the simple beam model with the 3D model for a maximum 600°C degrees with pinned end conditions.

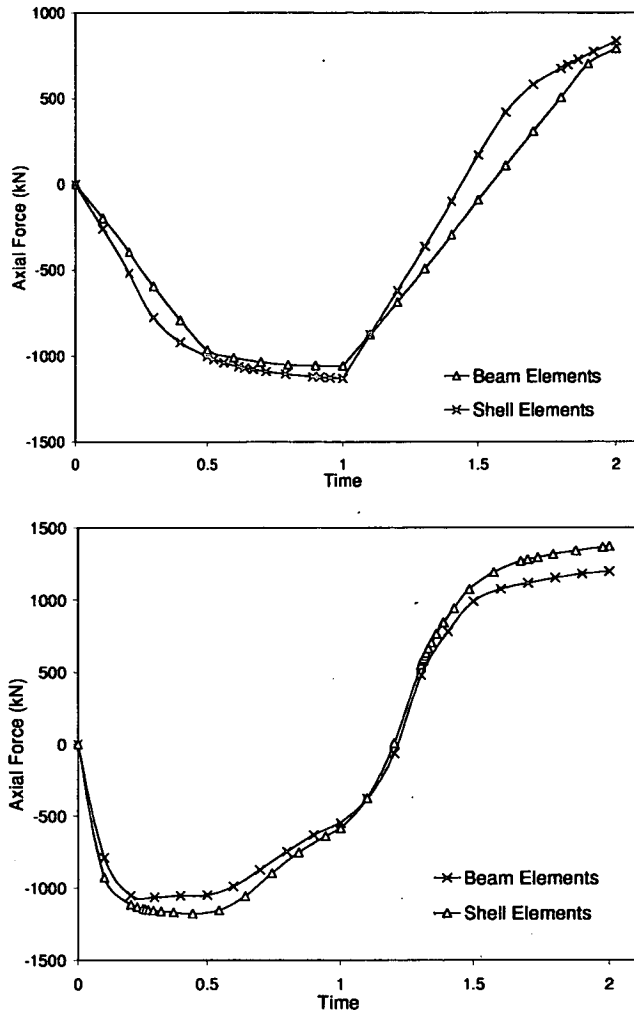


Figure 3-23 - Comparison of axial forces predicted by a beam element model and a 3D shell element model for maximum temperatures of 200°C and 800°C. Fixed end conditions.

A range of realistic connection types for this I section (fin plate, end plate and double angle web cleat) and their typical tying capacity can be obtained [62]. Considering these three connections, capacity predictions are between 250kN for an end plate and 328kN for a double angle web cleat. However, as is clear from Figure 3-17 to Figure 3-21, for each of the peak temperature scenarios reached, the axial force expected at the end of cooling is above 500kN. Clearly this is outside

the capacity of the connection if it is assumed the entire force is directly transferred onto the connection. In reality the connections may have some ductility which may relieve this force and prevent failure in some cases.

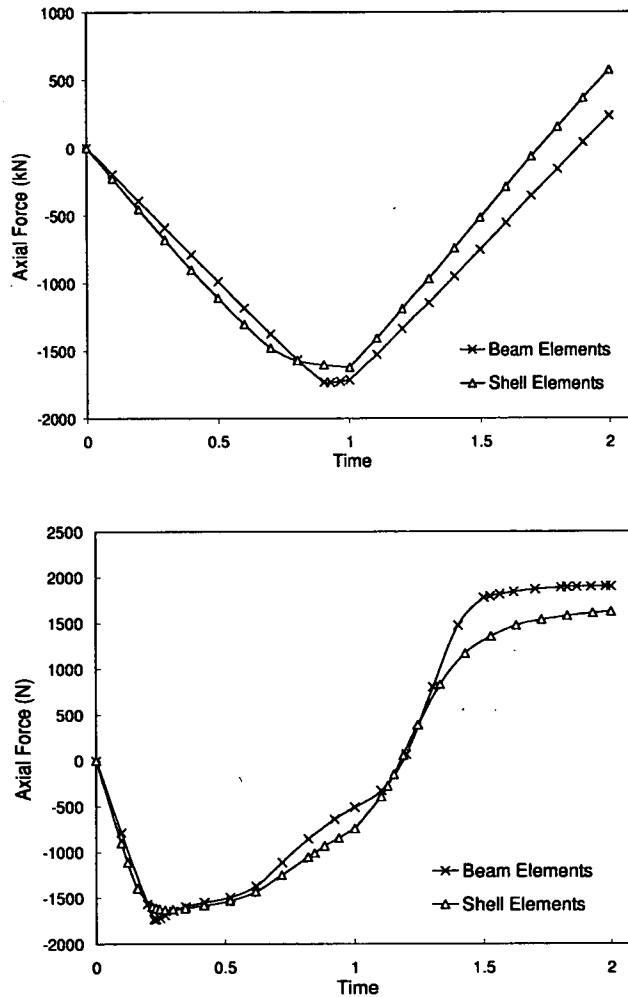


Figure 3-24 - Section forces in an I-beam comparing the simple beam model with the 3D model for a maximum of 200°C and 800°C degrees respectively with pinned end conditions.

The results show that the 1D models predict the behaviour well for most scenarios, fixed beams in particular. When pinned beams are considered and large thermal gradients are induced, buckling failure may occur which affects the force capacity of the section. In real structures the boundary condition is likely to be somewhere between pinned and fixed. As could be seen from section 3.2.4, even a small increase in rotational capacity significantly reduces the vertical displacements thus decreasing the likelihood of the failure observed in Figure 3-19. It should also be noted that the gradients for which the 3D beams buckle are extreme; a likely temperature distribution along the I-section would have high temperatures in the top flange as well thus reducing the total thermal curvature. The presence of the slab will also affect the behaviour to some extent. This is explored further in an example of a composite floor in section 3.4.

3.4. Cardington Test 1

A third, more complex 3D scenario was considered for comparison with the simple beam results. A simplified version of the first Cardington British Steel fire test conducted in 1996 on a composite steel-concrete structure in the UK is detailed by Gillie [64]. Figure 3-25 shows the geometry of the structural test as well as the dimensions for the sections. The secondary beam is heated linearly to 800°C and subsequently cooled linearly back to ambient temperatures. The concrete slab is heated with a linear gradient, with a peak temperature of 600°C at the bottom of the section and 0°C at the top.

The vertical deflection at mid-span of the heated beam, plotted against temperature is shown in Figure 3-26, which shows good comparison with the observed test results, thus validating the model [64]. This model is used here to compare the

behaviour with 1D beams as well as a variety of cooling rates which are discussed further in Chapter 5. The structural model described and shown in Figure 3-25 is subjected to a simplified parametric fire curve, the result of which is compared to a single beam element model subjected to the identical fire parametric fire.

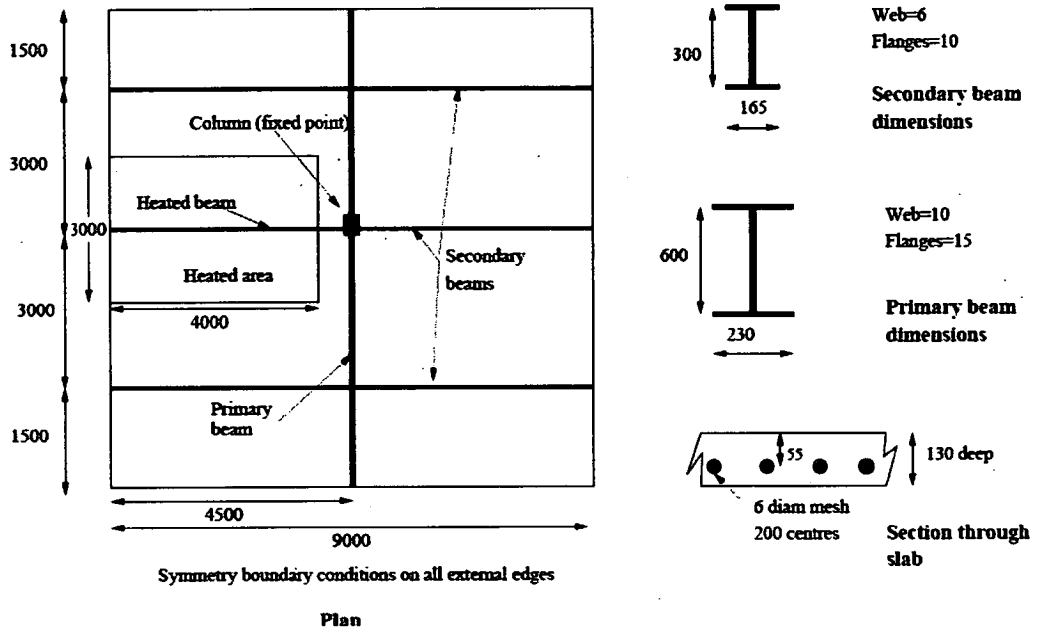


Figure 3-25 – Geometry of the structure and section dimensions [64]

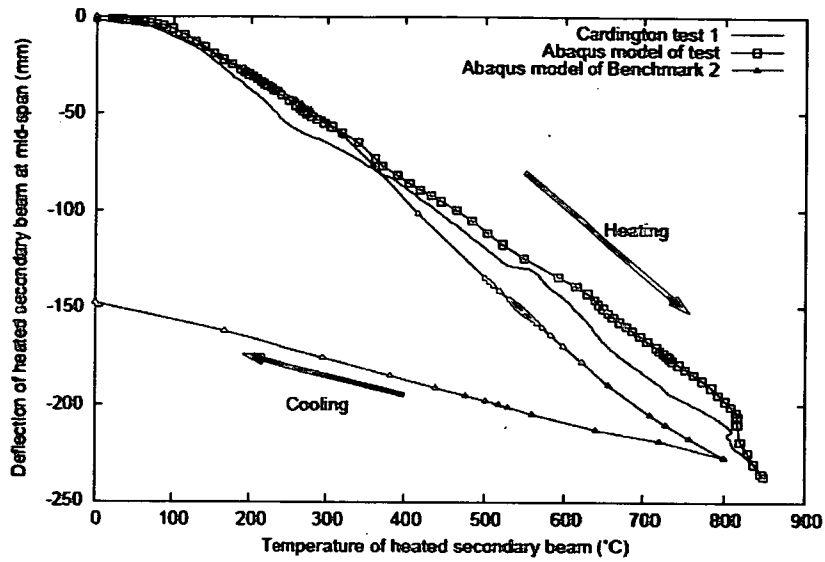


Figure 3-26 – Vertical displacement plotted against temperature [64]

Figure 3-27 shows a 3D representation of the beam element model and 3D beam and shell elements model of the Cardington Test 1 set up. The beam element model represents the central secondary beam which is being heated and is similar to all the beam element models considered in this chapter. Boundary conditions are identical (fixed) in both models whilst loading in the simple beam only incorporates the self weight, i.e. does not take the concrete slab into account in any way. The simplified parametric curve chosen has an arbitrary cooling length of 5600s for which a heat transfer analysis was done to obtain the concrete temperatures. More details on the heat transfer process are given in Chapter 5. The temperature distribution for both steel and concrete is shown in Figure 3-28.

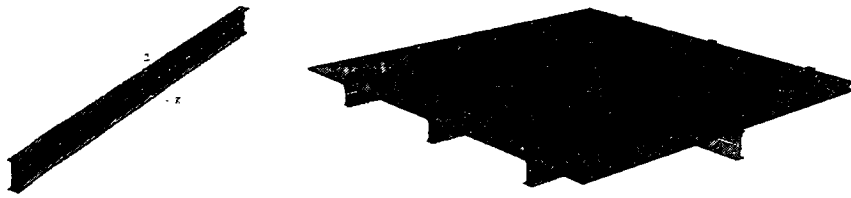


Figure 3-27 – 3D Representation of 1D and 3D model

Comparing the axial force in the heated beams in Figure 3-29 shows that the overall trend is very similar. The peak axial force in compression is identical; it is not until the cooling phase that a more substantial difference occurs. This is due to the presence of the slab which is still hot, thus reducing the tensile axial force to some extent. This gives confidence that the trends described in the previous sections are accurate as the concrete slab only has a limited effect on the axial force evolution.

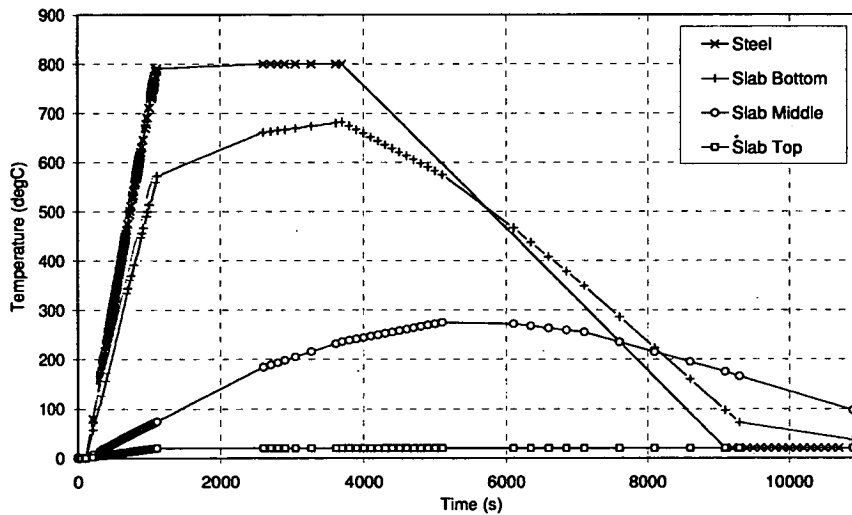


Figure 3-28 – Temperature evolution in steel and concrete

The vertical displacements and bending moments are also plotted in Figure 3-30 and Figure 3-31 respectively. The differences here are a little more obvious as the slab has some influence on the vertical displacements and associated bending moments and this is not taken into account in any way in the 1D beam model. The composite section deflects more than the beam due to the slab which is also hot and expands, causing the overall displacement to be larger. The recovery occurs when the steel beams cool, but in the case of the composite section this recovery continues as the slab cools. The bending moments in Figure 3-31 are similar during the heating phase but a more substantial difference is established during cooling. Once the steel beam in the 1D beam model has cooled, the bending moments stay constant (as do the displacements). In the composite section the slab cools more slowly and as seen with the displacements, this results in continuing recovery and thus increasing hogging (positive) moments. However, it is clear that the overall trend in behaviour is identical to the 1D beam model.

The buckling failure which was observed in the 3D beam validation of the previous section is not repeated in the Cardington Test 1 composite section. The beams in the composite scenario are heated uniformly to 800°C; no gradient is present and thus less thermal curvature. Although large displacements are induced, the beam does not buckle. This gives confidence that the use of 1D beam models to capture the global behaviour is appropriate.

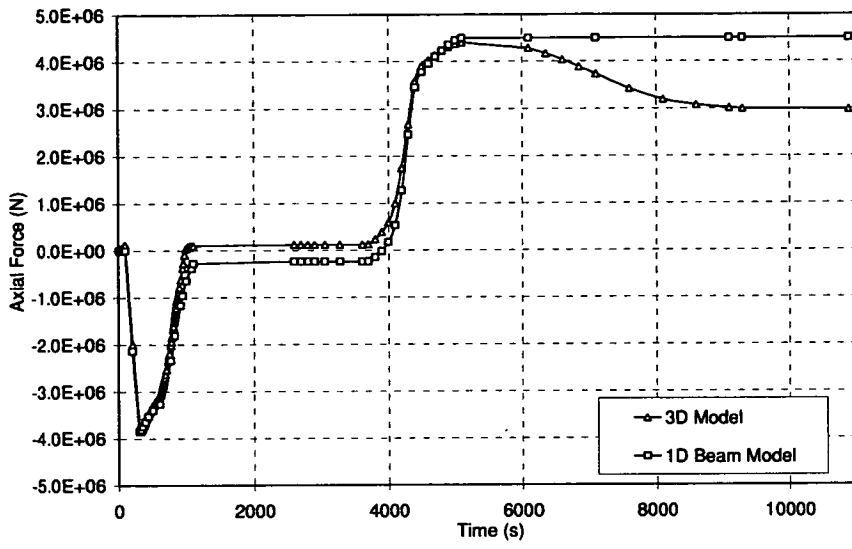


Figure 3-29 – Axial force comparison of 1D and 3D model

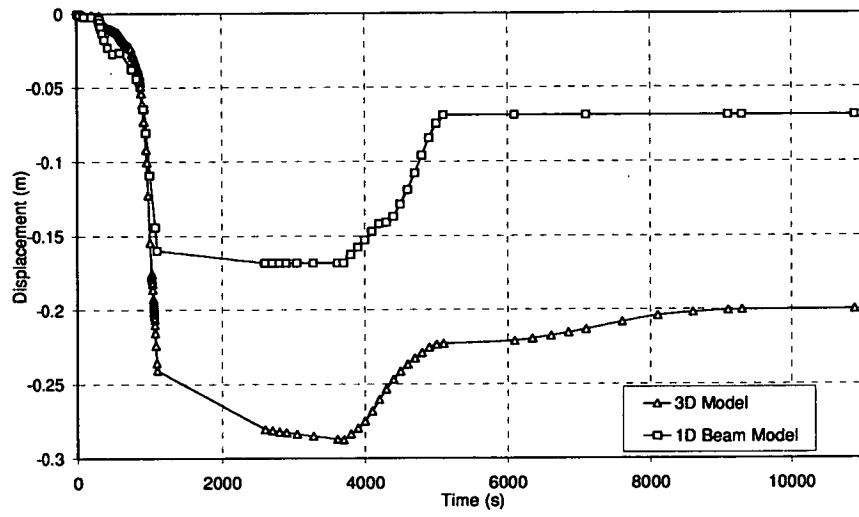


Figure 3-30 – Vertical displacement comparison of 1D and 3D model

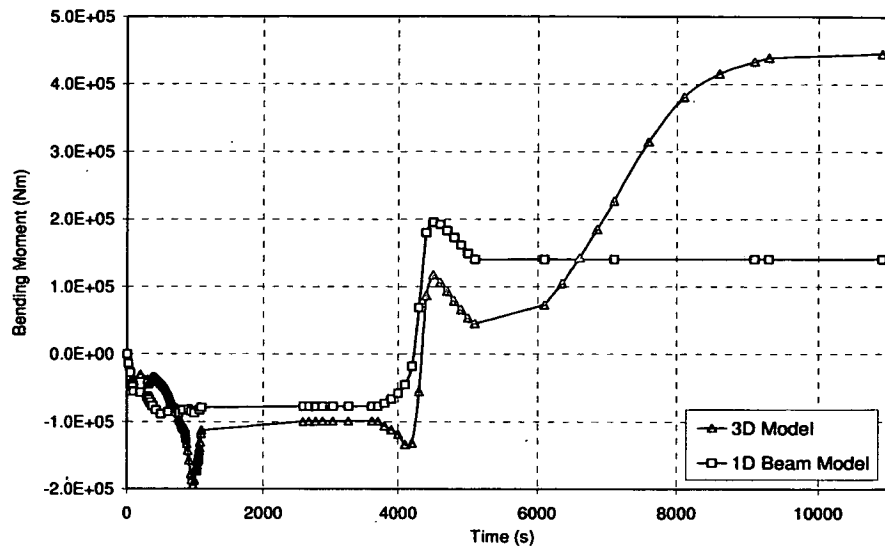


Figure 3-31 – Bending moment comparison of 1D and 3D model

3.5. Conclusions

This chapter has examined the fundamental mechanics of cooling structures by investigating the behaviour of beams subjected to heating and cooling. It has highlighted the patterns of forces and moments likely to be present in simple structural elements both during the cooling phase of a fire and in their residual state. Simple finite element models were used to examine several levels of complexity of support conditions and material behaviour. The results were validated against detailed 3D models.

It was found that a residual tensile force and sagging bending moments are always present, the only exceptions being when a boundary condition has zero capacity or heating is slight enough so as to not produce any plasticity. The values of the

residual forces and moments do, however, depend significantly on the scenario. It was found that both residual forces and moments are larger when the temperature dependent material properties are taken into consideration. Residual axial forces are largest when high temperature gradients were present in the structure. By contrast the largest residual bending moments occur with lower gradients (maximum at 300°C). Essentially the residual forces and moments represent an additional load on the structure, which should be taken into account when considering the use of a structure post-fire. The boundary conditions influence the behaviour strongly and as these are likely to vary to some extent during a real fire, some care is required when developing detailed models of structures. The 3D models showed that behaviour of the fixed ended beams compares very well with the simple beams. For pinned beams however, some buckling failure may occur during heating which is not captured by the 1D models. This failure may be prevented when the beam is part of a composite floor and a concrete slab is in place. The presence of a slab affects the boundary conditions which have been shown influence the behaviour significantly.

The results of the 1D beam analyses are compared with 3D shell models. These models may capture behaviour which is not observed by 1D modelling. It was found that the overall comparison was very good, especially for beams with fixed boundary conditions. For longer span, pinned beams however, buckling failure was observed. This failure occurred at mid-span where large deflections result in high compressive forces in the top flange. The pinned end conditions in combination with a steep temperature gradient across the section led to this failure; both the boundary conditions and temperature profile would be less extreme in

real structures. The presence of a concrete slab for instance would have an effect as the beam would be more restrained.

To evaluate this, a second comparison was made with a model of Cardington Test 1 to compare the modelling of simple steel beams with a beam in a composite floor section. The axial forces, displacements and bending moments were found to be very similar until the final stages of cooling which is when the hot concrete begins to affect the behaviour. This suggests that the global behaviour observed in the simplified 1D beams is generally representative of the behaviour of beams in a composite structure.

The fact that large tensile forces are likely during and after cooling has implications for connection design and robustness. At present connections in fire are not generally seen as critical because they will typically be cooler than the surrounding structure and on heating connection failures are rarely seen. If the full tensile yield values as presented in the results are applied directly to the connections, even assuming they are at ambient temperature, failure would result as connections are normally only designed for nominal axial forces.

This prediction is in line with experimental evidence from the Cardington tests where half-depth end plate connections failed in tension during cooling. If such a failure resulted in partial collapse, it would pose a serious risk to the lives of any remaining occupants of a structure and to fire fighters. During the Cardington tests collapse did not occur as the connection forces were redistributed through a composite floor slab. Alternative load paths such as this are clearly one means of avoiding the consequences of connection failure; however, they will not always be available, for example in non-composite construction. In these cases designers should consider other methods of reducing the chances of connection failure. One

possibility would be to design connections to have a large degree of axial flexibility.

Similarly it has been shown that fire-affected beams may carry large residual moments, which will also result in a residual strength lower than the initial strength. These effects would be present even if there were only very small residual deflections in the structure and so would not be apparent from a purely visual inspection. This suggests that the assessment of structures after a fire with a view to reinstatement should be undertaken with consideration of the residual forces and moments that will be present. Even minor fires that result in temperature increases of less than 200°C could produce considerable residual inelastic stresses. The fact that a beam that has been heated may be entirely yielded in tension after cooling implies that its residual bending strength will be substantially less than its initial strength at small displacements. For large displacements the beam would retain significant load carrying capacity by means of catenary action. Large displacements in a post-fire structure would prevent reinstatement and replacement of the sections would be required. Therefore the assumption that residual bending strength after cooling is substantially less remains valid as this considers small displacements only.

4.1. Introduction

Currently, it is normal structural fire engineering practice to assess structural stability assuming a fire that is uniform over an entire compartment. It is increasingly recognised though, through Rein [65] and others [47, 49, 66] that real fires are localised and may travel within a compartment. This aspect of fire behaviour is now sometimes accounted for by innovative structural designers because a localised but travelling fire is seen as less severe than a uniform fire. However, it has not yet been shown whether this is a valid assumption or if travelling fires may in fact result in a more severe structural response in some cases. To date the implications of travelling fires for structural behaviour have not been considered in a systematic manner. This chapter is an initial attempt to understand the effects travelling fires may have on structural behaviour and to identify the main consequences for design and safety. This chapter is not seeking to analyse real structures but instead attempts to identify the likely forms of structural response to travelling fires. It builds upon work in Chapter 3 where the behaviour of beams subject to cooling after a fire are considered, and also on work by Rein et al. [25, 65] who developed an approach for characterising non-uniform fires in a simple manner, detailed in Chapter 2.

In reality travelling fires will greatly depend on structural layout and fuel distribution and may be extremely complicated to predict. A simplified temperature profile is considered in this chapter which allows for heating and cooling to occur simultaneously and thus builds upon the work presented in Chapter 3.

This chapter considers the implications of travelling fires for simple beam structures only. Initially it describes the behaviour for a fully fixed beam with uniform temperature gradients, which is then extended to increasingly complex scenarios (linear temperature gradients, boundary conditions and loading). Larger, 3D structures subjected to non-uniform fires have also been researched as part of this thesis and are presented in Chapter 7.

4.2. Modelling

4.2.1. Structural Models

To examine the effects of a travelling fire on a beam, finite element models were used. For conducting parametric studies, a 1-d model consisting of 50 linear beam elements was constructed using ABAQUS, a representation of which is shown in Figure 4-1.

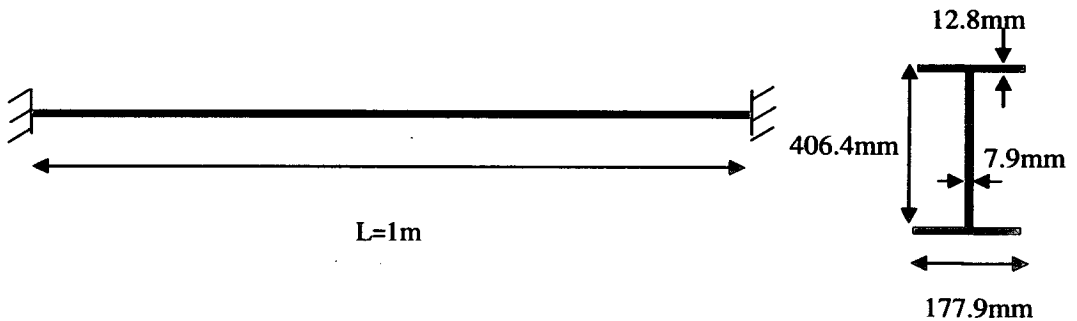


Figure 4-1 – Model geometry

The cross-section of the beam was taken to be a typical I-section (UB406x178x60). Material behaviour was taken to be elasto-plastic and typical of

a mild steel with a yield strength of 355MPa. Stress-strain relationships were taken from Eurocode 3 [54]. The beam length was taken to be 1m. At this stage this is an arbitrary length as no gravity loading is incorporated in the model thus making the length less important.

4.2.2. Fire definition

The fact that even in small compartments significant spatial temperature variations are likely is only beginning to be captured by simple fire models. Rein et al.[65] proposed a model consisting of “near-field” and “far-field” temperatures where the far-field temperatures result from hot gases and near-field temperatures from direct impingement of a flame as described in Chapter 2.

As the manner in which travelling fires should be characterized is still being developed, it was decided to apply simple, representative forms of temperature loading to the beam. This approach also has the advantage of allowing the underlying mechanics to be readily identified. The loading considered consists of a triangular patch of temperature, which was defined by two parameters: the patch length, d , and its peak temperature T , as shown in Figure 4-2. A triangular form of loading was chosen as this modelled the approximate linear decay of temperature with distance from the centre of the fire suggested by Rein et al. [65]. The peak temperature was varied between 200°C and 1000°C and patch lengths ranging from 20% to 100% of beam length were considered.

Initially a uniform temperature through the beam depth was modelled and no other loads were applied to the beam. This simple model was then extended to include a

thermal gradient, varying boundary conditions and loading scenarios, all of which are presented in section 4.3.

To model the temperature patches Fortran subroutines were used for each scenario. These user subroutines are referred to in the Abaqus input and define all aspects of the patches, including the length and peak temperature. An example of a subroutine is attached in Appendix B1.

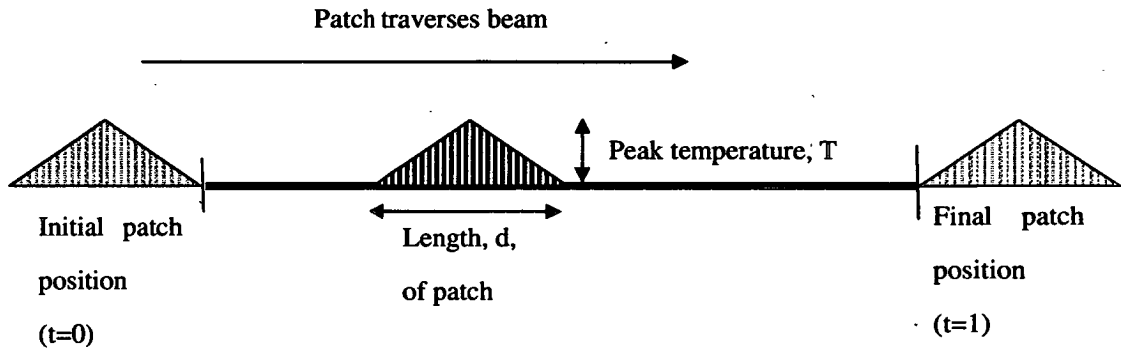


Figure 4-2 – Definition of patch loading showing the movement of the temperature along the length of the beam with the length, d , and peak temperature, T , indicated

4.3. Results

This section presents the results based on the structural models detailed in the previous section. The results have been divided into sections based on the temperature profile as well as the boundary conditions.

4.3.1. Linear temperatures gradients with fixed supports

The first case considered is of a fixed-end beam subject to a travelling triangular temperature patch load (Figure 4-2). Axial force in the beam, which must be constant along its length, is plotted against pseudo-time in Figure 4-3. As there are no time dependent phenomena in the model, the time axis is simply a proxy for the location of the temperature patch. At $t=0$ the beam is at ambient temperature immediately prior to heating, while at $t=1$ the temperature patch has traversed the entire beam with each section having been heated and then cooled.

It should be noted that as the thermal gradient is zero, no deflections or moments are produced.

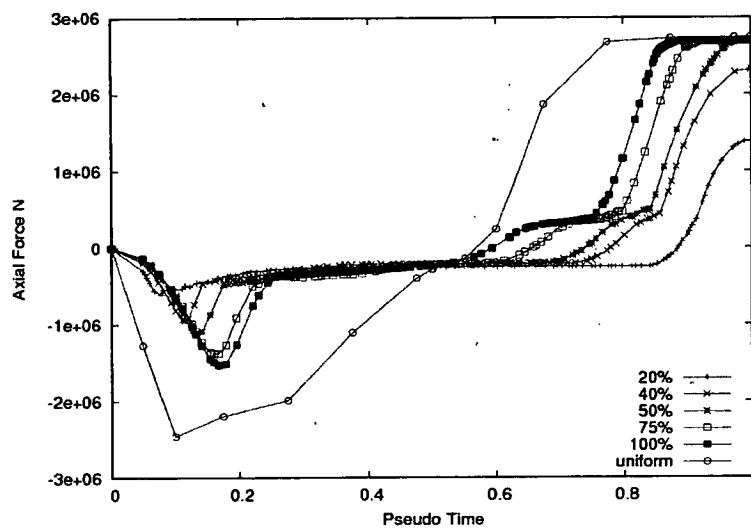


Figure 4-3 – Axial force evolution for peak temperatures of 800°C and varying patch lengths represented as a percentage of the beam length

The response of the beam can be divided into a number of distinct parts. Initially, as the temperature patch starts to heat one end of the beam, thermal expansion

results in compressive forces developing. As expected, the magnitude of these axial forces is greater for longer temperature patches as they result in a greater length of heated beam and hence a larger average thermal strain along the beam's length. After the initial sharp increase, the axial forces reduce as the material strength decreases with a continuing increase of temperature, thus resulting in a section of the beam yielding. The axial force has different peak values and this peak occurs at different times for each of the patch lengths. A shorter patch length means that the peak temperature (800°C in Figure 4-3) is reached within the beam sooner, but over a smaller area. Yielding therefore occurs sooner, but leads to a smaller peak axial force as a lesser section of the beam is heated.

The second stage of the response occurs once the cooling portion of the temperature patch is located within the length of the beam. As each section of the beam is heated, it plastifies in axial compression and so becomes permanently lengthened. Contraction of the plastified sections upon cooling produces tensile strains that largely counteract the compressive strains produced in the heated section of the beam. The final stage of the response occurs when the temperature patch traverses off the end of the beam and the full length returns to ambient temperature. At this point there is no thermal expansion to counteract the contraction of the plastified section and so large tensile forces result. This result is in line with the findings in Chapter 3 which consider the effects of cooling after uniform heating in section 3.2. Here, the larger patch length scenarios go into tension earlier than the shorter patch lengths, which is due to the fact that there is a longer duration of cooling when considering larger travelling patches. The longer the duration of the cooling, the greater the overall tensile force, until the beam yields in tension thus forming a plateau.

The effect of varying the length of the temperature patch is surprisingly small while the fire is in progress. Any increases in thermal strains caused by heating are largely offset by a corresponding increase in contraction of the cooling part of the beam. However, upon final cooling the longer patches result in significantly greater tensile forces being produced.

The response of the beam when subject to uniform heating and cooling is also shown in Figure 4-3. At all times the axial force based on a uniform fire is greater than that during the various travelling fires. The limiting case of uniform heating followed by uniform cooling shows significantly larger forces for the majority of the fire. It is only when the final cooling occurs and tensile yield is again reached that the force plateaus in an identical manner to the larger patch lengths. For patch lengths of less than 50% no tensile yielding occurs. For these cases the travelling fire is therefore less severe than a uniform fire. Figure 4-3 considers the peak temperature to be constant and the patch length to be variable. For identical structural models it is also possible to review a constant patch length with varying peak temperatures. Figure 4-4 shows the axial force for a range of peak temperature from 200 °C to 1000 °C with a constant peak patch length of 20%.

Again, the behaviour can be separated into three distinct parts. Initially the beam is subjected to heating only. The larger peak temperatures (i.e. 800 °C and 1000 °C) cause the beam to yield and thus to plastify in compression quite early on, whereas the cases with lower peak temperatures do not yield at all and maintain the peak axial force until final cooling occurs.

The second distinct part of the behaviour is identical to that seen in the previous graphs where heating and cooling counteract each other, thus resulting in a constant force until the third and final part. During final cooling, those beams

which did not yield in heating unload elastically and no residual tensile force remains. For the higher peak temperature cases, large tensile forces are induced as expected.

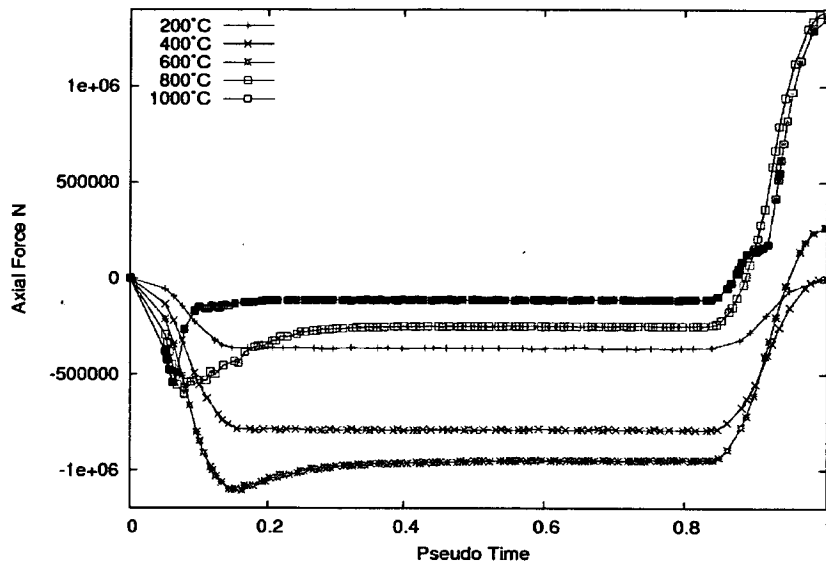


Figure 4-4 – Axial force evolution for 20% patch length and varying peak temperatures

4.3.2. Temperature gradients with fixed supports

The second form of loading is similar to that in section 4.3.1, but the temperature within the beam now includes a thermal gradient such that the lower surface reached the peak temperature while the upper surface remained at ambient temperature, rather than a uniform temperature. Most steel beams in fire would be subject to loading somewhere between these two extremes of thermal gradient.

Figure 4-5 shows the axial forces from the second load case where a temperature gradient is applied. A constant peak temperature of 800°C with varying patch

lengths, ranging from 20% to 100%, is considered. The difference in behaviour with that seen in section 4.3.1 is obvious as there are no longer three clear parts to the behaviour. Initially the beam goes into compression as heating commences. However, the upper portions of the section are not being subject to heating and thus only partial yielding occurs across the depth of the beam. This makes for more complex behaviour as a combination of yielding and loss of strength occurs in the heated sections of the beam, whilst contraction of the beam and material recovery occurs in those sections being cooled. In addition the thermal gradient also results in vertical displacements, which vary greatly along the length of the beam. These displacements cause additional plastic strains, in some parts of the beam before the heating patch has reached that particular section. The combination of all these effects is represented in the variation of axial force seen in Figure 4-5 between pseudo time of 0.1 and 0.5. The behaviour observed at this phase of the travelling fire is further amplified by vertical loading and this is discussed in more detail in Section 4.3.4.

Finally, as the heated section moves off the end of the beam the total amount of thermal expansion in the beam reduces, whilst the amount of thermal contraction remains constant. This results in a reduction of compressive force, continuing until the entire fire patch has moved off the beam and a large tensile force remains. Figure 4-5 also shows the axial force based on a uniform fire along its length compared to the patch lengths. The gradients in the uniformly heated beam are identical to those in the travelling fire scenarios, i.e. 800°C at the bottom surface and 0°C at the top, with a linear gradient. The axial forces based on a uniform fire are consistently greater than those in the travelling fires. The beam does not fully

yield in tension (or compression), due to the temperature gradient, which ensures the top part of the beam remains relatively cold.

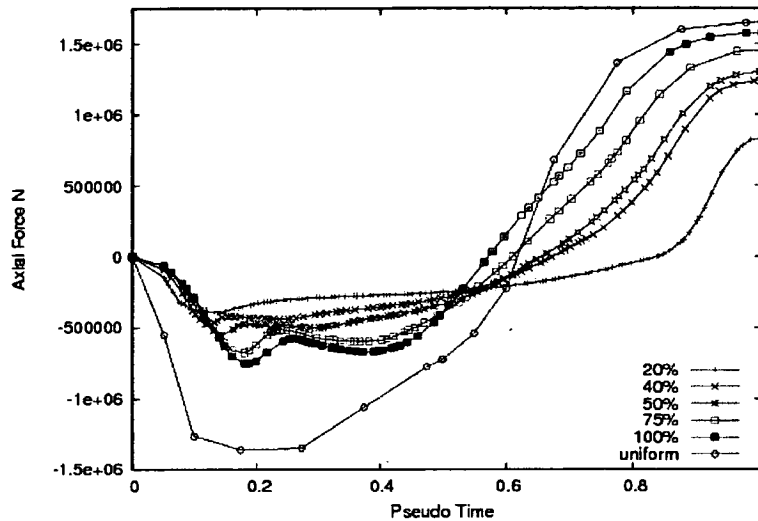


Figure 4-5 – Axial force evolution for peak temperatures of 800°C with gradients and varying patch lengths and uniform fire

Figure 4-6 shows the axial force evolution for a constant patch length of 50% with varying peak temperatures. Again, the beam subjected to a peak temperature of 200°C does not yield in tension or compression. As the peak temperature increases the section of the beam that yields also increases and thus the peak of the axial force in compression reduces whilst the peak axial tensile force increases.

The temperature gradients through the depth of the beam result in different rates of thermal expansion through the cross-section. This leads to associated displacements and bending moments. Figure 4-7 shows the bending moments at mid-span for beams subjected to a travelling fire with patch length 50% and varying peak temperatures, whilst Figure 4-8 shows displacement at mid-span for the 50% and 1000°C case plotted at various points along the beam. These points

are given as values between 0 and 1, where 0 represents the left hand support of the beam and 1 the right hand support.

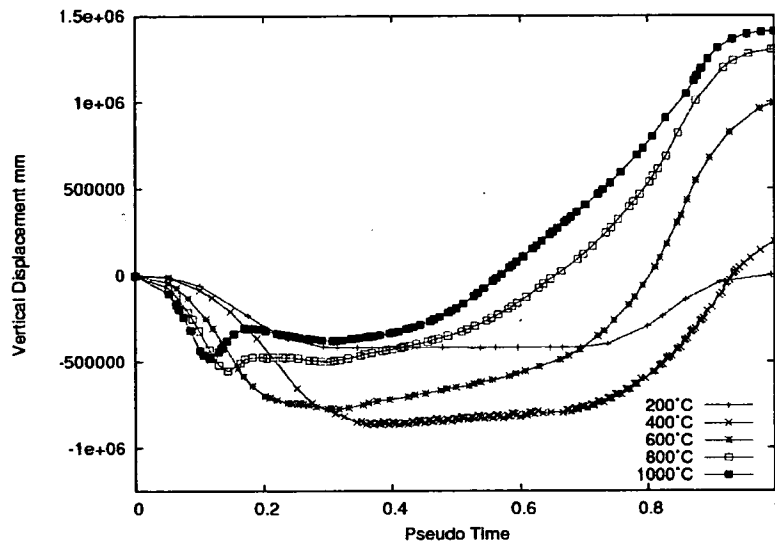


Figure 4-6 – Axial force evolution for 50% patch length and varying peak temperatures

When the heating part of the patch initially moves onto the beam, a positive moment is induced in this heated section. This is due to the lower parts of the cross section being heated whilst the top parts remain cold, thus inducing a positive bending moment as well as a downward displacement. Because of continuity this results in upward displacements along the rest of the beam, shown in Figure 4-8. At mid-span this upward displacement causes initial negative moments for each of the peak temperature cases considered (Figure 4-7). Consistently, the section which is being heated displaces downward. Subsequently, to maintain continuity, this downward displacement in the heated section of the beam results in negative moments adjacent to this heated section, which is accompanied by upward displacements shown in Figure 4-8.

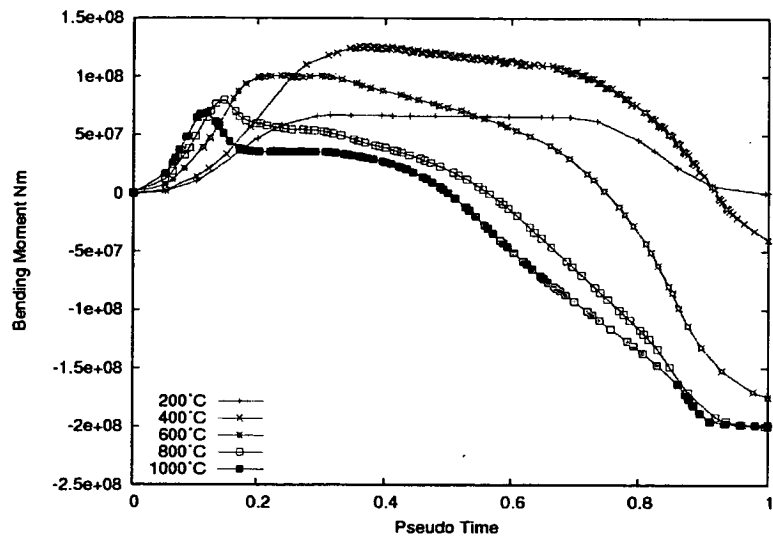


Figure 4-7 – Bending moments at mid-span for 50% patch length and varying peak temperatures

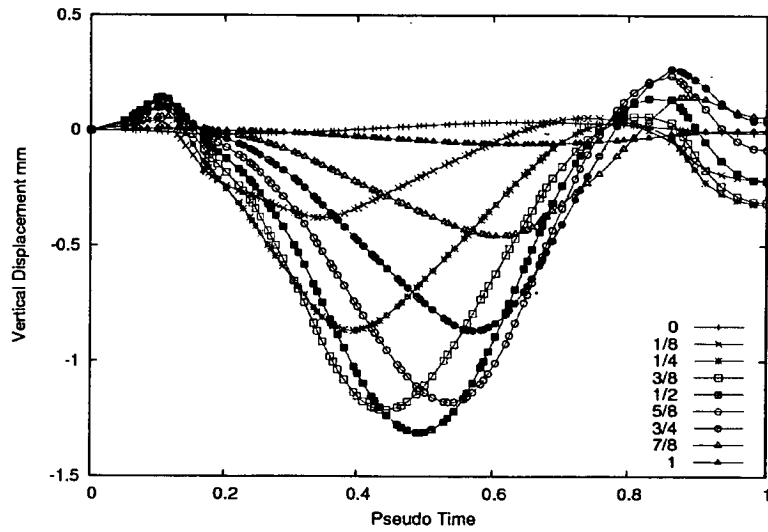


Figure 4-8 – Mid span displacement for 50% patch length and 1000°C peak temperature at various points along the beam length

As the temperature patch moves along the beam and local yielding occurs, the upward displacement reduces until it becomes a downward displacement along the entire beam length. The peak downward vertical deflection is reached as the peak temperature is at mid-span. Figure 4-9 gives a representation of the deflected shape of the beam at three different points in the travelling fire scenario. Figure 4-9 (a) shows the deflected shape when only the heating part of the fire patch is located on the beam, Figure 4-9 (b) shows the fire patch at midpoint and Figure 4-9 (c) shows only the cooling part of the fire patch remaining on the beam. From these figures it is clear that the displaced shape of the beam is highly dependent on the location of the fire and changes substantially during the various phases of the travelling temperature patch.

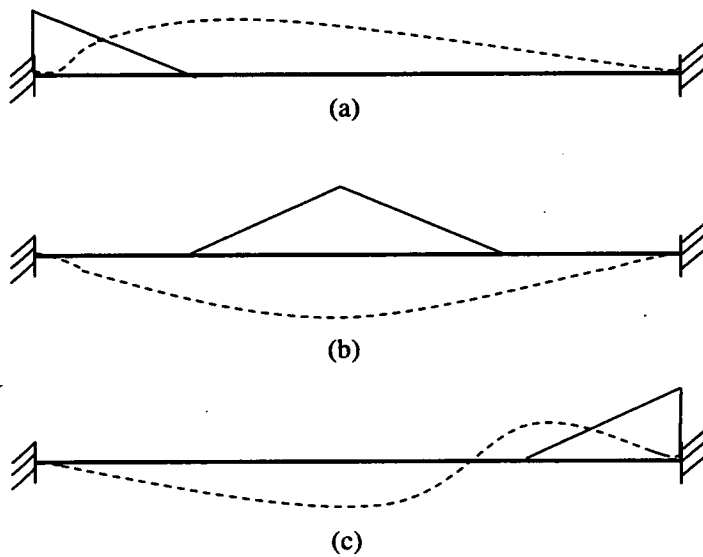


Figure 4-9 – Representation of the beam deflection for different fire patch positions

This is quite different from uniform heating and cooling along the length of the beam, where no such variation occurs and the displaced shape looks similar to Figure 4-9 (b) at all times. For this particular scenario the overall displacements for a uniform fire are also significantly smaller and close to zero. The deflection pattern shown in Figure 4-8 only covers the 50% and 1000°C case in detail. Figure 4-10 shows the mid-span deflection for a 50% patch length at various peak temperatures. The overall pattern is similar for each case; some initial upward movement occurs before a peak vertical displacement is reached when the peak temperature reaches mid-span. This is followed by another small upward displacement when only the cooling phase remains on the beam. The higher peak temperatures result in larger downward displacements.

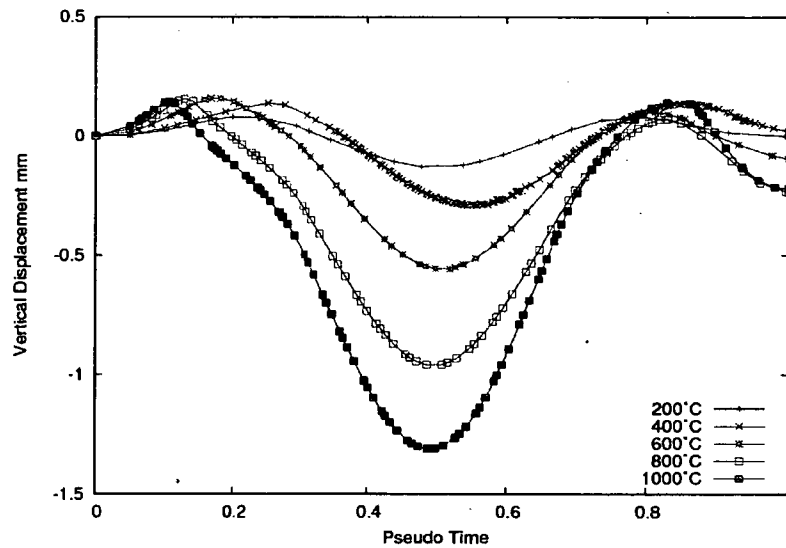


Figure 4-10 – Mid span displacement for 50% patch length and varying peak temperatures

4.3.3. Temperature gradients with pinned supports

Thus far only fully fixed supports have been considered. Support conditions in real structures will be somewhere between the two extremes of fully fixed and pinned. To explore the range of boundary conditions, both conditions require exploration. The results presented in this section are for pinned connections. The temperatures are applied as a gradient as in section 4.3.2 and the beam dimensions remain identical to the previous models. Figure 4-11 shows the axial forces for a constant peak temperature of 800°C and varying patch lengths.

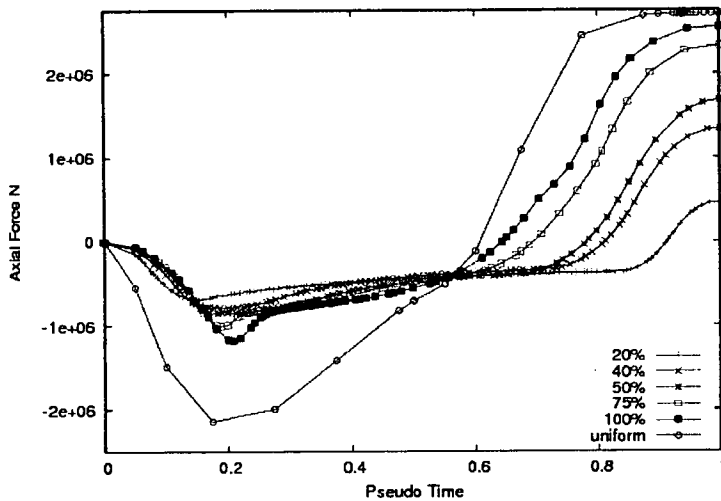


Figure 4-11 – Axial force evolution for 800°C temperature and varying patch length. Uniform fire case included

The pattern is identical to that seen for the fixed beam case, although the peak forces in both compression and tension are higher for the pinned boundary conditions. This is due to the interaction of axial force and bending moments which result in axial yielding. Axial yielding occurs later in the pinned scenario

than in the fixed beam case as the bending moments are substantially lower. This is due to the lack of rotational supports, thus allowing the axial force to continue to increase for longer until yielding occurs.

Again, the uniform fire case shows that the axial forces expected for the duration of the fire, are higher than those as a result of a travelling fire. The uniformly heated beam yields in tension at the end of the cooling phase, whereas none of the travelling fire scenarios reach tensile yield. Although the axial force evolution is very similar to the previous models, the bending moments and deflection pattern are quite different. Figure 4-12 shows the bending moments at mid-span for the duration of the fire. As the beam is not restrained from rotation, the initial heating causes a negative moment along the entire length of the beam.

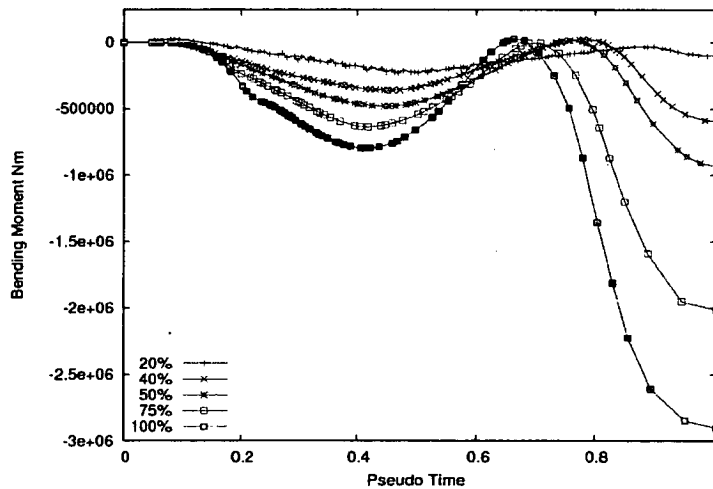


Figure 4-12 – Bending moments at mid-span for 800°C temperature and varying patch length

As the fire patch moves further along the length, this negative moment increases until the peak temperature has reached the mid-span, thus inducing a peak negative moment. As the patch moves away from mid-span, the effect of the locally induced moment becomes smaller and the negative moment reduces again. This reduction in negative moment continues until only the cooling section of the patch remains on the beam. The part of the beam which is cooling is subjected to a positive moment. As this is now the only effect on the beam, the local positive moment induces a negative moment along the cool part of the beam to maintain continuity. For the larger patch lengths this results in a greater residual moment as the duration of cooling is more significant. By plotting the deflection at mid-span in Figure 4-13 the behaviour described above can be reinforced. Initially there is a downward deflection as a result of the beam being heated locally.

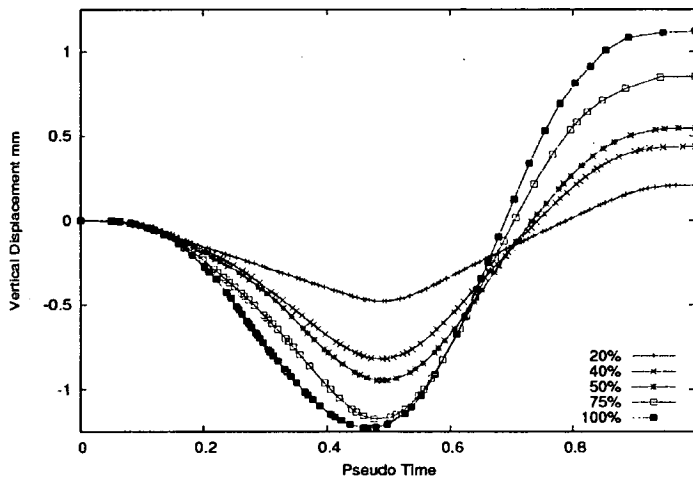


Figure 4-13 – Mid-span deflection for varying patch lengths and a peak temperature of 800°C

The deflections increase until the peak temperature occurs at mid-span. A decrease in deflections follows as the patch moves away from mid-span. Just as the initial

heating caused the remainder of the beam to deflect downwards, the final cooling causes an upward displacement which increases along the length of the beam and peaks at around $\frac{1}{4}$ length. This is clearly seen from Figure 4-14 where the vertical displacements are plotted at various points along its length, for one scenario; 50% patch length and 800°C peak temperature.

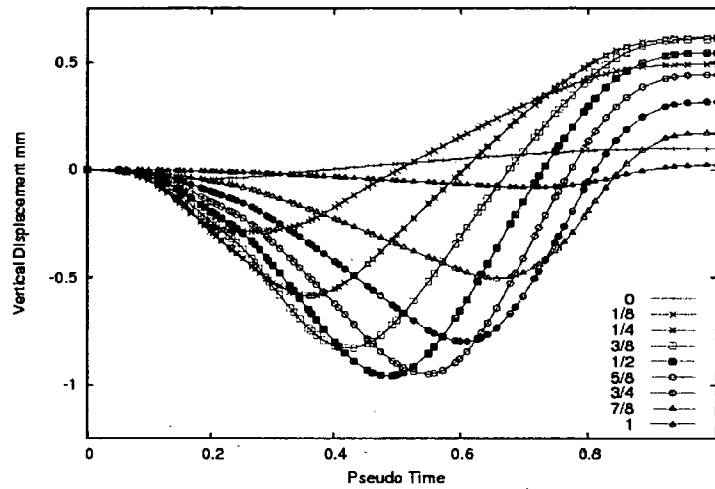


Figure 4-14 – Deflection at mid-span for 50% patch length and 800°C peak temperatures, plotted at various points along its length

4.3.4. Loading

The effect gravity loading has on the behaviour during travelling fires is investigated in this section. The loading is applied uniformly across the length of the beam and remains in place for the duration of the fire. The amount of loading is determined as a percentage of the ultimate load at ambient temperature. The applied load is 20% of the ultimate bending moment capacity and also includes the self-weight of the beam.

The loading is applied linearly over a pseudo time of 0.1, which is added to the pseudo time of the fire. The following graphs therefore show a time of 1.1, where the first 0.1 is the load phase and the remaining time represents the travelling fire.

Simplified material behaviour

The behaviour observed is a combination of the applied load, the changing temperature profile across the beam length as well as material degradation. To understand how each of these aspects impact the behaviour, Figure 4-16 to Figure 4-19 show the results for a loaded beam with a travelling fire but without temperature dependent material properties. These simplified material properties are shown in Figure 4-15. All analyses incorporate non-linear geometric behaviour, which is critical in fire modelling.

Figure 4-16 shows the axial force, which is constant along the length of the beam. The applied loading results in a small initial tensile force. As the heating patch starts to move across the beam, thermal expansion induces a compressive force. Although the section of beam heating remains constant after about 0.25 pseudo time for the 100% patch length, the compressive force continues to increase. The sections of the beam which are heated will partially yield and once cooling begins full recovery is no longer possible. This therefore results in a continually increasing compressive force. It is not until the heating part of the fire begins to move off the beam that these compressive forces begin to reduce significantly. This eventually leads to large tensile forces which remain in the beam after the fire.

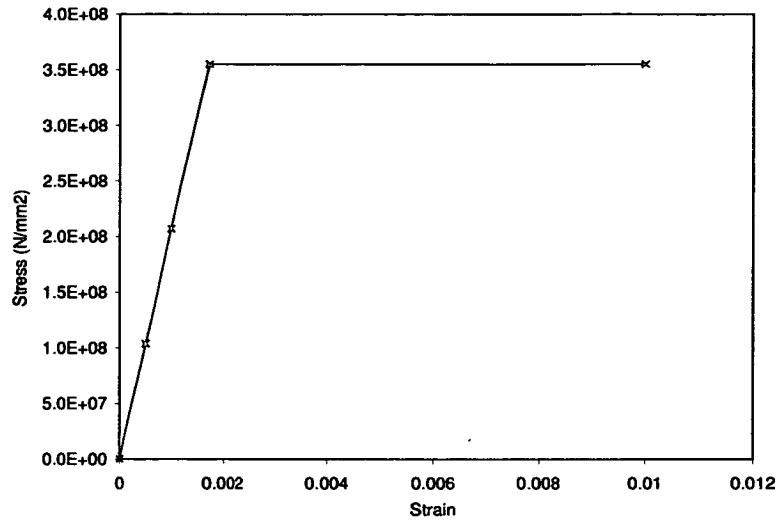


Figure 4-15 – Assumed simplified stress-strain relationship

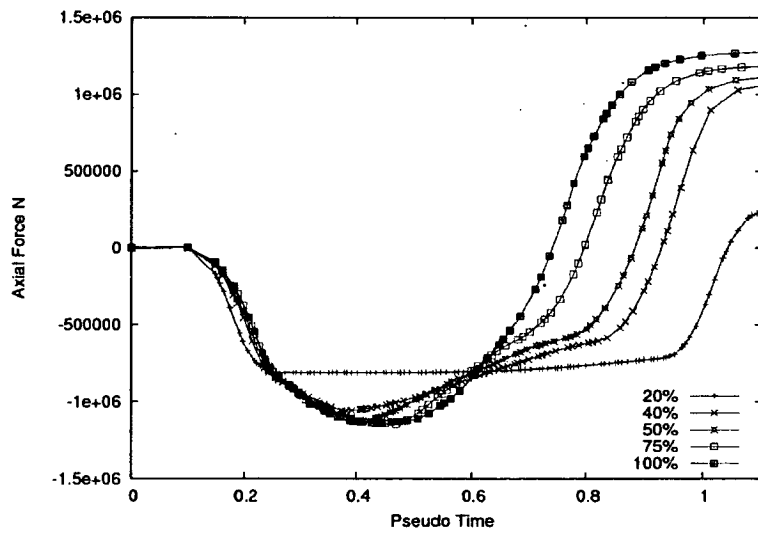


Figure 4-16 – Axial force evolution for 1000°C temperature and varying patch length

Figure 4-17 shows the vertical displacements at mid-span. A downward displacement results from the application of load. As the beam begins to heat at the far left of the beam, a local increase in displacement occurs. Subsequently, this causes a small decrease of displacement at mid-span as the beam maintains continuity. This is represented in Figure 4-18 where the displaced shapes for different stages in the fire are shown. Figure 4-18 (a) shows the displaced shape when subjected to loading only, whilst (b) and (c) show the shape at the start and end of the travelling fire respectively.

As the fire continues to move along the length of the beam the vertical displacements at mid-span continues to increase. When the fire patch moves away from mid-span the vertical displacement reduces until only the cooling part of the fire patch remains on the beam. This induces a further increase in vertical displacement at mid-span.

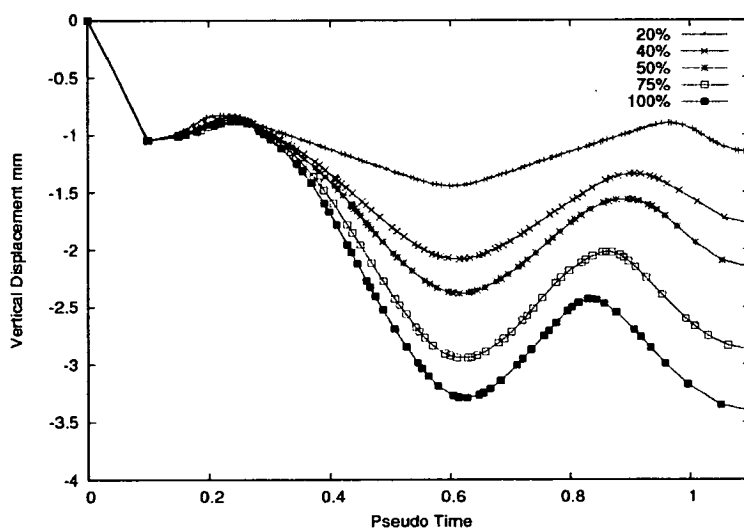


Figure 4-17 – Vertical displacements for 1000°C peak temperature and varying patch length

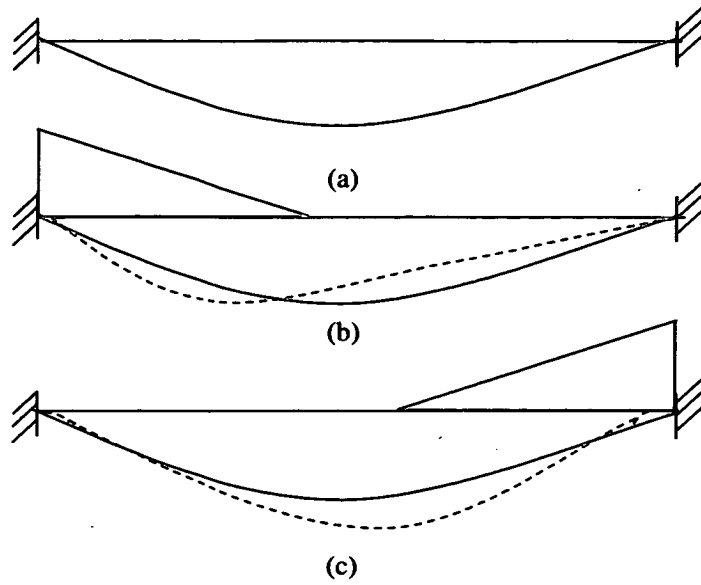


Figure 4-18 – Representation of the beam deflection for different fire patch positions

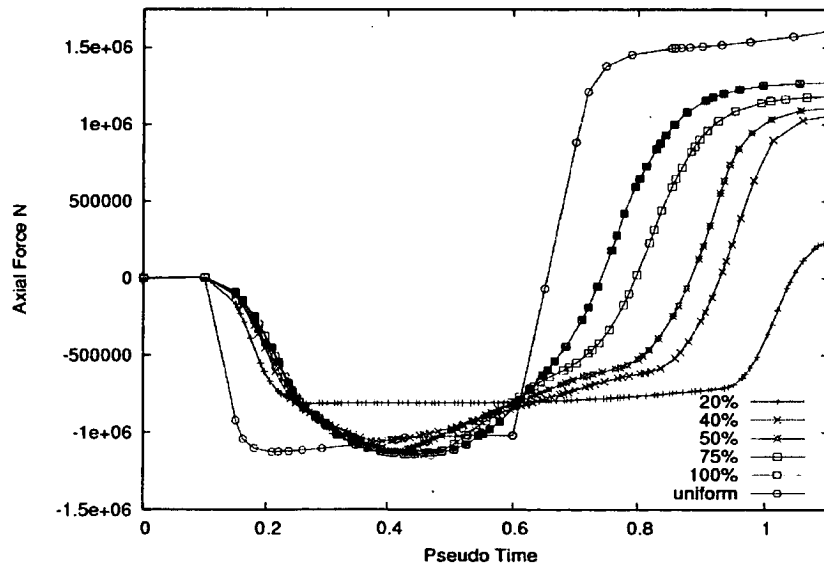


Figure 4-19 – Axial force evolution for 1000°C temperature and varying patch length compared with uniform heating and cooling

In Figure 4-19 the axial forces for 1000°C peak temperatures are plotted for varying patch lengths as well as a uniform fire. The peak forces in compression for a uniform fire are generally a little less than those for travelling fires, whereas the peak tensile forces are substantially larger.

Temperature dependent material behaviour

The behaviour observed in Figure 4-16 to Figure 4-19 is a result of load and increased temperatures. However, the material properties for this scenario are simplified and are not temperature dependent. The results shown here are for identical models with respect to the structure and temperature, but the material properties are now temperature dependent. The stress strain relationship which varies with temperature is shown in Figure 4-20.

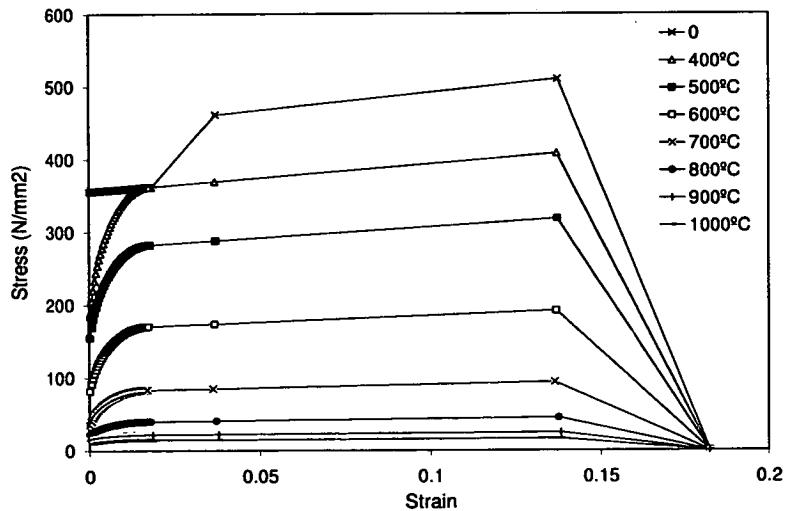


Figure 4-20 – Temperature dependent plastic stress-strain relationship

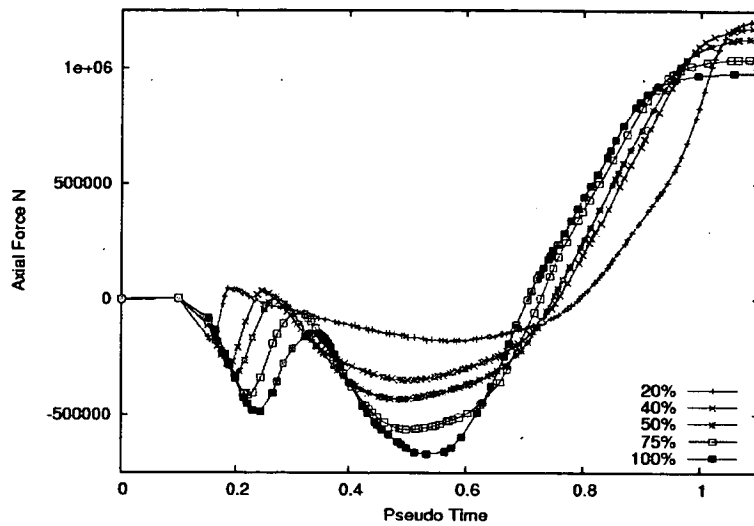


Figure 4-21 –Axial force evolution for 1000°C temperature and varying patch length

Figure 4-21 shows the axial force for a peak temperature of 1000°C and various patch lengths. The applied loading again results in a small initial tensile force. When heating commences a compressive force is induced as a result of the thermal expansion of the heated part of the beam. The larger patch lengths affect a greater section of the beam, thus causing larger compressive forces. Following this initial compression, a sudden reduction in force occurs followed by another increase. Similar behaviour was seen in Section 4.3.2, where the model was identical apart from the applied loading.

To analyse this behaviour in more detail, one of the scenarios is isolated. Figure 4-22 shows the axial force for the 1000°C temperature and 100% patch length case. Only part of the total time is shown to illustrate the different phases in behaviour more clearly.

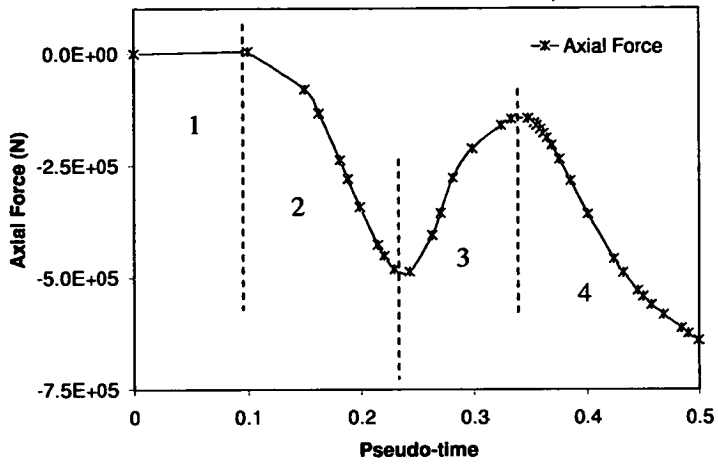


Figure 4-22 – Axial force plotted for part of the analysis duration with the four distinct phases indicated

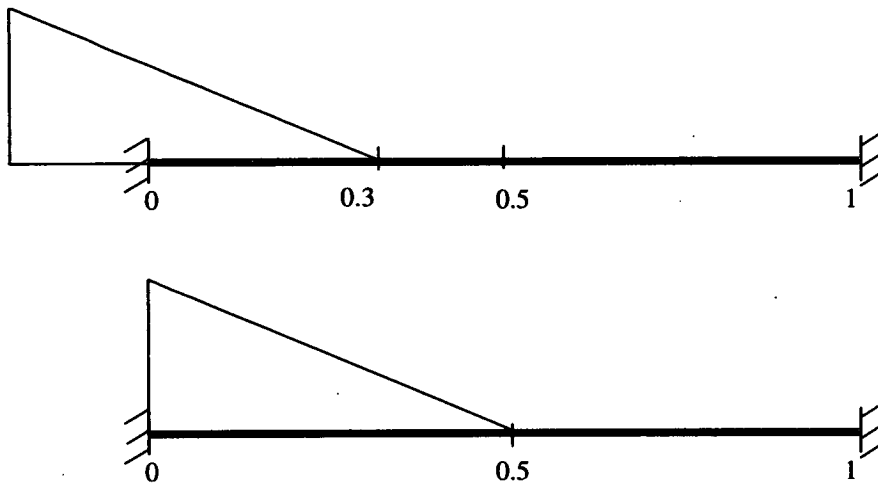


Figure 4-23 – Representation of the beam with locations of fire at 0.25 and 0.35 (total time) corresponding to the start of phase 3 and 4, respectively

Figure 4-23 shows the location of the fire patch on the beam for the phases which occur during heating as indicated in Figure 4-22. Phase 1 represents the application of loading. This causes a small tensile force in the beam. Phase 2 shows an increasing compressive force as a result of initial heating on the beam causing thermal expansion. The behaviour observed during phase 3 and 4 is less obvious and will be explained in the following section.

Vertical displacements are induced as a result of loading and subsequent heating. These displacements induce strains and bending moments along the length of the beam, not just in the locations which are being heated. Figure 4-24 shows the total strains along the length of the beam at the end of the load step and after 0.1 of the heating phase (i.e. total time of 0.2). At the end of the load step the strain distribution is as expected from basic principles as the peak values occur at mid-span and the supports. At 0.1 of the heating step, the total strains in the heated part of the beam are substantially larger.

As the fire progresses along the length, the heated sections expand and go into compression with some parts yielding. However, these parts may already have substantial strains, which means the total compressive force induced is lower. This causes the reduction in axial force seen around pseudo time 0.2 in Figure 4-21.

The elastic, plastic, thermal and total strains are plotted at the bottom surface at mid-span and shown in Figure 4-25. The heating patch reaches mid-span at 0.35 total time. At this point the thermal strains increase rapidly, as do the total strains. Up to that point, the plastic and thermal strains are zero at mid-span. However, the total strain up to that point is not zero as elastic strains are induced by the displaced shape and associated bending moments.

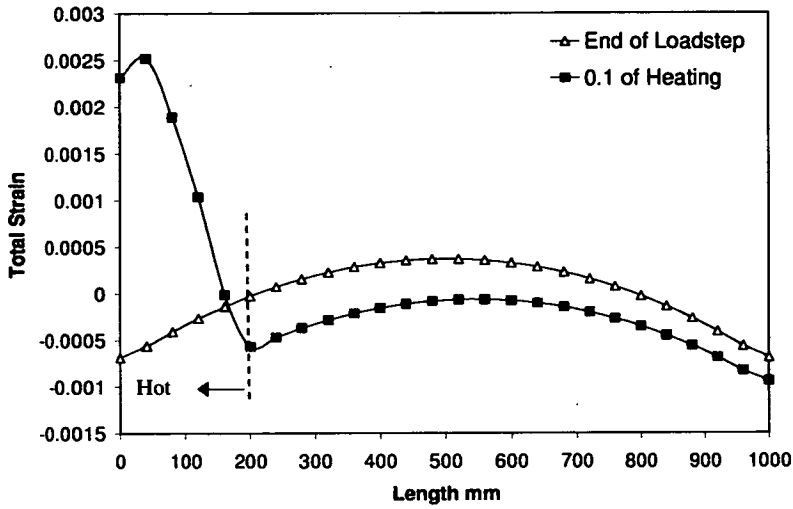


Figure 4-24 – Total strains plotted along the length of the beam for load step and partial heating (1000°C peak temperature and 100% patch length)

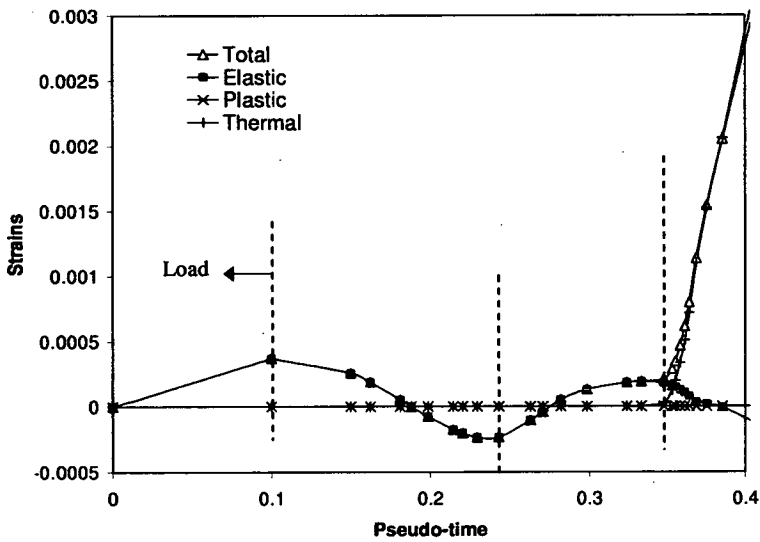


Figure 4-25 – Strain evolution at the bottom surface at mid span of the beam plotted for part of the analysis (1000°C peak temperature and 100% patch length)

The bending moments at different points along the length of the beam are shown in Figure 4-26. At the end of the load step, a positive moment is present nearer the support, whereas this moment becomes increasingly negative toward mid-span. As the temperature patch moves onto the beam the bending moment increases at all locations as the deformed shape changes with the localised thermal expansion as shown previously in Figure 4-18. The mid-span displacement for this scenario is shown in Figure 4-27.

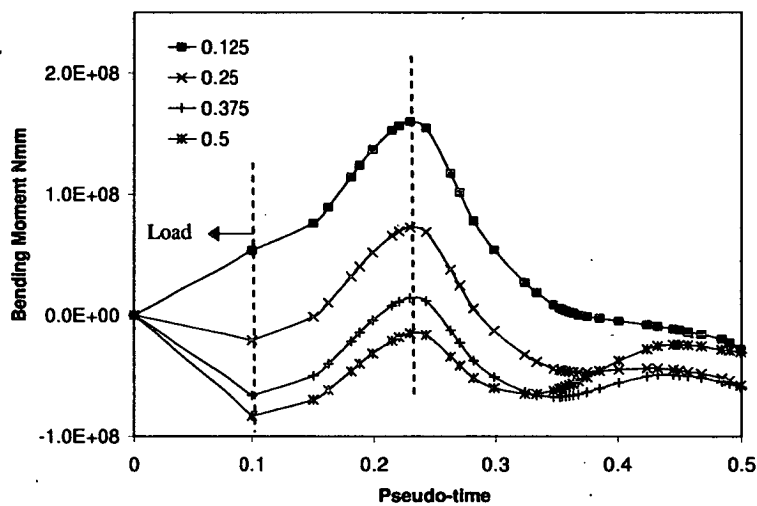


Figure 4-26 – Bending moment evolution for several locations in the first half of the beam plotted for part of the analysis. The location given in the beam means for example that 0.25 at a quarter of the length and 0.5 at mid-span (1000°C peak temperature and 100% patch length)

When the fire patch initially reaches the section, there is an additional positive moment induced by the thermal gradient. This additional positive moment also results in a small increase in vertical displacement. However, as the heating is only

affecting a small area of beam near the support, at mid-span this subsequently causes a small decrease of the negative moment and a decrease in vertical displacement due to beam continuity. As the patch moves further along the beam and the section affected by increased temperatures gets closer to mid-span the overall displaced shape results in further downward mid-span displacements, again represented by Figure 4-18.

It has been shown that displacements and bending moments in the beam exist even in locations where no heating has yet occurred. These then result in substantial elastic strains, again in yet unheated parts of the beam as well as significant bending moments. The capacity of a section is affected by the combination of axial force and bending moment as is shown schematically in Figure 4-28.

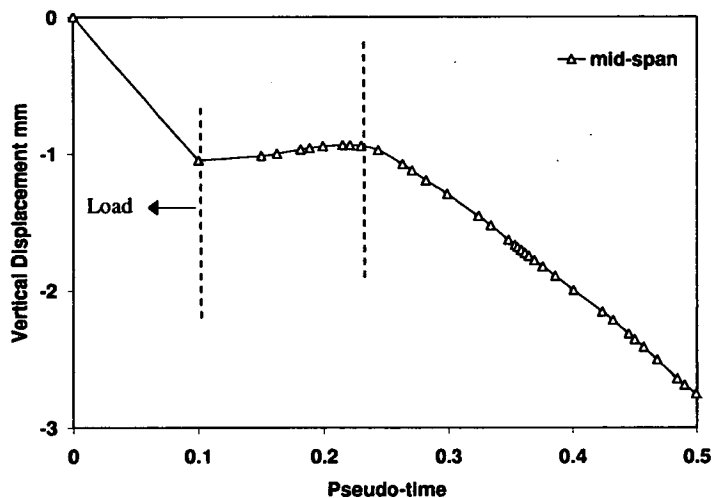


Figure 4-27 – Vertical Displacements at mid-span plotted for part of the analysis
(1000°C peak temperature and 100% patch length)

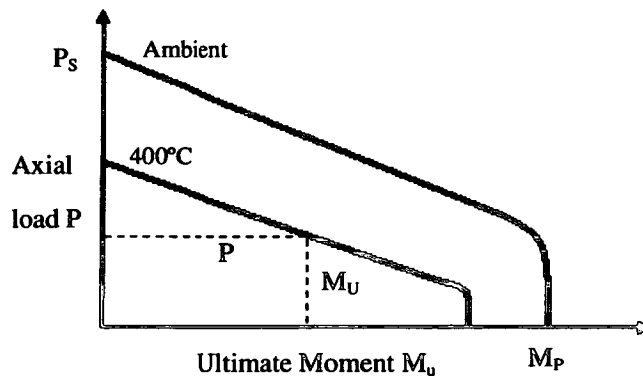


Figure 4-28 – Capacity of an I-section – relationship between axial force P and bending moment M , dependent on temperature

So when bending moments are present in the beam, the axial force required for yielding becomes less. The capacity also decreases significantly with an increase in temperature, which is indicated in Figure 4-28. Therefore, when those parts are eventually affected by an increase in temperature the section will reach plastic yield at a lower axial force and at a lower strain rate. Figure 4-29 shows the plastic strain evolution at several points along the beam. The plastic strain at which full yielding occurs (represented by constant plastic strain in the figure) reduces as the location moves toward mid-span. Beyond mid-span the strain at which full yield occurs increases again. When both the heating and cooling part of the fire patch are on the beam, thermal expansion and contraction occur simultaneously. In the case of uniform temperatures across the section, these cancelled out and the total axial force in the beam remained fairly constant. However, as explained, the thermal gradients across the section cause displacements, bending moments and strains, which vary significantly with time and location. Partial yielding occurs

during the heating phase resulting in permanent displacements; therefore making full recovery upon cooling impossible.

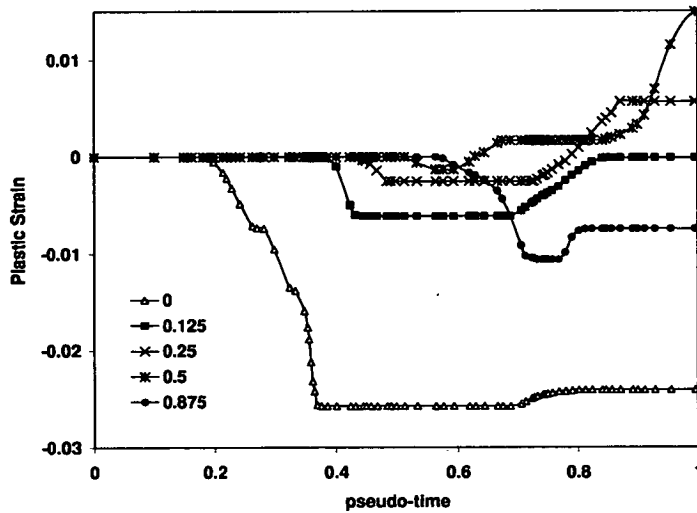


Figure 4-29 – Plastic strain evolution at the bottom surface at different locations along the beam (1000°C peak temperature and 100% patch length)

As the heating patch moves beyond mid-span (correlating to 0.35 total time and Phase 4 in the graphs) the pre-existing vertical displacements and thus bending moments and strains are less substantial. As the fire reaches this part of the beam, yielding again occurs at increasing strain rates. This allows the thermal expansion to materialise more thus resulting in another increase in compression. Once the heating part of the fire moves off the beam, a larger overall amount of thermal contraction occurs and the total axial force reduces and becomes tensile. The axial force in a beam subjected to a travelling fire is compared to the force based on uniform heating and cooling in Figure 4-30. A uniform fire results in larger axial forces during both heating and cooling.

This suggests that a uniform fire is a worse case scenario when doing performance based design, especially when considering the tensile forces in cooling. However, axial force is not the only output which should be taken into account to make an accurate assessment of the real structural behaviour.

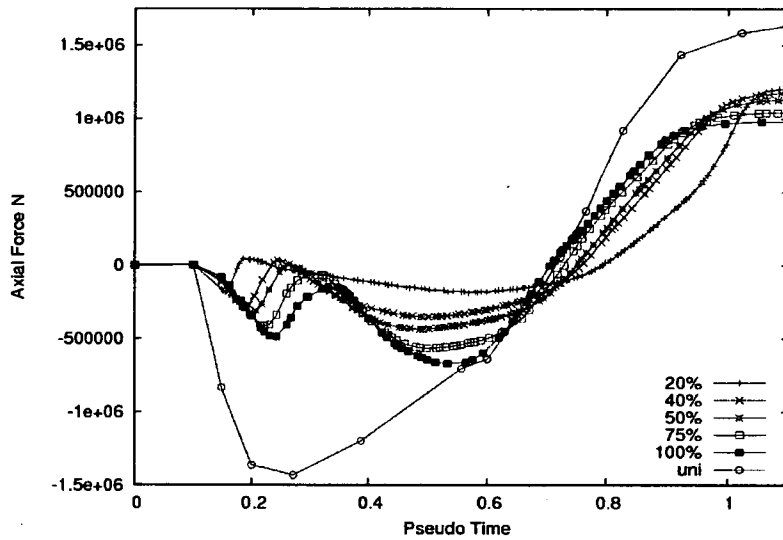


Figure 4-30 – Axial force evolution for 1000°C peak temperature and varying patch lengths compared with uniform heating and cooling

Figure 4-31 shows the bending moments at mid-span for a range of patch lengths and constant peak temperature of 1000°C. This illustrates the changing direction of the moments in the first part of the travelling fire as well as the large residual moments which remain as the fire has ended. It should be noted that although the bending moments during heating are higher for a uniform fire, the residual moments for all patch lengths are larger than when the fire is subjected to a uniform fire.

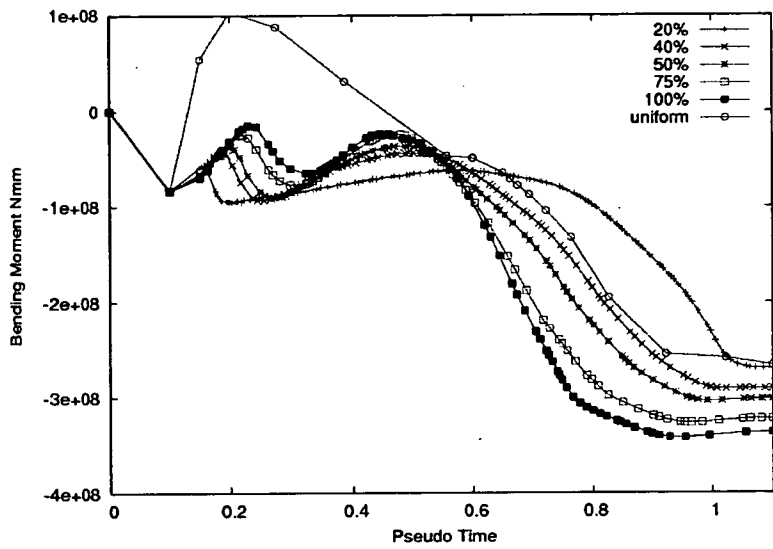


Figure 4-31 – Bending moments for 1000°C peak temperature and varying patch length, including for a uniform fire

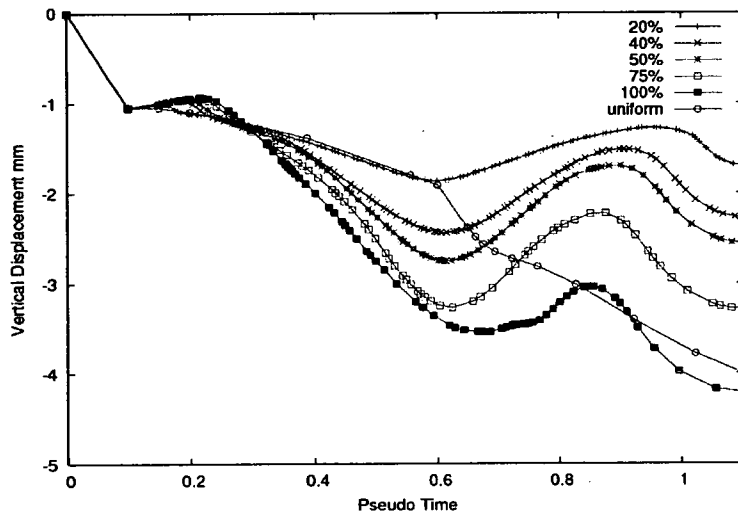


Figure 4-32 – Vertical displacements for 1000°C peak temperature and varying patch length, including for a uniform fire

Figure 4-32 shows the vertical displacements at mid-span for a range of patch lengths and constant peak temperature of 1000°C as well as the uniform fire case. The uniform fire displacements during heating are generally lower than the travelling fire scenarios. In cooling however, the uniform fire displacements are higher than all but the 100% patch length. The uniform fire is therefore not the worst case scenario when considering displacements only. Figure 4-31 and Figure 4-32 clearly illustrate that the assumption of uniform fires is not always conservative, especially when considering post-fire use of a structure.

4.4. Conclusions

The effects of travelling and localized fires on the behaviour of structures have until recently been ignored. Recent experimental and theoretical work has shown that assuming uniform temperatures in structural elements is not realistic, even for small compartments. Results in this chapter indicate that the development of forces produced by travelling fires may be significantly different to those produced by uniform fires. In particular beams will likely be subject to both tensile and compressive forces within the duration of a realistic compartment fire. Thermal expansion and possibly compressive yielding would occur in some areas, while other areas would be contracting and possibly yielding in tension. The effects of temperature gradients within the depth of a beam subject to a travelling fire may be significant and lead to tensile forces early in the fire development. The axial forces in the uniformly heated beams are consistently greater than in any travelling fire scenario. However, this is not the case for the displacements and bending

moments where uniform fires are shown to be less conservative in some cases. Large residual bending moments are observed for the entire range of patch lengths and displacements were seen to vary greatly with time, often displaying cyclic movements.

The structural effects of localised travelling fires are clearly complex and it should therefore not be assumed that travelling fires are always less severe for a structure than uniform fires. Any performance-based design should take account of this.

5.1. Introduction

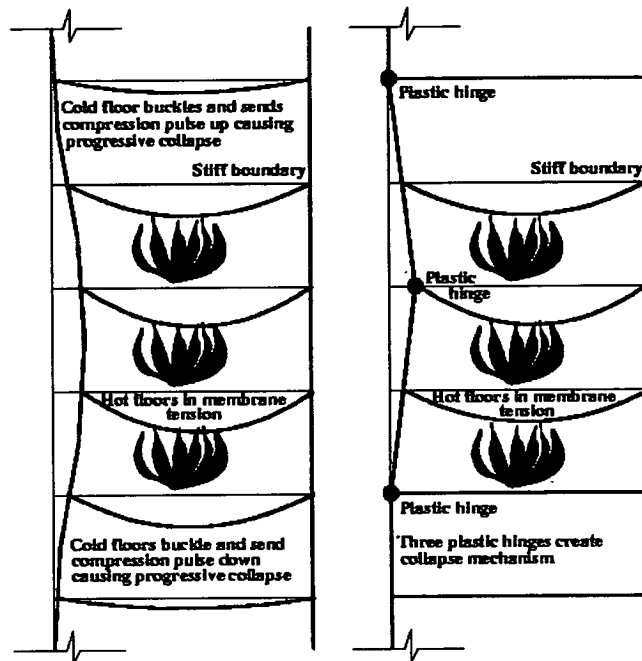
This chapter introduces and discusses a study of the behaviour of tall buildings in fire. It considers a generic composite multi-storey structure when subjected to simultaneous multiple floor fires, both in heating and cooling. The first part of the chapter gives a brief overview of previous work done on global collapse scenarios of the same structure during the heating phase of a fire. In these models progressive failure of the structure was observed during heating for some scenarios, but for the purpose of investigating cooling behaviour some adaptations to the structural models were made to ensure failure prior to cooling did not occur. Often the cooling branch of a fire is modelled to be linear with time, the duration of which may be varied. To investigate the importance of the duration of the cooling branch and to establish the overall structural response during this phase of a fire, a variety of cooling scenarios are investigated and compared. Finally the model of the Cardington Test 1, introduced in Chapter 3, is also subjected to a similar range of cooling phases. As this is a 3D model it may capture behaviour not observed in the 2D frame.

5.1.1. Background

The extreme events of September 11, 2001 led to the first full collapse of very large multi-storey composite structures. Both World Trade Centre towers 1 and 2 as well as WTC 7 collapsed as a result of these events. With an aim to understand these complex structural responses and to establish the precise collapse mechanisms, analyses on WTC tower like structures were carried out at the

University of Edinburgh in collaboration with Arup. This research led to several collapse theories specific the WTC buildings 1 and 2 [43, 44]. The two suggested collapse mechanisms for the WTC towers which results from this research are shown in Figure 5-1 and consist of a buckling mechanism and plastic hinge mechanism. The mechanism which occurs was found to depend on the relative stiffness of the floors and columns. Figure 5-1 (a) shows the collapse mechanism predicted when a strong column was supported by a relatively weak (in membrane compression) floor system [67]. In such a case the collapse mechanism consisted of Euler buckling of the column as its effective length was increased by the floors failing and no longer providing lateral restraint. Floors above and below the fire floors are not able to resist the increased forces distributed to them due to the failure of the fire floors and so also fail. This leads to a progressive collapse of the structure. If however the floors were stiff enough, a conventional plastic hinge mechanism seems to establish as a result of the moments imposed upon the column by the floors in tension and $P-\delta$ moments, shown in Figure 5-1 (b) [67]. No buckling of the non-fire floors would occur as the floors are strong enough to resist the increased force. The predictions of these mechanisms were based on analyses which assumed no local failures occurred, such as connection failure, local cracking of concrete or failure of shear connectors. Flint also showed that the behaviour observed in complex 3D models could accurately be captured by simplified 2D representations of the structure [43]. It was shown that identical collapse mechanisms also occur in these simplified, 2-d models when they are made up of universal beam and column sections rather than long span truss systems as in the WTC design [67]. This simplification of the models led to an

opportunity to investigate a large number of parameters influencing the collapse mechanisms [51].



(a) Weak floor collapse mechanism (b) Strong floor collapse mechanism

Figure 5-1 Suggested Collapse mechanisms for WTC towers structure in fire [68]

To date, almost all studies of multi-storey fires have considered the heating phase of a fire which was applied to all affected floors simultaneously and uniformly [43, 67-69]. These studies initially also only considered the heating phase of the fire as early collapse was the primary research interest. However, not all the structural models considered in these studies collapsed during the heating phase of the fire which was assumed to finish after two hours having reached its peak temperature. In reality the gas temperatures would return to ambient and the

structure would cool down. In this chapter the behaviour during this cooling phase is analysed. Temperatures during heating and cooling vary across the compartment with time but this variation is not considered in this chapter and uniform temperatures are assumed on each floor. Non-uniform temperatures across compartments are considered in Chapters 4 and 7.

It has already been shown (in Chapter 3) that cooling can result in large forces in structures as they cool from an inelastic state. These forces may result in connection failure which could subsequently result in a progressive collapse. However, connection failure is not explicitly modelled in the structural models presented here and thus this behaviour can not be captured fully. The focus therefore is on global behaviour.

5.2. The Structure

The analyses presented in this chapter are designed to represent the behaviour of the generic multi-storey structure shown in Figure 5-2. A plan view is shown on the left of Figure 5-2. This representative structure consists of a concrete core (considered rigid) supporting a steel-concrete composite floor system, the form of which is also indicated in Figure 5-2. The beams are laterally restrained at their internal ends by a stiff concrete core but are free to rotate. They are fully fixed to the columns, which are in turn fixed at the base but restrained only horizontally at the top. This is not an uncommon form of design for high rise construction; the WTC 1 and 2 towers were built according to this general layout, with trusses instead of I-beams spanning from the core to the perimeter. High rise structures will typically have a core which contains the building facilities such as lifts and

escape stairs. The remaining structure will then extend from this core, which does not necessarily have to be in the centre of the structural layout. In this case the columns are assumed to be placed on a 10m by 6m grid, with an inter-storey height of 4m as indicated in Figure 5-2.

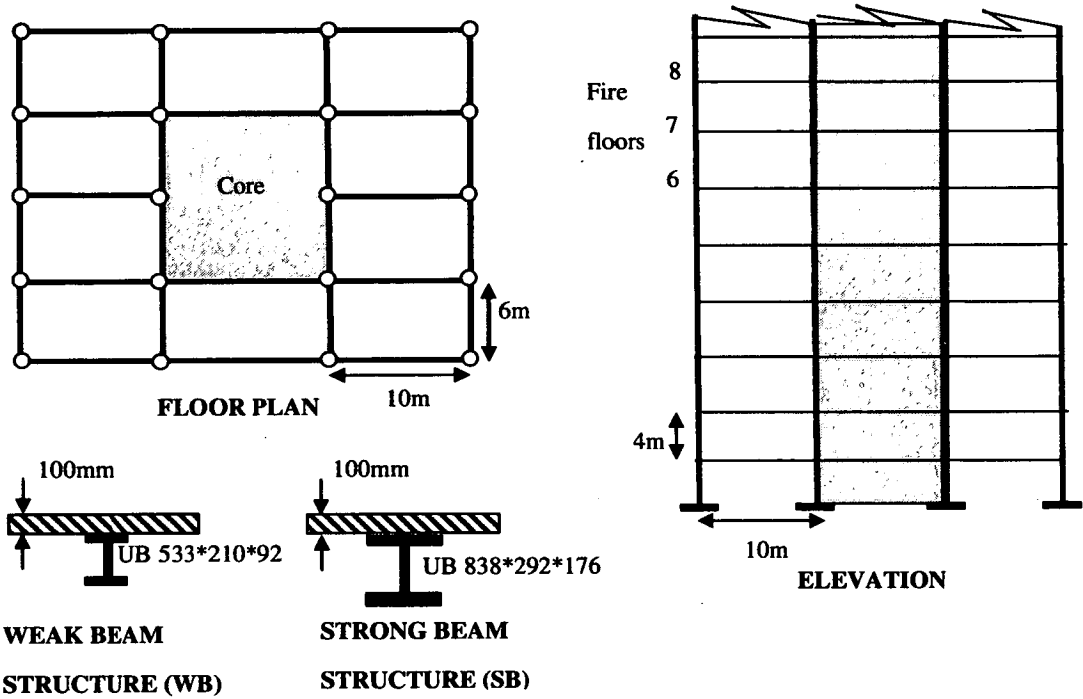


Figure 5-2 – Plan view and 2D representation of the structure considered. The three fire floors (Section 5.4) are indicated as are the differences between weak and strong beam versions of the structure

5.2.1. Structural variables

For the previous study of collapse scenarios during the heating phase, several variables were investigated to explore their effects on the behaviour [70]. These

included, amongst others; beam length, slab width, beam and column sizes and loads. The relative size of the steel beam in relation to the column was found to be the most critical variable, having significant effects on the mechanism of collapse [67, 68]. All other variables had some affect on the structure, but these either prevented collapse happening or only changed the time at which collapse occurred. Therefore, for the purpose of modelling cooling as part of the fire cycle and its effect on the structural model, only the effect of the size of the steel beam was investigated and the remaining variables were kept constant. Two realistic design scenarios were chosen, which are identified as Strong Beam (SB) and Weak Beam (WB) structures, where the relative axial capacity of the strong beam is almost twice that of the weak beam. The section sizes of the SB and WB beams are UB 838x292x176 and UB 533x210x92 respectively. The floor slabs are taken to have a thickness of 100mm in all of the analyses. The design of the beams was checked according to the British Standard BS5950 [71] and the details are shown in Appendix C. The columns size is UC 356x406x467, which is of a significant size to ensure no collapse would occur during the heating phase of the fire.

5.3. Structural Modelling

Structural modelling calculations were undertaken using an ABAQUS explicit dynamic analysis. A 2D representation of the model and the structure as it is modelled in Abaqus (with the slabs shown as the section they represent even though they are modelled as beam elements) is shown in Figure 5-3. This figure also indicates the location of the three fire floors. All sections are modelled using 2-D linear B31-type beam elements, including the concrete slab, which is

modelled as a beam with an equivalent rectangular cross-section and an appropriate offset to the beams.

The numerical model can be thought of as a plane strain representation of the structure. This approach to representing the behaviour of multi-storey structures has been shown to capture the key aspects of their behaviour while allowing for numerical models of manageable size. Detailed comparison between 2-d and 3-d modelling approaches were undertaken by Flint [43] who showed there was good agreement between the results obtained. Quiel [72] also compared behaviour in 2-d and 3-d models of the perimeter of a high-rise steel frame. The 2-d models were found to accurately predict the behaviour observed in the more complex 3-d models. Axial loads and bending moments showed particularly close agreement, while the deflections of the beams were marginally over predicted by the 2-d models as the continuous slab provides added rigidity in three dimensions. Axial forces were predicted accurately in terms of both peak values and time of occurrence. In the light of this previous work, the author chose to use a 2-d representation of the structure for ease of calculation and analysis.

The model incorporates twelve floors and thus represents only part of the whole height of the structure. Each floor slab supports a uniformly distributed load (UDL) which includes the self weight of the concrete slab and steel beam, as well as an imposed load. Based on a total of 5kN/m^2 , this results in 40kN/m on the beam.

The twelve-storey model is a representation of a section of a high rise building and thus could be located at any point within this structure. A point load is applied to the top of the column to represent the load due to the remaining upper floor levels. This point load would be close to zero if the section is located near the top of the

structure, or similarly would be very large if 40 or so higher storeys are assumed to be transferring load through the column.

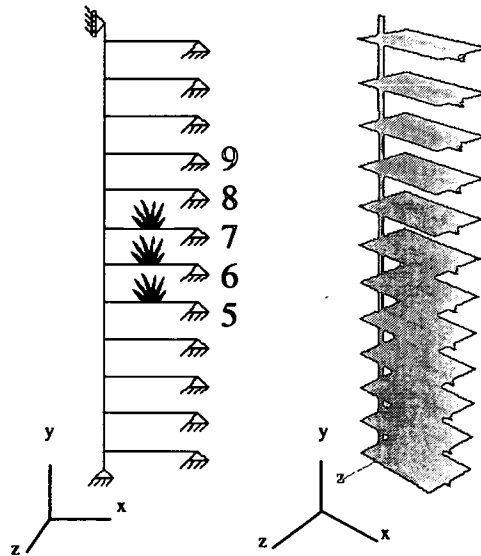


Figure 5-3 – 2D representation of the structure as modelled with Abaqus. The three fire floors are indicated together with selected floor numbers

During previous analyses of the frame during heating, noted in Section 5.1.1, a parametric study was done to explore the effect of this loading which was found to have very little impact on the collapse mechanism. It did however affect the time at which collapse occurred, with higher loads inducing collapse earlier in the fire duration [70]. In all models considered in this chapter the point load is chosen as 100kN, which represents a section of building somewhere near the top of the building. This was chosen to ensure the structures would not show failure during the heating phase and therefore could be analysed during cooling.

5.3.1. Material properties

The material properties for steel are taken from Eurocodes 4 [1] and a yield strength of 355 MPa is assumed. The compressive strength of concrete at ambient temperature is taken to be 35MPa. The stress-strain relationships assumed for concrete, in compression and tension, are shown in Figure 5-4. As the concrete slab is modelled as a 2D beam using beam elements, no reinforcement was included. The reinforcement in such a slab would only be anti-cracking mesh and thus not of very significant size. Parallel to the beam, this reinforcement has little effect as the concrete is mostly in compression. As the section is modelled as a 2D slice, any effect of the reinforcement perpendicular to the beam cannot be included; this is part of the structural model assumption.

Stresses on cooling are governed by Von Mises and Drucker-Prager yield criterion for steel and concrete respectively. It was assumed the materials properties returned to their original ambient values after the cooling phase. Assumptions such as these are necessary to establish a first estimate of the structural behaviour during cooling; many details in this area of research remain uncertain at present. In reality there is likely to be a reduction in the overall capacity of the concrete and steel after having reached high temperatures, although this reduction is difficult to quantify in particular for concrete [28, 55-57]. Studies of steel in fire have shown that the ultimate strength is not usually permanently reduced after a fire, although the strength can be temporarily reduced and permanent deformations can result [73]. The input of material properties in Abaqus is detailed in Appendix D.

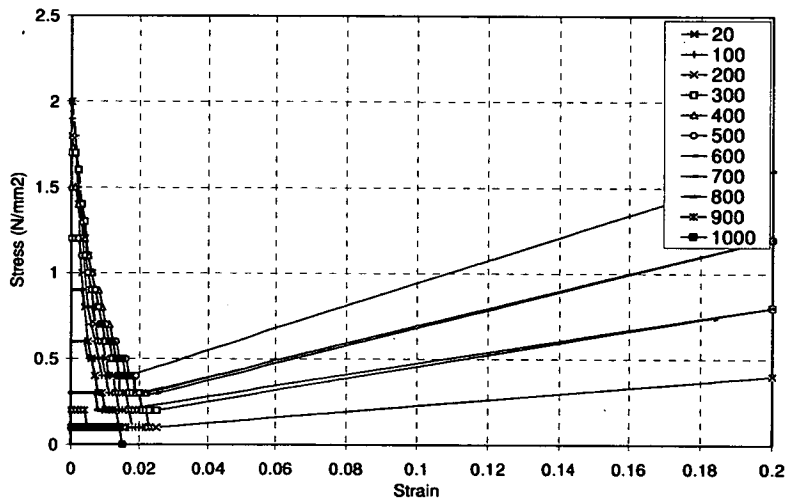
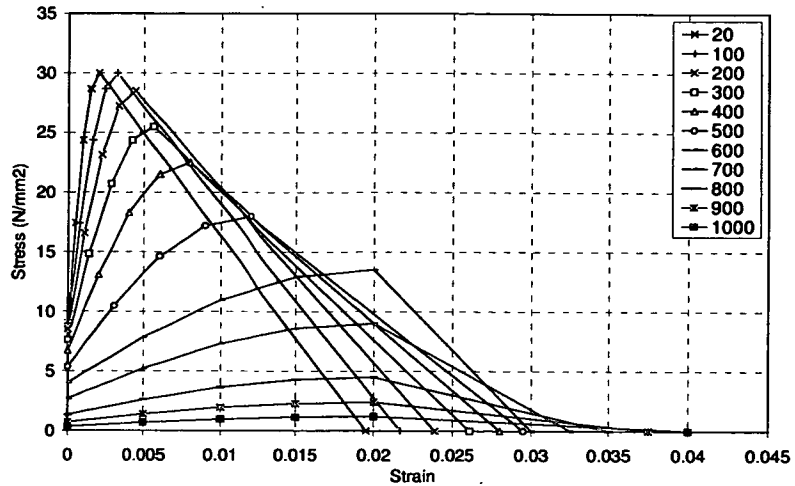


Figure 5-4 – Stress-strain relationship for concrete in both compression and tension respectively

It is not straightforward in ABAQUS to model material properties which are different during heating and cooling. The only material property affected by this, which can be properly quantified, is the specific heat capacity of concrete which has a peak value during heating when the moisture in the concrete evaporates. As during heating there will be moisture migration and most of the moisture will escape from the concrete, this peak will not occur upon cooling. Analyses were

performed to determine the influence of this brief increase in specific heat on the overall heat transfer analysis and the corresponding temperature distribution through the slab.

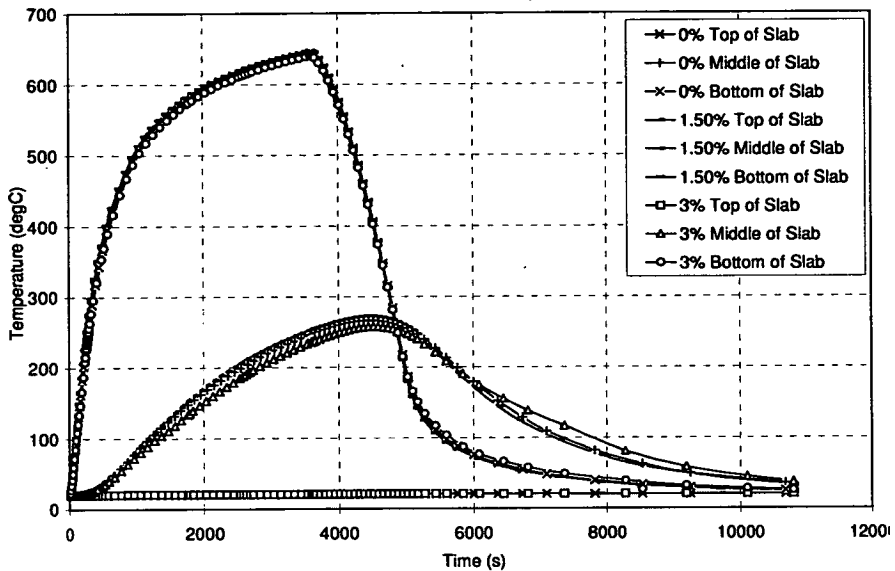


Figure 5-5 – Comparison of temperature evolution in the concrete slab for a typical fire scenario with varying moisture contents

The effect was found to be minimal as is shown in Figure 5-5 which shows the temperature evolution in a typical concrete section. This was also shown in research by Chung [11]. Although the latent heat of water at 100°C is something to consider, for the following analyses the assumption is made that this does not influence the specific heat of the material. The analysis therefore relates to dry concrete as defined in the Eurocode 4, rather than concrete with 1.5% or 3% moisture. The moisture content will however have a significant influence on spalling, but this is not considered in this research.

5.4. Fire scenarios

For the purpose of this study the number of fire affected floors was limited to three. These are located in the centre of the model as shown in Figure 5-3 , so as to include the possible effects on the surrounding structure. It was assumed that the fires only affect the floor above the fire compartment, and thus no heating of the top of the slab is taken into account.

Hot smoke is the main contributor to the heating of the slab which affects the floor above. The source of the fire is generally localised and thus only affects a small part of the slab below. A reasonable amount of insulation is also usually in place, in the form of floor coverings, thus again reducing the effect of a fire on the floor slab below. It was also assumed each floor was subjected to increased temperatures uniformly and hence horizontally travelling fires were not considered. This method is also applied in structural fire engineering design practice where a total floor fire is considered to be the worst case scenario. Whether uniform fires are actually the most conservative is addressed in more details in Chapters 4 and 7 which consider 1D beams and 3D structures subjected to non-uniform fires. A vertically travelling fire has also been considered in Chapter 6.

5.4.1. Gas Temperatures

To understand the behaviour of the structure during the cooling phase of fires, several possible fire scenarios are developed. Two separate comparisons are made; referred to as Case 1 and Case 2.

In Case 1 a comparison is made between two models. The heating phase is constant in both and the cooling phase is determined using two different methods. These methods are described further in section 5.5. In Case 2 the method for obtaining the structural temperatures is identical, but now a range of heating and cooling rates is compared. Two heating phases are considered to establish the effect this has on the cooling behaviour. Four linear cooling rates are considered. The time-temperature relationship during heating used for both Case 1 as well as the first heating curve for Case 2 is described by the generalised exponential curve previously used by Flint [43].

$$T(t) = T_0 + (T_{max} - T_0) (1 - e^{-\alpha t}) \quad (5.1)$$

where, T_{max} is the maximum compartment temperature, T_0 is the initial or ambient temperature, t time (this is a local time on each floor for analyses where the fires travel vertically), and α an arbitrary ‘rate of heating’ parameter. For the purpose of this research, T_{max} and T_0 were taken as 800°C and 20°C respectively, α as 0.005 and the total time of heating as 3600s. This fire will be referred to as ‘800’ for the remainder of the chapter. Equation (5.1) was used to model the gas temperatures as fire dynamics analyses undertaken by Flint [43] showed it to be a better approximation for large compartments than the more commonly used “natural fire” curves given, for example, in the Eurocodes [9].

The second temperature-time relationship during heating, used for Case 2 only is a standard fire based on ISO 834, taken from the British Standards, Eurocode 1 [9]. This fire is referred to by ‘SF’ in the remainder of the chapter. The equation is given in Section 2.2.1 in Chapter 2. The duration of the fire prior to cooling for both types of heating is constant at 60 minutes or 3600 seconds.

Neither of these fire definitions includes a cooling phase. Codes often show gas temperatures in cooling reduce linearly over a period of time. In reality the gas temperature reduces rapidly after burning has ended because a large degree of ventilation is likely to be present. However, radiation from surfaces (e.g. walls) may cause the temperature of solids to remain high for some time. Little research has been done on quantifying the thermal environment in cooling fire compartments and therefore assumptions are made to simplify the study. Two cooling assumptions are made for Case 1. First is a slow linear temperature decrease over time for all parts of the structure. Secondly, a heat transfer analysis is done (as outlined in Section 5.5.2) based on a decrease of the gas temperature over 30 minutes as the fire finishes and consequently rapid cooling of exposed surfaces.

For Case 2, a range of cooling times is considered to bound all possible cooling scenarios, where all concrete temperatures are defined using the heat transfer method. For the purpose of this research, linear decreases in gas temperature were used where ambient temperature was reached 5s, 1400s, 2800s and 5600s after the end of the heating. The gas temperature evolution for all Case 2 scenarios is shown in Figure 5-6 and Figure 5-7. The naming convention used in these graphs is shown in Table 5-1 below. This table also includes the naming convention on aspects of the concrete slab and structural details which are referred to throughout the chapter. Although these gas temperature figures are for Case 2, one of the two temperature cases considered in Case 1 is very similar to Figure 5-6. The heating phase is identical ('800') and the cooling phase is somewhere between C2 and C3.

Table 5-1 – Naming convention 2

Naming convention	Abbreviation
Weak Beam	WB
Strong Beam	SB
Standard Fire 'SF'	F1
Parametric fire '800'	F2
Floor level 5	L5
Floor level 9	L9
Cooling 5 seconds	C1
Cooling 1400 seconds	C2
Cooling 2800 seconds	C3
Cooling 5600 seconds	C4
Bottom of Slab	B
Middle of Slab	M
Top of Slab	T

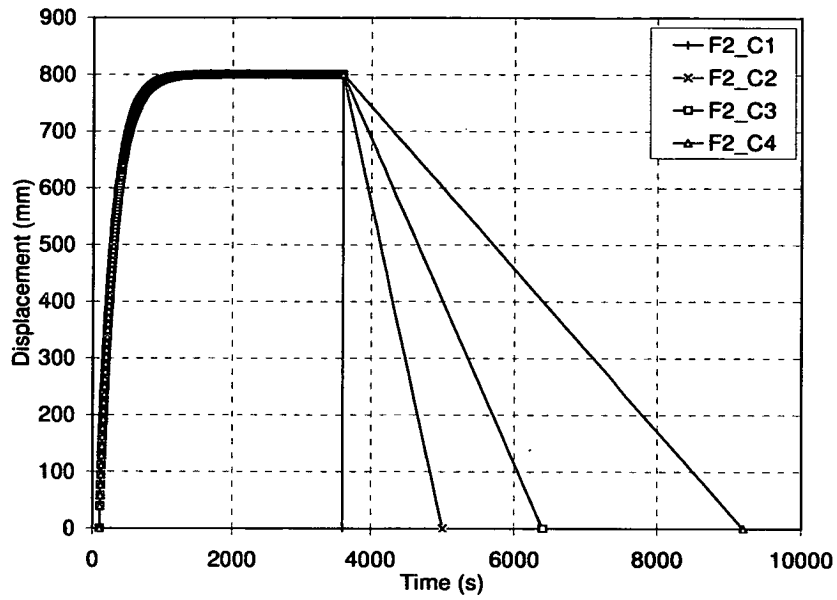


Figure 5-6 – Range of fires with '800' heating for Case 2. This heating curve also applies to Case 1

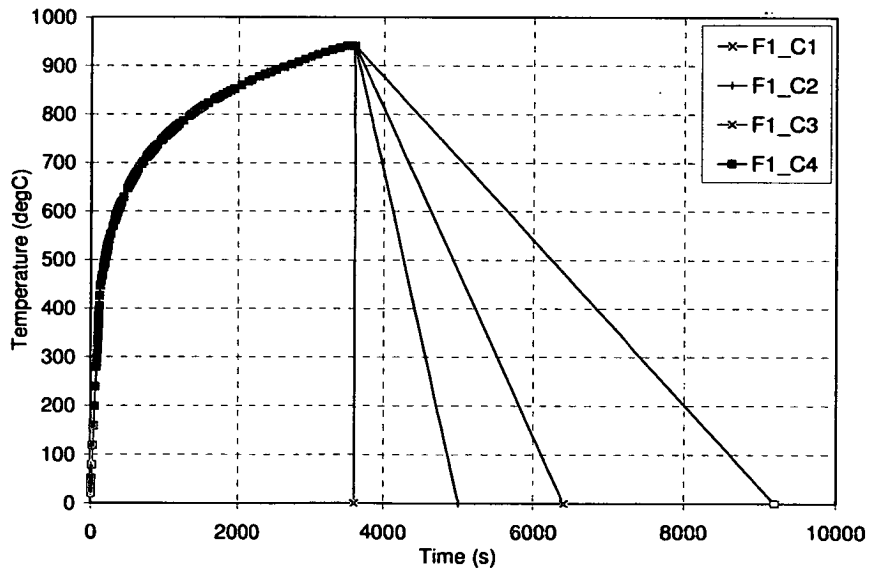


Figure 5-7 – Range of fires with 'SF' heating for Case 2

5.5. Structural Temperatures

Establishing the appropriate gas temperature-time curve for a structural fire analysis is only the first step in the analysis process. The defined gas temperatures will result in structural temperatures which need to be calculated. Several methods may be used to obtain these temperatures. For steel sections, such as columns and beams, tabular or graphical data may be used. These temperatures are based on standard tests which specify a minimum protection thickness depending on the section dimensions, protection material and fire exposure. Alternatively, simple or detailed numerical models can be used to obtain accurate temperature profiles using computer programs. For concrete slabs 1D heat transfer numerical models exist [74] which calculate the temperature evolution through the thickness of the slab when subjected to arbitrary heating. Detailed heat transfer analysis using finite element analysis programs are also available. Although greater computational resources are required, numerical modelling allows for more flexibility with the temperature input. In this thesis, the finite element software package Abaqus [35] is used to determine the temperature distributions in the concrete slabs.

In the fire scenarios described, the concrete slabs, the steel beams and columns were all subjected to heating. The steel columns were assumed to be protected and therefore reach a maximum temperature of 400°C. The steel beams supporting the concrete slab were assumed to be unprotected and thermally thin and therefore follow the gas temperature without a temperature gradient through the section.

In this chapter, two different methods of determining concrete temperatures are used. For Case 1, a simplified temperature distribution is used, referred to as

Linear Input whereby the cooling in concrete is assumed to be linear with time. The second scenario in Case 1 required a detailed heat transfer analysis to be done on the concrete slab to determine the exact temperature distribution through the section based on the gas temperatures. This heat transfer method is also used for Case 2. Both methods and the temperature profiles resulting from these are described in the sections below.

5.5.1. Linear Temperatures

The linear temperature definition is a simplified temperature input during cooling. Rather than using a heat transfer analysis (Section 5.5.2) to obtain the concrete temperatures during the cooling phase, it is assumed they reduce linearly over a period of 180 minutes.

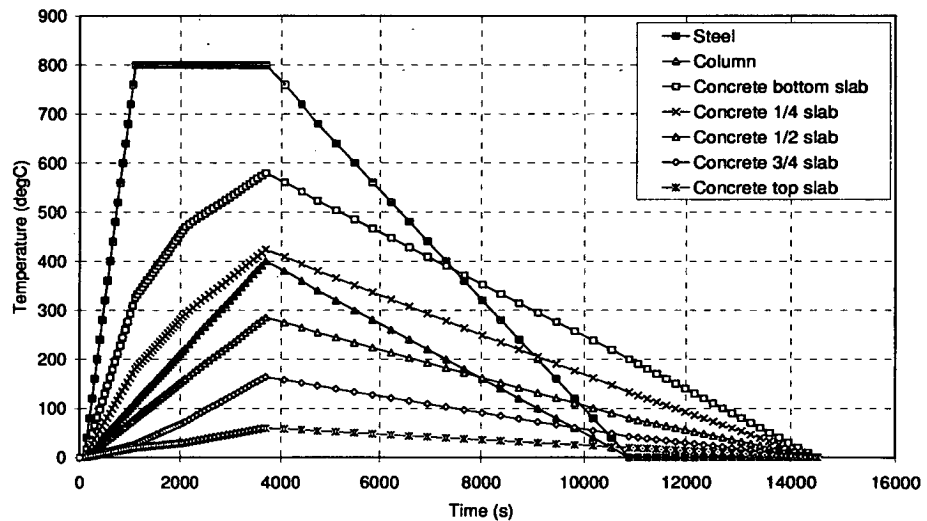


Figure 5-8 – Linear temperature input for Case 1

Although this is not a realistic temperature evolution through concrete, the simplified example serves to show the importance of the cooling phase and its

correct representation in design. The temperature evolution in the concrete as well as the steel beams and columns is shown in Figure 5-8. The steel is assumed to return to ambient after 120 minutes. The heating phase is based on the '800' fire, but is simplified to linear increments.

5.5.2. Heat Transfer Temperatures

To obtain realistic temperature-time curves for the cooling concrete, heat transfer analyses were performed on a cross-section of the slab. Several different heating and cooling curves are considered in both Case 1 and 2, and for each scenario a heat transfer analysis was done to ascertain the associated concrete temperature profile.

The heat transfer analysis in Abaqus assesses the temperature distribution through the concrete slab from the convective and radiative effects at the boundaries. These are calculated based on the gas temperature. Convection is associated with the transfer of heat by motion of a fluid onto a solid. The heat flux q'' due to convection is given by the following equation:

$$q''_c = h (T_g - T_s) \quad (5.2)$$

where h is the heat transfer coefficient, T_g the gas temperature and T_s the solid surface temperature [8]. The heat transfer coefficient for steel is generally taken between 5 and 25W/m².K [75]. Temperature, velocity of the hot gas and geometry are some of the factors which influence the exact value. A value of 25 W/m².K is assumed here.

Thermal radiation involves heat transfer by electromagnetic waves. Heat-flux due to radiation is given by the following equation:

$$q''_r = \sigma \varepsilon (T_g^4 - T_s^4) \quad (5.3)$$

where ε is emissivity and σ the Stefan-Boltzmann constant ($5.67E^{-8} \text{ W/m}^2\text{K}^4$). [8] Emissivity is a measure of the efficiency of the surface as a radiator and ranges from 0 to 1, where 1 indicates a perfect emitter. For all heat transfer analyses done in this study a value of emissivity of 0.8 is chosen [9].

A cross-section of the composite floor was modelled as indicated in Figure 5-9. In Figure 5-9(a) the temperature distribution through the section is shown when the fire is at the maximum temperature.

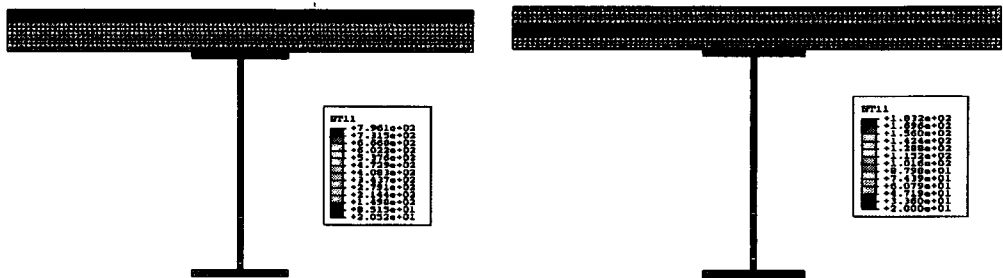


Figure 5-9 – Temperatures through the section predicted by heat transfer analysis, (a) when gas temperature is at a maximum, (b) when gas temperature has returned to ambient. The steel section pictured does not form part of the heat transfer analysis

Figure 5-9(b) shows the temperature distribution after the fire has ended and the section has been given some time to cool. This particular heat transfer example is based on an ‘800’ fire with a cooling phase of 1400s. It is clear from Figure 5-9 and Figure 5-10 that the bottom of the concrete slab heats up rapidly as this is directly exposed to the fire. The area of high temperature gradually expands towards the centre of the slab as the fire continues to heat the lower surface. Once

the fire has ended, the surfaces of the concrete slab quickly return to ambient temperature while the centre of the slab continues to heat and remains quite hot. The cooling of the centre of the slab is much slower and this section continues to be subjected to higher temperatures long after the fire has died out.

For the structural analyses ABAQUS beam elements were used to model a suitable width of the concrete slab that formed part of the composite section. These elements only allow temperatures to be specified at 3 locations through their depth while the heat transfer analyses described predicts temperatures at 11 locations, as shown in Figure 5-10.

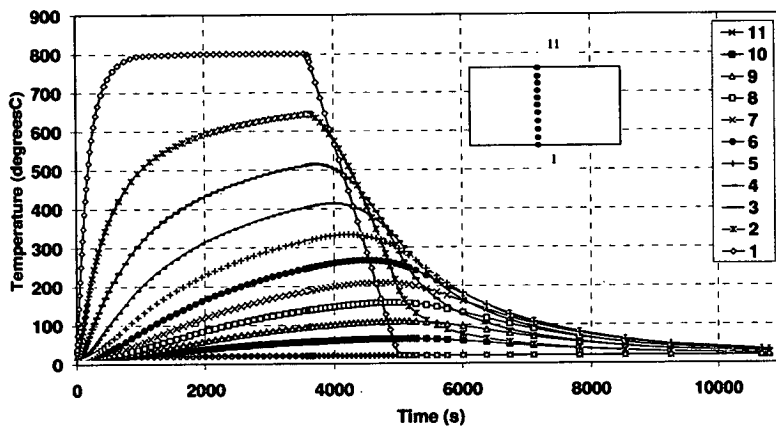


Figure 5-10 – Temperature distribution through the concrete slab as given by the heat transfer analysis

These 11 readings needed to be reduced to 3 representative points for the temperature input to the beam elements. Figure 5-11 shows the input points ABAQUS requires for beam elements on the left and the temperature predictions provided by the heat transfer analysis on the right. Of the 11 predictions, the 2

readings at the extremities of the section will be very similar to the gas temperature on each surface. These values are therefore not representative of the temperatures through the section and so would not give an accurate approximation of the temperature profile through the slab thickness.

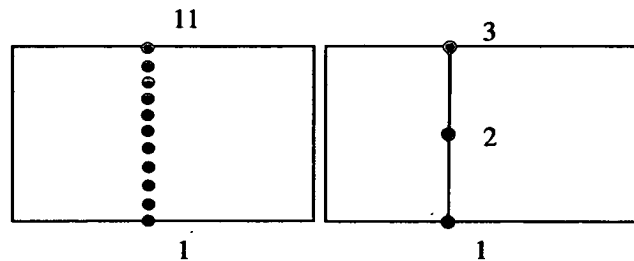


Figure 5-11– Temperature output points through the concrete slab from the heat transfer analysis and the linear approximation at three points used for the input into the structural model

This is especially true of the reading at the bottom of the slab where the temperature quickly reaches temperature similar to the gas temperature. This section of the concrete is also very susceptible to spalling and may therefore be ignored in the analysis. To more accurately represent the temperature distribution the values are taken from the first reading in the slab itself, that is, the second of the 11 points in Figure 5-11. The temperature-time distribution through the slab for Case 1 is shown in Figure 5-12. This shows both the temperature output from the heat transfer analysis as well as the multi-linear approximations applied to the structural models. Similar temperature input is created for each of the fire scenarios described. The calculated concrete temperatures for each of the scenarios in Case 2 are shown in Figure 5-13 and Figure 5-14. These are for the 'SF' and '800' fires respectively. The naming convention used here is referred to in Table 5-1. From these graphs it can be seen that the concrete cools slower as a result of a

long cooling phase and subsequently the middle of the slab reaches a higher temperature. It is again assumed that the steel temperatures follow the gas temperatures.

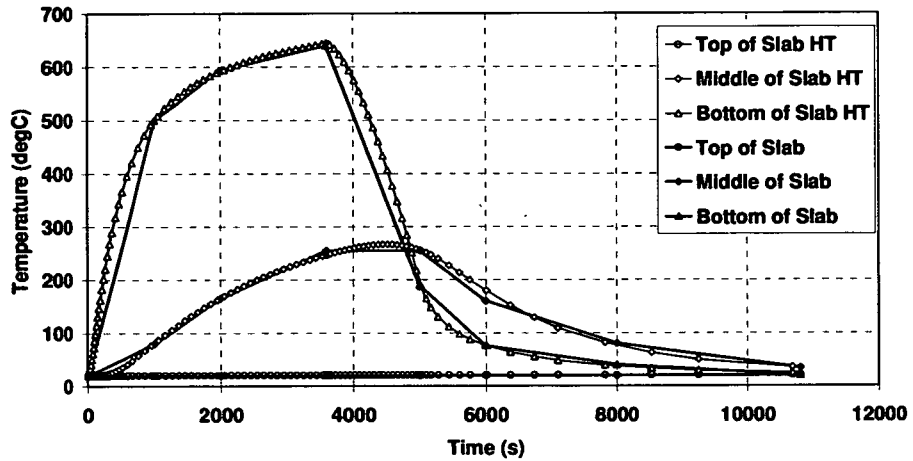


Figure 5-12 – Temperatures as given by the heat transfer analysis and linear Abaqus input

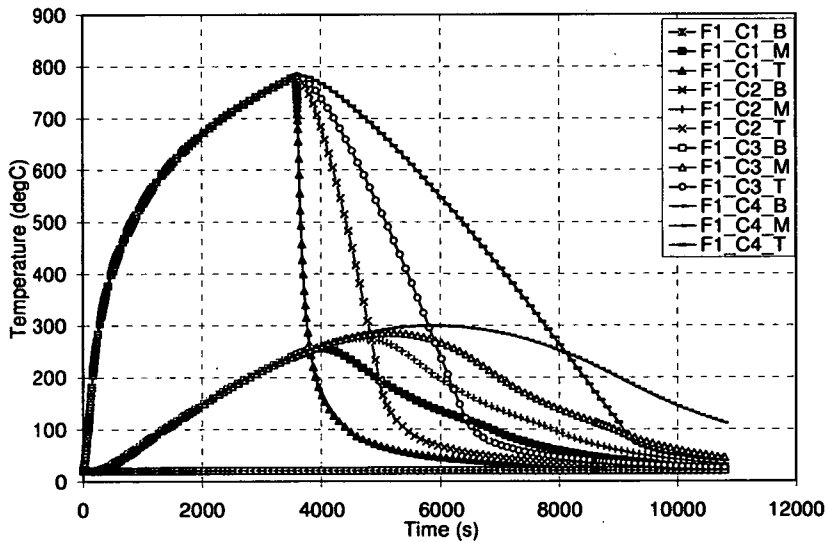


Figure 5-13 – Concrete temperatures with 'SF' fire for Case 2

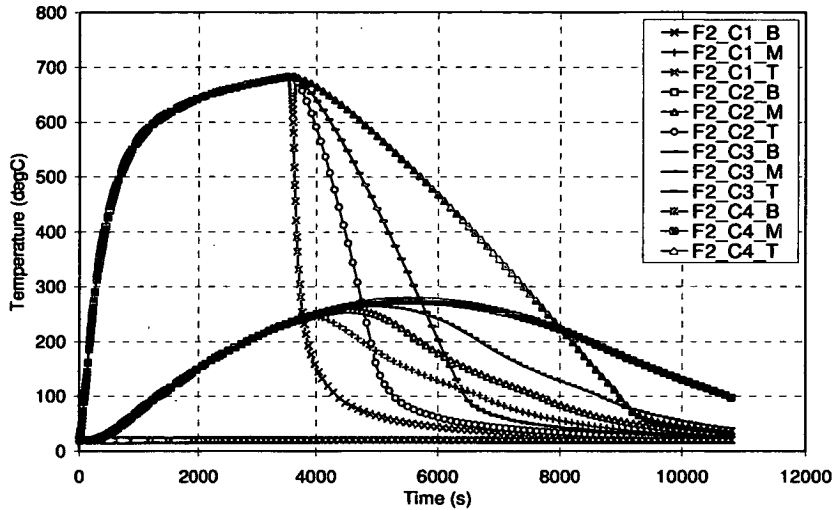


Figure 5-14 – Concrete temperatures with ‘800’ fire for Case 2

5.6. Behaviour during Cooling

This section will present the observed behaviour in the described structures during cooling only. Previous work has been done on the behaviour during heating and the possible collapse mechanisms induced. This is described in detail by Røben [67, 70, 76] and is not covered further in this thesis. A conference and journal paper on this can be found in Appendix D.

Several fire regimes are considered as described in Section 5.4. Case 1 investigates a linear cooling phase to understand the basic effects of cooling on the structural frame considered which is then compared to a more realistic cooling regime taken from the output of a heat transfer analysis based on a rapid decrease of the gas temperature. Case 2 considers four different cooling rates, as well as two different heating phases, to compare the effect these have on the overall behaviour.

5.6.1. Case 1: Linear cooling vs. heat transfer analysis

Here the temperature distributions described in Section 5.5 for both the linear cooling analysis and those obtained from the heat transfer analysis are applied in structural analyses to investigate and compare the structural behaviour. Both the WB and SB models are considered for the linear cooling and heat transfer temperature input.

The deflected shapes of the structures after having been subjected to the thermal regimes are shown schematically in Figure 5-15. The final deflected shapes are almost identical for both the heating regimes and so Figure 5-15 represents both.

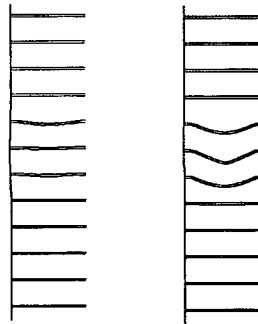


Figure 5-15 – Final deformed shape of two models regardless of linear or HT heating regime. SB on left, WB on right

In both the WB and SB models the thermal expansion of the floors has caused the column to be pushed out. In the following figures this is indicated as Phase 1. As the floors continue to expand they start deflecting downwards because of the through depth thermal gradient and P- δ moments imposed by the end reactions to their expansion. This was the initial stage of the collapse mechanism seen in previous studies [67, 70] and described in Section 5.1.1. The column is not pulled inwards by the floors in the SB model as these floors do not deflect downwards

enough and hence do not apply a significant pull-in force to the column. The higher overall capacity of the floors due to the larger beam section reduces the downward movement, whilst the column also provides less relative stiffness to the floor expansion thus allowing further outward movement of the column and floors. In the WB model the column does get pulled inwards somewhat, albeit not sufficiently to cause collapse. The results are separated into the weak and strong beam types, where each type is subjected to linear and heat transfer temperatures. Table 5-2 shows the naming convention used in the following graphs.

Table 5-2: Naming convention

Naming convention	Abbreviation
Weak Beam	WB
Strong Beam	SB
Temperature Profile 1 – Linear	TP1
Temperature Profile 2 – Heat Transfer	TP2
Floor level 5	L5
Floor level 9	L9

Weak Beam model

To compare the behaviour of the two cooling regimes, the axial forces as well as displacements are considered. The total forces in the composite sections of the WB structure are plotted in Figure 5-16 and Figure 5-17 for the linear temperature decay and heat transfer (HT) predicted temperature decay respectively.

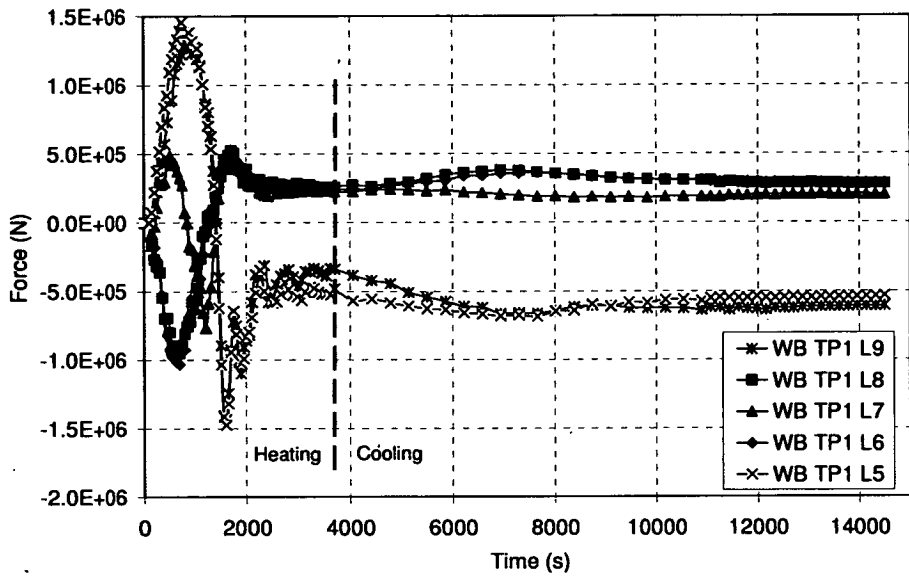


Figure 5-16 – Section forces for whole floors at the connection with the core, WB model with linear temperature analysis

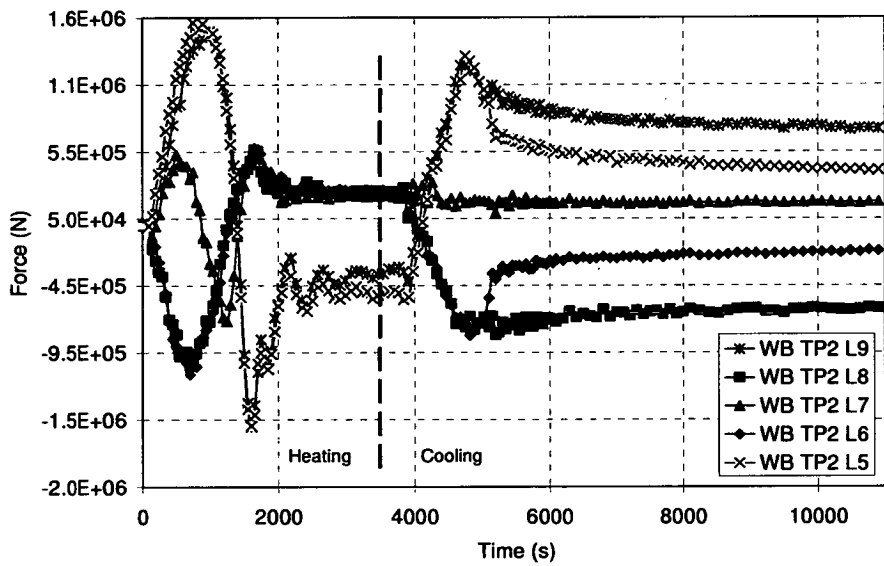


Figure 5-17 – Section forces for whole floors at the connection with the core, WB model with HT analysis

The behaviour during the heating phase is identical, as expected. During cooling however, the total floor forces in the two cases differ substantially. The behaviour during both these parts of the fire is discussed. Initially the fire floors are expanding and are therefore in compression (negative axial force). To accommodate the shape of the column which is being pushed out by the fire floors, the floors above and below the fire need to be in tension, as does the middle fire floor, floor 7, for compatibility.

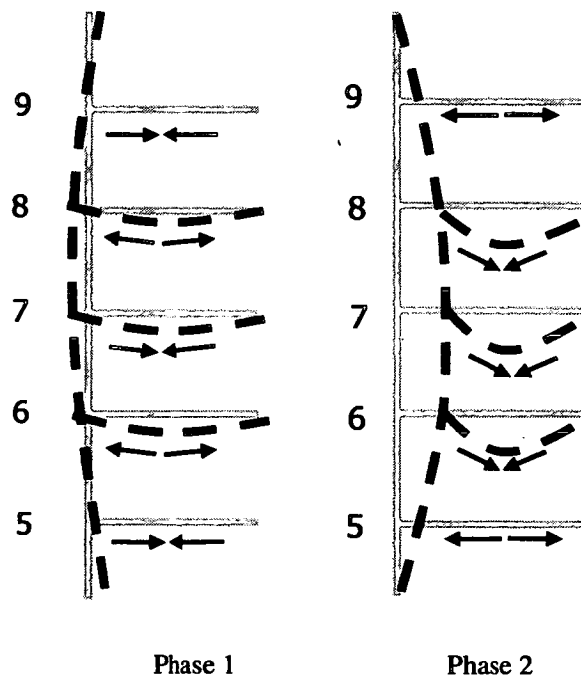


Figure 5-18 – Displaced shape of the weak beam structure during phase 1 and 2 respectively for either heating-cooling regime

This is referred to as Phase 1 which is schematically shown in Figure 5-18. At a later stage, when the fire floors deflects substantially they are in catenary and thus floors 5 and 9 have high compressions to support the column, correlating to Phase

2 again shown in Figure 5-18. Minor oscillations in the force predictions in this and other figures arise from the inertia forces that are represented in the numerical model.

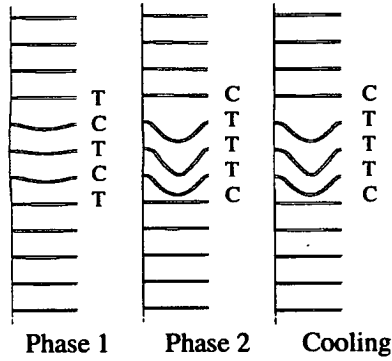


Figure 5-19 – Diagram of compression (C) and tension (T) forces for the WB model at the early stage of heating, the end of the heating phase and the end of the cooling phase of the linear temperature profile analysis

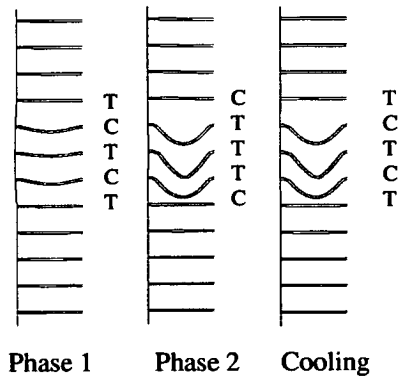


Figure 5-20 – Diagram of compression (C) and tension (T) forces for the WB model at the early stage of heating, the end of the heating phase and the end of the cooling phase of the HT profile analysis

In the linear temperature analysis, the section forces at the end of the cooling phase show the three fire floors are in tension. This is as a result of the floors contracting as they cool from an inelastic state. Floors 9 and 5, those above and below the fire floors, are forced into compression by compatibility requirements. The forces at the end of the cooling phase of the HT analyses are quite different. Here floors 9 and 5, together with the middle of the three fire floors, are in tension. The other two fire floors are in compression. The total force here is dominated by the concrete which continues to expand after the steel has begun to cool. The steel beam has insufficient area to counteract this effect and so the net force is compressive. The diagram in Figure 5-19 shows the variation for the linear cooling analysis, whilst Figure 5-20 shows the variation of tension and compression in the floors at three points in time during the HT profile analysis.

The deflected shapes of the structures support this explanation of the behaviour. During the heating phase the column is pushed out by the thermal expansion of the fire floors (Phase 1). As these floors start to deflect downwards the column is pulled back through its original position (Phase 2). This is shown by Figure 5-21 which shows the horizontal displacement of the column at floor 6 to 8 for the linear and HT analysis. Negative values indicate outward movement and positive values inward movement. For the HT analysis, the column can be seen to cross the x-axis, representing its original location, twice, once during heating where the column is pushed out (0-1700s) and once during cooling before being pulled in (1700-4000s). It is noticeable that the inward deflection of the column peaks at around 1800s and then reduces again.

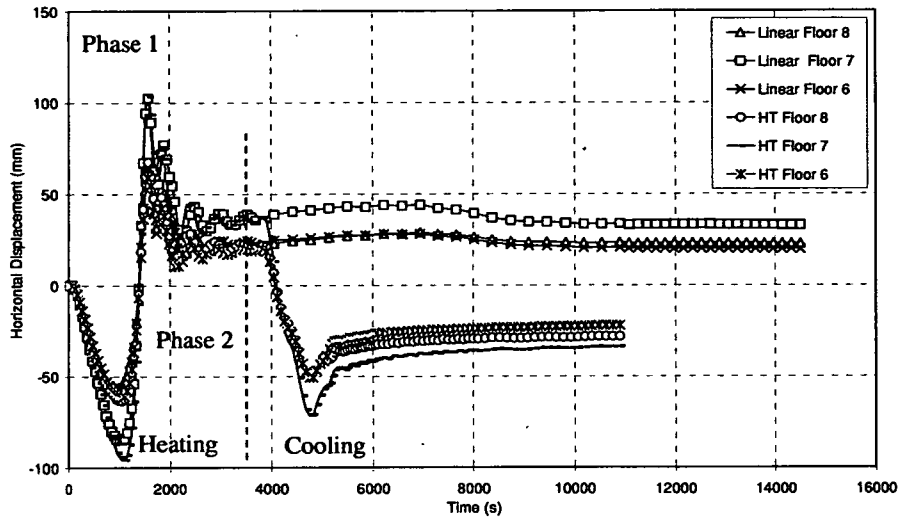


Figure 5-21 – Horizontal displacement of the column at the connection with the floors, WB model with Linear and HT analysis

The column in the linear model on the other hand does not move back through its original position for the second time. This difference is caused by the different temperature profiles in each of the two models. In the HT analysis the concrete continues to heat as it is a thermally thick material. The steel is cooling rapidly but as it is a relatively small beam the concrete dominates the behaviour.

This continuing expansion therefore causes the column to be pushed out once again before stabilising as the sections cool further. In the linear model on the other hand, the steel and concrete do not continue to heat but both cool linearly over a long period of time. This results in a more or less unchanging horizontal displacement. It can be seen from Figure 5-21 that the horizontal displacement of the column remains constant once cooling has commenced in both the steel and concrete.

Strong Beam model

The section forces and displacements of the SB model are discussed in the following section. The behaviour during heating is again identical for both analyses. Figure 5-22 shows the section forces for the linear temperature profile while Figure 5-23 shows those for the HT temperature profile. During the cooling phase the overall section forces also remain similar for both temperature profiles. The axial capacity of the strong beam is almost twice that of the weak beam. The forces generated during cooling by the contraction of the steel are therefore also substantially larger. In this case this force dominates the behaviour of the floor as a whole and thus the overall behaviour is not affected as much by the difference in thermal regime, which differs mostly in the concrete.

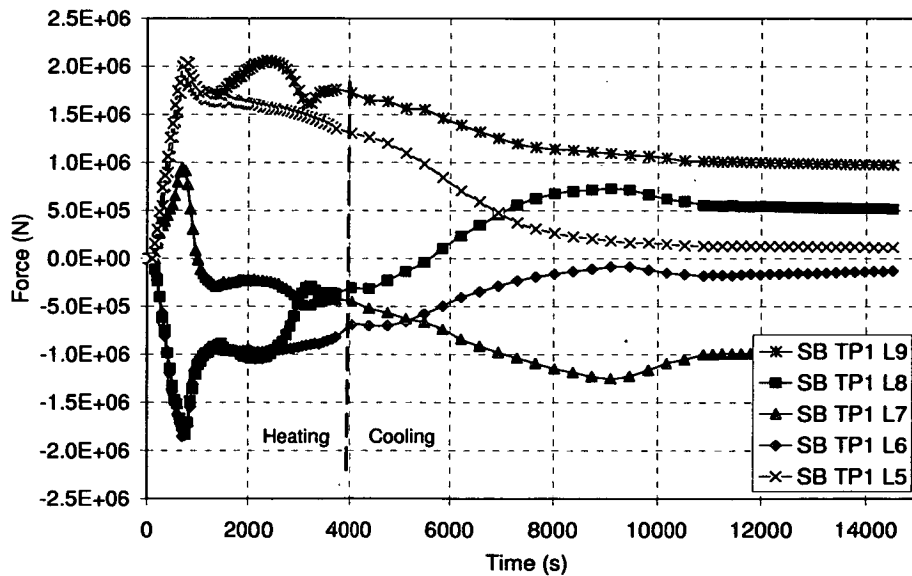


Figure 5-22 – Section forces for whole floors at the connection with the core, SB model with linear temperature analysis

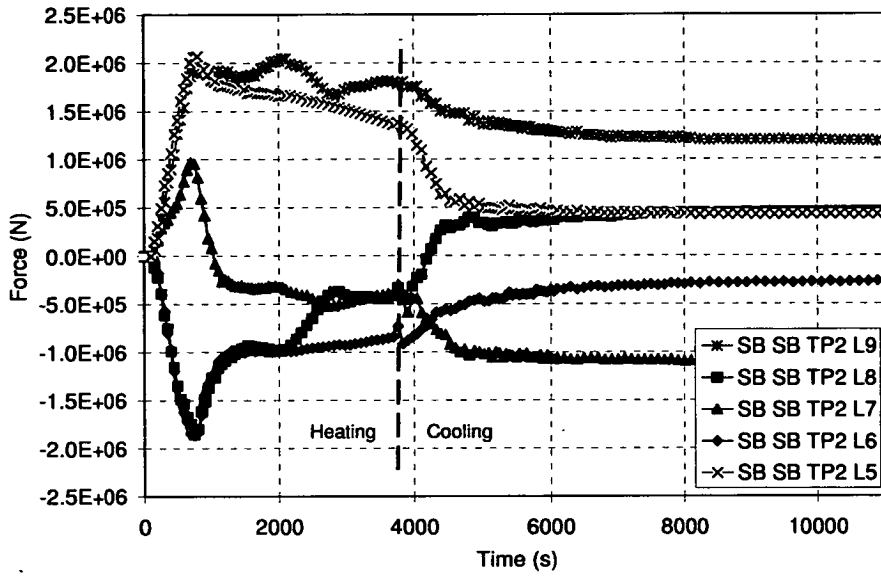


Figure 5-23 – Section forces for whole floors at the connection with the core, SB model with HT analysis

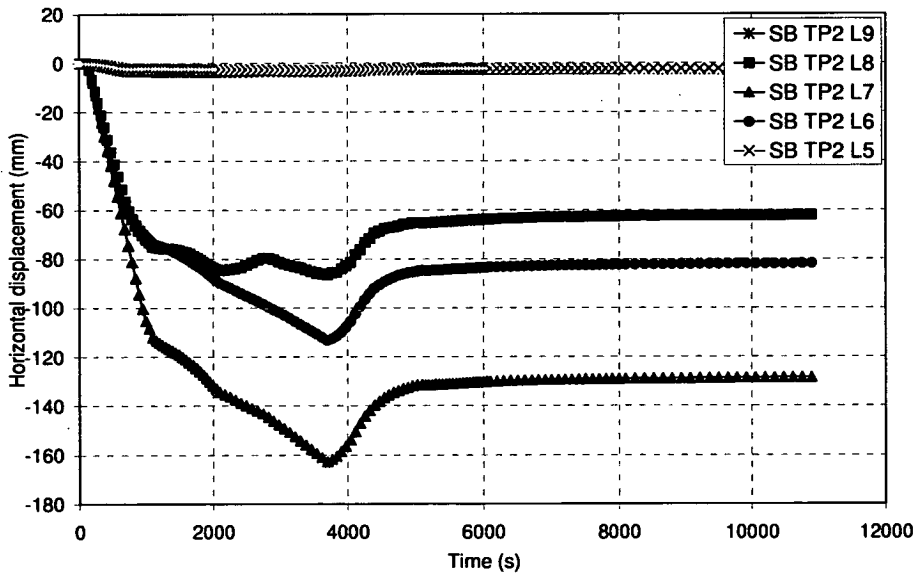


Figure 5-24 – Horizontal displacement of the column for the Strong Beam scenario

The horizontal displacements at the fire floors and those directly above and below are shown in Figure 5-24 where negative values indicate outward movement and positive indicates inward. In the SB models, the column is not pulled inwards as the fire floors do not deflect downwards enough to apply a significant pull-in force to the column. This is very different behaviour from the WB model where the column is pulled inwards past its original position as described in the previous section.

Local failure of connections

High tensile forces are generated in the steel beams when they cool from an inelastic state. In the Strong Beam model especially, the section forces during cooling are significantly higher than those encountered during heating, this is shown in Figure 5-25.

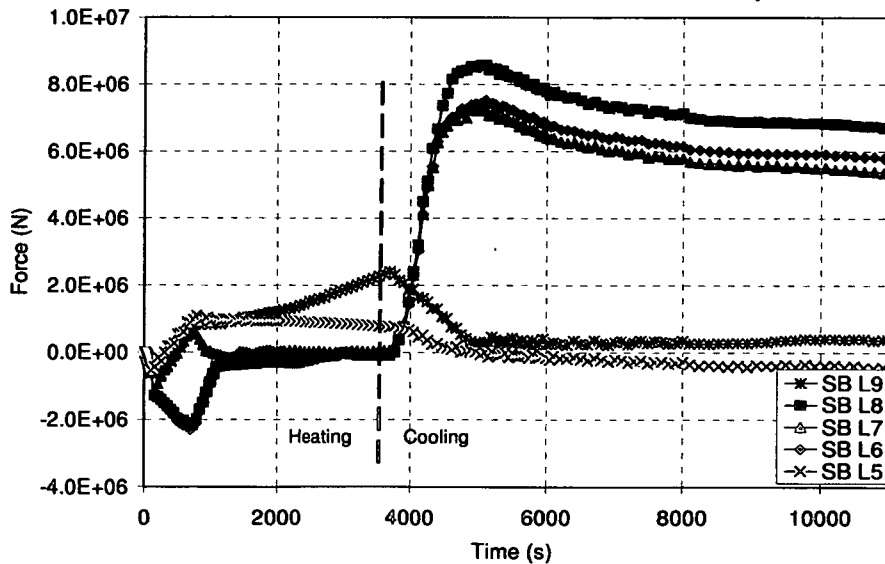


Figure 5-25 – Section forces for the steel beams in the SB model for the HT analysis

A maximum tensile force of approximately 9MN is present in floors 6 and 8 during cooling, while the maximum compressive force reached during the heating phase is approximately 2MN. The forces in the WB model are of a similar magnitude during the heating phase, however during the cooling phase there is not a significant increase and the maximum value reached is approximately +2.3MN (tensile). Although these forces are very large, the axial capacity of the composite floor is not reached for either model. However, typical beam to column connections, which would not be designed for significant axial forces, are not able to resist axial loads of this magnitude. Considering a range of realistic connection types (fin plate, end plate and double angle web cleat) and a range of beam sizes, their typical tying capacity can be obtained from the guidance on Joint Construction [62].

For double angle web cleats the tying capacity may range from 100kN to 1200kN, from 113kN to 990kN for flexible end plates and from 105kN to 1300kN for fin plates. The range depends on the size of the beam as well as the details of the connections such as single or double lines of bolts. Clearly the observed peak tensile forces of 2MN and 7.5MN are outside the capacity of the connections, regardless of the type. Local failure of the beam would therefore be likely to occur. In reality the connections may have some ductility which may partially relieve this force which may in some cases prevent failure occurring. To check this it would require detailed connection modelling which is outside the scope of this research.

5.6.2. Case 2: Varying cooling times

Several gas temperature cooling periods were considered, ranging from 5 seconds to 5600 seconds. The temperatures of the concrete slab in each case were obtained by a heat transfer analysis as described in Section 5.5.2.

Both the WB and SB models were subjected to these four different cooling periods and two different heating regimes. This allows for a comparison of the cooling phase as well as the effect different heating regimes have on the cooling behaviour.

Figure 5-26 shows the horizontal displacement of the column at the three floors affected by fire for the WB models with an '800' fire and each of the four cooling regimes.

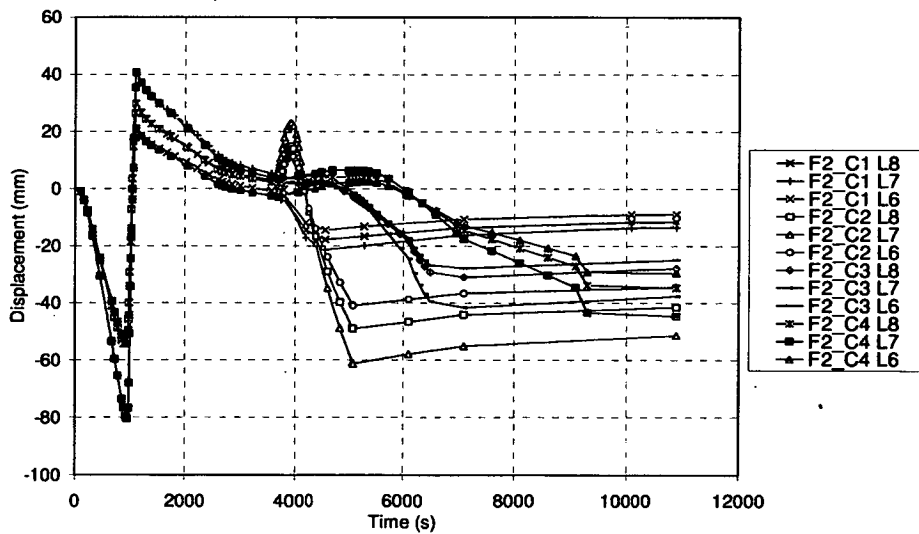


Figure 5-26 – Horizontal displacement of the column at the three fire floors for the WB '800' scenario

It is clear that the displacement is reversed more rapidly when the cooling occurs during a shorter time frame. Subsequent to the initial pushing out and pulling in of the column, there is a slow move back to the column's original position. This is due to the expansion of the column itself. As this is a relatively strong column, this upward movement overrides the pulling in force from the beams, thus resulting in the visible behaviour. This is identical for each scenario as it is not until cooling that the temperature profile changes. For the 5s cooling case the horizontal displacement is quickly increased which again can be explained by the column itself. As this is cooling very rapidly there is significant shortening of the section which, in combination with the sudden high tensile forces in the steel, causes the small but sudden increase in movement.

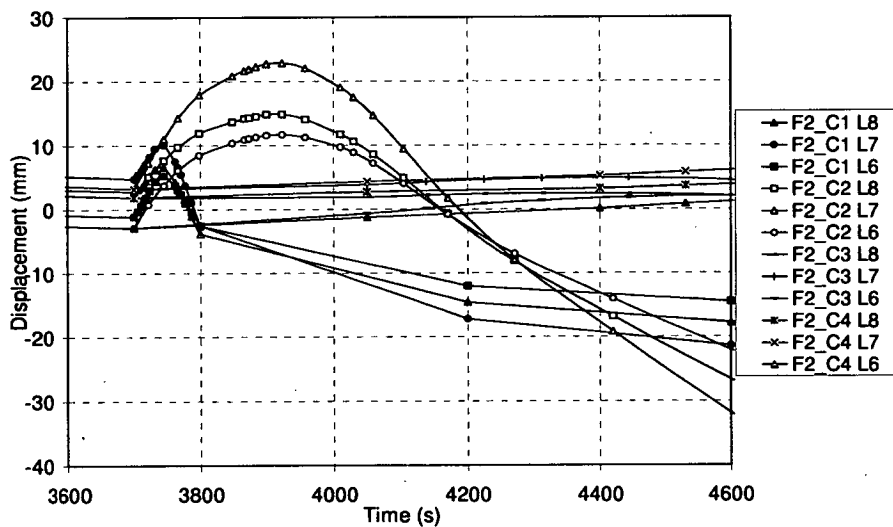


Figure 5-27 – Horizontal displacement of the column at the three fire floors for the WB '800' scenario, focussed on the first part of cooling

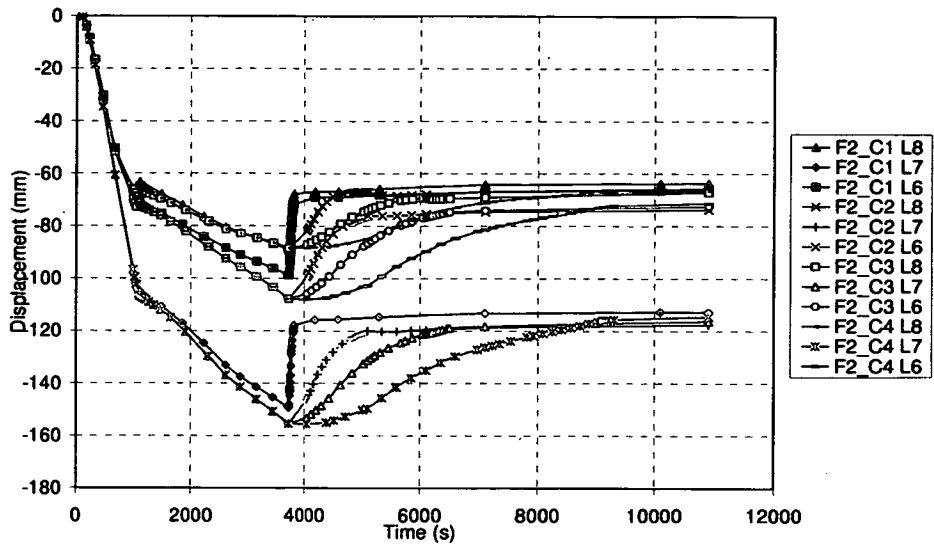


Figure 5-28 – Horizontal displacement of the column at the three fire floors for the SB ‘800’ scenario

As the length of the cooling phase increases, this rapid movement of the column becomes smoother and eventually disappears altogether. This is shown in Figure 5-27 where the horizontal displacement for all four cooling scenarios is shown in more detail during the first stage of the cooling phase. The behaviour observed in the SB models changes very little with varying cooling durations as shown in Figure 5-28. The rate at which recovery occurs varies significantly, with rapid cooling resulting in rapid recovery etc, but the final displacement for each of the floors is very similar. The overall structural behaviour does not appear to change much. The steel beam appears to be dominating the behaviour as it cools rapidly while the concrete continues to heat.

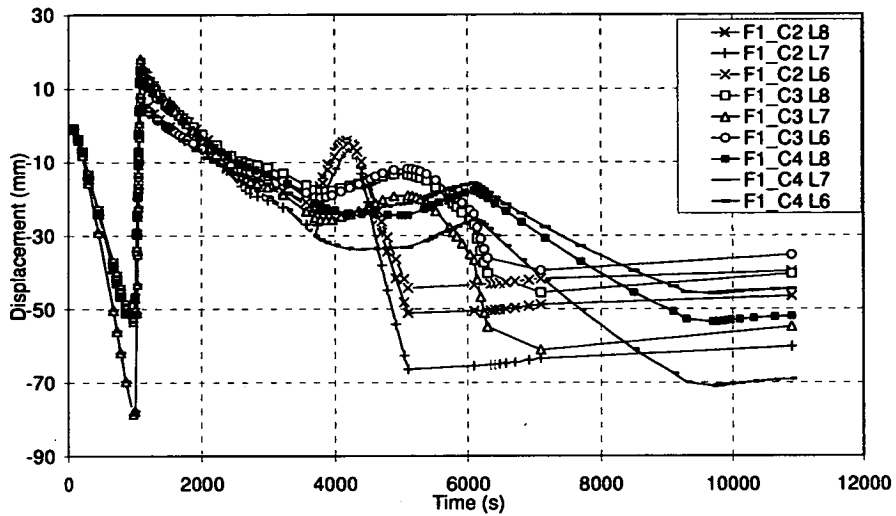


Figure 5-29 – Horizontal displacement of the column at the three fire floors for the WB ‘SF’ scenario

All the results presented here are for the ‘800’ fire. The output for the ‘SF’ fire is different during the heating phase, however the behaviour observed during cooling is very similar. Figure 5-29 shows the horizontal displacements for the ‘SF’ fire with each of the cooling phases.

The pattern is very similar to that observed for the ‘800’ fire, shown in Figure 5-26. For one of the cooling scenarios, 1400s, the displacement is compared directly; it can be seen that there is a small difference during the heating phase. The temperatures reached in the steel during the heating phase are higher, leading to more thermal expansion. This results in the heated floors deflecting downwards earlier thus causing the column to be pulled back somewhat sooner. Once cooling commences in both models, the behaviour is very similar in principle; both models see the sudden upward trend in the graph caused by the contracting of the steel beam and column.

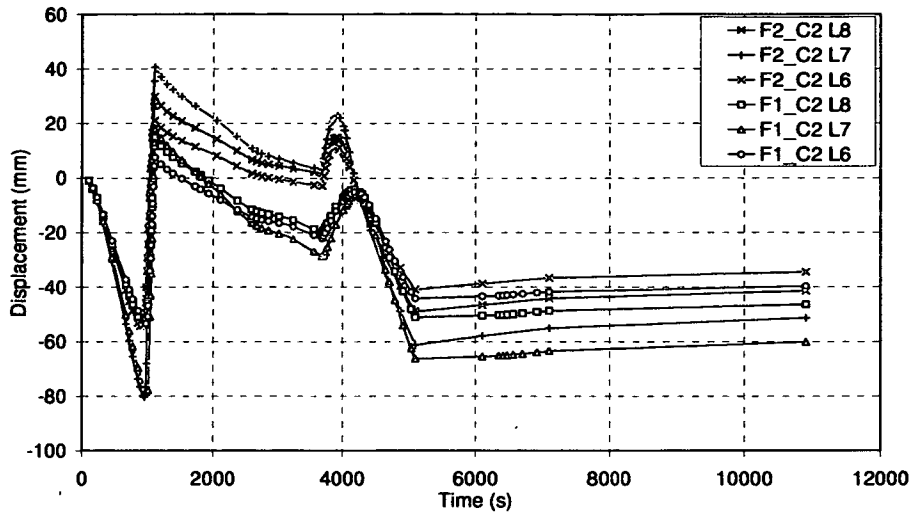


Figure 5-30 – Comparison of horizontal displacements for both the ‘800’ and ‘SF’ fires with the 1400s cooling phase

Due to the different rates of heating, the displacement pattern is not identical once cooling starts, with the ‘800’ fire displacements being positive and the ‘SF’ fire negative. The final displacements however are all negative and quite similar but with the ‘SF’ results consistently greater. This may be explained by the larger temperature reached, resulting in larger axial forces during heating and cooling, which was also observed in Chapter 3. To illustrate this, Figure 5-31 shows the axial forces in the steel beams at floor level 5 and 6, for the ‘SF’ and ‘800’ fire scenario and with two cooling phases each, C3 and C4. As cooling commences at 3600s the results for the two cooling regimes diverge as the C3 case beams regain strength more quickly. When comparing the axial forces at the end of the analyses, the axial forces are similar although forces from the ‘SF’ fires are consistently higher than from the ‘800’ fires, as expected. Another point to note is that slower cooling leads to higher residual forces in these models.

Overall it is shown that the rate of cooling causes some temporary differences in behaviour, but the general trend is similar.

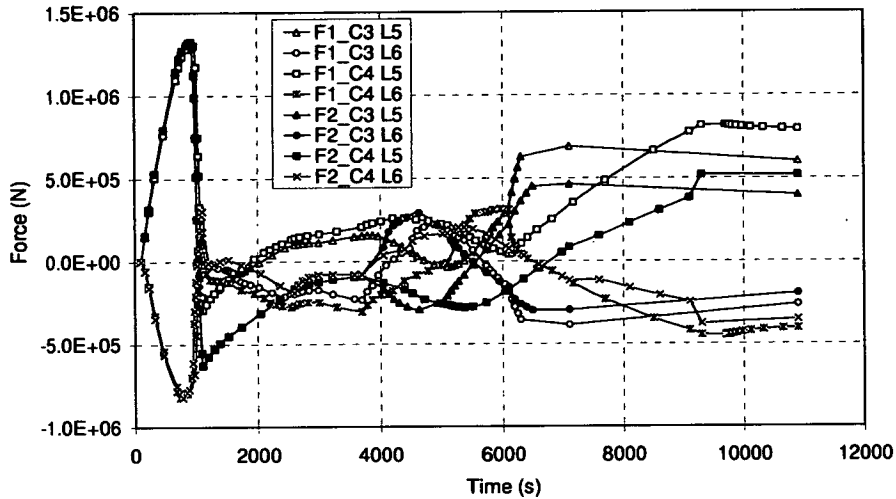


Figure 5-31 – Axial force in steel beams for both heating scenarios and two cooling phases

5.7. Cardington Test 1

The 3D model of the Cardington Test 1 described in Chapter 3 is also used to compare cooling rates. The rate of cooling is not found to be of great significance thus far, but this may be different when considering a 3D, single floor fire compartment. In this model the slab is based on shell elements, rather than beam elements which may affect the results.

The heating phase is identical to that considered for the model in Chapter 3. Three different rates of cooling are considered and compared. Very rapid cooling (5s) and two more gradual cooling rates (2800s and 5600s) are chosen. Heat transfer analyses were done to obtain the correct temperature distribution through the

concrete slab for each scenario. The axial force is plotted for each case in Figure 5-32. As the temperatures do not vary between analyses until the cooling phase starts (after 3700s) this is where the first differences are obvious. It can be seen that the axial force reduces rapidly for faster cooling rates, however the peak and final axial forces are almost identical.

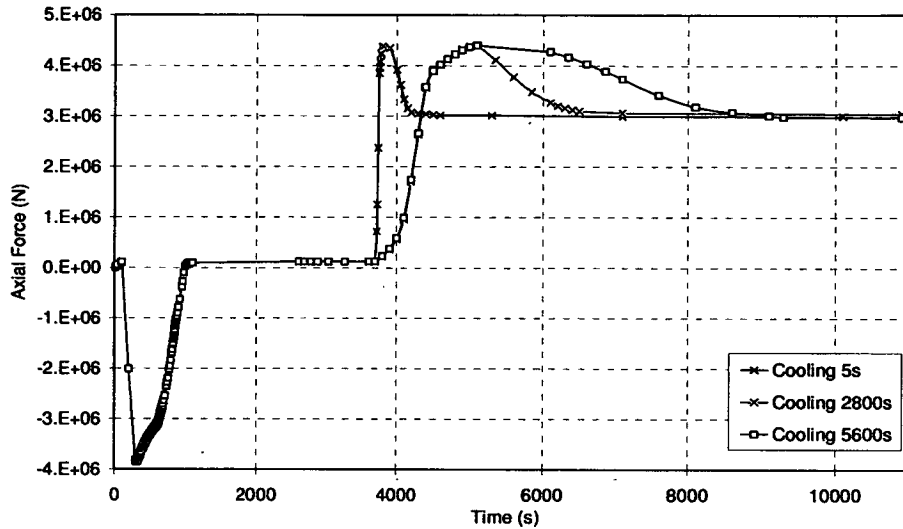


Figure 5-32 – Axial force comparison for various cooling rates

This is also the case for the vertical displacements at mid-span which recover at different rates, but to very similar final location shown in Figure 5-33. This is different from the behaviour in the 2D structural models where some difference in peak and final axial force was observed but the displacements finished at the same value. Finally, as the bending moments depend on the axial force and displacement evolution, there are also some temporary differences during the cooling phase, in Figure 5-34. The rate at which the moments become increasingly hogging is much slower for the longer cooling rates. The final, residual bending moment however is very similar.

This suggests that the cooling rate does not significantly affect the overall structural behaviour which agrees with results from earlier in this chapter.

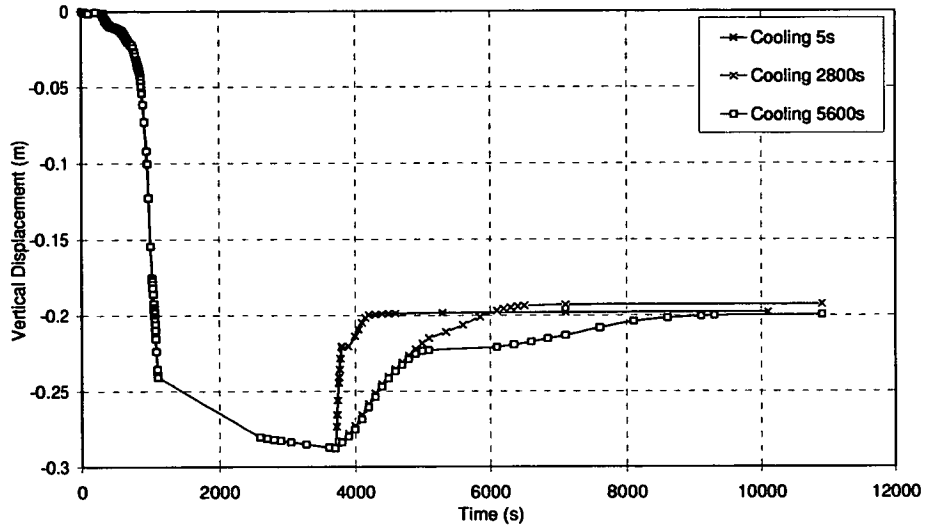


Figure 5-33 – Vertical displacement comparison for various cooling rates

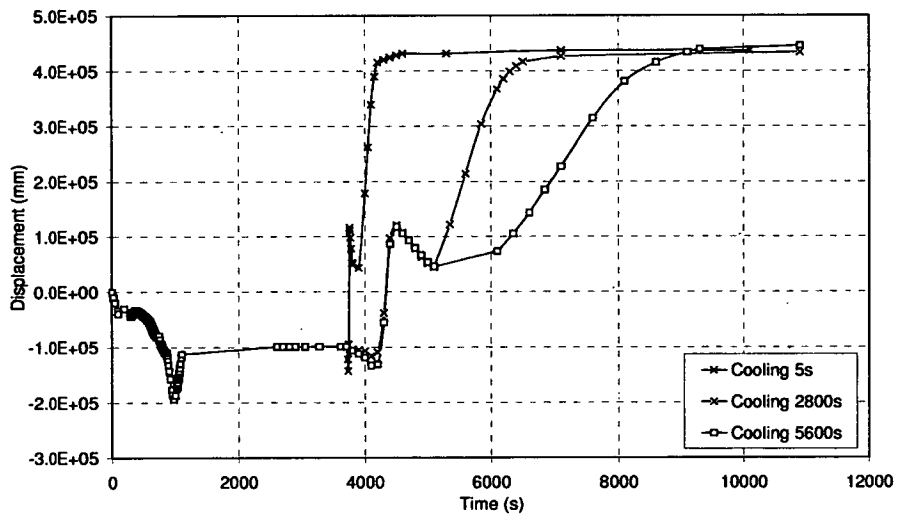


Figure 5-34 – Bending moment comparison for various cooling rates

5.8. Conclusions

This chapter discussed the investigation of the effect of cooling on a simple 2-D model representing a multi-storey building. Three of the twelve floors in the model were subjected to a fire with varying cooling regimes.

Two heating regimes were considered. A heat transfer analysis was performed to ascertain the temperatures in the structure through the full fire cycle. These temperatures were then applied to the structure and its behaviour is analysed. The structural behaviour observed was then compared with the behaviour of the structure when linear cooling is applied.

Firstly it was shown that the behaviour of the type of structure studied here during cooling depends on the relative areas of steel and concrete in the composite sections. In design at present unprotected steel beams are generally not considered during a fire as they rapidly lose almost all their strength on heating. During cooling however they will regain much of their strength and this study showed this strengthening will influence overall structural behaviour. If the area of steel is sufficiently large, the contraction forces in the steel beams dominate the floor behaviour. For smaller beams high forces in the (still hot) concrete dominate the behaviour. Secondly, it was shown that consideration of connection forces on cooling is required. It was also shown that forces during cooling can be more than three times those during heating, albeit of the opposite sign. Therefore the structure may remain globally stable while the structural elements are at high temperatures, but may be susceptible to local failures during the cooling.

The different heating regime had little effect on the global behaviour of the structures. The main difference was caused by the peak temperature reached;

higher temperatures result in relatively more cooling and thus higher axial forces.

This is in accordance with the observations in Chapter 3.

The different rates of cooling which were considered for both the 2D and 3D models showed that the overall behaviour during cooling is very similar. There are differences in the rate of recovery of vertical displacements and the rate at which moments and forces becoming increasingly hogging and tensile respectively. Importantly however, it was shown that the behaviour once ambient temperatures are reached is almost identical with similar residual forces and moments. Although cooling in itself has been shown to be extremely important to the behaviour of a structure during a fire, the rate of cooling appears to have limited effect on this.

6.1. Introduction

This chapter extends Chapter 5 by studying the effect of fires that travel vertically rather than occurring simultaneously on several floors; this is more realistic as it accounts for the time it takes for severe fires to spread between floors in high rise structures. The models described in Chapter 5 for behaviour during cooling are used to explore the global behaviour during a variety of travelling fires. The different beams sizes (WB and SB) are again compared to explore how this affects the global behaviour in the travelling fire scenarios. A range of vertical fire spread rates are chosen based on observations from real fires and these represent slow and fast fire spread. The resulting structural behaviour is compared with that observed during uniform fires.

6.1.1. Background

It is only recently that multiple floor fires have been considered in research on structural fire behaviour. Until this point single floor fires were the general assumption. Several high profile fires have led to a move in multiple floor fire research, some of which is discussed in Chapter 5 [43, 44, 68, 70]. Even in this research, the assumption has been to consider multiple simultaneous fires. In reality however, fires generally start in one location and then travel vertically up the building, affecting several floors in the process [22-24]. Fire in high-rise structures also tends to be difficult or impossible for fire-fighters to tackle, so much so that full burn-out may occur on one or more floors while evacuation or fire-fighting on other floors is still taking place. In such situations ensuring the stability of the overall structure has clear life safety implications. This leads to a requirement to understand the behaviour of structures subject to fires that travel between floors, perhaps with some floors cooling after burning-out while other floors are in the early stages of heating. This chapter aims to build on the very limited work that has so far

been devoted to understanding the global response of high-rise structures subject to multiple-floor fires.

As large fires can occur and spread relatively easily in modern open-plan office floors and extensive glazing is common which could break and provide sufficient air., the idealised structural model of a 2D high rise building as discussed in Chapter 5 is a reasonable assumption, where the fires occur in the outer floor plate and move progressively upward through broken windows as described in Chapter 2.

6.2. Travelling Fires Scenarios

Three different fires are considered; simultaneous heating on all three floors (discussed in Chapter 5), rapid vertical spread and the slow vertical spread. Inter-floor time intervals for the latter two cases are based on estimates from the Windsor Tower fire in Madrid; these varied from 6 to 30 minutes [5]. Here 500s and 1500s are chosen to represent this range. The temperature-time profiles for the steel beams (assumed to be equal to the gas temperature) and the concrete floor slabs for the travelling fires are shown in Figure 6-1 and Figure 6-2. Fire 1, 2 and 3 refer to the fires which occur on different floors, i.e. Fire 1 occurs first on floor 6, followed by Fire 2 on floor 7 and Fire 3 on floor 8. The gas temperature is based on the '800' fire described in Chapter 5. The cooling phase assumes a linearly decreasing temperature over 1500s.

The temperatures in the slab are based on heat transfer analyses as these are more realistic than an assumption of a linear temperature profile. The simultaneous fire situations with which the travelling fires are compared are the HT analyses from Chapter 5. For each scenario two versions of the structure were modelled; these are referred to as the strong beam (SB) model and the weak beam (WB) model. The cross-sectional area of the steel beams in the SB models was twice that in the WB models. The structural behaviour under

simultaneous heating was previously considered in more detail by Röben et al. [70, 77] and in Chapter 5.

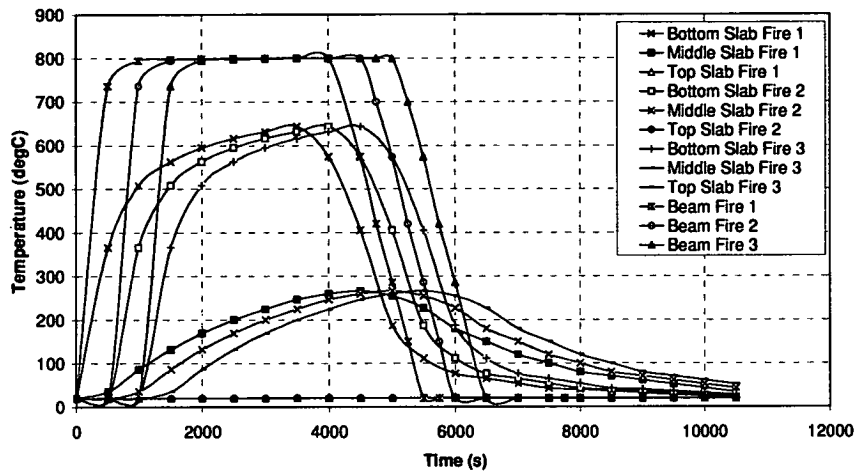


Figure 6-1 – Plot of the time temperature profile of the concrete slabs and steel beams for rapid fire spread between floors.

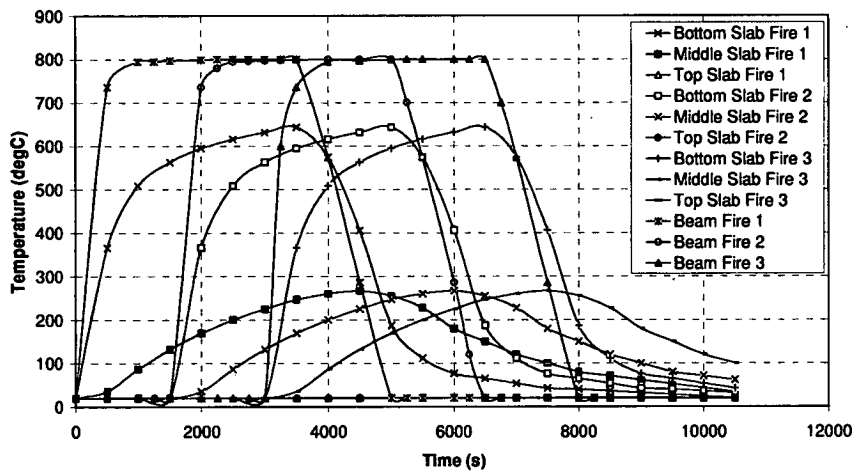


Figure 6-2 – Plot of the time temperature profile of the concrete slabs and steel beams for slow fire spread between floors.

6.2.1. Rapid vertically travelling fire scenario for WB model

This scenario considers a WB model and assumes an inter-floor time delay of 500s. The time interval is in accordance with several sources which suggest flame spread between floors is rapid and may take as little as 5-10 minutes [5]. The total floor section forces are shown in Figure 6-3 for the entire fire duration. Figure 6-4 also shows the total axial forces for the floors but this has been magnified during the heating stage to clarify the complex behaviour. Floor 6 is the first subjected to fire. As the temperature in the steel and concrete increase the floor expands, thus inducing compression. This process results in the column being pushed out, which requires the beams above and below the fire floor to be in tension for compatibility. However, only 500s into the heating phase of floor 6, floor 7 starts to heat and so also develops compression as it expands against the restraint of the column. At around 1000s floor 6 has reached sufficiently high temperatures to deflect rapidly and go into tensile membrane action.

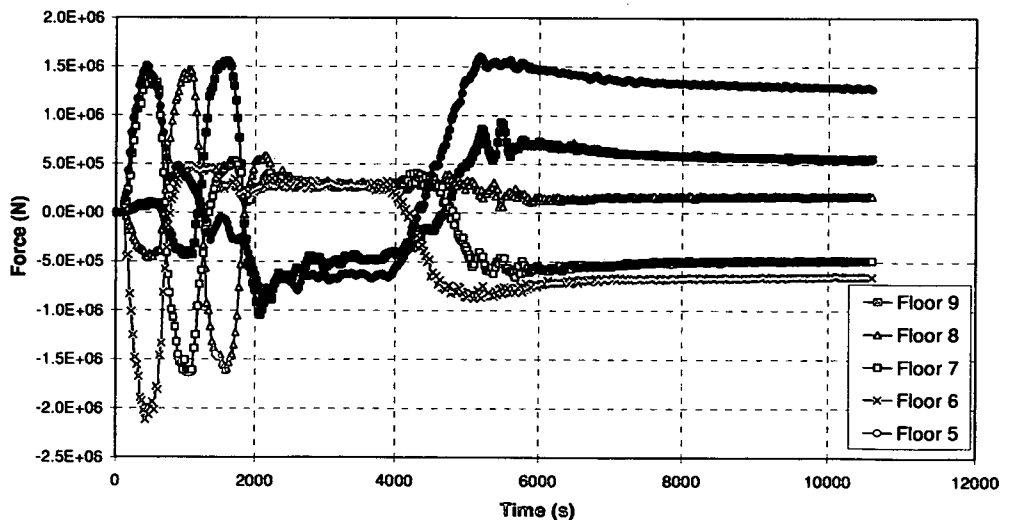


Figure 6-3 – Total axial forces in floors for the WB model with rapid fire spread for the whole fire duration.

This means that although the floor continues to expand, it is now in tension. At this stage floor 8 is also in tension, again for compatibility. At 1000s the heating of floor 8 starts, which is the last of the three fire floors considered here. This floor goes into compression as it expands, causing floor 9 to go into tension. At 1500s floor 7 deflects rapidly and therefore goes into tension. Finally floor 8 also develops large deflections, thus going into tension. Now the three fire floors are all in tension whilst the two floors above and below are in compression as a result of compatibility requirements.

The process described induces a cyclic movement of the column as it is pushed out and pulled back in repeatedly. This is also clear from Figure 6-5 where horizontal displacements of the column at the level of each floor are shown.

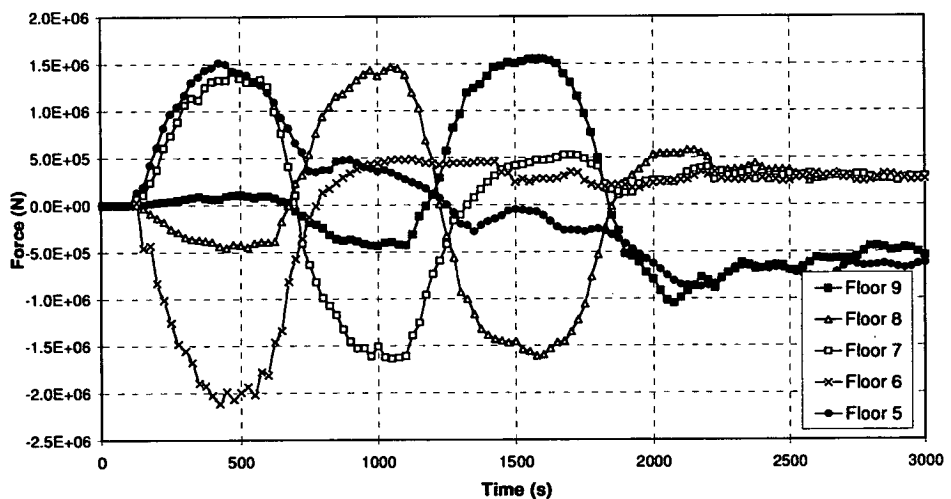


Figure 6-4 – Total axial forces in floors for the WB model with rapid fire spread, shown for the magnification of the heating phase on the right

Once all the floors have gone through this cyclic motion and all three are in tensile membrane action, the forces no longer change significantly until cooling begins. From Figure 6-5 it is also clear that the column is pushed out at all three floors during this

cyclic movement and moves in past its original position only when all three floors are in tensile membrane action.

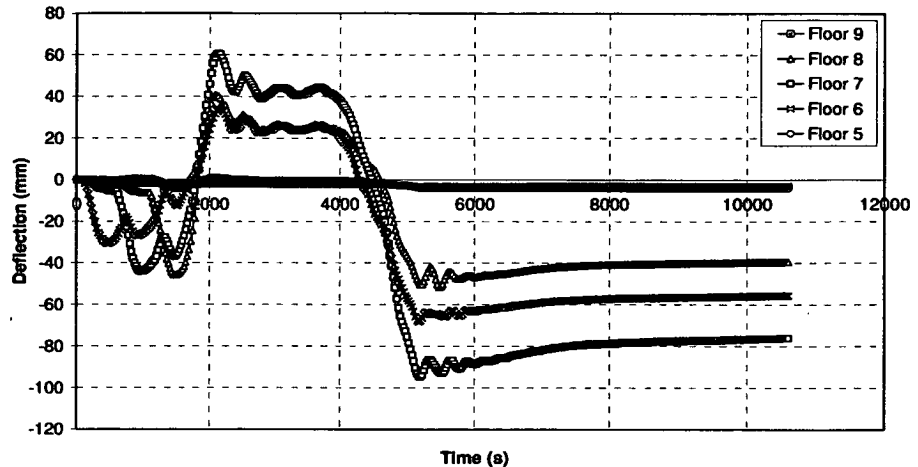


Figure 6-5 – Horizontal displacements of the column at each floor level, WB model

6.2.2. Rapid travelling fire scenario for SB model

The scenario discussed here is the same as in the previous section except the SB model is considered. Initially floor 6 goes into compression as it expands against the column as can be seen from Figure 6-6 which shows the total axial forces of the floors. Figure 6-7 shows the axial forces with a focus on the heating phase. As seen in the WB model behaviour, the floors above and below go into tension. As floor 7 starts heating this too goes into compression. However, the floors are much stiffer than in the previous scenario and do not deflect significantly at these high temperatures but continue to expand. Hence floor 6 does not go into tensile membrane action, which means floor 5 continues to be subjected to high tensile forces whereas these had reduced significantly at this stage for the WB model. When floor 8 starts heating, this behaviour repeats itself and only floors 5 and 9 are in tension as all three fire floors are continuing to expand in compression. This is very

different behaviour from the WB model during heating; however it does compare well with the SB simultaneous three floor fires discussed in Chapter 5.

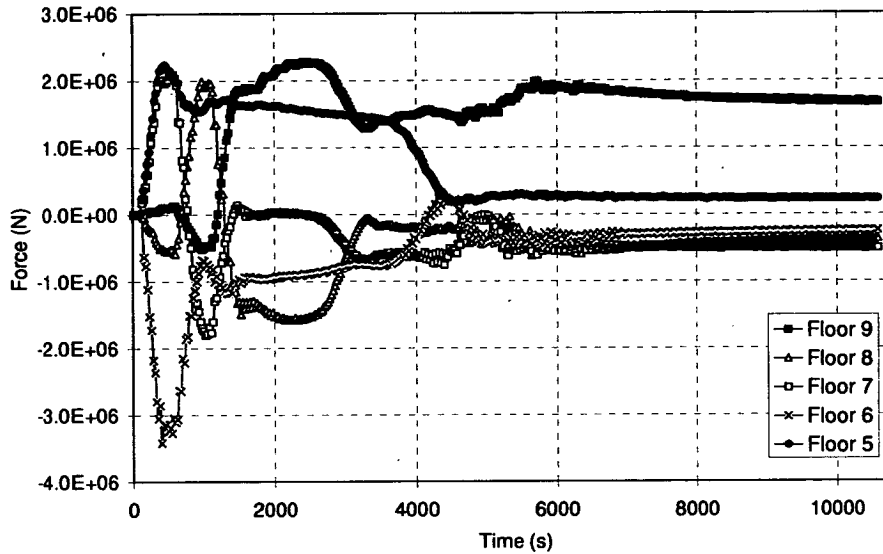


Figure 6-6 – Total axial forces in floors for the SB model with rapid fire spread, whole heating-cooling cycle

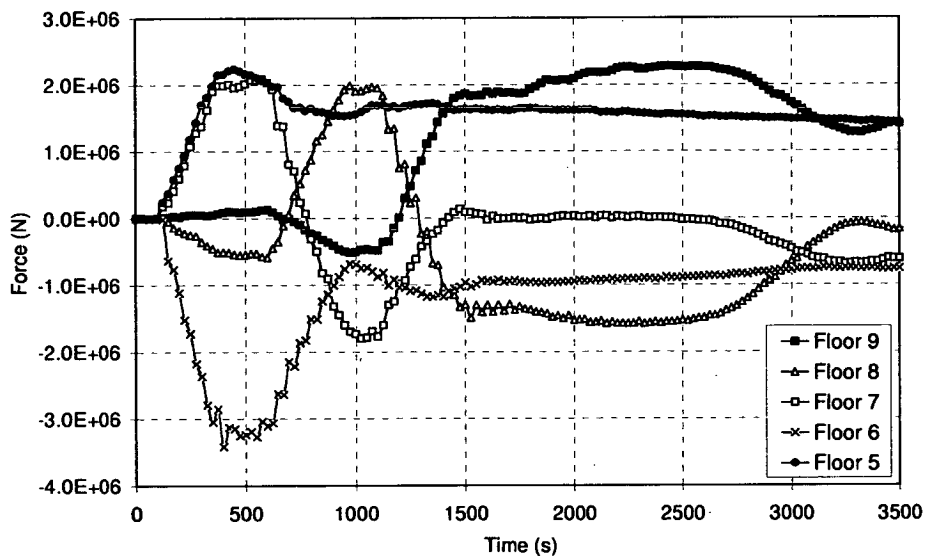


Figure 6-7 – Total axial forces in floors for the SB model with rapid fire spread, magnification of the heating phase

Figure 6-8 shows the horizontal displacements at the column for the 500s spread rate. Once the column has been pushed out by the thermal expansion of the fire floors, it remains there for the duration of the fire. This is very similar behaviour as for the simultaneous fires described in Chapter 5. Clearly the SB model is not significantly affected by a rapid fire spread rate.

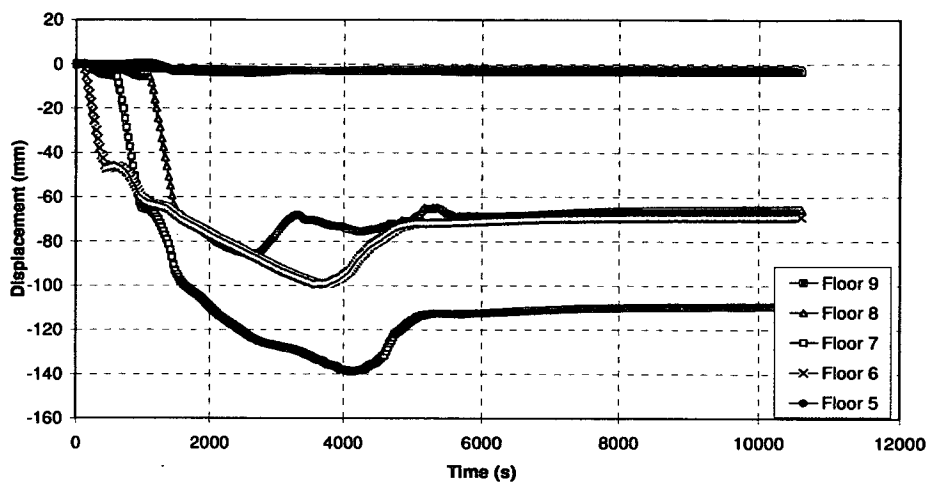


Figure 6-8 – Horizontal displacements for the column at the SB floors for the 500s time interval

6.2.3. Slow travelling fire scenarios

The previous two scenarios assumed an inter-floor time delay of 500s, which may be regarded as representing rapid fire spread. Alternative inter-floor time delays of 1500 and 3500s were also considered. It was found that these slower rates induced very similar behaviour as for the 500s spread rate, for the WB models. However, for SB models a significant difference occurs when changing the inter storey fire speed.

This is most clearly illustrated when comparing the 500s and 1500s models. Figure 6-8 and Figure 6-9 show the horizontal column deflections of the SB model at the level of each floor for both the inter-floor time delay of 500s and 1500s respectively.

In the simultaneous fire and 500s fire spread rate models for the Strong Beam, the fire floors did not deflect downwards significantly as the fire progressed as the expanding floors were able to push the column out. In the 1500s case the column provides more restraint as it is not being pushed out by three floors at once. This additional restraint causes each floor to deflect downwards allowing it continued thermal expansion. This process occurs with each fire floor and therefore induces the same cyclic effect on the movement of the column as was seen in the WB models. The 3500s time delay also results in this behaviour and is therefore not discussed further.

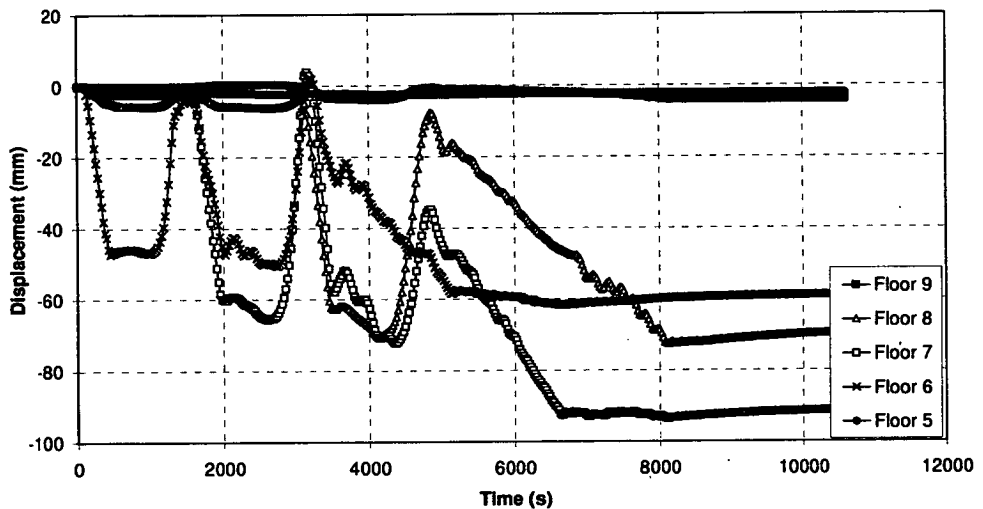


Figure 6-9 – Horizontal displacements for the column at the SB floors for the 1500s time interval

Both the 500s and 1500s models have the cyclic floor forces induced by the thermal expansion of the fire floors. However, this does not lead to cyclic movement of the column for both cases. The SB model subjected to 500s time interval fires resembles the uniform scenario where similar deflections are seen, whereas the column in the 1500s model is affected significantly by these changing forces. It should also be noted that the

final displaced shape is similar, although the maximum values encountered are much higher for the rapid fire spread situation.

6.3. Conclusions

This chapter has discussed the findings of research into structural behaviour during vertically travelling fires in generic, multi-storey, steel-concrete composite structures.

Three fire scenarios were considered as well as two sizes of floor beam.

Currently multi-storey fires are considered during design of buildings when the structural layout would suggest such a severe fire scenario is a possibility. At present a simultaneous fire on several floors is assumed to be the worst case scenario and some work has been done to investigate the effects of such fires on global structural behaviour. Multi-storey fires in real structures however do not normally occur simultaneously on several floors but spread from an initial, single-floor compartment. This situation is currently not considered in design.

There is limited information about the likely rate of fire spread between floors in multi-storey fires. The rates used in this chapter are based on observations from a single multi-storey fire. The most appropriate rate of vertical spread to use in design is currently not known and is likely to depend on the form of construction and the nature of fire. Given these uncertainties it is recommended that designers consider a range of fire scenarios and ensure that structures have sufficient robustness for each. No consideration was given here to differences between internal and external fire spread. It was also assumed that each floor is subjected to a horizontally uniform fire. This is a common assumption in structural fire design. However, horizontally travelling fires would give a more realistic representation of the fire spread through a compartment and research in this area is recommended.

It has been shown that in general neither a simultaneous nor vertically travelling fire can be considered a worse case scenario as they result in different structural responses, either of which may be the most serious. For short inter-floor time delays the structural behaviour was found to be very similar to when fires occur simultaneously on the same number of floors. However, a key difference observed was the cyclic movement induced in columns at each floor level as the fire progressed upwards. This cyclic deflection pattern has not previously been considered when designing against fire. It will be of significance for fire design, particularly for connections which will already have severe demands made on their ductility capacity under fire loading.

With larger inter-floor time delays the global structural behaviour changed. This is particularly clear for the strong beam structure. Whereas with small inter-floor delays, floors expand against the relatively weak column restraint and do not deflect substantially, in the slow travelling fire the cold surrounding columns provide more restraint and large deflections do occur. This has an effect on the overall floor forces in the non-fire floors as well. Cyclic movement of the columns also occurs here, albeit with a larger time interval.

Overall it is therefore clear that travelling fires cause a different load case which is not normally considered in fire design. Different time delays may also affect the global structural behaviour and should therefore be given careful consideration in the design.

7.1. Introduction

Current methods of describing the temperature-time evolution within a fire compartment are based on many assumptions. This leads to a limited applicability to real structures. As described in Chapter 2 large variations of temperature occur even in small compartments which are within the code limitations. In larger compartments, fires which move across the compartment therefore need to be considered to establish what structural behaviour may result when non-uniform heating occurs.

Chapter 4 gives a first indication of the expected behaviour of simplified beams during travelling fires. However, many real structures are composite in that they consist of steel beams and columns as well as a concrete floor slab. Composite behaviour has been researched extensively [13, 60, 78-80] but again mostly during uniform fire conditions. This chapter extends the work presented in Chapter 4 and describes the structural behaviour of composite structures during travelling fires. The details of the travelling fire considered here are in line with more recent research in this field than that which was available at the time the research for Chapter 4 was undertaken.

7.2. Structure

To examine the effects of a travelling fire on composite structures, a finite element model of a composite structure is used. The structure is based on the Cardington Test 1 layout, which was extended from Chapter 3 and 5 to multiple bays. The layout of the structure is shown in Figure 7-1, where the dimensions are indicated.

Four bays are modelled, each 9m by 9m with symmetry conditions around all edges taken at mid-span of the smallest spanning slab distance. The floor section is therefore assumed to be located within an office building, but not near the extremities of the structure. As the travelling fire will induce highly unsymmetrical behaviour it was considered necessary to keep the structure as symmetrical as possible to aid the understanding of the behaviour induced by the fires. The dimensions of the primary beam, secondary beam and concrete slab are shown in Figure 7-2. Only the four central bays are heated (18 by 18m); the surrounding areas are modelled for symmetry and remain at ambient temperature throughout the duration of the fire.

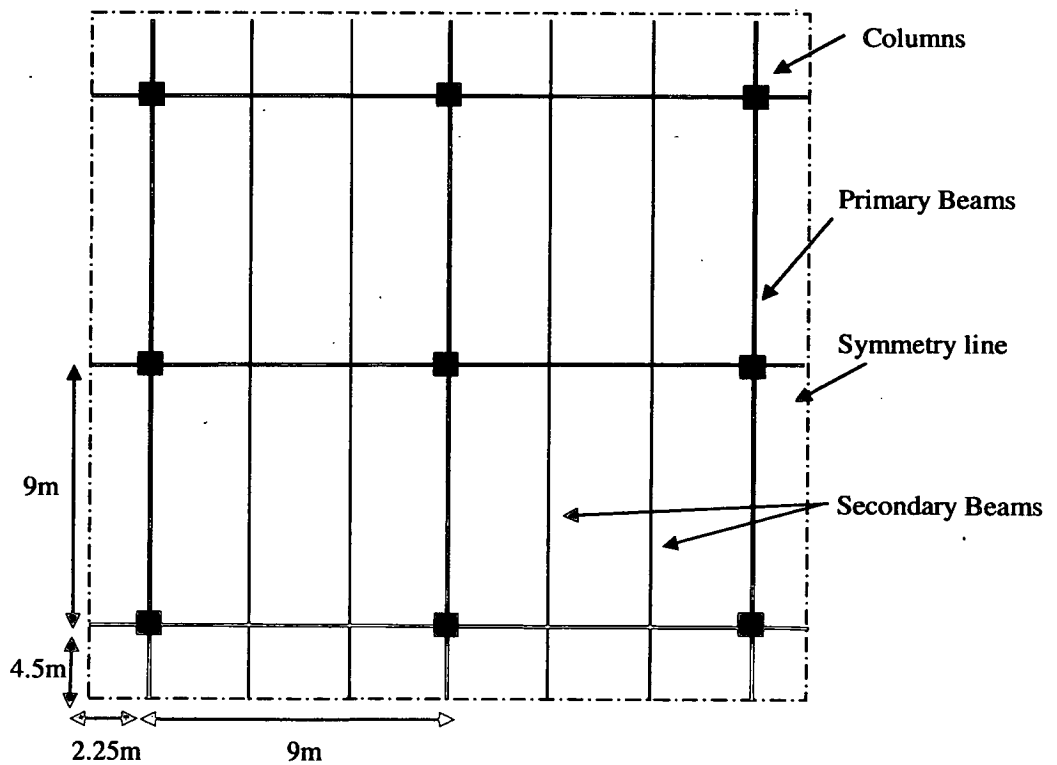


Figure 7-1 – Plan layout of the composite structure

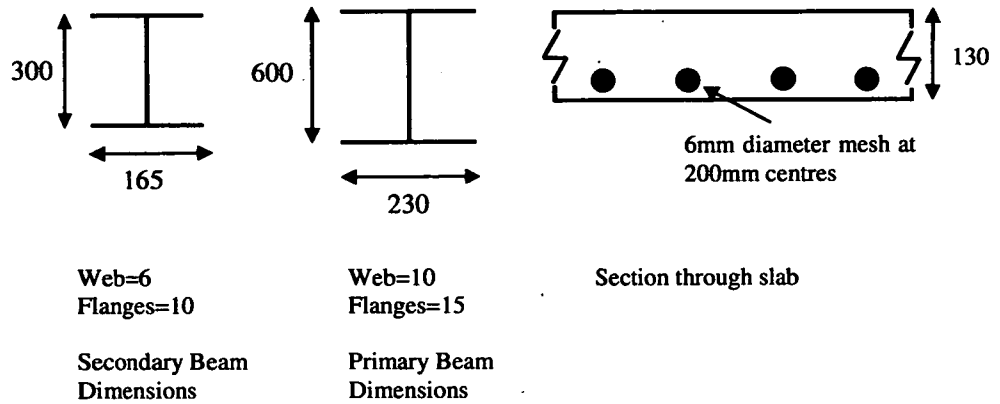


Figure 7-2 – Dimensions of Structural Sections in mm

7.3. Fires

The following section describes the assumed gas temperatures in the various design fires for which the structure is analysed. These include several travelling fires as well as three uniform fires.

7.3.1. Travelling Fires

The manner in which travelling fires should be characterized is still being developed and some recent progress has been made [25, 26, 65]. In Chapter 4 it was appropriate to apply simple, representative forms of temperature loading to a beam in the form of triangular patches. This approach had the advantage of allowing the underlying mechanics to be readily identified. This very simple form of temperature profile is not adopted for the composite section considered in this

chapter, as a more realistic temperature distribution in travelling fires has since been developed.

The gas temperature evolutions considered here represent the fire scenarios described by Rein and Stern-Gottfried [25, 26] which is described in some detail in Chapter 2. Rein suggested there would be an area of 'near field' temperatures in the area in which the burning is occurring and the gas temperature here is assumed to be equal to the flame temperature. The near field only incorporates a percentage of the floor area and moves across a compartment until the entire fuel load has been consumed. The remainder of the compartment is subjected to a 'far field' temperature which results from hot gases. The far field temperature depends on the size of the fire. As described in Chapter 2, each area of the compartment is subject to near field temperatures for a constant time. This time depends on the fuel load density and the heat release rate per unit area, which for a standard office fire equates to 19 minutes [26]. This is based on the assumption that the fuel load is evenly distributed across a compartment. The near field temperature is more or less constant at 1200 to 1300°C for an office fire and for these analyses is assumed to be constant at 1200°C.

The far field temperature is highly dependent on the compartment considered. As the distance away from the fire increases, the gas temperature decreases. This relationship can be described by the ceiling jet correlation by Alpert [81] in Equation 7-1.

$$T_{\max} - T_{\infty} = \frac{5.38 \left(\frac{\dot{Q}}{r} \right)^{2/3}}{H} \quad (7-1)$$

where T_{max} is the maximum ceiling jet temperature (K), T_{∞} is the ambient temperature (K), \dot{Q} is the total heat release rate (kW), r is the distance from the centre of the fire (m) and H is the floor to ceiling height (m).

This equation is used to obtain the far field temperatures only, as the near field temperatures are assumed to be constant. It will give a complex temperature distribution away from the near field, an example of which is shown in Figure 7-3. As described by Stern-Gottfried [26] it is desirable to approximate this by a single characteristic temperature value, T_{ff} , as this simplifies the input into the structural analysis. To obtain T_{ff} the far field temperature is taken as the fourth-power average of T_{max} . The fourth-power average is calculated to favour high temperatures in a bias towards radiation heat transfer and worst case conditions [26]. The temperature is calculated over the full far field length, ranging from r_{nf} to r_{ff} representing the distance between the end of the near field temperature and the end of the far field.

$$T_{ff} = \frac{\left[\int_{r_{nf}}^{r_{ff}} (T_{max})^4 dr \right]^{1/4}}{(r_{ff} - r_{nf})^{1/4}} \quad (7-2)$$

To illustrate how the Alpert curve and the T^4 average compare, these are both plotted in Figure 7-3 for a typical case. It can be seen the temperatures predicted by the Alpert curve have been capped at 1200°C as this is the assumed flame temperature and thus cannot be exceeded. Temperatures exceeding 1200°C are not considered in the T^4 average calculation, but instead taken as this peak value. The total far field length is taken as 18m, which is the equivalent of the compartment size considered here.

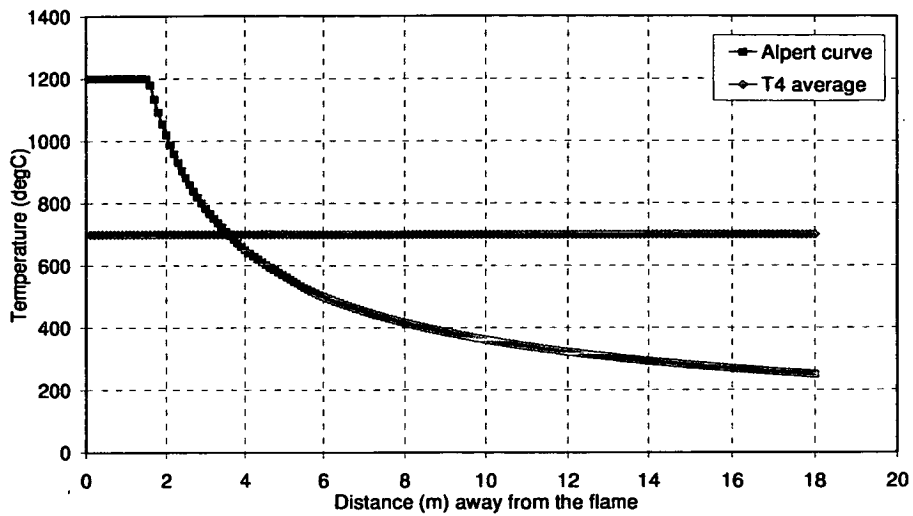


Figure 7-3 – Alpert curve and T^4 average comparison a typical case

Based on the structural layout described in section 7.2 and this approach to defining travelling fires, a family of fires can be created. As the near field temperature is constant for all scenarios, only the far field temperatures are calculated. Figure 7-4 shows the family of fires specific to the structure considered. From this it can be seen that the fires where a larger percentage of floor is burning at a time, the shorter the duration of the fire and the hotter the far field. This is also given in tabular form (Table 7-1) where the total fire duration and far field temperatures are shown to vary significantly depending on the percentage of floor burning.

The cases of 25, 33, 50 and 100% are considered for these analyses. This represents a reasonable range of fire sizes; any smaller than 25% and the fire would be unrealistically small for this compartment. As this is an initial attempt at

modelling the behaviour of a structure under these travelling fire conditions, some assumptions had to be made.

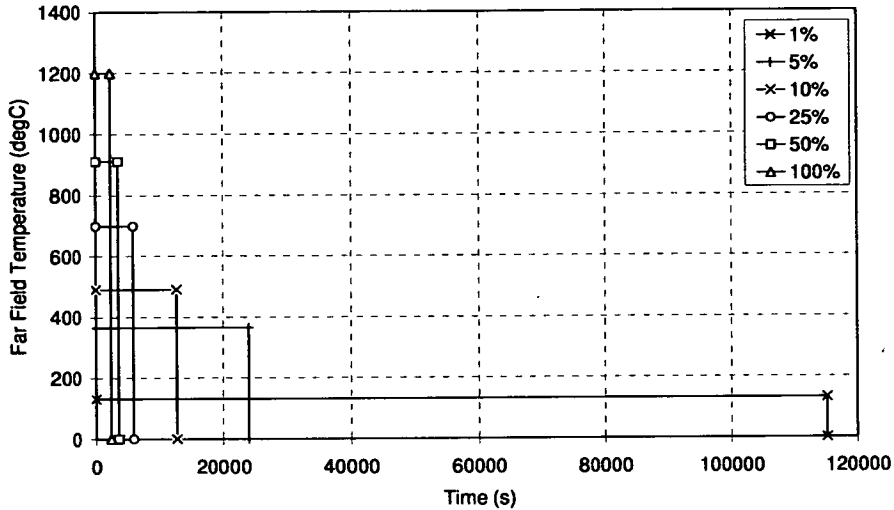


Figure 7-4 – Family of fires (far field temperatures) for the considered fire compartment

Table 7-1 – Family of Fires for the analysed structure

Percentage floor burning (%)	Total Fire Duration (s)	Far Field Temperature (°C)
1	115140	132
5	23940	365
10	12540	491
25	5700	700
33	4560	780
50	3420	911
100	2280	1200

For the purpose of calculating the far field temperatures, the length of the far field is taken as 18m, i.e. the entire length of the compartment. The near field is assumed to be completely outside of the compartment at time 0, before it moves across the compartment burning for 19 minutes at each location and then moving completely off the edge of the compartment by the time the fire is finished as is shown in Figure 7-5. This assumption allows for the fire to be moved onto the compartment gradually, rather than starting with the near field temperature on part of the compartment at $t=0$.

The total duration of the travelling fire is therefore equal to the time it takes for the entire floor area to burn for 19 minutes plus an additional 19 minutes for the near field to move on and off the compartment. Using this method also allows for an additional time for the development stage of the fire, which is ignored in the original fire as defined by Rein [65]. The fire durations shown in Figure 7-4 and Table 7-1 include these times.

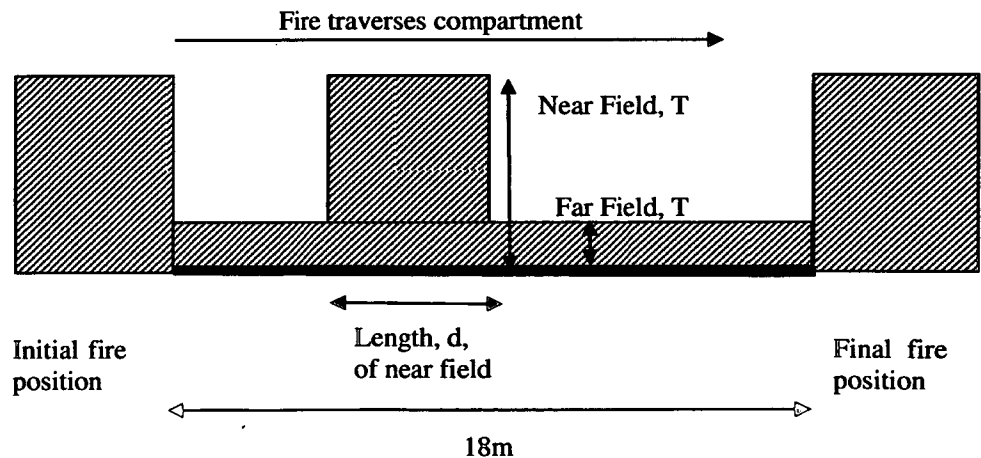


Figure 7-5 – Definition of fire loading

While cooling and heating occur simultaneously during a travelling fire, once the entire compartment has burned out, the temperature will return to ambient from the far field values. One major shortcoming of the temperature definition by Rein and Stern-Gottfried is that no assumption is made regarding this cooling phase. It is therefore assumed here that ambient gas temperatures are reached shortly after the compartment has completed the full travelling fire cycle. The cooling phase in the structure is modelled for 2 hours (7200 seconds) beyond this time the temperatures in the slab have also returned to near-ambient values. This allows for a more reasonable comparison with uniform fires (below); the parametric fire in particular, which also includes cooling.

It is assumed the near field fire moves across the compartment along the path indicated in Figure 7-6. The fire is uniform along the y-axis and varies along the x-axis as shown. The width of the fire (d) as indicated in the figure, changes depending on the particular travelling fire case considered.

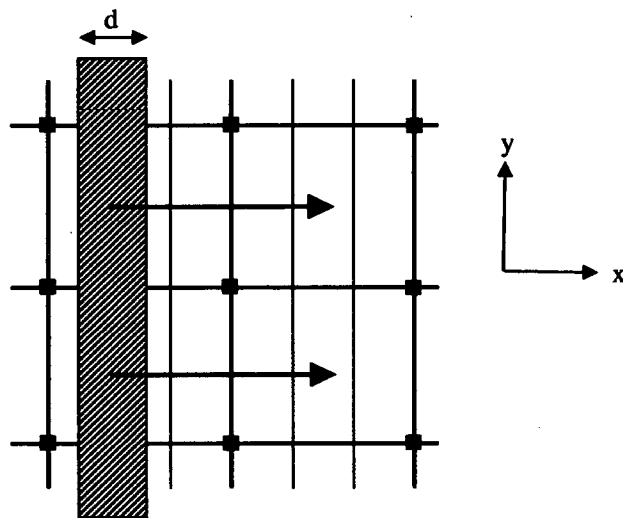


Figure 7-6 – Path of travelling fire

7.3.2. Uniform Fires

To compare the behaviour of a structure when subjected to travelling fires, uniform fires need to be considered. Three uniform fires are modelled. Firstly a constant temperature of 1000°C is assumed. Secondly a Standard Fire (SF) is considered (ISO 834 [9]) and lastly a Parametric Fire. All these fires are assumed to continue for 12500s. Although this is an unrealistically long period of time for a uniform fire, the duration is extended to ensure no critical behaviour is missed for the purpose of comparison.

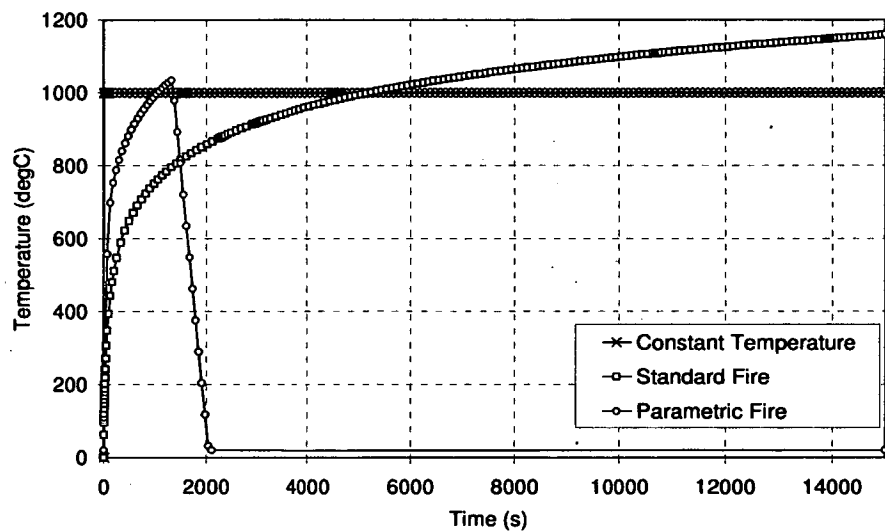


Figure 7-7 – Temperature evolution of three uniform fires

The 'constant temperature' fire and SF do not include a cooling phase. For the Parametric Fire the compartment dimensions have to be considered to determine an appropriate temperature evolution for the specific structure. This is calculated based on the recommendations in Annex A of Eurocode 1 [9], with an assumed 25% openings contributing to ventilation and a compartment height of 4m. The

fire reaches a peak temperature of 1034°C after 1320 seconds and cools linearly until the gas temperature has returned to ambient after a total of 2100 seconds. Figure 7-7 shows the gas temperature-time curves for all three uniform fires.

7.4. Modelling

7.4.1. Structure

The structure described in section 7.2 is modelled with the Abaqus Finite Element software. All models are subjected to gravity loading and an imposed load of 5kN/m² representing a generalised office load. [82]. Figure 7-8 shows the layout Abaqus model of the beams. The beams are modelled by beam elements; however they are shown in the figure as the I-section each beam element represents in the analysis. The slab is also modelled but is not visible in this image to show the beam layout more clearly. The slab is modelled by shell elements. It has a uniform thickness and the steel deck has been omitted from the finite element model; both are common assumptions [13, 59] to simplify the modelling of the section. Rebar is modelled in the section as a ‘smeared’ layer with an equivalent area of steel.

The beams and concrete slab are connected using tie constraints. Symmetry boundary conditions were applied around all edges of the structure. The columns are not explicitly modelled; instead the slab is fixed where columns would be present. Material behaviour was taken to be elasto-plastic and typical of a mild steel with a yield strength of 355MPa. Stress-strain relationships and thermal properties are taken from Eurocode 3 [54]. The stress-strain relationship for concrete in compression is as shown in Figure 5-4 but fully ductile concrete is

assumed in tension as shown in Figure 7-9. The material properties are temperature dependent apart from the tensile concrete strength.

The numbering of the primary and secondary beams, which will be used throughout this chapter, is shown in Figure 7-10.

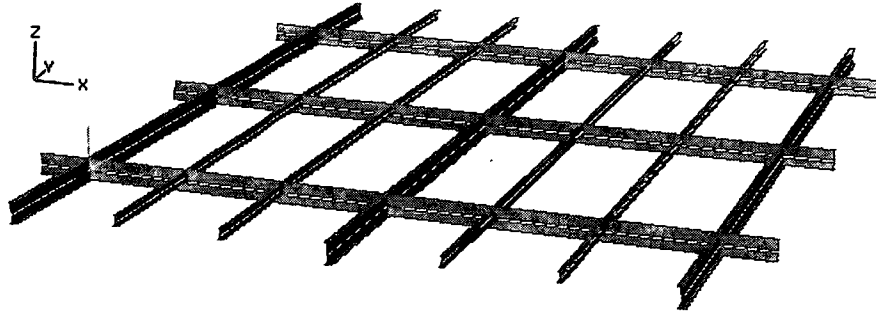


Figure 7-8 – Abaqus view of primary and secondary beam layout

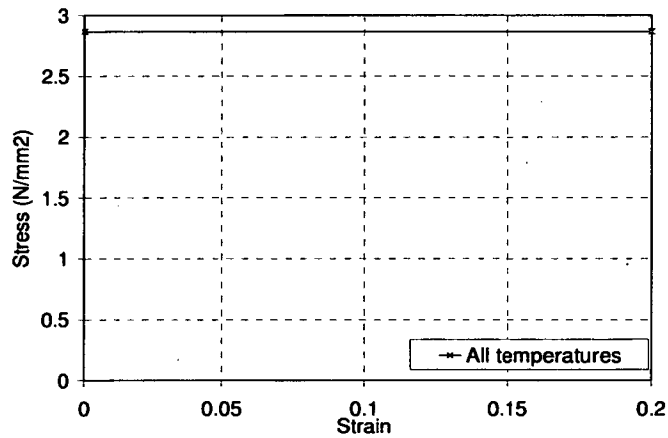


Figure 7-9 – Tensile stress-strain relationship of concrete

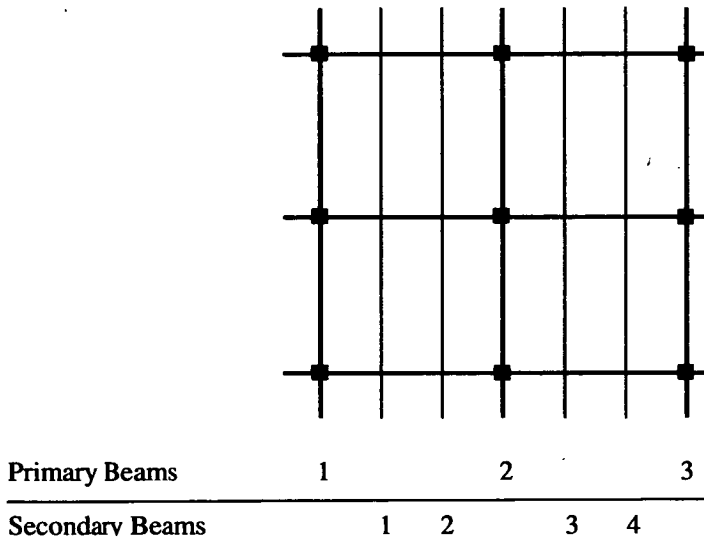


Figure 7-10 – Numbering of primary and secondary beams

7.4.2. Structural Temperatures

The following section describes how the structural temperatures are obtained based on the gas temperature definitions assumed in section 7.3.

Travelling Fires

To obtain the structural temperatures based on the gas temperature definitions described for travelling fires, user subroutines were created with FORTRAN. These subroutines describe the gas temperatures varying with time and location and are compatible with the Abaqus software thus allowing more complex heating scenarios to be applied than is otherwise possible. These subroutines are referred to in the Abaqus input and define all aspects of the temperature field, including the length and peak temperature.

The analysis has to be separated into two parts; a heat transfer to obtain the slab temperatures and a mechanical analysis where the steel temperatures are read in directly from a subroutine as the steel is assumed to closely follow the gas temperature. A separate heat transfer analysis has to be done for the slab as the non-uniform heating will result in quite a complex temperature distribution. The subroutine defining the gas temperatures is therefore modified to suit a heat transfer analysis by defining the flux. The gas temperatures are calculated as for the steel temperatures and from these values the radiative and convective heat flux components are calculated. These equations are given in Chapter 5, section 5.3.2. The temperature output from the heat transfer analysis is then read directly into the structural analysis where the temperature subroutine for the steel beams is also applied. An example of both user subroutines can be found in Appendix B2.

As in previous chapters, the steel beams are assumed to be unprotected and closely follow the gas temperature. However, a small gradient is modelled through the steel sections. Temperatures in Abaqus beam elements are defined at 5 points, which are shown in Figure 7-11. Also indicated in this figure are the gradients by factors giving the relative value of the temperatures that will be applied.

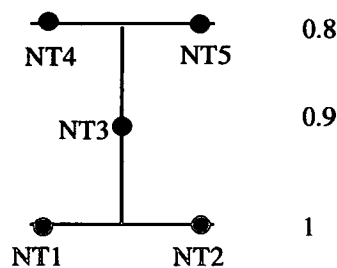


Figure 7-11 – I-beam cross-section with temperature points and gradients indicated

The bottom flange is the hottest (temperature points 1 and 2) and the temperature is lowest in the top flange (temperature points 4 and 5) which is connected to the slab. It is generally accepted that a gradient through a steel beam is accurate; this is also observed in fire tests where the temperature in the beams is monitored, such as in the Cardington Tests [19].

The steep temperature difference between the near field and far field areas causes numerical issues in the smaller fire sizes. The subroutine for the steel temperatures was therefore altered slightly to simplify the numerical analysis. This is done by introducing a slope which eliminates the sudden jump in temperature and allows for a more gradual increase. In reality, the steel temperature will not increase instantly with the gas temperature but more gradually, in a similar way to the temperature distribution in the concrete slab. Modelling a linear increase in temperature for part of the near field incorporates this delay in temperature rise during the heating phase. The slab temperatures are still based on the original temperature profile as suggested by Rein and Stern-Gottfried [25, 26].

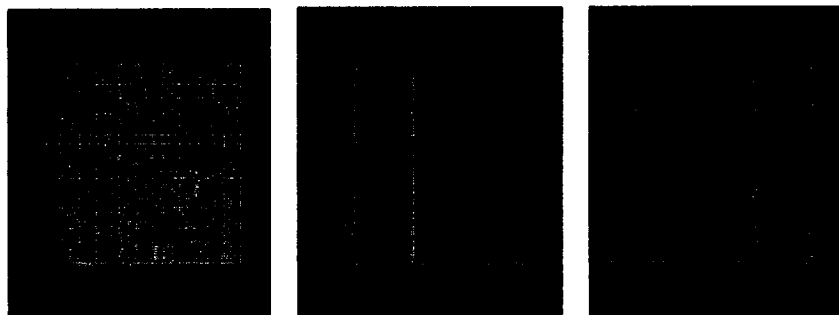


Figure 7-12 – Temperature in the slab for 25% travelling fire scenario at times 500s, 2000s and 4500s respectively

A visual example of the how the temperatures develop in the slab is shown in Figure 7-12 for the case of a 25% travelling fire. The colours indicate the temperature range, where the red colour indicates the near field temperature which can be seen moving across the slab.

Figure 7-13 shows the temperature of primary beam 2 for two of the travelling fires scenarios. Primary beam 2 is in the middle of the compartment and therefore will be at its peak temperature exactly halfway through the fire duration. Figure 7-13 shows that the far field temperatures differ, whilst the near field temperatures are identical. It is also clear that the total duration for which the beams are heated to near field temperatures is identical for each scenario; 19 minutes or 1140 seconds.

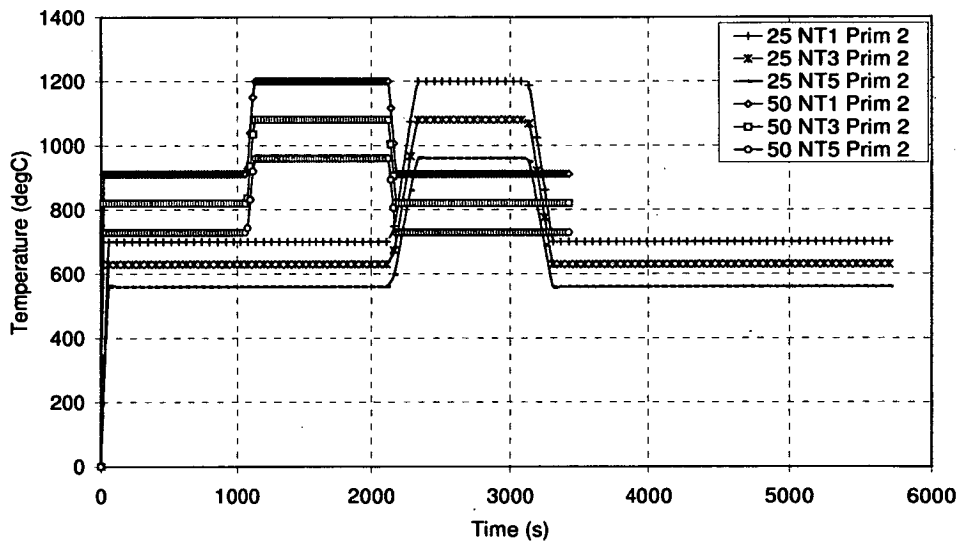


Figure 7-13 – Steel temperature in primary beam 2 for two travelling fire scenarios at points shown in Figure 7-11

This temperature plot is with respect to real time which is why for each analysis the total time is different and the near field temperatures are reached at a different

time. If the time were normalised however, as shown in Figure 7-14 the peak temperatures occur simultaneously. The duration of the near field now also relates to the travelling fire case, i.e. the near field temperature area for the 50% case has twice the length of the 25% case fire, etc. It should be noted that real time is only of importance when considering the heat transfer analysis as this is dependent on the duration of the fire. Although the steel temperatures could be applied over an arbitrary time, all analyses consider real time to accurately include the slab heat transfer.

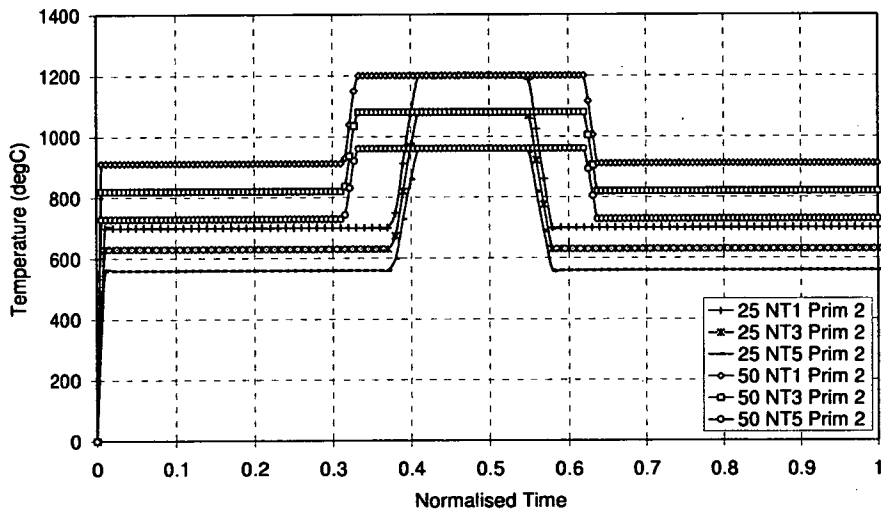


Figure 7-14 – Steel temperature in primary beam 2 for various travelling fire scenarios with respect to normalised time at points shown in Figure 7-11

The temperatures through the slab are plotted at three different locations in the compartment in later figures. These three locations are indicated in Figure 7-15. At each location the temperatures are plotted at five points through the depth of the slab, which are shown in Figure 7-16. The notations in these two figures are also used in the temperature graphs.



Start Middle End

Figure 7-15 – Plan view of the compartment with heated area in lighter colour.

Locations of slab temperature output points indicated

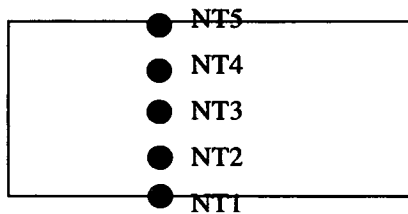


Figure 7-16 – Location of temperature points through the depth of the slab

The temperatures in the slab obtained through a heat transfer analysis are plotted in Figure 7-17. Only the 25% travelling fire case is shown here. All locations immediately begin to increase in temperature as the entire slab is subjected to fire, whether near or far field temperatures. Initially the near field is at the start of the slab. The high local temperatures lead to a rapid increase locally. The remainder of the slab is subjected to the far field and the temperature rise is therefore much slower.

As the near field fire moves away from the 'start' location the temperatures at the bottom of the section reduce. The temperatures at the remaining points through the depth of the slab continue to increase as the far field remains active at the 'start'

location and this far field temperature is higher than the values reached in the slab thus far. As the fire moves on and reaches the 'middle' slab location temperatures here also start to increase rapidly. This repeats itself again at the 'end' location. What should also be noted is that the slab temperatures reached towards the right of the slab will be higher than those near the left of the slab as this is subjected to heating for a longer period of time. Note that NT5 (temperature at the top of the slab) is not plotted in this graph as these are almost identical to NT4.

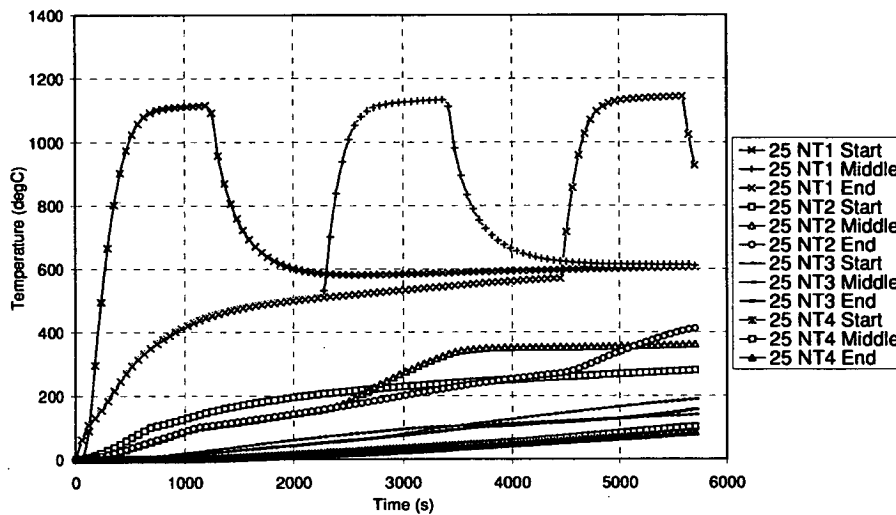


Figure 7-17 – Concrete temperature in the slab for 25% travelling fire case

Figure 7-18 considers two travelling fire scenarios and compares the slab temperatures for each case with respect to normalised time. Only the bottom slab temperatures for both the 25% and 50% travelling fires are plotted. It is interesting to note that the maximum temperatures reached at the bottom of the slab do not change significantly depending on the fire size; at other locations through the section a greater difference occurs. The trend for both scenarios is identical at each

location with the main difference being the far field temperature which affects the slab temperature when it is not subjected to the near field fire.

The fire duration is extended to include a cooling phase (7200s) which occurs once the near field temperatures have moved off the compartment. For the heat transfer analysis of the slab gas temperature is assumed to return to ambient (20°C) immediately. The steel temperature definition incorporates a cooling gradient which is identical to that calculated for the parametric fire (as described in section 7.3.2). The duration of cooling will therefore be slightly different for each travelling fire case (ranging from 520 to 900s for 25% and 100% respectively) but the temperature gradient is identical.

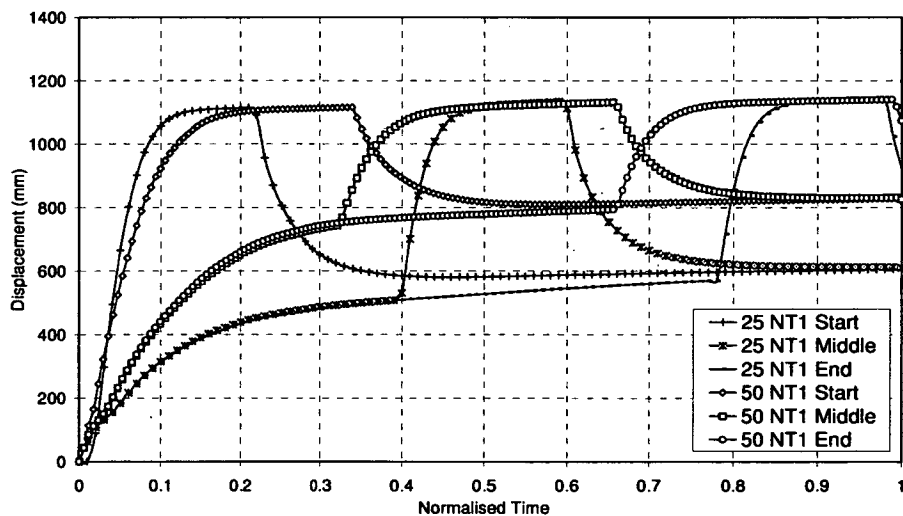


Figure 7-18 – Concrete temperature in the slab for 25% and 50% travelling fire case, bottom slab temperatures only

location and this far field temperature is higher than the values reached in the slab thus far. As the fire moves on and reaches the 'middle' slab location temperatures here also start to increase rapidly. This repeats itself again at the 'end' location. What should also be noted is that the slab temperatures reached towards the right of the slab will be higher than those near the left of the slab as this is subjected to heating for a longer period of time. Note that NT5 (temperature at the top of the slab) is not plotted in this graph as these are almost identical to NT4.

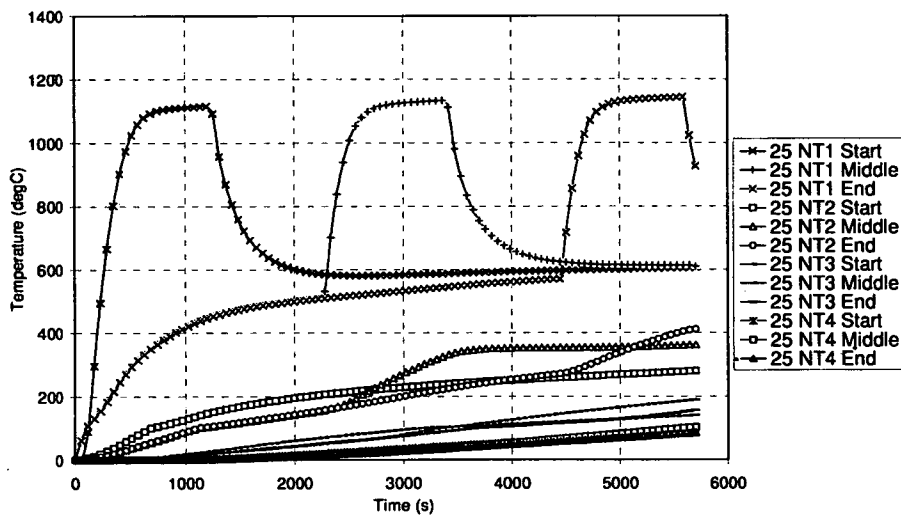


Figure 7-17 – Concrete temperature in the slab for 25% travelling fire case

Figure 7-18 considers two travelling fire scenarios and compares the slab temperatures for each case with respect to normalised time. Only the bottom slab temperatures for both the 25% and 50% travelling fires are plotted. It is interesting to note that the maximum temperatures reached at the bottom of the slab do not change significantly depending on the fire size; at other locations through the section a greater difference occurs. The trend for both scenarios is identical at each

location with the main difference being the far field temperature which affects the slab temperature when it is not subjected to the near field fire.

The fire duration is extended to include a cooling phase (7200s) which occurs once the near field temperatures have moved off the compartment. For the heat transfer analysis of the slab gas temperature is assumed to return to ambient (20°C) immediately. The steel temperature definition incorporates a cooling gradient which is identical to that calculated for the parametric fire (as described in section 7.3.2). The duration of cooling will therefore be slightly different for each travelling fire case (ranging from 520 to 900s for 25% and 100% respectively) but the temperature gradient is identical.

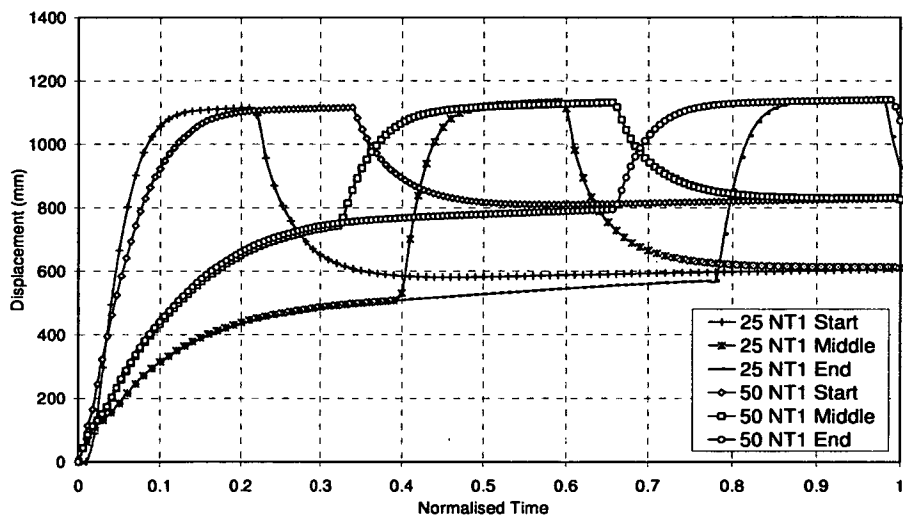


Figure 7-18 – Concrete temperature in the slab for 25% and 50% travelling fire case, bottom slab temperatures only

Uniform Fires

Figure 7-19 and Figure 7-20 show the temperature evolution in the concrete for all of the uniform fires. They show that the concrete temperatures reach substantial values after 12500s of the Standard and Constant Fires (circa 250°C on top surface). The Parametric fire includes a cooling phase and the concrete temperatures therefore return to near ambient values.

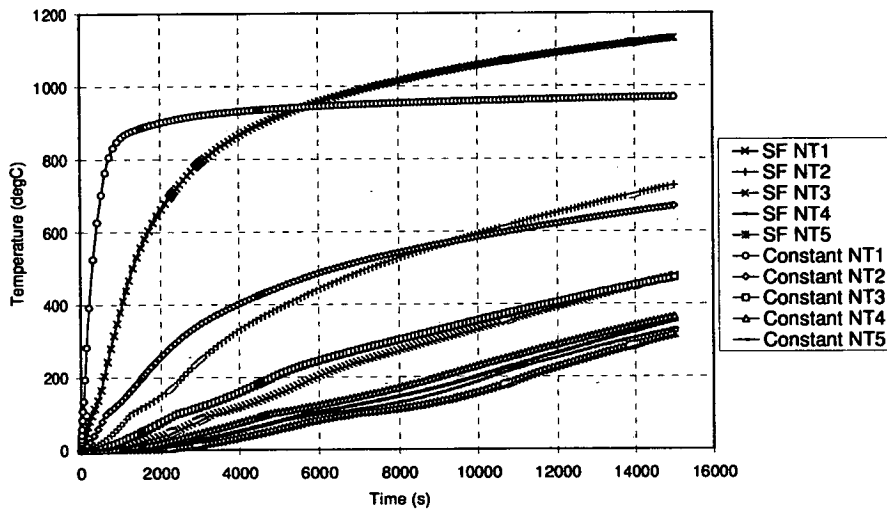


Figure 7-19 – Concrete temperature evolution based on the standard fire (SF) and constant temperature fire cases

To aid the numerical modelling for the parametric fire scenario an additional assumption was made for the steel temperature. Rather than taking the steel temperature as equal to the gas temperature during the cooling phase, the steel cools more gradually. Figure 7-21 gives a plot of the steel and gas temperature assumed in the parametric fire. It shows that the steel follows the gas temperature during heating and during the early stages of the cooling phase. Once the steel has reached 300°C the cooling of the steel slows down and linearly reduces over the

remaining time. The steel has regained most of its strength at this stage and so this changed cooling gradient does not significantly affect the structural behaviour. The temperature of the slab remains based on a heat transfer analysis with the original gas temperature cooling branch.

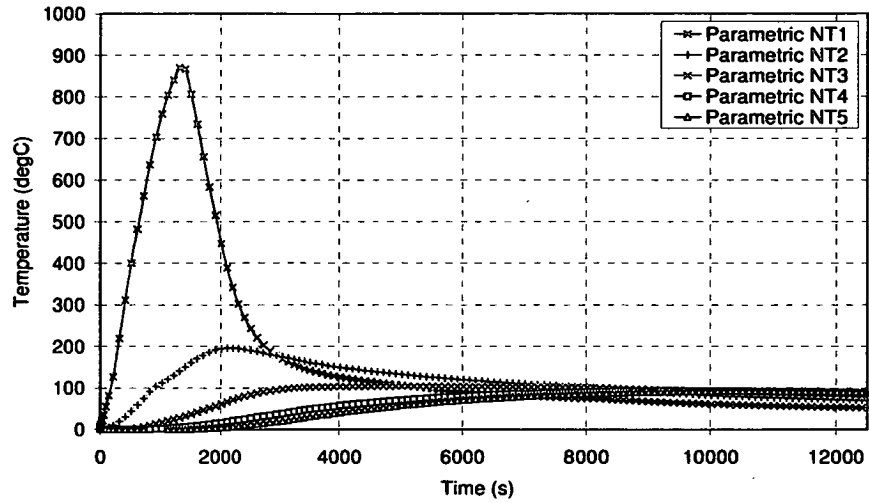


Figure 7-20 – Concrete temperature evolution based on Parametric fire case

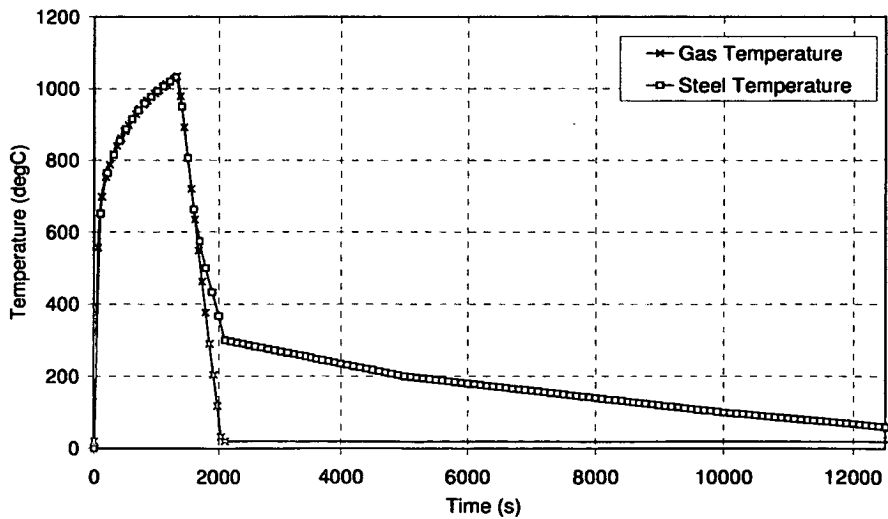


Figure 7-21 – Gas and steel temperature for the parametric fire

7.5. Results

This section presents predictions of structural behaviour based on the heat transfer models and fire scenarios detailed in the previous sections. Firstly the results are described for the uniform and travelling fires separately. These are then compared and finally the behaviour during the final cooling stage is considered.

Some of the displacement output in the following sections is shown along a path as indicated in Figure 7-22. This path goes across the entire length of the structure and crosses the centre of the bays where the peak displacements will occur.

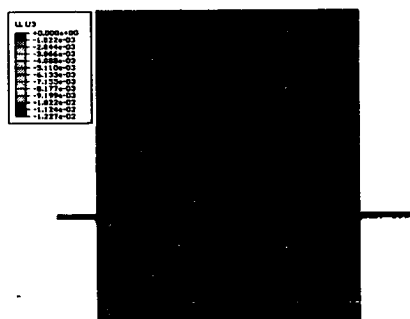


Figure 7-22 – Location of path across the slab along which results are plotted

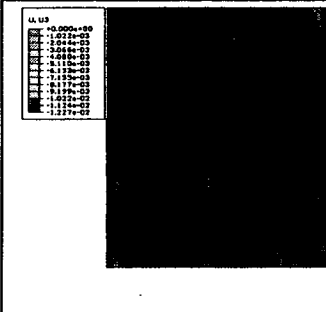
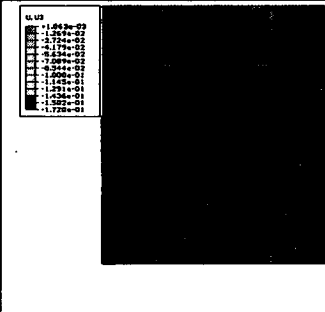
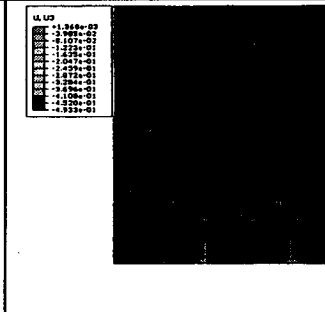
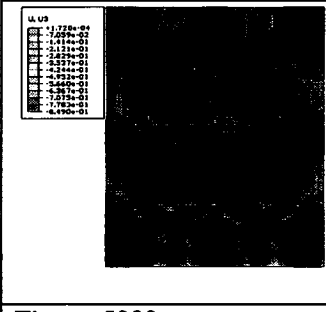
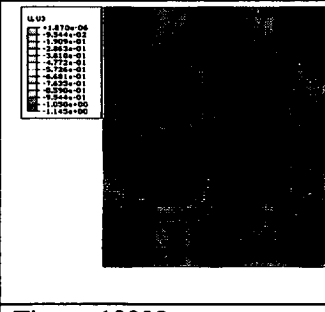
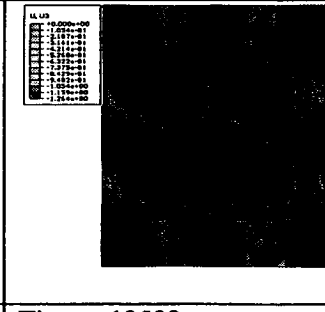
7.5.1. Uniform Fires

Three uniform fires are considered. All uniform fires take 12500s. The three time-temperature evolutions are described and shown in Section 7.3.2.

Table 7-2 shows the displacement evolution for the Standard Fire. As the temperature is applied uniformly the displacement is symmetrical in both directions. As the temperature increases the deflections also increase. The plot is for the standard fire, but the response to the constant fire and parametric fire is

identical in principle (although the parametric fire displacements recover some what during the cooling phase). Figure 7-23 compares the maximum vertical displacement for the SF and constant temperature scenarios. The constant temperature case deflects more rapidly to begin with but the standard fire ends up with a larger overall displacement. This can be explained by looking at the temperature evolution for each case; the constant temperature causes rapid heating at the early stages, but the standard fire reaches much higher temperatures towards the end of the analysis (both in the steel and concrete) thus leading to larger displacements.

Table 7-2 – Standard Fire displacement pattern

		
Time = 0s	Time = 200s	Time = 1000s
Max. Displ. =12mm	Max. Displ. =173mm	Max. Displ. =493mm
		
Time = 5000s	Time = 10000s	Time = 12500s
Max. Displ. =849mm	Max. Displ. =1145mm	Max. Displ. =1264mm

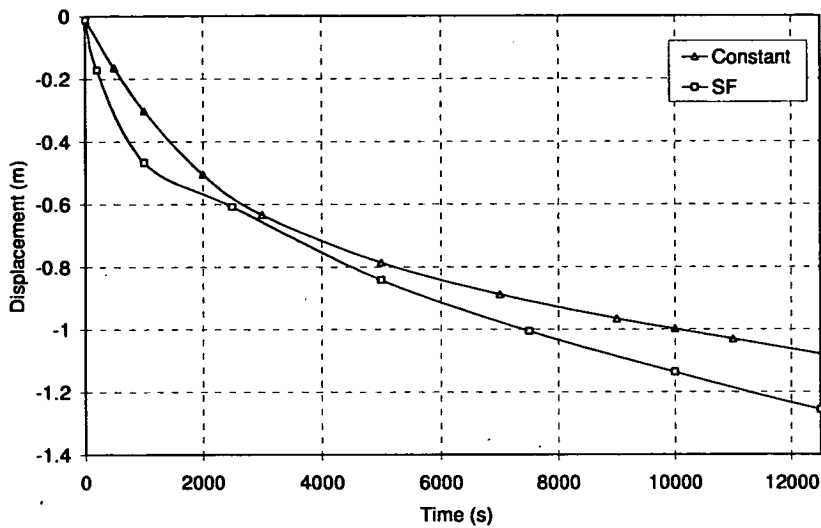


Figure 7-23 – Peak vertical displacement during uniform fires

Figure 7-24 shows the vertical displacement of the steel beams in the parametric fire. Due to symmetry, primary beam 3 and secondary beams 3 and 4 are not included in the graph. Substantial displacements occur during the heating phase. As cooling begins all beams show some recovery; the primary beams more so than the secondary beams. Once the temperatures in the steel remain more or less constant (from 2100s onwards) very little movement is observed. The concrete slab remains hot and continues to expand even though the steel beams are contracting. The concrete is clearly dominating the behaviour, which is also why the larger primary beams recover more than the smaller secondary beams which have less axial capacity. Similar behaviour was observed in Chapter 5 where the behaviour was also dominated by the concrete, especially for the ‘weak beam’ model. Figure 7-25 shows the section forces in the primary and secondary beams

for the uniform fire cases. For all three scenarios the beams initially go into compression as they are heating and expanding.

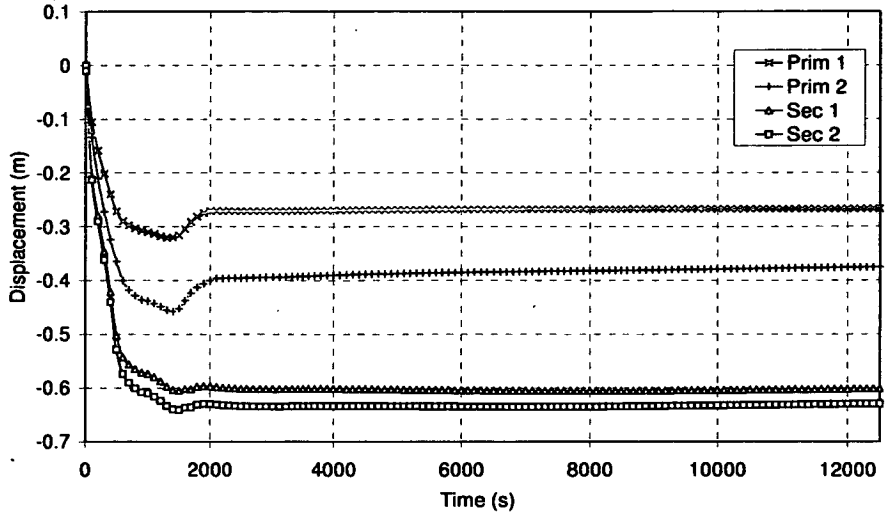


Figure 7-24 – Vertical displacement of steel beams in the parametric fire

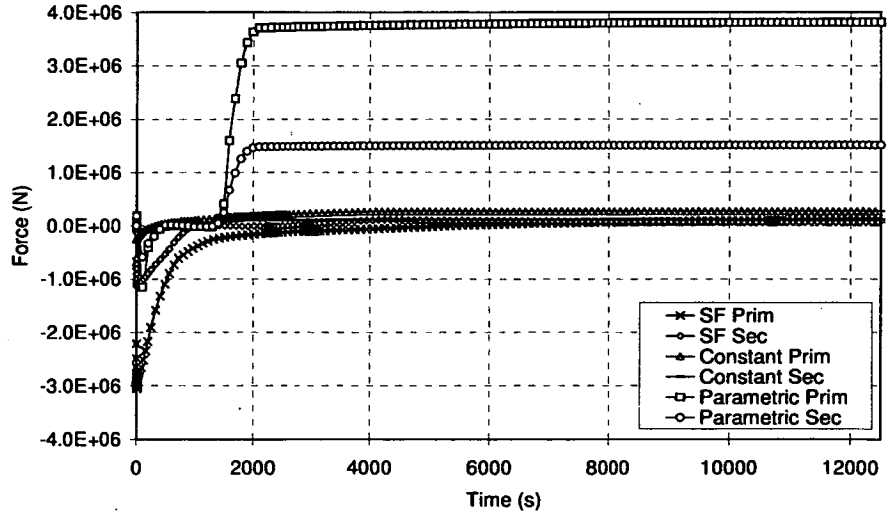


Figure 7-25 – Section force in primary and secondary beams for uniform fires

For the uniform fires which do not include cooling, the overall behaviour is almost identical. As large displacements begin to form, the forces in the steel beams also suddenly reduce and remain more or less constant, either just in tension or still with a very small constant compressive force. The parametric fire scenario also starts with large compressive forces in both primary and secondary beams in a similar way to the other two uniform fires. These then reduce as the sections lose strength and large displacements occur, before becoming tensile as the steel cools rapidly. This leads to very large tensile forces, similar to that observed in the 1D beams analysed in Chapter 3. The forces in the primary beams are larger than those in the secondary beams as these have a smaller capacity.

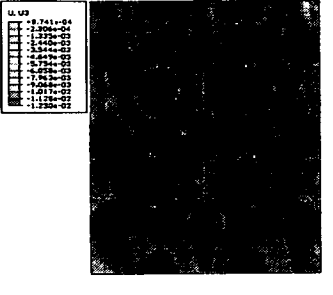
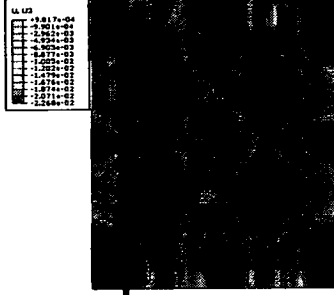
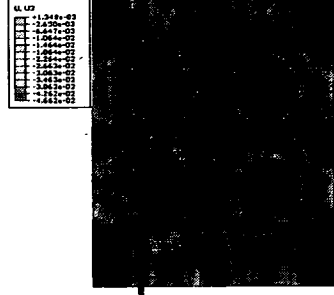
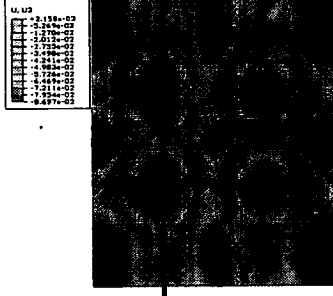
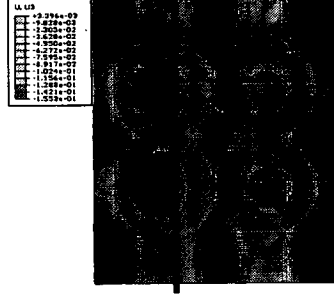
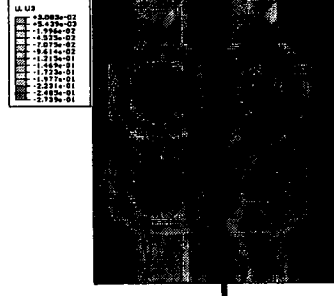
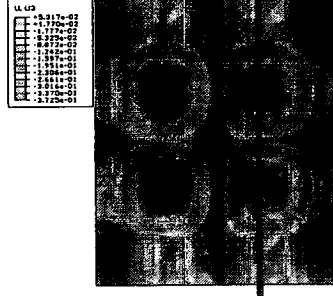
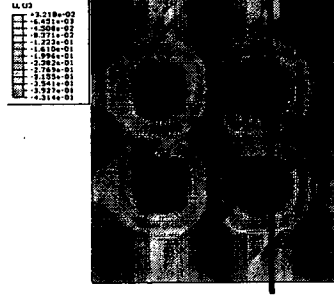
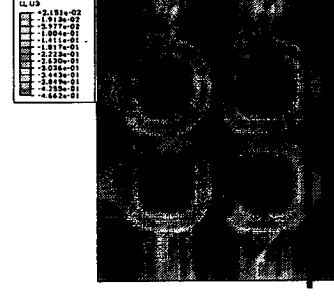
7.5.2. Travelling Fires

Four travelling fire scenarios are chosen. The percentage burning areas range from 25 to 100%; the time-temperature evolutions for each of these are as described in section 7.3.1. The results of the structural response to the fires are presented in this section. Effectively the 100% case is a uniform fire as the far field temperature and the near field temperature are identical. For this case the displacement evolution is similar to that shown in Table 7-2. When considering smaller fire percentages however, a different pattern becomes clear. Table 7-3 shows the displacement evolution for the 50% travelling fire scenario with the location of the centre of the fire indicated in each figure. The pattern shown here is typical of each of the travelling fires. As the near field temperature moves onto the structure from the left hand side, it initially deflects more than the right side which is subjected to far field temperatures only. The left hand bay continues to deflect more as the near

field fire moves across the compartment. When the near field moves past the midpoint and the right hand bay becomes hotter, larger displacements begin to form there as well and eventually the displacements are comparable on both sides. This behaviour is also obvious from Figure 7-26 where the displacements are plotted along the path shown in Figure 7-22. Although this is for the 33% scenario, the behaviour is very similar to that shown in Table 7-3. The time is normalised, so that at time 0.5 the fire is halfway along the compartment. Large displacements occur in both bays as the fire progresses, although the amount of vertical displacement in each bay differs as is shown in Figure 7-27.

Initially the trend is quite similar in both bays (up to time 0.22) but as the fire moves towards mid-span the displacements in the left bay increase more rapidly. As the near field moves towards the end of the compartment, the displacements increase more quickly in the right hand bay, whereas the steel beams in the left bay have regained most of their strength and so the downward trend slows. The concrete remains hot or continues to heat depending on the location, which continues the downward displacement in both bays; no recovery occurs.

Table 7-3 – 50% Travelling Fire displacement pattern with the centre line of the fire indicated

		
Time = 0s	Time = 200s	Time = 500s
Max. Displ. =12mm	Max. Displ. =23mm	Max. Displ. =47mm
		
Time = 1000s	Time = 1500	Time = 2000s
Max. Displ. =87mm	Max. Displ. =155mm	Max. Displ. =274mm
		
Time = 2500s	Time = 3000s	Time = 3420
Max. Displ. =372mm	Max. Displ. =431mm	Max. Displ. =466mm

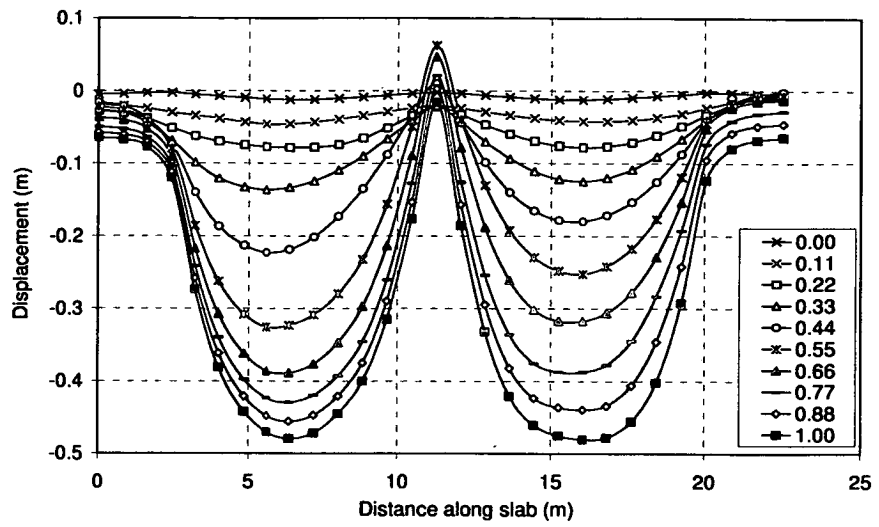


Figure 7-26 – Displacements along the slab for the 33% travelling fire case at various normalised times

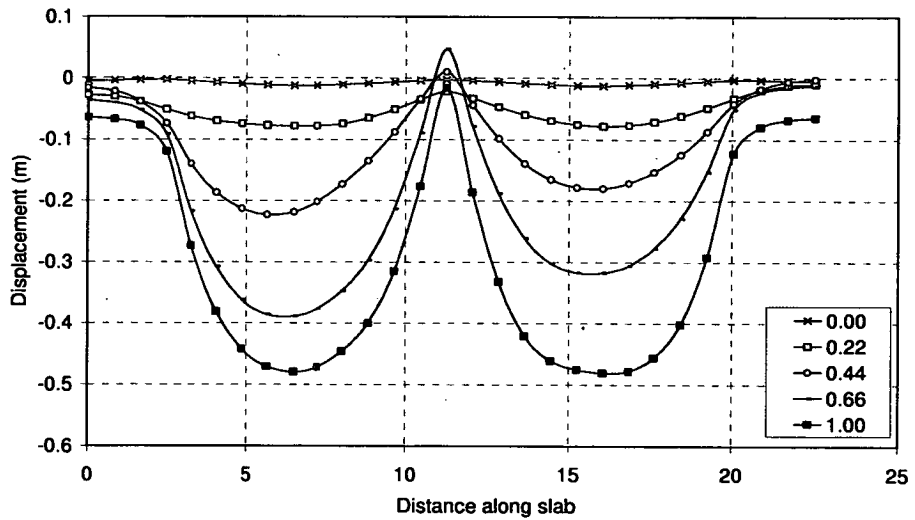


Figure 7-27 – Selected displacements along the slab for 33% travelling fire case at selected normalised times

At the end of the analysis the total vertical deflection in each bay is almost identical. The displacement pattern changes a little after each steel beam is heated; the affected beam always deflects a little more than any others around it and so the shape of the bay 'leans' a little towards the most recently heated secondary beam. Although this is only a small phenomenon, it can be seen from the displacements in Figure 7-27.

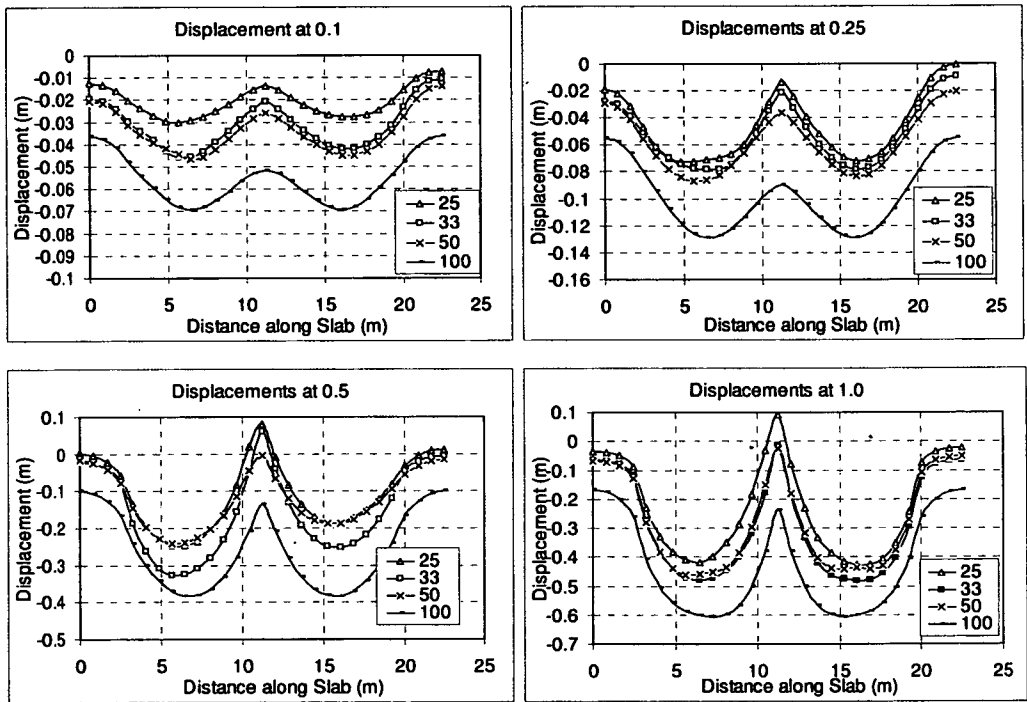


Figure 7-28 – Displacements along path for all travelling fires at various normalised times

Figure 7-28 compares the displacement pattern for each of the travelling fire scenarios at four points in time. As the time is normalised this represents a location of the fire, rather than actual time. At the early stages of the fire there is a wide range in deflections between the different fires; the 100% case is substantially

hotter across the entire compartment than the other fires which is reflected by the relatively large difference in displacement. As the fire moves across however, this difference becomes less and less pronounced. The three smaller travelling fire scenarios in particular become very similar as the fire progresses. There remain local differences, but the trend is consistent. It should also be noted that although this is plotted for normalised time, the actual fire durations are quite different. So although the 25% case for example is subjected to lower far field temperatures than the 100% case, the duration of the fire is also substantially longer. The displacements therefore end up being quite similar.

Something which occurs in the 50, 33 and 25% scenarios is the upward displacement seen at mid-span. This is not observed in the 100% travelling fire and becomes more pronounced as the fire percentage decreases. How the four travelling fire scenarios compare in this respect is shown in Figure 7-29 where the mid-span displacement of the slab is plotted against normalised time.

This upward trend begins just before normalised time 0.45 for all cases, i.e. when the near field first begins to affect primary beam 2 and this upward displacement continues as the fire moves across the beam and on towards the end of the compartments. The time at which the displacements reduce again varies for each case. There is only permanent upward displacement for the 25% scenario.

The primary beams along the top and bottom edge of the compartment are not being heated uniformly but instead the fire moves along the length of the beam. At the same time the two secondary beams attached to the primary beam are deflecting and as this is a fully fixed connection, rotations are caused. These rotations result in the central primary beam (primary beam 2) to be rotated also, causing some upward movement at mid-span. The upward movement occurs

primarily in the beam, only if the movement is significant (as in the 25% case) does the slab also move upwards to accommodate for this.

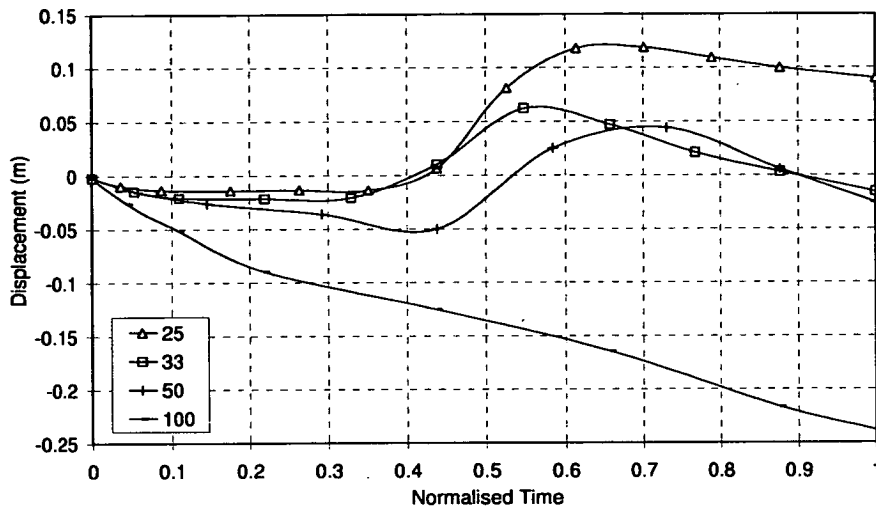


Figure 7-29 – Vertical displacement at mid-span for all travelling fire scenarios

Similar behaviour was observed in 1D beams described in Chapter 4. Here continuity of the beam caused upwards movement at mid-span when the fire moved on from this location and local cooling has occurred. The composite action caused by the presence of the slab has an effect on the overall behaviour with respect to this deflection pattern but continuity of the floor section remains a requirement. The cooling effect is more significant for smaller travelling fire percentages as the far field temperature is lower resulting in a larger temperature difference and thus a larger local upward movement.

Apart from displacement patterns the structural behaviour can be compared by looking at the section forces in the steel beams. Figure 7-30 shows the section forces in the steel beams for the 25% travelling fire case. The numbering of the

primary and secondary beams is shown in Figure 7-10. Initially all beams go into compression as they increase in temperature simultaneously. In primary beam 1, which is immediately subjected to the near field temperatures, the force quickly reduces before it yields in compression.

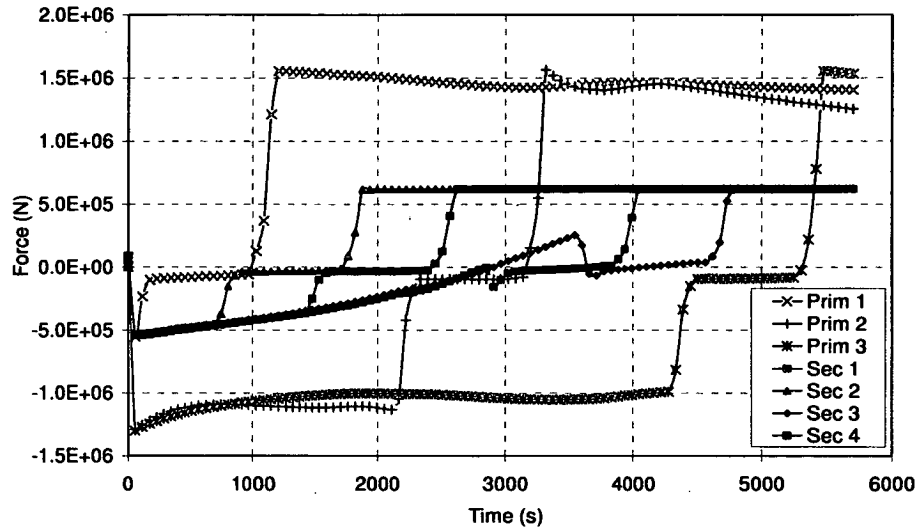


Figure 7-30 – Axial forces in the steel beams for the 25% travelling fire scenario

This is closely linked to the temperature evolution in this beam which is shown in Figure 7-31 combined with the section force. As the beam reaches the peak temperature, the strength reduces and the section yields; the large compressive force can no longer be sustained and reduces quickly before reaching a plateau. The fire gradually moves across all the beams and all go through a similar pattern (Figure 7-30) as they are briefly subjected to higher and then lower temperatures once again. The secondary beams are significantly smaller than the primary beams and therefore have a smaller capacity; yield occurs at a lower axial force. It is also

clear that there is a gradual reduction in compressive force for all beams apart from primary beam 1 even before the near field has reached it.

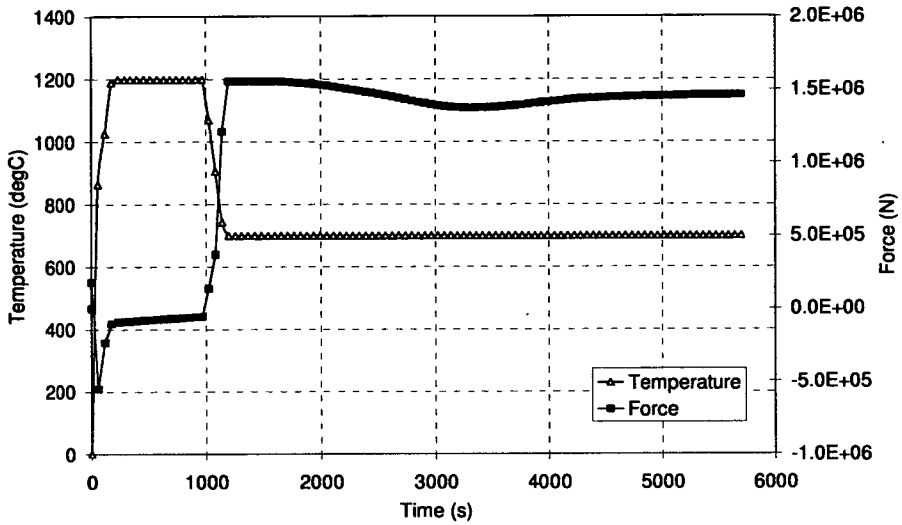


Figure 7-31 – Force and temperature plot for Primary Beam 1 in 25% scenario

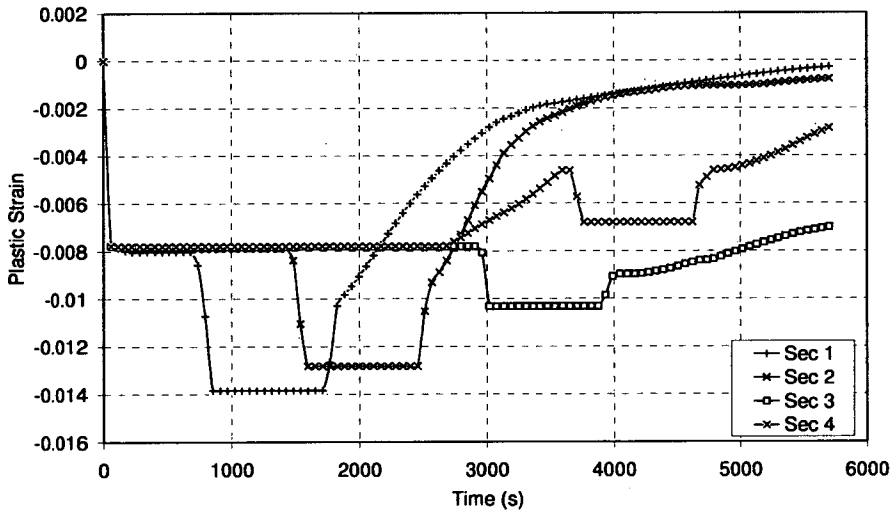


Figure 7-32 – Plastic strain in the lower flange in each of the secondary beams for the 25% fire scenario

As the fire moves onto the structure, displacements are induced across the entire compartment. These displacements have an effect on the force capacity of the beams as this also leads to increased plastic strains and bending moments. To illustrate this Figure 7-32 shows the plastic strains in each of the secondary beams for the 25% scenario.

To fully understand the plastic strain behaviour observed in Figure 7-32 it is necessary to consider a simpler example. Figure 7-33 shows the strains and vertical displacements for one of the 1D beams discussed in Chapter 3 section 3.2.6. This beam is subjected to gravity loads and has fully fixed supports. It is being heated uniformly along its length to a linear gradient with 900°C at the bottom surface and 0°C at the top. The thermal strain in Figure 7-33 follows the heating and cooling evolution; linear heating from 0.1 to 1.1 and linear cooling from 1.1 to 2.1. The load is applied over the initial 0.1.

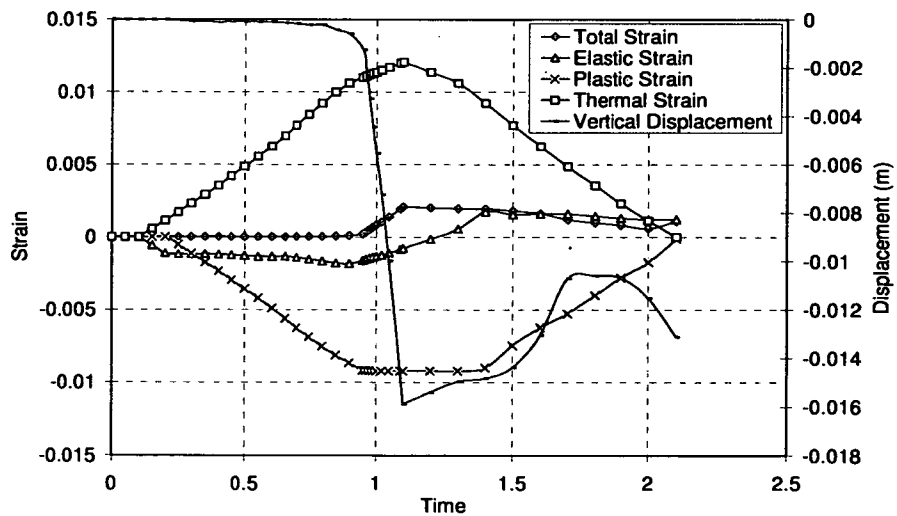
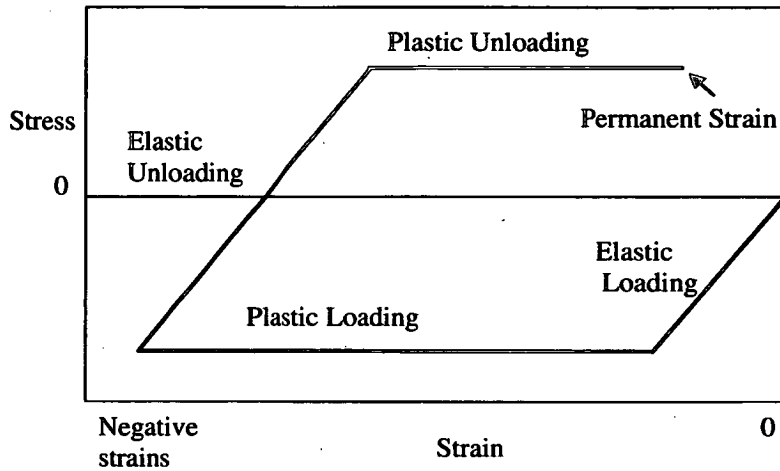


Figure 7-33 – Strain and displacements for 1D beam example

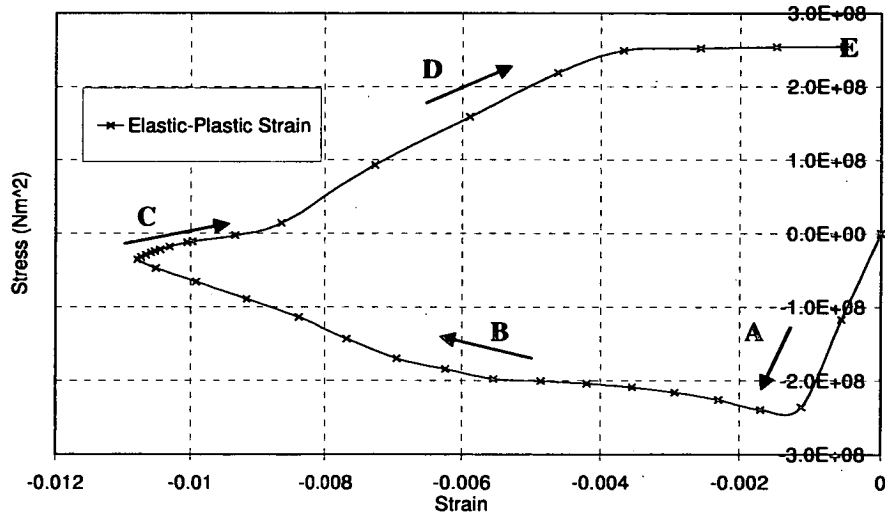
The application of load alone does not result in significant displacements and hence all strains appear as zero until the temperature is applied. The elastic strains increase linearly as the beam starts to heat and the beam is expanding against the supports. This results in plastic strains developing which increase linearly as thermal expansion continues. The elastic strains are almost constant at this stage as there is very little downward displacement. However, at time 0.9 the displacement at mid-span suddenly increases rapidly. This releases the load induced by thermal expansion and effectively results in unloading of the beam; the elastic strains reduce (they become increasingly tensile) whilst the plastic strains are constant. At time 1.1 cooling commences, which is also a form of unloading as the beam is now contracting. The elastic strains therefore continue to reduce and the plastic strain still remains constant. Once the elastic strains have reduced and elastic unloading is complete, the plastic strains begin to reduce until the fire has ended and some permanent plastic strains remain. This becomes even clearer when considering the stress-strain curve for this particular example in Figure 7-34. This plot shows stress plotted against the combination of elastic and plastic strains for both an idealised case as well as the specific output for the 1D beam example.

The strains initially increase linearly (A) which represents the elastic strains, after which the gradient of the strain changes and the strains increase over a slightly reducing stress (B). This is the plastic strain. Due to the material degradation occurring simultaneously, this is not a plateau as described by the classic stress-strain relationship (Figure 7-34 (a)), but a reducing plastic strain as the section is losing strength.

The next point of interest occurs when there is another change in direction of the strains (C). This occurs when the deflections suddenly increase and the strains are released; the stresses reduce and become tensile as the elastic unloading occurs.



(a)



(b)

Figure 7-34 – Stress-strain plot (a) idealised and (b) for 1D beam

This does not happen at the same rate as the elastic loading did as the beam has now been heated to a high temperature, affecting the material properties. Finally the plastic strains also reduce (D) linearly as the beam cools until some permanent strain (E) is present.

Keeping in mind this behaviour observed for a simple beam, the strains in the travelling fire compartment may be explained more clearly. The total, elastic, thermal and plastic strains for secondary beam 4 are plotted in Figure 7-35. Secondary beam 4 is chosen as this beam behaves in a different manner to the others, as can be seen in Figure 7-32.

The plastic strains increase in all beams simultaneously as the entire compartment is heated to the far field temperature. The plastic strain remains constant as there is no further change in temperature. As secondary beam 1 is heated to the near field temperature a rapid increase in plastic strain occurs, which subsequently reduces as the temperatures reduce again. This takes place in each of the secondary beams, but as is clear from the graph, the value at which plastic yield occurs reduces as the beams are located closer to the end of the compartment and the displacements continue to increase. Only secondary beam 4 shows different behaviour; here the plastic strain reduces before a temperature change has occurred. Figure 7-35 shows all the strains (at the bottom flange) changing with time and Figure 7-36 shows the stress-strain (elastic and plastic strain only) evolution. As the temperatures increase in the beam, the thermal strains quickly increase and remain constant until the near field reaches the section.

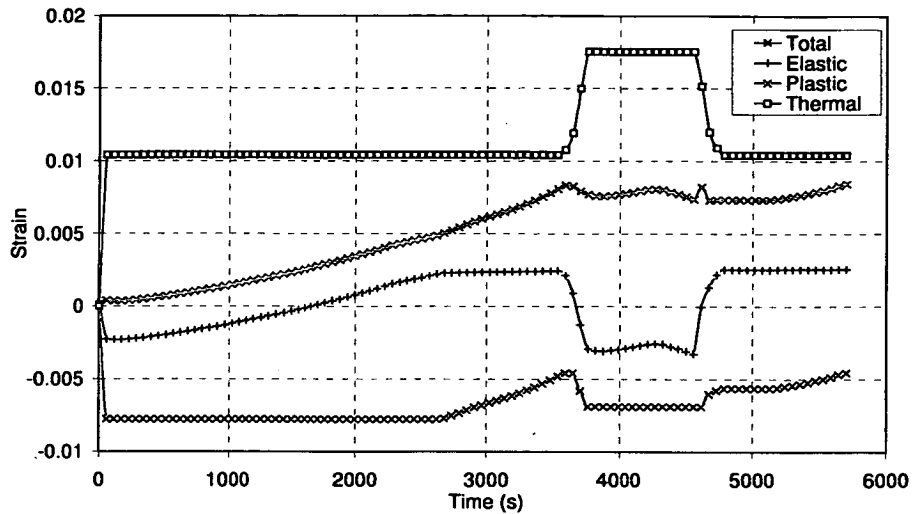


Figure 7-35 – Total, Elastic, Plastic and thermal strains in secondary beam 4 in the 25% fire scenario

The elastic strains rapidly increase as do the thermal strains. Large displacements immediately begin to form, leading to elastic unloading (represented by a linearly decreasing elastic strain). The elastic unloading results in constant plastic strains. At the same time the total strains continue to increase as the beam is deflecting downwards continuously. Up to this point, this behaviour is observed in all secondary beams (the plastic strains for all secondary beams are shown in Figure 7-32). Once the elastic unloading has completed, the strains reduce plastically. This reduction of plastic strains continues until the end of the cooling phase when large tensile plastic strains are induced as the beams contract.

In Figure 7-36 the elastic-plastic strains are only shown up to the point where the near field heating reaches the beam. The elastic strains increase initially under loading (positive) and then the plastic strains increase rapidly as heating is applied (negative). This appears to be a sudden jump in the graph; this is due to the

number of outputs taken from the results; in reality the strains will follow the elastic-plastic path but this is happening very quickly. Elastic unloading then follows until plastic yield in tension is reached and plastic unloading commences. As the near field then begins to heat secondary beam 4 (Figure 7-35), the thermal strains increase, the elastic strains increase (they become compressive as further thermal expansion occurs) and the plastic strains increase for this reason also. Figure 7-37 shows the plastic strain in secondary beam 4 only, plotted alongside the bending moment at the same location. As the plastic strains reduce, the bending moments also reduce. The plastic strains are plotted for the bottom flange of the beam.

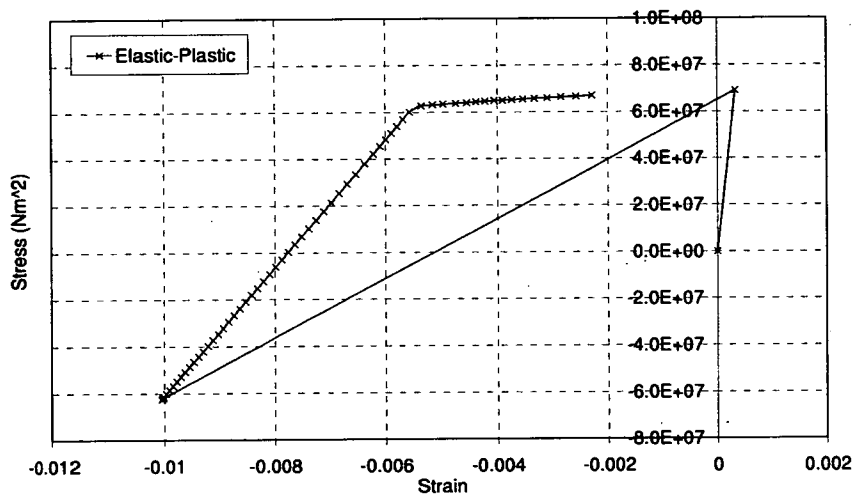


Figure 7-36 – Stress-strain plot for secondary beam 4

As they reduce and become less compressive, the bending subsequently becomes less sagging. Although this is only observed for secondary beam 4 in the 25% scenario, the number of beams affected by this effect increases as the percentage burning area is increased; this is due to larger deflections causing more rapid

elastic unloading as well as higher far field temperatures reducing the material strength of the sections. Another effect which may be adding to the reduction of the bending moment is the force-moment interaction affecting the section capacity. As the axial forces move towards zero, the section capacity is mostly governed by the bending moments. However, as the force goes from compression into tension, the large bending moments combined with increasing tensile forces come closer to the section capacity, thus causing an additional reduction in bending moments.

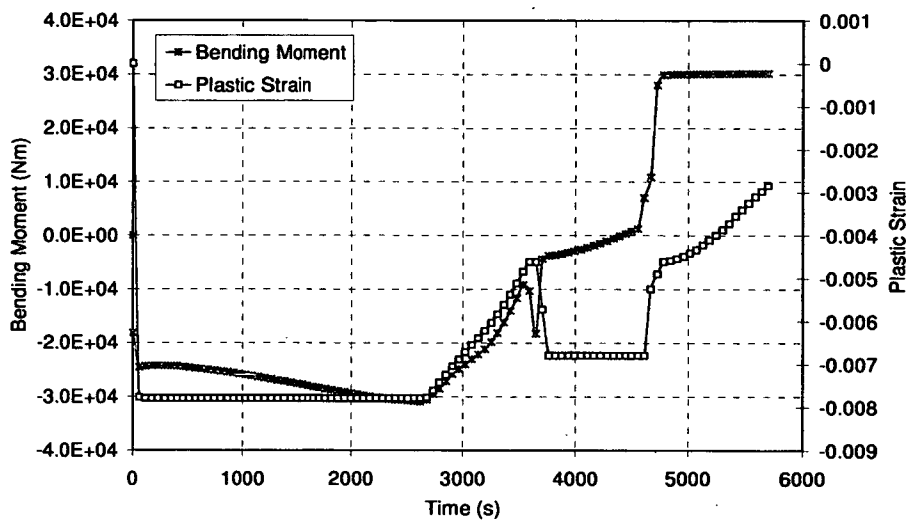


Figure 7-37 – Plastic strain and bending moment in secondary beam 4 for the 25% travelling fire scenario

The axial force in the secondary beam crosses the x-axis shortly before the sudden increase decrease in plastic strain and bending moment (Figure 7-30). The small increase which occurs at around 0.65 normalised time is due to the sudden increase in temperature, which causes the axial force to drop to almost zero. The forces and moments then remain more or less constant during the near field fire,

before rapidly increasing in tension and hogging respectively during partial cooling.

Similar trends in behaviour (axial forces, bending moments and strains) are observed for each of the other travelling fire scenarios, apart from the 100% case, which is effectively a uniform temperature. However, as the length of the near field fire increases so does the far field temperature which influences the capacity of the beams as they remain substantially hotter for the entire duration of the fire.

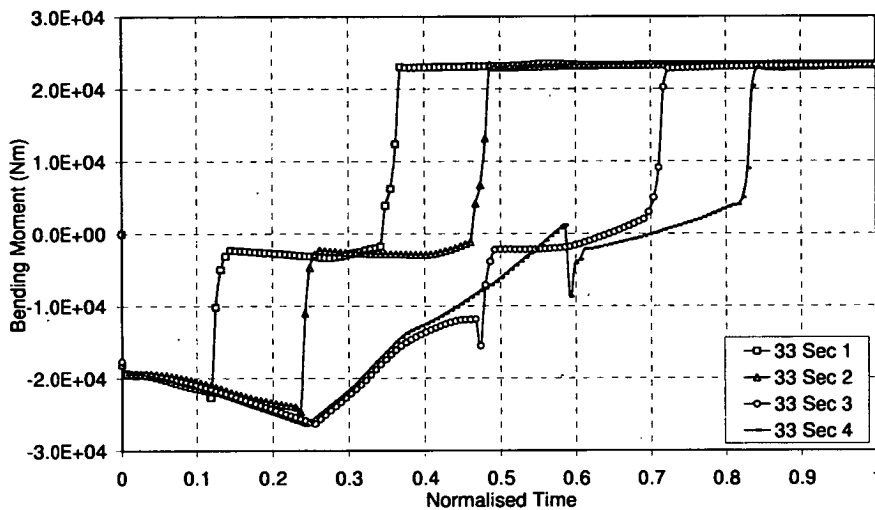


Figure 7-38 – Bending moments in the secondary beams for the 33% scenario

Figure 7-38 shows the bending moments for the all secondary beams in the 33% travelling fire scenario. The bending moment increases in each of the secondary beams until the near field reaches it, it then reduces rapidly as the section loses most of its strength. For this scenario both the third and the fourth secondary beam see their bending moments reduce suddenly before the near field has reached them, due to larger displacements and lower material strength. The behaviour

becomes less obvious when considering beams further along the compartment. It is no longer just the temperature which influences the behaviour, but clearly there are several factors which have an influence simultaneously; temperature, displacements, moments and strains.

7.5.3. Comparison

Thus far the results have been described for each of the travelling fires separately.

In this section the results of all travelling fire scenarios are compared directly.

Figure 7-39 shows the axial force in primary beam 1 for all travelling fire scenarios against normalised time.

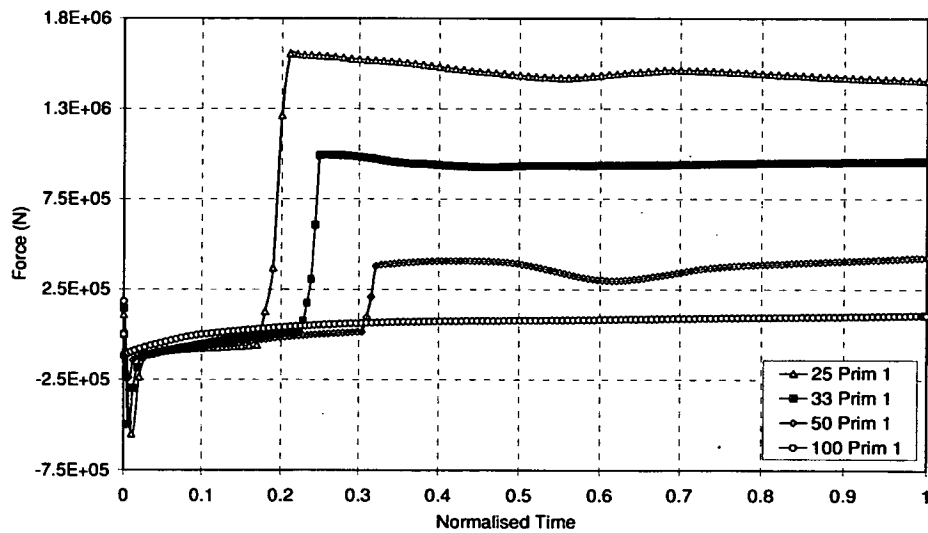


Figure 7-39 – Section forces in Primary Beam 1 for all travelling fire scenarios against normalised time

This plot clearly shows that the pattern in this beam for each case is very similar but that the time at which the force becomes tensile changes. The peak

compression force is lower for the larger near field percentages as the far field temperature is higher and subsequently the section capacity is lower. The smaller the fire length the earlier the beam goes into tension as the return to far field temperatures occurs sooner. As this far field value is lower for smaller fires this results in a larger tensile force as the temperature difference is greater.

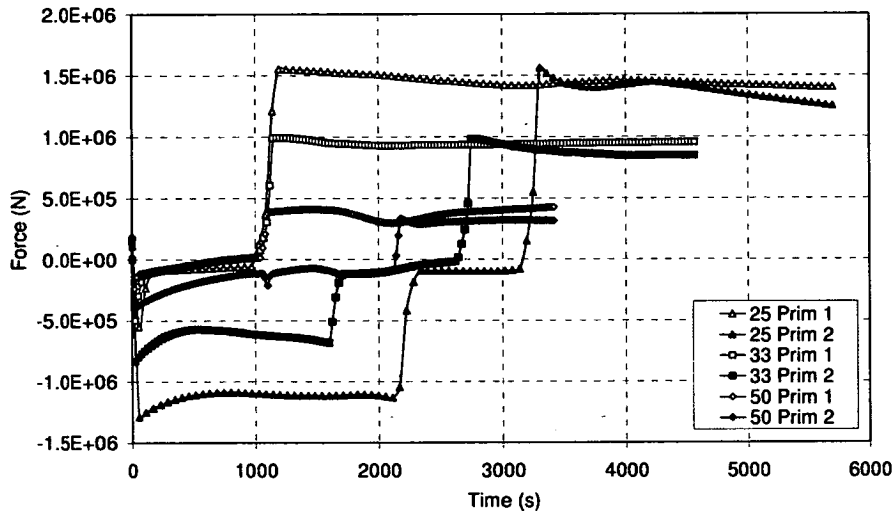


Figure 7-40 – Section forces in Primary Beam 1 and 2 for travelling fire scenarios 25, 33 and 50 plotted against real time

This is even clearer when considering Figure 7-40 where the axial forces in primary beams 1 and 2 are plotted for travelling fire scenarios 25, 33 and 50%. As all beams are heated to either the near field or far field temperature, all go into compression. The axial force in primary beams 2 does not reduce immediately (as it does in primary beam 1) as the beam retains much of its capacity and relatively small displacements are induced. Primary beam 1 goes into tension at an identical time for all travelling fire scenarios, i.e. 19 minutes after the start of the fire.

However, as the fire length is different, the speed at which it travels also changes; hence primary beams 2 are affected at different times, with larger fire length heating and cooling earlier than the smaller fire lengths.

Figure 7-41 shows the bending moments in secondary beam 1 for travelling fire scenarios 25, 33 and 50. Similarly to the axial forces, the peak sagging moment during the initial heating is lower for the larger near field percentages, as the beam capacity is affected by the higher far field temperatures. The bending moments continue to increase until the near field reaches the secondary beam which is when the moments begin to reduce. This occurs sooner for the larger travelling fires. The moments become hogging in cooling as the near field moves off the beam; this occurs sooner for the smaller fires and these reach larger hogging moments.

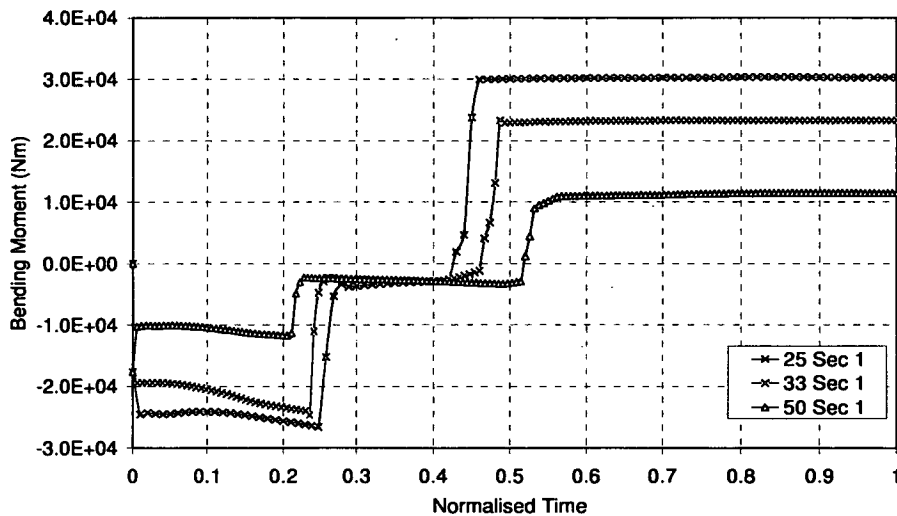


Figure 7-41 – Bending moments in secondary beam 1 for the travelling fire scenarios

Figure 7-42 shows the bending moments plotted against real time for secondary beam 3 and 4. These are the beams where the effect of the displacements and

strains result in a reduction of the moments prior to the fire reaching them. It can be seen that the bending moments start off in a sagging manner for all cases with the larger fires again with the lowest moments. In all three travelling fire scenarios a reduction in bending moments is then observed. This occurs first for the 33% case, closely followed by the 50% and lastly 25%.

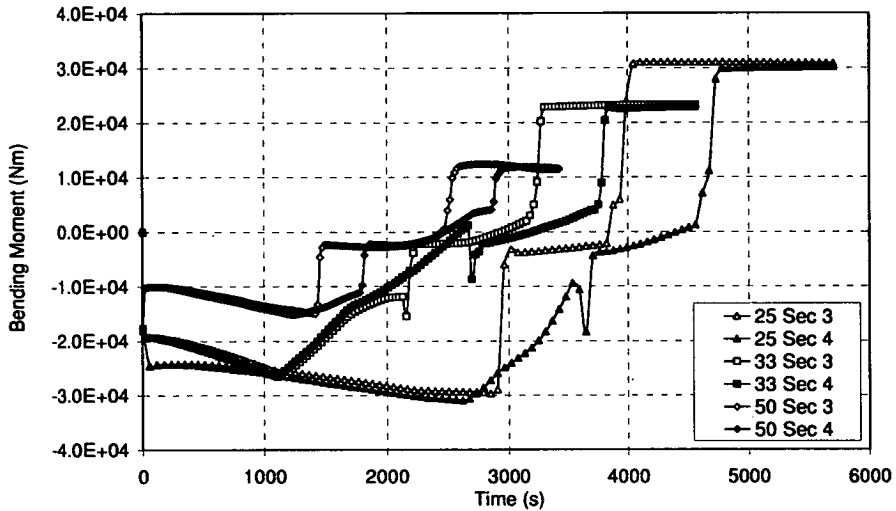


Figure 7-42 – Bending moments for secondary beam 3 and 4 for travelling fire cases 25, 33 and 50%

Figure 7-43 shows the maximum vertical displacement in the left hand bay for each fire scenario, both uniform and travelling. The uniform fires have been reduced to 90 minutes as this is a more realistic fire duration than the 208 minutes assumed originally. It can be seen that the maximum displacements in the travelling fire cases gradually increase with larger fire percentages. Only the 50% case is not completely in line with the other results, the displacements seem to increase at a marginally slower rate than in the other cases. This may also explain the reason for the slower bending moment reduction in Figure 7-42.

The models presented here are numerically challenging; steep temperature gradients moving across the compartment complicates the analysis significantly. To ensure a numerical solution, small amounts of stabilization were used. For the 50% case the required stabilization was slightly higher than for the other cases; this may have a very small effect on the behaviour. This may explain why the displacements and bending moments react more slightly slowly than in the other scenarios.

Overall though, the trend is very clear. Both the standard fire and constant temperature cases result in substantially larger displacements. The parametric fire has comparable displacements, even when including the cooling phase. It should be noted that the actual duration of each of these fires is quite different. When these deflections are plotted in real time, as in Figure 7-44 it is clear that the 100% fire scenario is very similar to the uniform fires.

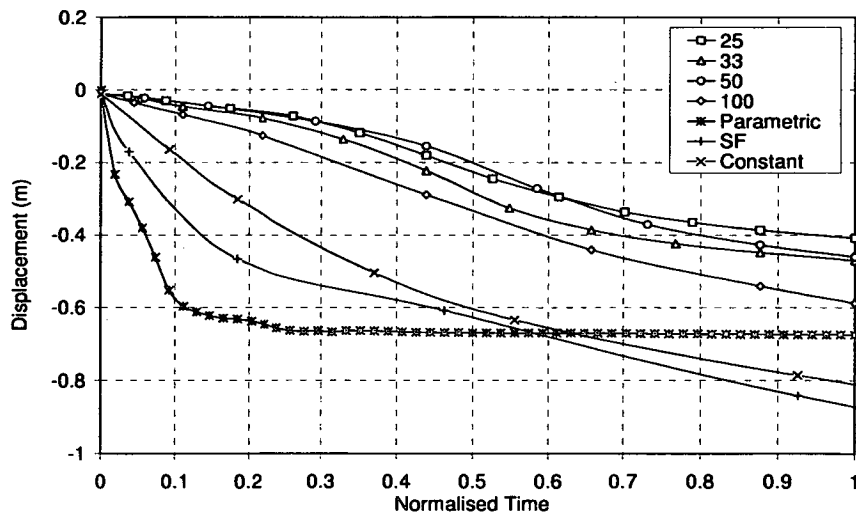


Figure 7-43 – Maximum vertical displacements for all fire scenarios with uniform fires reduced to 90 minutes in normalised time

However, as it is assumed there is a realistic fuel load in the compartment the fire can only continue for a limited amount of time before cooling commences. Therefore, although the trend is similar, the standard fire and constant temperature scenarios continue to deflect, whilst the 100% case has finished burning. It is also clear that the smaller travelling fires deflect more slowly, but that the final displacement is quite similar for all travelling scenarios. Here the 50% scenario which previously did not fit exactly in the trend has greater displacements than the 33% case and smaller than the 100% case for the duration of the fire, as expected. All uniform fires (including the 100% travelling fire scenario) increase in vertical displacement at a faster rate than the travelling fire scenarios.

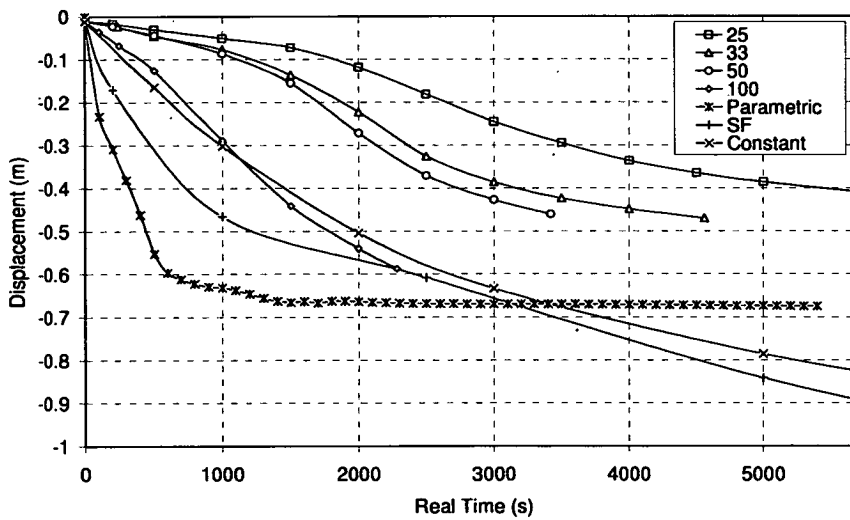


Figure 7-44 – Maximum vertical displacements for all fire scenarios with uniform fires reduced to 90 minutes in real time

Another aspect of behaviour often considered in structural fire engineering is the plastic strain in the rebar. For areas of high strain, additional rebar would be suggested to prevent excessive cracking. Figure 7-45 shows the plastic strains for a travelling fire scenario and the standard fire after 90 minutes of heating. The peak plastic strains are more widespread for the uniform fire, whereas for the travelling fire they are located near the (most recently) heated bay. The peak values observed in the analyses also varies substantially. Figure 7-46 plots the plastic strains at three locations in the slab (start, middle and end as indicated in Figure 7-15. These locations are directly above the primary beams, where the highest strains are usually observed. Each plot shows the strain evolution at a particular point for three travelling fires (25, 33 and 50%) and two uniform fires (standard and parametric fires). For all three locations the strains in the travelling fires initially increase much slower than in the uniform fires. However, for the travelling fires the strains then suddenly increase rapidly at the start location. The duration of the standard fire is 12500s, which is much longer than may be expected in a real fire. If taking the standard fire strains after 90 minutes of heating, which can be considered a more realistic time duration for the standard fire, the strains are much lower than for any of the travelling fires.

At the centre of the slab, directly above primary beam 2, the strains are the largest for all cases. This can be explained as there are two bays deflecting immediately adjacent to this point, causing the slab to bend in both directions and increasing the strain in the rebar at that location. The strain in the standard fire is significantly higher than in any other scenario. This is mostly due to the very large displacements observed in both bays.

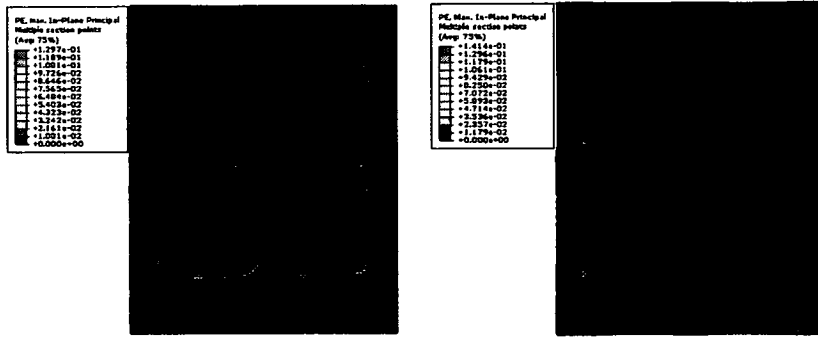


Figure 7-45 – Plastic strains in the rebar for (a) 33% travelling fire at the end of heating at 4560s and (b) standard fire after 90 minutes of heating

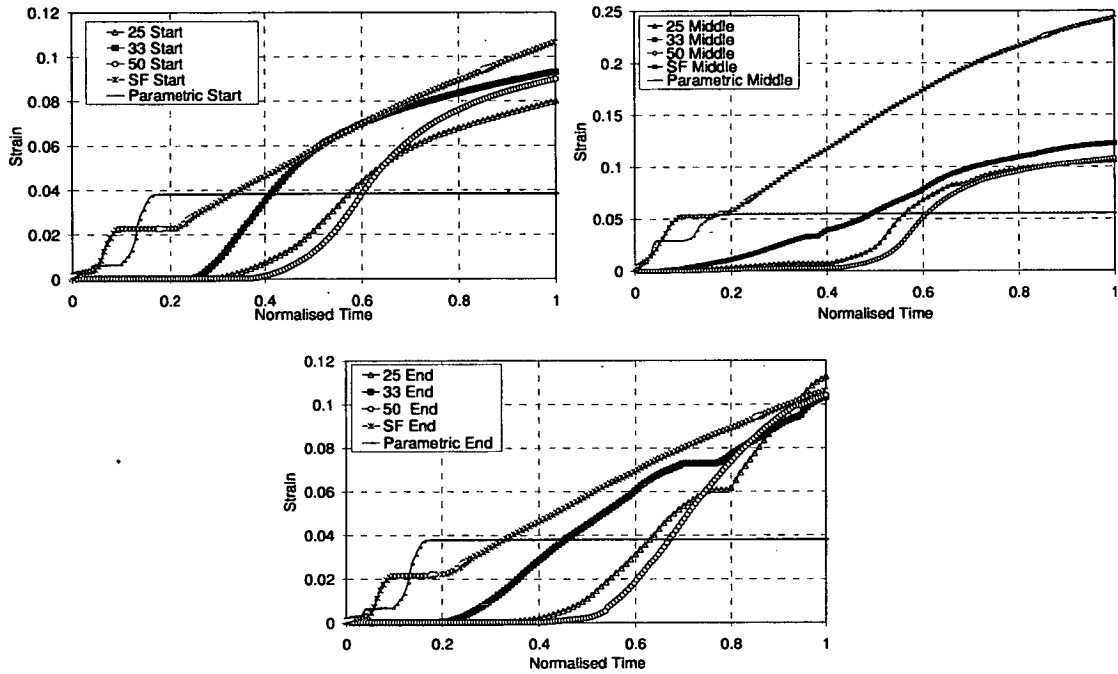


Figure 7-46 – Plastic strains (where strain of 1 relates to 100%) at three locations in the slab compared for travelling and uniform fires

The final plot shows the strains at the end of the compartment, above primary beam 3. The strains for the standard fire and parametric fire are identical as those

in the start location. This is as expected as the section is symmetrical and heated uniformly. For the travelling fires however, the strains are similar at each beam with only marginal differences at the three locations. There are bigger differences in strains for the travelling fires during the fire itself, but at the end of heating for the strains are more similar, especially when closer to the end of the compartment. In the parametric fire the strains are quite small at each of the three locations. Also, the fire duration includes a cooling phase (constant strain) and so the actual time of heating is much shorter than for any of the other cases. Up to the point where heating stops, the plastic strains are comparable with those in the standard fire.

Neither the uniform or non-uniform fires can be considered a worst case for plastic strains in the rebar. Higher strains are observed in the standard fire, and although these occur after almost four hours of heating which may be deemed unrealistic they remain higher at mid-span. At the start and end location however, the strain in the non-uniform fires are equal to the standard fire after the entire heating phase. The non-uniform fires induce significant strains at each location; the near field heating which moves across the compartment induces an irregular displacement pattern in the slab. This leads to additional strains in the rebar across the beams.

7.5.4. Cooling

To compare the behaviour of the travelling fires with the uniform fires it is necessary to include a final cooling phase for all travelling fires. As described in section 7.3, the main shortcoming of the travelling fire definition set out by Rein and Stern-Gottfried [26] is that cooling is not included. All the travelling fire

models were extended by 7200s during which cooling occurred. The steel beams follow a cooling branch similar to that in the parametric fire as shown in Figure 7-21. The gas temperature was assumed to return to ambient immediately and a heat transfer analysis was done for each scenario to calculate the temperature evolution accordingly. Figure 7-47 and Figure 7-48 show the axial force for the primary and secondary beams respectively in the 33% travelling fire scenario as well as the parametric fire. The time has been normalised. It can be seen that the total tensile force in both types of beams is higher as a result of the travelling fire than after the parametric fire. However, the peak temperature reached in the steel beams is higher during the travelling fires (1200°C) than in the parametric fire (1030°C).

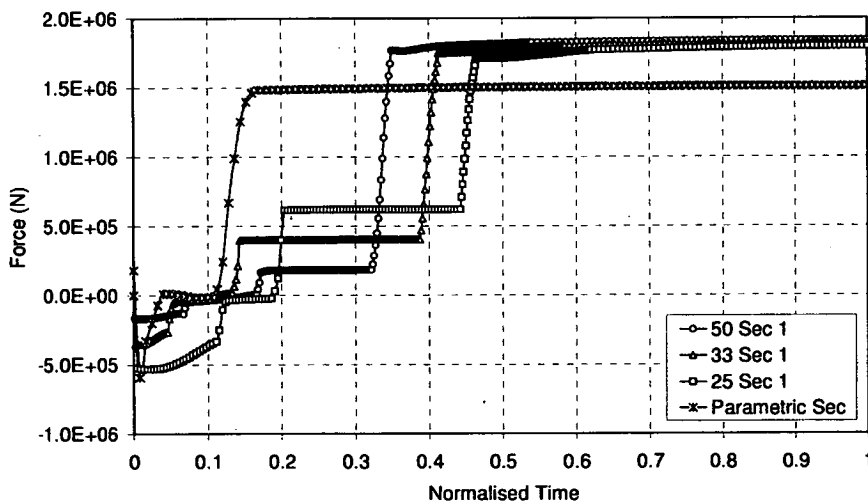


Figure 7-47 – Axial force comparison of primary beams for 33% travelling fire scenario and the parametric fire

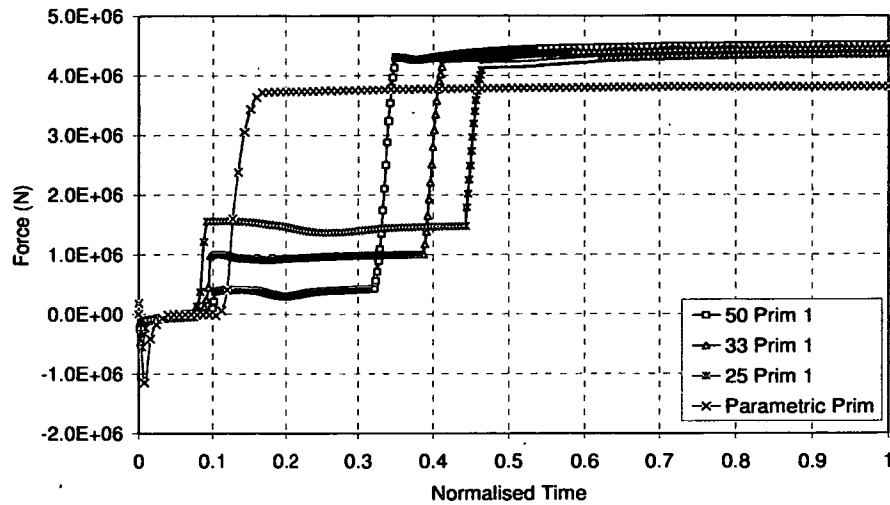


Figure 7-48 – Axial force comparison of secondary beams for 33% travelling fire scenario and the parametric fire

It was already observed in Chapter 3 that the residual axial force upon cooling is higher when higher temperatures are reached during cooling. However, there is a small difference in axial force between each of the travelling fire scenarios and these have reached identical peak temperatures. The larger percentages result in a slightly larger tensile force. Although the peak temperature in heating dictates the residual axial force, some variations may still be induced by the specific heating regime.

The bending moments during cooling are also compared to the parametric cooling phase. Figure 7-49 and Figure 7-50 show the bending moments for the secondary and primary beams respectively, for a range of travelling fires as well as the parametric fire. It can be seen that the bending moments at mid-span for the parametric scenario remain constant from 0.2 of normalised time. This

corresponds to the end of the heating phase; the bending moment stays constant during cooling.

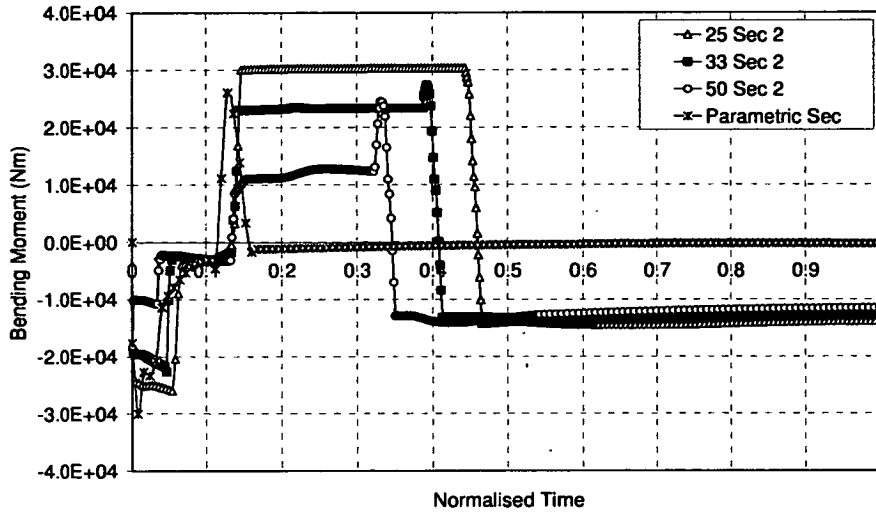


Figure 7-49 – Bending moment comparison of secondary beam 2 for range of travelling fire scenarios and the parametric fire

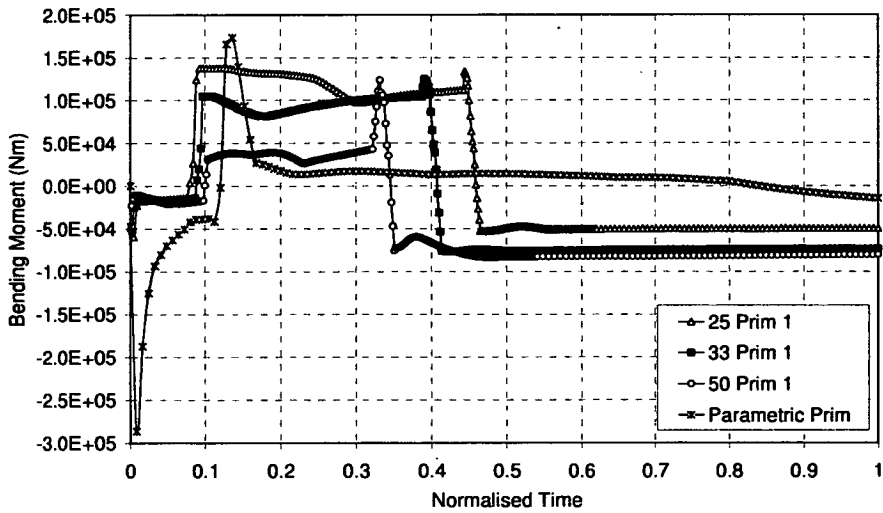


Figure 7-50 – Bending moment comparison of primary beam 1 for range of travelling fire scenarios and the parametric fire

A small sagging moment remains in the primary beams, whereas the secondary beams have a very small residual hogging moment. Upon cooling for all scenarios the large sagging moments, caused by the large vertical displacements during heating, suddenly reduce as thermal contraction results in tensile plastic yield and hogging bending moments. Large residual hogging moments remain upon cooling in both the primary and secondary beams for the travelling fire scenarios. These moments stay more or less constant once the steel beam has cooled to ambient temperatures. During the cooling phase little change is also observed in the axial force and displacements. Similarly to the axial forces upon cooling, in the primary beams the larger fire percentages results in higher residual moments. However, the difference between the final values of moments is quite small. For the secondary beams the opposite is true; the smaller fires results in larger residual moments but again the difference is minor.

7.6. Alternative direction of travel

Up to this point the assumption has been that the fire travels along the x-axis in all scenarios as shown in Figure 7-6. The path of the fire has to be assumed as this is dependent on the fuel distribution and ventilation parameters. To ensure no aspects of the behaviour are missed, a comparison is done for the 33% travelling fire case where the fire moves along the y-axis as shown in Figure 7-51.

The fire now travels along the primary and secondary beams causing non-uniform heating along the length of the section. In all the other models most beams are heated uniformly along their length, but with a time delay between the individual

beams. For the purpose of this comparison the final cooling stage is not included and only the duration of the travelling fire is considered.

Axial forces, bending moments and plastic strains are compared to ensure similar behaviour is observed for both directions of travel.

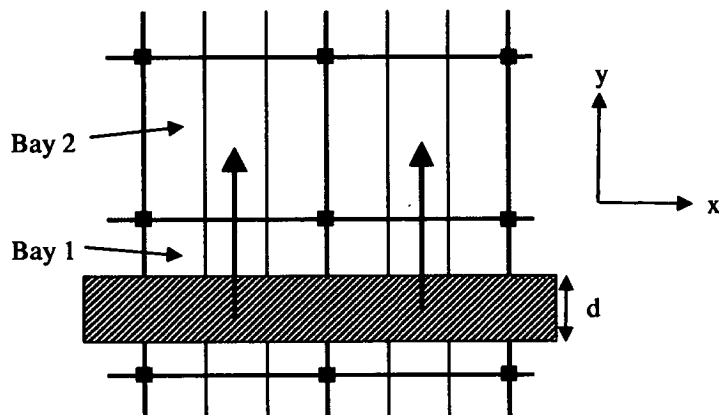
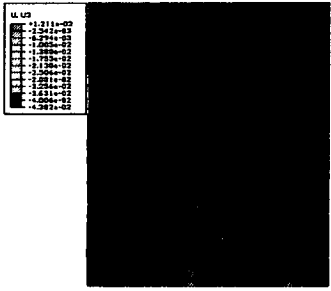
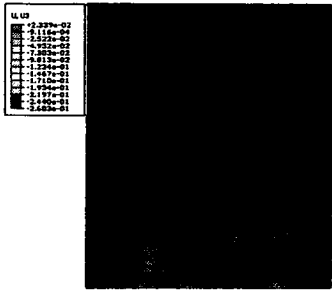
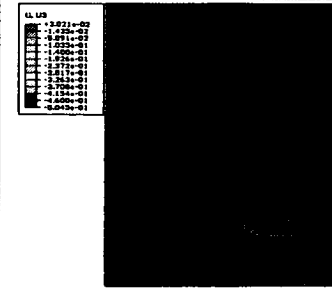


Figure 7-51 – Path of travelling fire along y-axis with the width of the fire, d , indicated as well as the naming convention for the bays

For this purpose output is taken from secondary beam 1 at mid-span in both bays as indicated in Figure 7-51. Due to the direction of travel, the heating is applied to all beams simultaneously; the results for the other secondary beams are therefore identical.

Figure 7-52 shows the vertical displacements along the path for both fire scenarios. The path for the y-direction fire runs across the mid-span of bays 1 and 2, thus capturing the peak displacements at the centre of the bays. The total length of the structure is different from the x-direction; for the purpose of this graph the original result have been moved along by 2.25m to align the fire compartments. The displacement is plotted for four points in time which are represented as a fraction of the total time, 4560 seconds.

Table 7-4 – Displacement pattern for 33% case travelling along y-axis

		
Time = 500s	Time = 2280s	Time = 4560s
Max. Displ. =44mm	Max. Displ. =268mm	Max. Displ. =505mm

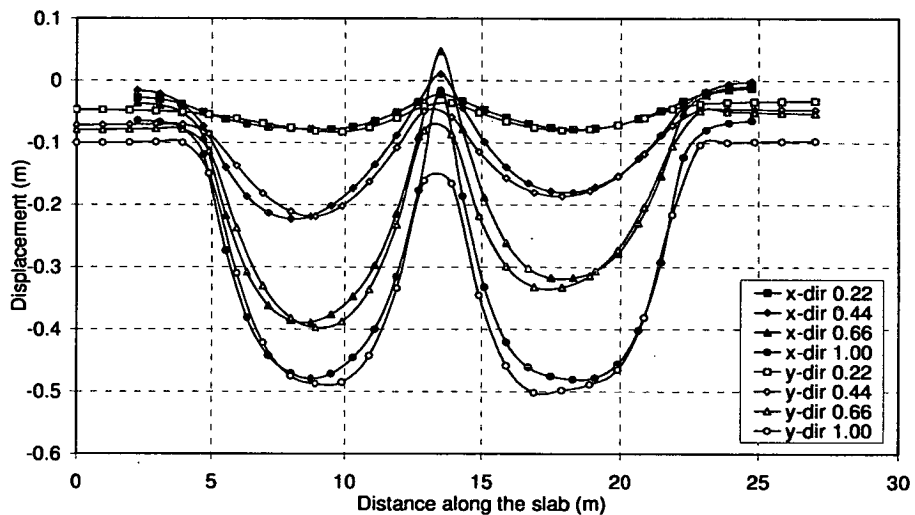


Figure 7-52 – Vertical displacements along the path for both the x-direction and y-direction fires

At mid-span of both bays the vertical displacement is consistently similar; peak values differ only 25mm at the centre of the slab at the end of the fire (before final cooling). The only difference occurs at mid-span of the compartment where no upward displacement is predicted. The non-uniform heating of the edge primary

beams were responsible for this upward displacement, as described in section 7.5.2. In this scenario, the only primary beams which are heated non-uniformly along their length have no secondary beams connecting to them which eliminates the cause of the upward movement.

The axial forces shown in Figure 7-53 compare those in the original 33% case (x-direction travel) to those obtained at similar locations from the y-direction fire scenario. It should be noted that the points at which the output is taken are not identical; secondary beams 1 and 3 are plotted at mid-span for the original fire case, whereas secondary beam 1 at mid-span in bay 1 and bay 2 is plotted for the new fire case. Secondary beams 1 and 3 in the x-axis travel case are 3m and 12m from the start of the compartment respectively, whereas secondary beam 1 in bay 1 and 2 in the y-axis travel case are at 4.5m and 13.5m respectively. This affects the time at which the fire arrives at each location.

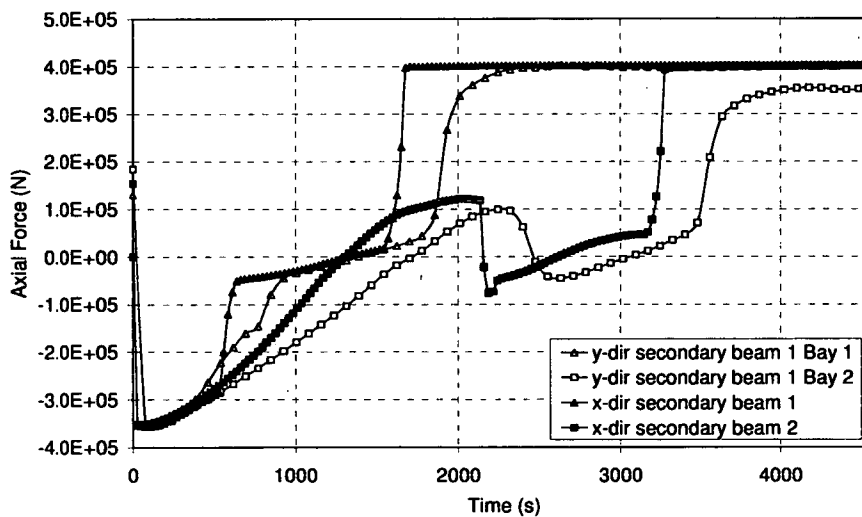


Figure 7-53 – Axial forces in the secondary beams at comparable locations for both the x and y-axis travelling fires

All beams reach an identical compressive force due to initial heating conditions caused by the far field. The force in all the beams then reduces at an identical rate until the fire reaches it. The trend which is observed once the fire moves onto the beam at both locations is very similar, although the timings are a little different, as explained. The peak values at each stage of the analysis are very similar.

The bending moments and plastic strains are plotted for the travelling fire along the y-axis only in Figure 7-54.

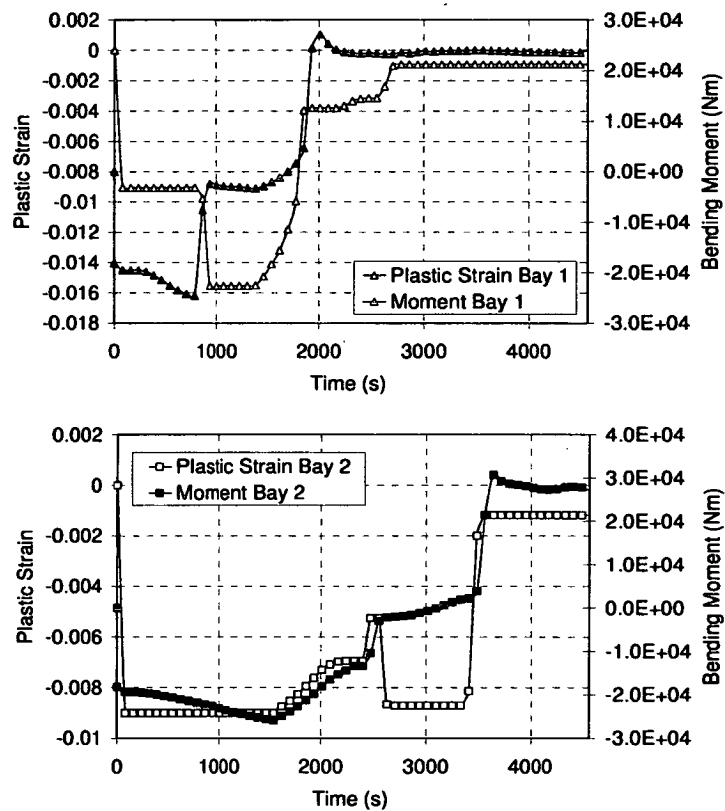


Figure 7-54 – Plastic strains and bending moments plotted in secondary beam 1 at mid-span of bay 1 and bay 2

Again this is plotted at mid-span of both bay 1 and 2. Comparing these results to the behaviour observed in Figure 7-32, Figure 7-37 and Figure 7-38 it can be seen the behaviour is almost identical. In bay 1 (comparable with secondary beams 1 and 2 for the original scenario) the strains are constant until the fire reaches it when a sudden increase in plastic strain occurs.

At the same time the bending moments suddenly reduce. Once the fire has moved on, both the moments and strains reduce further until an almost constant value is reached until the end of the analysis. In bay 2 (comparable to secondary beams 3 and 4) the bending moment and strain reduce prior to being subjected to the near field temperatures. This is identical to the behaviour observed in all the other models and explained in further detail in section 7.5.2. Similarly to the axial force and displacements, the peak values observed for both the bending moments and the strains are very similar for both scenarios.

7.7. Conclusions

Design fires have an important role in structural fire engineering. An assumption on the fire scenario in a given compartment must be made in order for the structural response to that scenario to be evaluated. The current design fires are limited to relatively small compartments in the codes and observations from real fires have confirmed that large temperature variations may occur, even in small spaces, so it becomes increasingly important to find alternative ways of defining the fire scenario. Recent developments in this field have led to a need to investigate the structural behaviour when subjected to these newly defined fire scenarios.

It has generally been assumed that uniformly applied standard fires pose the most serious threat and thus designing for this is deemed conservative. However, it has never been investigated whether this is actually true.

The results presented in this chapter show that the maximum displacements expected are larger for uniform fires. This is expected as the entire compartment loses strength simultaneously; there are no parts of the floor section which retain significant strength thus restraining the vertical movement. What is observed in the travelling fires however and not captured by uniformly applied temperatures is the irregular displacement pattern. Some beams deflect rapidly early on in the fire only to remain almost stable at the later stages and vice versa. Some beams even show upward movement, in this compartment that was observed at mid-span only. This coincides with the results from Chapter 4 and to some extent Chapter 6, where non-uniform fires led to cyclic movement in the beams or columns respectively.

The axial forces observed in the travelling fires are comparable to those observed in the parametric fire and constant temperature case. The standard fire had much higher compressive axial forces. This is due to the rate at which the steel beams heat; rapid heating leads to rapid loss of strength, whereas slower heating allows for the force to build up as the beams expand. As the fire moves across the compartment, these forces change significantly, with the trend comparable for each travelling fire scenario. Once cooling has completed however, all beams have yielded in tension. The residual axial force observed in the travelling fires is higher than in the parametric fire case. However, this can be explained by the higher temperature reached during heating (1200°C near field temperatures, 1030°C peak parametric temperature). As was observed in Chapter 3, higher peak

temperatures during heating result in higher residual tensile forces. The observations here support that, even though this is a much more complicated structure and fire scenario.

The residual bending moments are also quite different. Whilst after a parametric fire the bending moments reduce to values close to zero, after the travelling fires substantial residual moments remain. This is in contrast to Chapter 3 where lower peak temperatures resulted in higher residual bending moments. Clearly it is not only the peak temperature in the steel which affects this value, but also the way in which this heating takes places. It was shown in Chapter 4 that the bending moments change significantly when non-uniform heating is applied to the section. This is mostly induced by the irregular displacement pattern, which is also observed in the 3D compartment models described in this chapter.

Plastic strains in the rebar are also compared. It is shown that the strains in the parametric fire are much smaller than those expected in non-uniform fires, whereas the standard fire induces higher strains. However, this is dependent on the location where strains are measured. The non-uniform fires generally have greater strains, again caused by the irregular deformation of the compartment.

An alternative fire path is considered to ascertain the importance of the direction of travel. It was found that the behaviour for both cases was almost identical. Only very small differences occurred between peak values of displacement, force and bending moments. For the compartment considered here it can therefore be concluded that the direction at which the fire travels is not of great importance. This is in part due to the symmetry in both directions; were the bays rectangular rather than square, greater differences could be expected. Both fires travel along these lines of symmetry; were fires at another angle modelled (for example

diagonally) this would also be expected to result in greater differences in behaviour.

It is clear that the behaviour of the structure when subjected to a non-uniform fire does not respond in an identical manner as when subjected to design fires. Although similar peak displacements may be expected, the axial force, moment and strain evolution during the heating and cooling phase may be quite different. Some differences also occur depending on which travelling fire scenario is chosen for the particular compartment. Smaller fires result in smaller downward displacements of the bays, but a higher temperature difference between the near and far field leads to more continuity issues in some cases resulting in some upward movement at mid-span (for this specific compartment). This temperature difference also results in larger tensile forces and larger hogging moments, prior to the final cooling stage for the smaller fire percentages.

These results indicate that uniform fires are not necessarily more conservative than non-uniform fires. Neither is a worst case scenario on all aspects of structural behaviour. However, as the non-uniform fires provide much more realistic temperature evolutions for any given compartment, it is recommended that this type of fire should be designed for instead of the limited uniform fires.

Chapter 8

8. Conclusions and Further Work

8.1. Conclusions

This thesis has examined structural behaviour during cooling and non-uniform fires. The previous chapters have investigated a range of structures, from 1D beams to a 3D composite structure. The conclusions drawn at each stage of the research are considered here to present a total overview as well as recommendations on the improvement of design.

8.1.1. General observations

This section describes some of the general observations which have led to this research.

- Design fires have an important role in structural fire engineering. An assumption on the fire scenario in a given compartment must be made in order for the structural response to that scenario to be evaluated.
- The design fires currently available in codes have significant limitations and their use in performance-based structural fire design is an inadequate method. They have been shown to be an unrealistic temperature assumption for most compartments.
- Observations of real fires and large fire tests have shown that the cooling phase of a fire may lead to failure.
- Observations of real fires have also shown that large variations in temperature may occur, even in very small compartments. This contrasts with the assumption of currently used design fires that temperatures will be uniform.

-
- It has generally been assumed that uniformly applied standard fires pose the most serious threat to a structure and thus designing for this is deemed conservative. However, it has never been investigated whether this is accurate.

8.1.2. General conclusions

Here the conclusions from all chapters are combined and generalised. This therefore provides an overview of the main findings.

- The inclusion of a cooling phase is a necessity as failure (of connections in particular) may occur which will not be captured unless cooling is considered. Forces in the steel beams during cooling can be more than three times those during heating. Therefore the structure may remain globally stable while the structural elements are at high temperatures, but may be susceptible to local failures of connections during the cooling.
- The linear rate of cooling of the gas temperature is shown to have little effect on the overall behaviour of structures, in all 1D, 2D and 3D models. This was shown to be the case for both single beams and composite structures where a concrete slab is present. The rate of cooling does affect the temperature evolution in the concrete slab, which accounts for some of the observed differences in the results.
- Although the concrete slab does affect the behaviour, this is primarily during the final stages of the cooling phase when the steel beams have regained most of their strength but the concrete remains hot. Regardless,

the results predicted remain similar and the final expected force, displacement and moments are comparable.

- It is shown that the behaviour of the 2D type of multi-storey structure studied in Chapters 5 and 6 during cooling depends on the relative areas of steel and concrete in the composite sections. In design at present unprotected steel beams are generally not considered during a fire as they rapidly lose almost all their strength on heating. During cooling however they will regain much of their strength and this study shows this strengthening will influence overall structural behaviour. If the area of steel is sufficiently large, the contraction forces in the steel beams dominate the floor behaviour. For smaller beams high forces in the (still hot) concrete dominate the behaviour.
- The results from Chapters 4 and 7 indicate that uniform fires are not necessarily more conservative than non-uniform fires. Neither is a worst case scenario for all aspects of structural behaviour. However, as the non-uniform fires provide much more realistic temperature evolutions for any given compartment, it is recommended that this type of fire should be designed for instead of the limited uniform fires. A range of travelling fires appropriate for the compartment should be considered to capture the upper and lower bound of behaviour. This range would depend on the size of the compartment and ventilation parameters.
- In the case of vertical fire spread between individual floors, it is shown that in general neither simultaneous nor vertically travelling fire can be considered a worse case scenario as they result in different structural responses, either of which may be the most serious. When designing for

multi-storey fires it is therefore recommended that both a simultaneous fire as well a range of travelling fires is considered. A slow and rapid fire spread as described in Chapter 6 can be adopted, although further research into realistic fire spread rates may be required.

8.1.3. Specific conclusions

In this section the specific conclusions from all chapters are summarised.

Cooling

- After cooling residual tensile forces and bending moments are always present; the values of which are dependent on the structural variables such as load, boundary conditions, section size and length, as well as the fire variables such as peak temperature and the gradient through the section.
- Boundary conditions significantly affect the structural behaviour, both during heating and cooling and these must be carefully considered in design.
- Residual axial tensile forces are greater when higher peak temperatures are reached during heating.
- The largest residual bending moments occur when lower temperatures are achieved (maximum at 300°C in 1D beams examples) resulting in a lower bending capacity post-fire than prior to the temperature exposure. These temperatures are also reached in sections which are fire protected. Fire protection is therefore not sufficient to prevent significant damage to fire affected structures.

-
- Residual forces and moments essentially represent an additional load on the structure and should be taken into account when considering post-fire use of the structure. The effects of residual forces and moments would be present even if there were only very small residual deflections in the structure and so would not be apparent from a purely visual inspection. This suggests that the analysis of structures after a fire with a view to reinstatement should be undertaken which goes beyond a visual inspection.
 - The comparison of 3D shell models with the 1D beam models in Chapter 3 show that behaviour of the fixed ended beams compares very well with the simple beams. For pinned beams however, some buckling failure may occur during heating (to high temperatures) which is not captured by the 1D models.
 - The 1D beams models in Chapter 3 are compared to a 3D model of the Cardington Test 1. The results show that the 1D model predicts the general behaviour of more complex structures well, even though the concrete slab is not considered. The axial forces and bending moments are found to be very similar until the final stages of cooling which is when the hot concrete begins to affect the behaviour. The composite section predicts larger displacements but the trend is found to be similar. This suggests that the global behaviour observed in the simplified 1D beams is representative of the behaviour of beams in a composite structure.
 - 1D beams can accurately represent the behavioural trends of structures in cooling, although do not necessarily predict the behaviour quantitatively.

Non-uniform fires (horizontal)

- Results in Chapter 4 indicate that the development of forces produced by horizontally travelling fires may be significantly different to those produced by uniform fires.
- Beams are likely to be subjected to both tensile and compressive forces within the duration of a realistic compartment fire. Thermal expansion and possibly compressive yielding would occur in some areas, while other areas would be contracting and possibly yielding in tension.
- Large residual bending moments are observed for the entire range of patch lengths and displacements were seen to vary greatly with time, often displaying cyclic movements.
- The axial forces in the uniformly heated beams are consistently greater than in any travelling fire scenario.
- Bending moments in uniformly heated beams are not necessarily greater than in travelling fire scenarios. The bending moments and displacements vary significantly depending on the temperature profile as well as the structural variables such as boundary conditions and loading. The uniform fire is therefore not the most conservative design scenario.
- The results in Chapter 7 show that the maximum displacements expected are larger for uniform fires than for any of the travelling fires. This is expected as the loss of strength occurs across the entire compartment; there are no parts of the floor section which retain significant strength thus restraining the vertical movement.

-
- In the travelling fires an irregular displacement pattern is observed which is not captured by the uniform fire cases. Across the compartment different rates of displacement occur, depending on the location of the near field temperature.
 - Irregular displacement patterns are also observed in Chapters 4 and 6, where non-uniform fires led to cyclic movement in the beams and columns respectively.
 - As the fire moves across the compartment, the axial forces change significantly, but the observed trend remains comparable for each travelling fire scenario. Once cooling has completed however, all beams have yielded in tension and a residual force remains.
 - The residual axial force observed in the travelling fires is higher than in the parametric fire case. This can be explained by the higher temperature reached during heating (1200°C near field temperatures, 1030°C peak parametric temperature). As was observed in Chapter 3, higher peak temperatures during heating result in higher residual tensile forces.
 - The residual bending moments are quite different between the uniform and non-uniform fires. Whilst after a parametric fire the bending moments reduce to values close to zero, after the travelling fires substantial residual moments remain. This is in contrast to Chapter 3 where larger lower peak temperatures resulted in higher residual bending moments. The bending moments are not only affected by the peak temperature, but also by the global structural behaviour. It was shown in Chapter 4 that the bending moments change significantly when non-uniform heating is applied to the

section. This is mostly induced by the irregular displacement pattern, which is also observed in the 3D compartment models in Chapter 7.

- Plastic strains in the rebar are compared. The strains are dependent on the location they are measured. The non-uniform fires generally have greater strains, again caused by the irregular deformation of the compartment. The strains in the parametric fire are much smaller than those expected in non-uniform fires, whereas the standard fire induces higher strains in some of the locations.
- The behaviour of a structure when subjected to a non-uniform fire does not respond in an identical manner as when subjected to design fires. Although similar peak displacements may be expected, the axial force, moment and strain evolution during the heating and cooling phase may be quite different. This has been shown in both Chapter 4 and 7.
- Differences also occur depending on which travelling fire scenario is chosen for the compartment considered. Smaller fires result in lower downward displacements of the bays, but a higher temperature difference between the near and far field leads to more continuity issues in some cases resulting in some upward movement at mid-span (for this specific compartment). This temperature difference also results in larger tensile forces and larger hogging moments, prior to the final cooling stage for the smaller fire percentages.
- Travelling fires capture all aspects of behaviour generally required for design; displacements, strains and forces.

Non-uniform fires (vertical)

- It is shown in Chapter 6 that a time delay considered between floor fires affects the global response of high-rise structures.
 - For short inter-floor time delays the structural behaviour was found to be very similar to when fires occurred simultaneously on the same number of floors.
- A key difference observed is the cyclic movement induced in columns at each floor level as the fire progressed upwards. This cyclic deflection pattern has not previously been considered when designing against fire. It will be of significance for fire design, particularly for connections which will already have severe demands made on their ductility capacity under fire loading.
 - With larger inter-floor time delays the global structural behaviour changed to the simultaneous multi-storey fire. This is particularly clear for the strong beam structure where significantly different behaviour was observed; not only in the fire floors but also in the rest of the structure. Cyclic movement of the columns also occurs here, albeit with a larger time interval.

8.2. Further Work

The work presented in this thesis provides an insight into global structural behaviour during cooling and non-uniform fires. A large amount of further work

could be undertaken to improve the understanding of structural behaviour during cooling and travelling fires.

The work presented on the cooling phase of the fire has shown that the linear rate of cooling of the gas temperature has very little effect on the overall behaviour of the structure. None of the models have explicitly modelled connections. The structural response to cooling has shown that very large axial tensile forces should be expected; connections are not normally designed to withstand these. Detailed research into connection behaviour would be essential to fully understand the risk of failure during a fire.

All the modelling in this thesis assumes the beams are unprotected and thus follow the gas temperature. When steel beams are protected a heat transfer analysis may be required to obtain the temperature evolution through the section. This could potentially affect the design as slower cooling may cause a continuing temperature rise in the steel once cooling has started. In situations where the limiting peak temperature in the sections is governed by loss of strength, the steel sections may require more protection to achieve this; this is likely to have consequences for the cost efficiency of the design. To what extent the temperature difference in protected steel as a consequence of various cooling rates will affect global behaviour should be investigated.

The work presented on travelling fires has incorporated several assumptions to simplify the analysis. Two directions of travel are considered but the fire is still assumed to be uniform along the one axis. Spatial variation is likely to occur in both directions, especially in very large compartments. Modelling the near field as a circle, with the far field affecting the remaining area of the compartment may be

the next step in increasing the accuracy of the temperature definition for structural analysis. However, this would also require a definition of the path the fire would take; something which has an almost infinite range of possibilities when considering all the variables which affect this behaviour. The ventilation conditions in particular are difficult to predict with accuracy but greatly affect the development of the fire. Doors and windows which are open or closed at the time the fire starts as well as glazing failure during the fire can affect the path significantly. Other factors such as the fuel load distribution would also require some quantification.

The compartment considered for travelling fires in this thesis is assumed to be completely enclosed by the surrounding structure; no edge conditions are considered. It would be interesting to explore the effect the irregular fire loading has on a compartment with irregular boundary conditions to explore the effects this may have.

It has been concluded that travelling fires are a more realistic design scenario for structural analysis than the currently used design fires. For this method to be generally applicable, some further considerations must be made. Rather than using a single uniform fire, a range of travelling fires could be considered. This range should be (at least) an upper and lower bound of the likely fire scenarios for any given compartment. For the compartment considered in this thesis this range was chosen as 25% to 100%, with any fires smaller than 25% being unrealistic. However, for very large structures, potentially with irregular layouts, this range could be very different. For example, a 1000m² compartment is unlikely to burn uniformly; an upper bound of 40 to 50% may be more appropriate. Similarly the lower bound may be as little as 5% which still represents a burning area of 50m².

If a 100% fire is deemed appropriate for a compartment this is effectively a uniform fire; although crucially it would burn for a much shorter duration as this is fuel dependent.

The appropriate range is clearly structure dependent and should be assessed with respect to the compartment size considered as well as possible ventilation conditions, e.g. worst case is the maximum possible ventilation with full glazing failure. Perhaps it would be possible to establish some guidelines on typical layouts, for example for square or rectangular floor areas with certain length to width ratios. On top of that it may be interesting to create tabulated data on the range of fires which may be expected depending on the compartment size and ventilation conditions (e.g. 25 or 50%). This would be an important step for developing this method into code recommendations.

The fire is currently modelled as a band of near field temperatures which moves across the structure. As the percentage fire is reduced, this band narrows. At some point the ratio of length to width becomes unrealistic from a fire science perspective. It would be interesting to explore this ratio for compartment fires as this would also give an insight towards determining realistic fire sizes and possible paths for a given structure.

One complication which does occur when modelling travelling fires is the requirement to model the entire fire compartment. Often simplifications are made and symmetry conditions are used to reduce the model size and complexity. However, as a travelling fire is an unsymmetrical load case the structure has to be considered in full. The fire compartment modelled in Chapter 7 is assumed to be part of a larger structure which is not affected by fire. This therefore allows for the slab and beams to be extended beyond the fire compartment and symmetry

conditions to be applied. Therefore care must be taken when modelling a structure for a travelling fire to ensure the boundary conditions are accurately represented. It may be interesting to explore the effect partial compartment modelling has when subjected to travelling fires and to what extent the symmetry conditions affect the response of the structure. This is in addition to the boundary conditions, such as edge beam which are mentioned earlier.

Vertically travelling fires have not been considered prior to the work done in this thesis. The results have indicated that a time delay between fire floors has an affect on the global structural behaviour, however the work has limitations in that it has only considered one structural form. Other structural layouts as well as internal vertical spread (through an atrium) or horizontal travel in combination with vertical spread may be interesting to consider next. Establishing a reasonable range of fire spread rates which would present an upper and lower bound for most structures would also be an important improvement.

References

1. *Eurocode 4 - Design of composite steel and concrete structures. Part 1-2: General rules - Structural fire design*, in *BS EN 1994-1-2:2005*. 2005, British Standards Institution.
2. Lamont, S., Lane, B., Flint, G., Usmani, A., *Behavior of structures in fire and real design - A case study*. *Journal of Fire Protection Engineering*, 2006. **16**(1): p. pp 5-35.
3. Gillie, M., Usmani, A., Rotter, J.M, *A structural analysis of the Cardington British Steel corner test*. *Journal of Constructional Steel Research*, 2001. **58**(4): p. 427-442.
4. Elghazouli, A.Y., B.A. Izzuddin, and A.J. Richardson, *Numerical modelling of the structural fire behaviour of composite buildings*. *Fire Safety Journal*, 2000. **35**(4): p. 279-297.
5. Huang, Z.H., I.W. Burgess, and R.J. Plank, *Modeling membrane action of concrete slabs in composite buildings in fire. II: Validations*. *Journal of Structural Engineering-ASCE*, 2003. **129**(8): p. 1103-1112.
6. *The behaviour of multi-storey steel framed buildings in fire*. 1999, British Steel Plc.
7. Lie, T.T., *Characteristic temperature curves for various fire severities*. *Fire Technology*, 1974. **10**(4).
8. Drysdale, D., *An Introduction to Fire Dynamics*. 2000, Chichester: John Wiley & Sons Ltd.
9. *Eurocode 1: Actions on Structures - Part 1-2: General Actions - Actions on Structures Exposed to Fire in EN 1991-1-2:2002*. 2002, British Standards Institution.
10. *ISO 834, in Fire resistance tests - elements of building construction*. 1975, International Standards Organization: Geneva, Switzerland.

-
11. Chung, K.F., *Fire resistance design of composite slabs in building structures: from research to practice*. The Structural Engineer, 2006. **84**(20): p. pp 30-36.
 12. Moss, P.J., Buchanan, A.H., Seputro, J., Wastney, C., Welsch, R., *Effect of support conditions on the fire behaviour of steel and composite beams*. Fire and Materials, 2004. **28**(2-4): p. 159-175.
 13. Huang, Z.H., I.W. Burgess, and R.J. Plank, *Three-dimensional analysis of composite steel-framed buildings in fire*. Journal of Structural Engineering-ASCE, 2000. **126**(3): p. 389-397.
 14. Lamont, S., Lane, B., Usmani, A., Flint, G., *Structural Behaviour in Fire and Real Design*. Fire Protection Engineering, 2006. **16**(5): p. 5-35.
 15. Kawagoe, K., *Fire Behaviour in Rooms*, in Report No. 27. 1958, Building Research Institute: Tokyo.
 16. Petterson, O., Magnusson, S.E, Thor, J, *Fire engineering design of structures*. 1976, Swedish Institute of Steel Construction.
 17. Kawagoe, K., Sekine, T, *Estimation of fire temperature-time curve in rooms*, in *BRI Occasional Report No. 11*. 1963, Building Research Institute, Ministry of Construction: Tokyo.
 18. Babrauskas, V., Williamson R.B, *Post Flashover Compartment Fires: Basis of a Theoretical Model*. Fire and Materials, 1978(2): p. 39-53.
 19. Bailey, C., *One Stop Shop in Structural Fire Engineering*, <http://www.mace.manchester.ac.uk/project/research/structures/strucfire/default.htm>.
 20. Cooke, G.M.E., *Tests to determine the behaviour of fully developed natural fires in a large compartment*, in *Fire Note 4*. 1998, Fire Research Station, Building Research Establishment.
 21. Gillie, M., Stratford, T., *Chapter 8, Behaviour of the Structure during the Fire*, in *The Dalmarnock Fire Tests: Experiments and Modelling*, G. Rein,

-
- Abecassis Empis, C., Carvel, R., Editor. 2007, School of Engineering and Electronics, University of Edinburgh: ISBN 978-0-9557497-0-4.
22. Gann, R.G., *Reconstruction of the Fires in the World Trade Center Towers*. NIST NCSTAR 1-5, September 2005.
 23. Fletcher, I. *Model-Based Analysis of a Concrete Building Subject to Fire*. in *Advanced Research Workshop on Fire Computer Modelling*. November 2007. Santander, Spain.
 24. Zannoni, M., *Brand bij Bouwkunde*. COT Instituut voor Veiligheids- en Crisismanagement, December 2008.
 25. Rein, G.Z., X., Williams, P. Hume, B., Heise, A., Jowsey, A., Lane, B., Torero, J.L. *Multi-storey fire analysis for high-rise buildings*. in *11th Interflam*. 2007. London.
 26. Stern-Gottfried, J., Rein, G., Lane, B., Torero, J., *An innovative approach to design fires for structural analysis of non-conventional buildings - A case study*. in *Application of Structural Fire Engineering*. February 2009. Prague, Czech Republic.
 27. BRE-FRS, *Fire Performance of external thermal insulation for walls of multi-storey buildings*. 2003.
 28. Fletcher, I., Borg, A., Hitchen, N., Welch, S. *Performance of concrete in fire: a review of the state of the art, with a case study of the Windsor Tower*. in *4th International Workshop 'Structures in Fire'* 2006. Aveiro, Portugal.
 29. NCE, *Madrid tower designer blames missing fire protection for collapse*, in *New Civil Engineer*. 2 July 2005.
 30. Bailey, C., Burgess, I.W., Plank, R.J., *Computer Simulation of a Full-Scale Structural Fire Test*. *The Structural Engineer*, 1996(74(6)): p. 93-100.

-
31. Huang, Z.H. and A. Platten, *Nonlinear finite element analysis of planar reinforced concrete members subjected to fires*. ACI Structural Journal. **94**(3): p. 272-282.
 32. Huang, Z.H., I.W. Burgess, and R.J. Plank, *Three-dimensional analysis of composite steel-framed buildings in fire*. Proceedings of the Institute of Civil Engineers, Structures and Buildings, 1999. **134**(1): p. 243-255.
 33. Vulcan, www.vulcan-solutions.com. 2008: Sheffield, UK.
 34. Izzuddin, B.A. and D.B. Moore, *Lessons from a full-scale fire test*. Proceedings of the Institution of Civil Engineers-Structures and Buildings, 2002. **152**(4): p. 319-329.
 35. Abaqus, in *Abaqus Users' Manual*. 2006, Abaqus: RI.
 36. Gillie, M., A.S. Usmani, and J.M. Rotter, *A structural analysis of the first Cardington test*. Journal of Constructional Steel Research, 2001. **57**(6): p. 581-601.
 37. Sanad, A.M., J.M. Rotter, and M. O'Connor, *Finite Element Modelling of Fire Tests on the Cardington Composite Building*. Proceedings of Interflam 1999, 1999. **2**.
 38. Gillie, M., Usmani, A., Rotter, M., O'Conner, M., *Modelling of heated composite floor slabs with reference to the Cardington experiments*. Fire Safety Journal, 2001. **36**(8): p. 745-767.
 39. Report, P.i.T., *Behaviour of steel framed structures under fire conditions*, in *Main Report*. 2001, University of Edinburgh.
 40. Bailey, C. *A Simple new fire design method to predict the structural response of steel frames with composite floors*. in *NSCC 2001 9th Nordic Steel Construction Conference*. 2001. Helsinki, Finland.
 41. Yin, Y.Z. and Y.C. Wang, *Analysis of catenary action in steel beams using a simplified hand calculation method, Part 1: theory and validation for uniform temperature distribution*.

-
42. Yin, Y.Z. and Y.C. Wang, *Analysis of catenary action in steel beams using a simplified hand calculation method, Part 2: validation for non-uniform temperature distribution.*
 43. Flint, G., *Fire Induced Collapse of Tall Buildings*, in *BRE Centre for Fire Safety Engineering*. 2005, University of Edinburgh.
 44. Usmani, A.S., Y.C. Chung, and J.L. Torero, *How did the WTC towers collapse: a new theory.* *Fire Safety Journal*, 2003. **38**(6): p. 501-533.
 45. Usmani, A.S., *Stability of the World Trade Center Twin Towers structural frame in multiple floor fires.* *Journal of Engineering Mechanics-ASCE*, 2005. **131**(6): p. 654-657.
 46. El-Rimawi, J.A., I.W. Burgess, and R.J. Plank, *The Treatment of Strain Reversal in Structural Members During the Cooling Phase of a Fire.* *Journal of Constructional Steel Research*, 1996. **37**: p. 115-135.
 47. Bailey, C., *Analysis of the Effects of Cooling and Fire Spread on Steel-framed Buildings.* *Fire Safety Journal*, 1996. **26**: p. 273-293.
 48. Wang, P., G. Li, and S. Guo, *Effects of the cooling phase of a fire on steel structures.* *Fire Safety Journal*. **43**(6): p. 451-458.
 49. Franssen, J.-M., D. Pintea, and J.-C. Dotreppe, *Considering the effects of localised fires in the numerical analysis of a building structure.* *Fire Safety Journal*, 2007. **42**(6-7): p. 473-481.
 50. Liu, T.C.H., M.K. Fahad, and J.M. Davies, *Experimental investigation of behaviour of axially restrained steel beams in fire.* *Journal of Constructional Steel Research*, 2002. **58**(9): p. 1211-1230.
 51. *Investigation of Broadgate Phase 8 Fire*, in *Report of Fire Engineering Consultant Ltd*. 1991, SCIF Fire Engineering Group.
 52. Fletcher, I., Welsh, S., Torero, J., Carvel, R., Usmani, A., *The behaviour of concrete structures.* *Journal of Thermal Science*.

-
53. Naus, D.J., *The Effect of Elevated Temperature on Concrete Materials and Structures - A Literature Review*. 2006, U.S. Nuclear Regulatory Commission: Washington.
 54. *Eurocode 3: Design of steel structures, General Rules - Structural Fire Design*, in *BS EN 1993-1-2:2005*. 2005, British Standards Institution.
 55. Luo, X., W. Sun, and S.Y.N. Chan, *Effect of heating and cooling regimes on residual strength and microstructure of normal strength and high-performance concrete*. *Cement and Concrete Research*, 2000. **30**(3): p. 379-383.
 56. Husem, M., *The effects of high temperature on compressive and flexural strengths of ordinary and high-performance concrete*. *Fire Safety Journal*, 2006. **41**(2): p. 155-163.
 57. Hertz, K.D., *Concrete strength for fire safety design*. *Magazine of Concrete Research*, 2005. **57**(8): p. 445-453.
 58. Burgess, I.W., J. Elrimawi, and R.J. Plank, *Studies of the Behavior of Steel Beams in Fire*. *Journal of Constructional Steel Research*, 1991. **19**(4): p. 285-312.
 59. Foster, S., Chladna, M., Hsieh, C., Burgess, I., Plank, R., *Thermal and structural behaviour of a full-scale composite building subject to a severe compartment fire*. *Fire Safety Journal*, 2007. **42**(3): p. 183-199.
 60. Usmani, A.S. and S. Lamont, *Key events in the structural response of a composite steel frame structure in fire*. *Fire and Materials*, 2004. **28**(2-4): p. 281-297.
 61. Usmani, A.S., Rotter, M., Lamont, S., Sanad, A.M., Gillie, M., *Fundamental principles of structural behaviour under thermal effects*. *Fire Safety Journal*, 2001. **36**(8): p. 721-744.

-
62. *Joints in Steel Construction*, in *Simple Connections (SCI-P212-2002)*. 2002, The Steel Construction Institute and The British Constructional Steelwork Association Ltd.
 63. PIT, *Behaviour of steel-framed structures under fire conditions*, in *Main Report*. 2001, University of Edinburgh.
 64. Gillie, M., *Analysis of heated structures: Nature and modelling benchmarks*. Fire Safety Journal, 2009. **44**(5): p. 673-680.
 65. Rein, G., J. Torero, and B. Lane. *On the design fire for non-conventional structures*. in *Advanced Research Workshop on Fire Computer Modelling*. 2007. Santander.
 66. Buchanan, A.H., *Structural Design for Fire Safety*. 2001: John Wiley & Sons.
 67. Usmani, A., Roben, C., Johnston, L., Flint, G., Jowsey, A., *Tall building collapse mechanisms initiated by fire*. in *4th Workshop on Structures in Fire*. 2006. Aveiro, Portugal.
 68. Usmani, A., Flint, G., Jowsey, A., Roben, C., Torero, J., *Collapse scenarios of WTC 1&2 with extension to generic tall buildings*. in *La seguridad contra incendios en edificios de gran altura 2006*. Santander, Spain.
 69. Heise, A., G. Flint, and B. Lane. *Effect of fire on tall buildings: Case study*. in *The Third International Conference on Steel and Composite Structures (ICSCS)*. 2007. Manchester, UK.
 70. Roben, C., *Fire Induced Instability in Multi-Storey Frames*, in *MEng Thesis*. 2006, University of Edinburgh.
 71. *Structural use of steelwork in buildings - Part 1: Code of practice for design - Rolled and welded sections*, in *BS5950-1:2000*. 2000, British Standards Institution.

-
72. Quiel, S. and M. Garlock. *3-D versus 2-D modelling of a high-rise steel framed building under fire*. in *Proceedings of the Fifth International Conference on Structures in Fire*. 2008. Singapore.
 73. Dexter, R.J. and L.W. Lu, *The effects of a severe fire on the steel frame of an office building*. Engineering Journal-American Institute of Steel Construction Inc, 2001. **38**(4): p. 167-175.
 74. Huang, H.C. and A. Usmani, *Finite Element Analysis for Heat Transfer - Theory and Software*. 1994, London: Springer-Verlag.
 75. Jowsey, A., *Fire Imposed Heat Fluxes for Structural Analysis*. 2006, University of Edinburgh.
 76. Usmani, A., Roben, C., and Al-Remal, A., *A Very Simple Method for Assessing Tall Building Safety in Major Fires*. International Journal of Steel Structures, 2009(9): p. 17-28.
 77. Roben, C., Gillie, M., Usmani, A., Torero, J., *Collapse scenarios for tall buildings in fire during cooling*. in *5th International Seminar on Fire and Explosion Hazards*. 2007. Edinburgh, UK.
 78. Elghazouli, A.Y. and B.A. Izzuddin, *Analytical assessment of the structural performance of composite floors subject to compartment fires*. Fire Safety Journal, 2001. **36**(8): p. 769-793.
 79. Sanad, A.M., Rotter, J.M., Usmani, A., O'Connor, M.A., *Composite beams in large buildings under fire - numerical modelling and structural behaviour*. Fire Safety Journal, 2000. **35**(3): p. 165-188.
 80. Wang, Y.C., *Performance of steel-concrete composite structures in fire*. Progress in Structural Engineering and Materials, 2005. **7**: p. 86-102.
 81. Alpert, R.L., *Calculation of Response Time of Ceiling-Mounted Fire Detectors*. Fire Technology, 1972. **8**: p. 181-195.

-
82. *Eurocode 1: Actions on structures - Part 1-1: General actions - Densities, self-weight, imposed loads for buildings*, in *BS EN 1991-1-2:2002*. 2002, British Standards Institute.

Appendix A

Variation of output with changing step time

When varying the rotational spring stiffness of the beam some inconsistent results were obtained. Certain combinations of stiffness and peak temperature seemed to lead to upward buckling. This behaviour was investigated to establish whether this was caused by a numerical instability or a physical buckling of the beam.

Removing any of the non-linear aspects (such as the material behaviour or boundary conditions) eliminates the issue of upward deflection. However, it was difficult to find a physical reason for this behaviour thus the possibility of a numerical instability was explored further.

It was found that changing the step time increment influences the behaviour substantially. Figure A-0-1 and Figure A-2 show the vertical displacement at mid-span of two of the beams considered. The graphs are associated with a peak temperature and two different spring stiffnesses. The variable is the defined maximum step increment. The mid-span deflections should be identical for each of the outputs as the analysis in itself remains the same. However, the results are very different depending on the step increment chosen for the analysis as is clearly shown in each of the graphs below. This must therefore be a numerical issue, rather than a physical one.

From Figure A-0-1 it can also be seen that the incorrect results are not constant. Not only are upward deflections predicted, but also zero deflections (as the beam buckles to the second order thus having a zero deflection at mid span) and incorrect downward deflections.

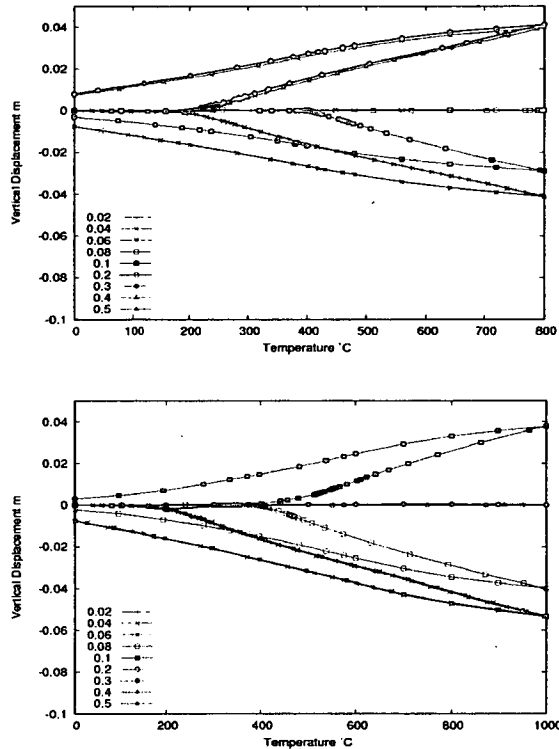


Figure A-0-1 – Displacements with spring = 43750000 (0.7) and peak 800°C and 1000°C respectively

Figure A-3 shows plots of the mid span displacement against the step increment for each of the four combinations of spring stiffness and peak temperature. In Figure A-4 these four outputs are plotted together.

As can be seen from all the graphs above and Figure A-4 in particular, there is no consistent pattern to the result output. However, for each case the results are

accurate when the step increment is sufficiently small (less than 0.04). This is promising as we can ensure the numerical issues are eliminated by choosing an appropriately small step increment value.

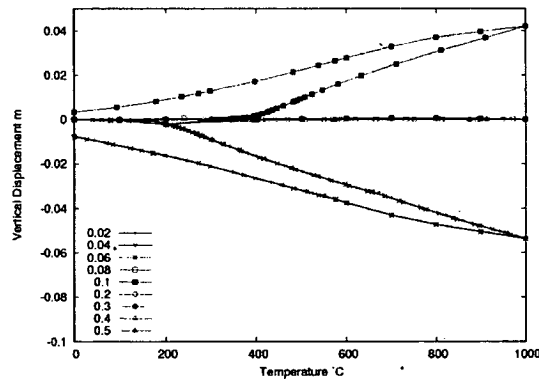
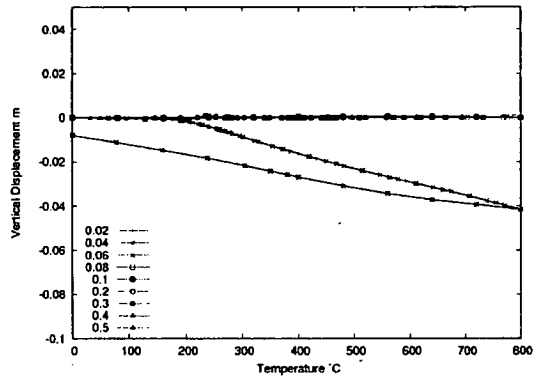


Figure A-0-2 – Displacements with spring = 37500000 (0.5) and peak with 800°C and 1000°C respectively

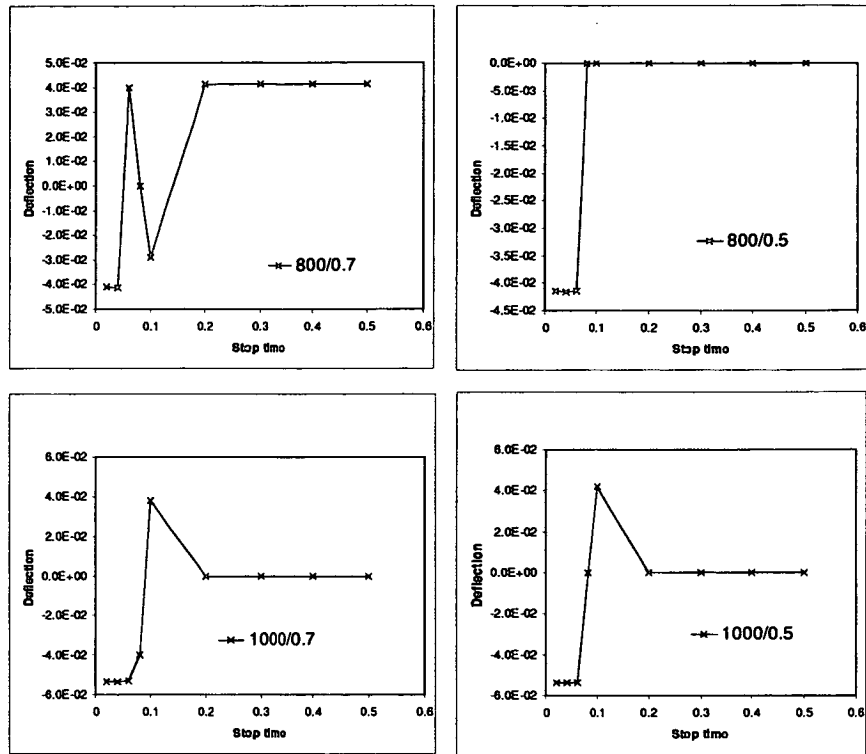


Figure A-0-3 – Displacements at mid-span against step increments for all four cases considered individually

After applying this smaller step increment the results are as expected – with downward displacements only as shown in the figure below.

Figure A-0-5 shows the results for a beam with varying rotational stiffnesses but with a constant step increment of 0.02 during heating. Figure A-0-6 shows the displacement with time for an identical beam but with an I-section rather than square. In this case it was found that similar problems are not experienced and that each of the chosen step times gives an identical result.

As the majority of work on structural behaviour during fire is done on I-beams rather than rectangular sections of steel, these numerical instabilities will not affect

results. It is however important to note that care must be taken when considering complex highly non-linear behaviour and that it may be necessary in some cases to do a sensitivity study to ensure the results are consistent.

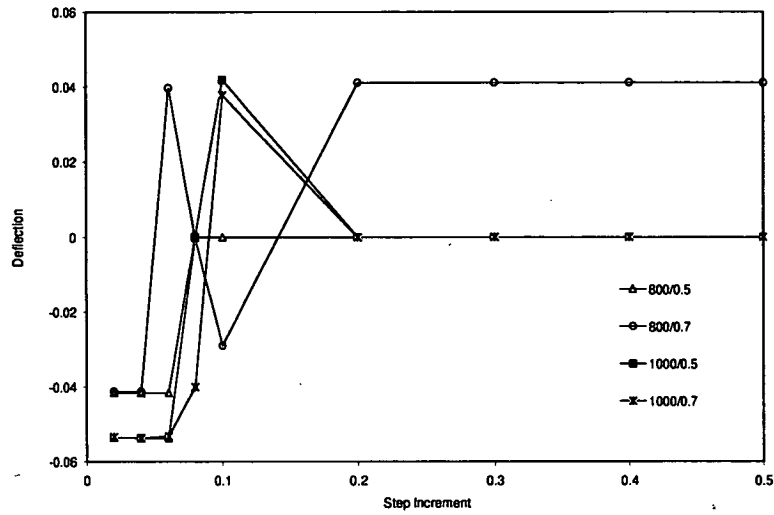


Figure A-0-4 – Displacements at mid-span against step increments for all four cases considered combined

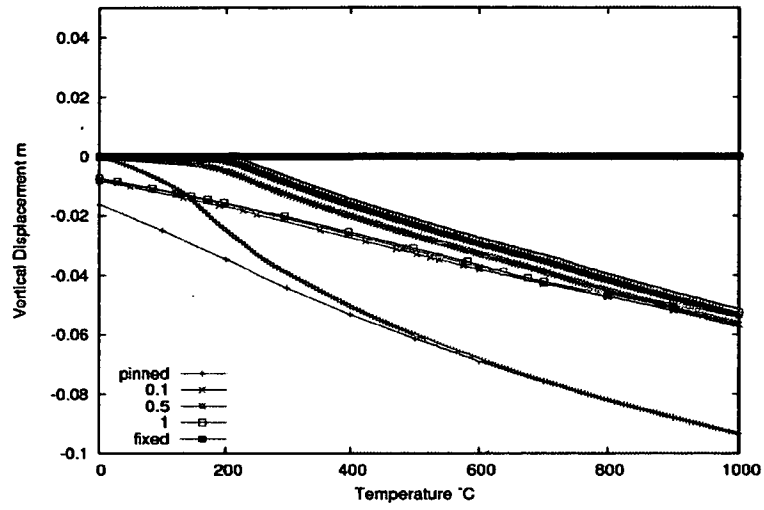


Figure A-0-5 – Displacements at mid-span with step increment reduced to obtain accurate results

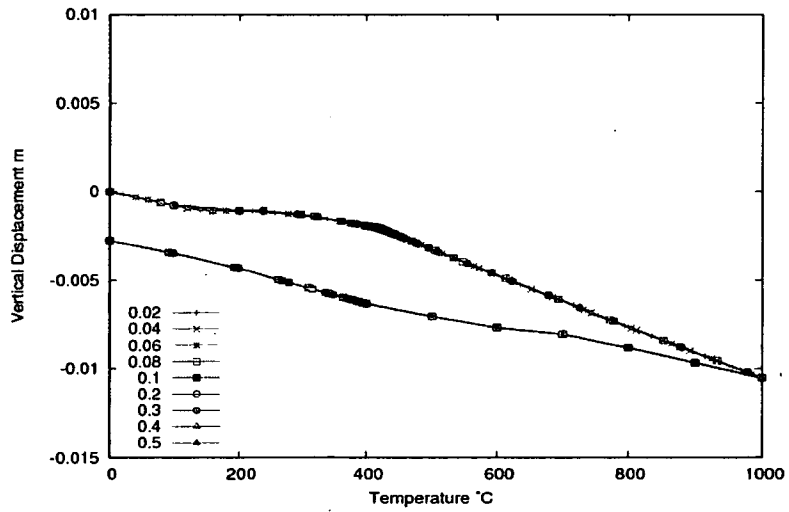


Figure A-0-6 - Displacements at mid-span for step increments for I beam

Appendix B1

User subroutines for travelling fires on 1D beams.

Temperature definitions for steel for travelling fire scenario with 40% patch length and 800°C peak temperature.

```

SUBROUTINE UTEMP (TEMP, NGCEPT, KSTEP, KINC, TIME, NODE, COORDS)
C
C   INCLUDE 'ABA_PARAM.INC'
C   DIMENSION TEMP (NGCEPT), TIME (2), COORDS (3)
C   Routine to model a "mountain" of temperature moving along a beam

INTEGER PEAK      !peak temperature at "summit" of mountain
INTEGER PLEN      !Total length of base of mountain
INTEGER BLEN      !Total length of beam
INTEGER FLEN      !Total length travelled by fire

PEAK=800
PLEN=400
BLEN=1000
FLEN=PLEN+BLEN

TEMP (1)=0      !Initialize midsurface temp

TEMP (1)=(PEAK/(PLEN/2))*(FLEN*TIME(1)-COORDS(1))      !Climbing mountain

IF (TEMP (1).GT.PEAK) THEN
TEMP (1)=PEAK-(PEAK/(PLEN/2))*(FLEN*TIME(1)-COORDS(1)-PLEN/2) !Descending mountain
END IF

IF (TEMP (1).LT.0) THEN
TEMP (1)=0      !Avoids negative temperatures
END IF

TEMP (2)=TEMP (1)/2
TEMP (3)=0

RETURN
END
```

Appendix B2

User subroutines for travelling fires on composite structures

Temperature definitions for steel for 50% travelling fire scenario

```
Dec 01, 09 9:14                                user50.f                                Page 1/2
SUBROUTINE UTEMP (TEMP, NSCEPT, KSTEP, KING, TIME, NODE, COORDS)
C
  INCLUDE 'ABA_PARAM.INC'
C
  DIMENSION TEMP (NSCEPT), TIME (2), COORDS (3)
C
  Routine to model a travelling fire across a compartment

  REAL PEAK      !peak temperature
  INTEGER PLEN   !Total length of base of mountain
  INTEGER BLEN   !Total length of beam
  INTEGER FLEN   !Total length travelled by fire

  PEAK=3500
  FARF=911
  PLEN=10583
  BLEN=18000
  FLEN=PLEN+BLEN

  TEMP (1)=FARF
  TEMP (1)=(PEAK/(PLEN/2))*(FLEN*(TIME (1)/3420)-((COORDS (1)*1000))+FARF
  !Increasing temperature

  IF (TEMP (1).GT.PEAK)THEN
    TEMP (1)=PEAK-(PEAK/(PLEN/2))*(FLEN*(TIME (1)/3420)-((COORDS (1)*1000))-PLEN/2)
    !Decreasing temperature
  END IF

  IF (TEMP (1).GT.1200)THEN
    TEMP (1)=1200
  END IF

  IF (TEMP (1).LT.FARF)THEN
    TEMP (1)=FARF
    !Avoids temperatures to go below the f
    ar field value during heating
  END IF

  IF (TEMP (1).LT.20)THEN
    TEMP (1)=20
  END IF

  IF (TEMP (1).GT.3420)THEN
    TEMP (1)=FARF-((TIME (1)-3420))
    !Linear cooling branch included for th
    e steel beam
  END IF

  IF (TEMP (1).GT.3600)THEN
    TEMP (1)=500-(0.667*(TIME (1)-3600))
  END IF

  IF (TEMP (1).GT.4200)THEN
    TEMP (1)=300-(0.055*(TIME (1)-4200))
  END IF

  IF (TEMP (1).GT.7000)THEN
    TEMP (1)=200-(0.05*(TIME (1)-7000))
  END IF

  IF (TEMP (1).GT.9000)THEN
    TEMP (1)=100-(0.0276*(TIME (1)-9000))
  END IF
```

Tuesday December 01, 2009

use

Dec 01, 09 9:14

user50.f

Page 2/2

```
TEMP(2)=TEMP(1)                                ! Gradients in the I-section
TEMP(3)=TEMP(1)*0.9
TEMP(4)=TEMP(1)*0.8
TEMP(5)=TEMP(1)*0.8

nt after cooling
IF (TEMP(2) .LT. 20) THEN                       ! Avoids temperatures lower than ambie
TEMP(2)=20
END IF

IF (TEMP(3) .LT. 20) THEN
TEMP(3)=20
END IF

IF (TEMP(4) .LT. 20) THEN
TEMP(4)=20
END IF

IF (TEMP(5) .LT. 20) THEN
TEMP(5)=20
END IF

RETURN
END
```

Flux definition for concrete slab for 50% travelling fire scenario

```

Nov 23, 09 14:11                               user_50HT3.f                               Page 1/2
SUBROUTINE DFLUX (FLUX, SOL, KSTEP, RINC, TIME, NOEL, NPT, COORDS,
1  JLTYP, TEMP, PRESS, SNAME)
C
  INCLUDE 'ABA_PARAM.INC'

  DIMENSION FLUX(2), TIME(2), COORDS(3), TEMP(2)
  CHARACTER*80 SNAME

C
  Routine to model a "mountain" of temperature moving along a beam

  REAL    PEAK    !peak temperature at "summit" of mountain
  INTEGER PLEN    !Total length of base of mountain
  INTEGER BLEN    !Total length of beam
  INTEGER FLEN    !Total length travelled by fire
  INTEGER FIRL    !Length of the fire patch
  INTEGER LASC    !length of triangular section
  INTEGER LPEA    !length of peak temperature patch
  INTEGER FARF    !FAR FIELD TEMP
  INTEGER PREF    !PRE DESCENDING SLOPE DISTANCE (LASC+PLEN)
  INTEGER POSF
  INTEGER LPAR    !LENGHT OF FAR FIELD SECTION BEFORE NF BEGINS
  REAL    PREC    !FUNCTION OF COORDS AND TIME FOR SLOPE DEF
  REAL    POSC    !FUNCTION OF COORDS AND TIME FOR SLOPE DEF
  REAL    GAST    !Gas temperature
  REAL    GAS1
  REAL    GAS2
  REAL    QCON
  REAL    QRAD

  PEAK=1200
  FARF=911
  PLEN=10
  BLEN=18000
  FLEN=BLEN+36020
  LASC=0
  PREF=LASC+PLEN
  LPEA=18000
  POSF=PLEN+LPEA
  PREC=FLEN*(TIME(1)/3420)-(COORDS(1)*1000)-PLEN
  POSC=FLEN*(TIME(1)/3420)-(COORDS(1)*1000)-POSF
  COOR=COORDS(1)*1000

  GAST=FARF    !Initialize midsurface temp

  IF (PREC.GT.COOR) THEN
    GAST=((FLEN*(TIME(1)/3420)-(COORDS(1)*1000)-PLEN)*((PEAK-FARF)/PLEN))
  END IF

  IF (POSC.GT.COOR) THEN
    GAST=PEAK-(PEAK/(PLEN))*(FLEN*(TIME(1)/3420)-((COORDS(1)*1000)-PREF))
  END IF

  IF (GAST.LT.FARF) THEN
    GAST=FARF
  END IF

  IF (GAST.GT.PEAK) THEN
    GAST=PEAK
  END IF

  IF (TIME(1).GT.3420) THEN

```


Nov 23, 09 14:11

user_50HT3.f

Page 2/2

```
GAST=0
END IF

QCON=25*(GAST-SOL)
QRAD=(0.8*5.67E-8)*(((GAST+273)**4)-((SOL+273)**4))

FLUX(1)=(QCON+QRAD)

RETURN
END
```

0HT3.f

1/1

Appendix C

Design of steel beams used in the 2D model in Chapters 5 and 6.

Design of UB 533x210x92 – Weak Beam	Reference
<p>Loading</p> <p>Live load = 3kN/m^2 (load factor = 1.6; live load = 5kN/m^2) Dead load from 100mm concrete slab $24\text{kN/m}^3 = 2.4\text{kN/m}^2$ (load factor = 1.4; dead load = 3.4kN/m^2) Dead load from steel beam (92.1 kg/m) 0.9kN/m or 0.15kN/m^2</p> <p>Total load = 8.55kN/m^2</p>	<p>BS 6399-1 and BS 6399-3</p>
<p>Shear Capacity</p> <p>$P_v = 0.6 \rho_y A_v$ $A_v = tD$ $\rho_y = 355\text{N/mm}^2$ $A_v = 10.1 \times 533.1 = 5384.31\text{mm}^2$</p> <p>Shear Capacity P_v: $P_v = 0.6 \times 355 \times 5384.31 = 1146.8\text{kN}$</p> <p>Check that $F_v < P_v$ $F_v = 8.55 \times 6 \times (10/2) = 256.5\text{kN}$ $F_v < 0.6 P_v$ ok Low shear</p>	<p>BS 5950-1:2000 Section 4.3.2</p>
<p>Moment Capacity</p> <p>$M_c = \rho_y S$ $S = 2360$ (plastic modulus)</p> <p>Moment Capacity: $M_c = 2360 \times 355 = 837.8\text{kNm}$</p> <p>Check that $M < M_c$ $M = WL^2/8$ $M = ((8.55 \times 6) \times 10^2) / 8 = 641\text{kNm}$</p> <p>$M < M_c$ ok</p>	<p>BS 5950-1:2000 Section 4.2.5</p>

Design of UB 838x292x176 – Strong Beam	Reference
Loading	BS 6399-1 and BS 6399-3
Live load = 3kN/m ² (load factor = 1.6; live load = 5kN/ m ²) Dead load from 100mm concrete slab 24kN/m ³ = 2.4kN/m ² (load factor = 1.4; dead load = 3.4kN/ m ²) Dead load from steel beam (175.9 kg/m) 1.72kN/m or 0.288kN/m ² Total load = 8.7kN/m ²	
Shear Capacity	BS 5950-1:2000
$P_v = 0.6 \rho_y A_v$ $A_v = tD$ $\rho_y = 355\text{N/mm}^2$ $A_v = 14.0 \times 761.7 = 10663.8\text{mm}^2$ Shear Capacity P_v : $P_v = 0.6 \times 355 \times 10663.8 = 2271\text{kN}$ Check that $F_v < P_v$ $F_v = 8.7 \times 6 \times (10/2) = 261\text{kN}$ $F_v < 0.6 P_v$ ok Low shear	Section 4.3.2
Moment Capacity	BS 5950-1:2000
$M_c = \rho_y S$ $S = 6808$ (plastic modulus) Moment Capacity: $M_c = 6808 \times 355 = 2417\text{kNm}$ Check that $M < M_c$ $M = WL^2/8$ $M = ((8.7 \times 6) \times 10^2) / 8 = 652.5\text{kNm}$ $M < M_c$ ok	Section 4.2.5

Appendix D

This appendix provides the Abaqus input for the material properties for both steel and concrete assumed in Chapters 3, 5 and 7.

The material properties for steel are taken from Eurocodes 3 [1] and a yield strength of 355 MPa is assumed. Isotropic hardening of structural steel is incorporated. The material properties for concrete are based on Eurocode [4]. The compressive strength of concrete at ambient temperature is taken to be 35MPa.

Stresses on cooling are governed by Von Mises and Drucker-Prager yield criterion for steel and concrete respectively. It was assumed the material properties returned to their original ambient values after the cooling phase. The unloading occurs at the same stiffness as the elastic loading path for both materials.

The material properties are defined in Abaqus as follows:

Steel:

```
*Material, name = [name]
*Density
[Density]
*Elastic
[Young's modulus, poissons ratio, temperature]
*Plastic
[Yield stress, plastic strain, temperature]
*Expansion
[Expansion coefficient, temperature]
```

Concrete:

```
*Material, name = [name]
*Density
[Density]
*Expansion
[Expansion coefficient, temperature]
*Elastic
[Young's modulus, poissons ratio, temperature]
*concrete damaged plasticity
[Dilation angle, flow potential eccentricity, ratio of initial equibiaxial compressive yield stress to initial uniaxial compressive yield stress, ratio of the second stress invariant on the tensile meridian, viscosity parameter]
*concrete compression hardening
[Yield stress, inelastic strain, inelastic strain rate, temperature]
*concrete tension stiffening
[Remaining direct stress after cracking, direct cracking strain, direct cracking strain rate, temperature]
```

Input for Chapter 3

*Material, name=STEEL

*Density

7.85e-09,

*Elastic

2.1E+11,0.3,0

2.1E+11,0.3,100

1.89E+11,0.3,200

1.68E+11,0.3,300

1.47E+11,0.3,400

1.26E+11,0.3,500

6510000000,0.3,600

2730000000,0.3,700

1890000000,0.3,800

1417500000,0.3,900

945000000,0.3,1000

472500000,0.3,1100

*Expansion

1.23e-05, 0.

1.25e-05, 100.

1.29e-05, 200.

1.33e-05, 300.

1.37e-05, 400.

1.41e-05, 500.

1.45e-05, 600.

1.49e-05, 700.

1.41e-05, 800.

1.34e-05, 900.

1.41e-05,1000.

1.46e-05,1100.

1.51e-05,1200.

*Plastic

250500000 ,0.0000 ,20

250625000 ,0.0013 ,20

250750000 ,0.0018 ,20

250875000 ,0.0023 ,20

251000000 ,0.0028 ,20

251125000 ,0.0033 ,20

251250000 ,0.0038 ,20

251375000 ,0.0043 ,20

251500000 ,0.0048 ,20

251625000 ,0.0053 ,20

251750000 ,0.0058 ,20

251875000 ,0.0063 ,20

252000000 ,0.0068 ,20

252125000 ,0.0073 ,20

252250000 ,0.0078 ,20

252375000 ,0.0083 ,20
252500000 ,0.0087 ,20
252625000 ,0.0092 ,20
252750000 ,0.0097 ,20
252875000 ,0.0102 ,20
253000000 ,0.0107 ,20
253125000 ,0.0112 ,20
253250000 ,0.0117 ,20
253375000 ,0.0122 ,20
253500000 ,0.0127 ,20
253625000 ,0.0132 ,20
253750000 ,0.0137 ,20
253875000 ,0.0142 ,20
254000000 ,0.0147 ,20
254125000 ,0.0152 ,20
254250000 ,0.0156 ,20
254375000 ,0.0161 ,20
254500000 ,0.0166 ,20
254625000 ,0.0171 ,20
254750000 ,0.0176 ,20
254875000 ,0.0181 ,20
255000000 ,0.0186 ,20
325000000 ,0.0377 ,20
359375000 ,0.1381 ,20
100 ,0.1823 ,20
250500000 ,0.0000 ,100
250625000 ,0.0013 ,100
250750000 ,0.0018 ,100
250875000 ,0.0023 ,100
251000000 ,0.0028 ,100
251125000 ,0.0033 ,100
251250000 ,0.0038 ,100
251375000 ,0.0043 ,100
251500000 ,0.0048 ,100
251625000 ,0.0053 ,100
251750000 ,0.0058 ,100
251875000 ,0.0063 ,100
252000000 ,0.0068 ,100
252125000 ,0.0073 ,100
252250000 ,0.0078 ,100
252375000 ,0.0083 ,100
252500000 ,0.0087 ,100
252625000 ,0.0092 ,100
252750000 ,0.0097 ,100
252875000 ,0.0102 ,100
253000000 ,0.0107 ,100
253125000 ,0.0112 ,100
253250000 ,0.0117 ,100
253375000 ,0.0122 ,100

253500000 ,0.0127 ,100
253625000 ,0.0132 ,100
253750000 ,0.0137 ,100
253875000 ,0.0142 ,100
254000000 ,0.0147 ,100
254125000 ,0.0152 ,100
254250000 ,0.0156 ,100
254375000 ,0.0161 ,100
254500000 ,0.0166 ,100
254625000 ,0.0171 ,100
254750000 ,0.0176 ,100
254875000 ,0.0181 ,100
255000000 ,0.0186 ,100
325000000 ,0.0377 ,100
359375000 ,0.1381 ,100
100 ,0.1823 ,100
216690841.2 ,0.0000 ,200
220307508.3 ,0.0013 ,200
223289058 ,0.0018 ,200
225864343.2 ,0.0023 ,200
228148274.9 ,0.0028 ,200
230208380 ,0.0033 ,200
232088383.2 ,0.0038 ,200
233818538.2 ,0.0042 ,200
235420813 ,0.0047 ,200
236911755.8 ,0.0052 ,200
238304196.3 ,0.0057 ,200
239608314.4 ,0.0062 ,200
240832341.4 ,0.0067 ,200
241983038.3 ,0.0072 ,200
243066032 ,0.0077 ,200
244086056.8 ,0.0082 ,200
245047133.9 ,0.0087 ,200
245952705.4 ,0.0091 ,200
246805736.9 ,0.0096 ,200
247608797.8 ,0.0101 ,200
248364123.3 ,0.0106 ,200
249073664.9 ,0.0111 ,200
249739130.1 ,0.0116 ,200
250362014.9 ,0.0121 ,200
250943630.5 ,0.0126 ,200
251485125 ,0.0131 ,200
251987501.2 ,0.0136 ,200
252451631.6 ,0.0140 ,200
252878270.9 ,0.0145 ,200
253268066 ,0.0150 ,200
253621564.6 ,0.0155 ,200
253939222 ,0.0160 ,200
254221407.3 ,0.0165 ,200

254468407.1 ,0.0170 ,200
254680429.9 ,0.0175 ,200
254857608 ,0.0180 ,200
255000000 ,0.0185 ,200
325000000 ,0.0375 ,200
359375000 ,0.1379 ,200
120 ,0.1823 ,200
175179499.5 ,0.0000 ,300
183867854.2 ,0.0009 ,300
190594072.9 ,0.0014 ,300
196223945.2 ,0.0018 ,300
201120506.2 ,0.0023 ,300
205477522.2 ,0.0028 ,300
209413053.9 ,0.0032 ,300
213005415.1 ,0.0037 ,300
216309737.3 ,0.0042 ,300
219366577.9 ,0.0047 ,300
222206799.4 ,0.0052 ,300
224854524.9 ,0.0056 ,300
227329021.8 ,0.0061 ,300
229645956.5 ,0.0066 ,300
231818256.5 ,0.0071 ,300
233856723.3 ,0.0076 ,300
235770476.6 ,0.0081 ,300
237567284.8 ,0.0085 ,300
239253814.7 ,0.0090 ,300
240835823.5 ,0.0095 ,300
242318308.7 ,0.0100 ,300
243705625.6 ,0.0105 ,300
245001582.3 ,0.0110 ,300
246209515.7 ,0.0115 ,300
247332352.5 ,0.0119 ,300
248372660.9 ,0.0124 ,300
249332691.2 ,0.0129 ,300
250214410.9 ,0.0134 ,300
251019532.9 ,0.0139 ,300
251749539.4 ,0.0144 ,300
252405701.6 ,0.0149 ,300
252989096 ,0.0154 ,300
253500617.9 ,0.0158 ,300
253940992.6 ,0.0163 ,300
254310783.5 ,0.0168 ,300
254610399.7 ,0.0173 ,300
254840100.8 ,0.0178 ,300
255000000 ,0.0183 ,300
325000000 ,0.0373 ,300
359375000 ,0.1376 ,300
120 ,0.1823 ,300
140969547.5 ,0.0000 ,400

152603420 ,0.0010 ,400
161985810 ,0.0014 ,400
169985413 ,0.0018 ,400
177015341 ,0.0023 ,400
183311024.5 ,0.0027 ,400
189021902.8 ,0.0032 ,400
194249935.8 ,0.0037 ,400
199068395.2 ,0.0041 ,400
203532037.2 ,0.0046 ,400
207683049.3 ,0.0051 ,400
211554737.2 ,0.0055 ,400
215173923.7 ,0.0060 ,400
218562568 ,0.0065 ,400
221738897.2 ,0.0070 ,400
224718216 ,0.0074 ,400
227513502.5 ,0.0079 ,400
230135852.8 ,0.0084 ,400
232594820.9 ,0.0089 ,400
234898680.6 ,0.0093 ,400
237054632.1 ,0.0098 ,400
239068964.6 ,0.0103 ,400
240947187.8 ,0.0108 ,400
242694137.6 ,0.0113 ,400
244314062.8 ,0.0117 ,400
245810695.8 ,0.0122 ,400
247187311.5 ,0.0127 ,400
248446775.7 ,0.0132 ,400
249591585.7 ,0.0137 ,400
250623903.9 ,0.0142 ,400
251545585.9 ,0.0147 ,400
252358203.6 ,0.0151 ,400
253063064.6 ,0.0156 ,400
253661227.7 ,0.0161 ,400
254153515.7 ,0.0166 ,400
254540524.7 ,0.0171 ,400
254822631.8 ,0.0176 ,400
255000000 ,0.0181 ,400
260000000 ,0.0375 ,400
287500000 ,0.1378 ,400
120 ,0.1823 ,400
116640053.7 ,0.0000 ,500
125033599.9 ,0.0010 ,500
131795173 ,0.0015 ,500
137557507.8 ,0.0019 ,500
142620266.3 ,0.0024 ,500
147153837.8 ,0.0028 ,500
151266220.1 ,0.0033 ,500
155031023.1 ,0.0038 ,500
158501106 ,0.0042 ,500

161715947.6 ,0.0047 ,500
164705950.9 ,0.0052 ,500
167495109.4 ,0.0056 ,500
170102740.1 ,0.0061 ,500
172544653.7 ,0.0066 ,500
174833970.4 ,0.0071 ,500
176981705.2 ,0.0076 ,500
178997196.9 ,0.0080 ,500
180888428.9 ,0.0085 ,500
182662274.2 ,0.0090 ,500
184324684.6 ,0.0095 ,500
185880838.5 ,0.0100 ,500
187335259.2 ,0.0104 ,500
188691908.9 ,0.0109 ,500
189954265.1 ,0.0114 ,500
191125382.7 ,0.0119 ,500
192207945.5 ,0.0124 ,500
193204307.9 ,0.0129 ,500
194116530.5 ,0.0133 ,500
194946408.5 ,0.0138 ,500
195695496.5 ,0.0143 ,500
196365128.6 ,0.0148 ,500
196956434.6 ,0.0153 ,500
197470354.7 ,0.0158 ,500
197907650 ,0.0163 ,500
198268911.9 ,0.0168 ,500
198554569.1 ,0.0172 ,500
198764892.8 ,0.0177 ,500
198900000 ,0.0182 ,500
202800000 ,0.0376 ,500
224250000 ,0.1380 ,500
120 ,0.1823 ,500
62942985.21 ,0.0000 ,600
68703400.76 ,0.0009 ,600
73370808.06 ,0.0014 ,600
77359446.26 ,0.0018 ,600
80869272.57 ,0.0023 ,600
84015188.73 ,0.0027 ,600
86870518.23 ,0.0032 ,600
89485475.43 ,0.0036 ,600
91896245.93 ,0.0041 ,600
94129929.07 ,0.0045 ,600
96207438.96 ,0.0050 ,600
98145309.54 ,0.0055 ,600
99956871.33 ,0.0059 ,600
101653048.3 ,0.0064 ,600
103242914.8 ,0.0069 ,600
104734096 ,0.0074 ,600
106133061.5 ,0.0078 ,600

107445345.6 ,0.0083 ,600
108675715.7 ,0.0088 ,600
109828302.1 ,0.0093 ,600
110906700.2 ,0.0097 ,600
111914051.8 ,0.0102 ,600
112853109.7 ,0.0107 ,600
113726290.9 ,0.0112 ,600
114535719.4 ,0.0117 ,600
115283261.2 ,0.0121 ,600
115970554.1 ,0.0126 ,600
116599031.4 ,0.0131 ,600
117169942.1 ,0.0136 ,600
117684368.1 ,0.0141 ,600
118143237.6 ,0.0146 ,600
118547337 ,0.0150 ,600
118897320.7 ,0.0155 ,600
119193718.3 ,0.0160 ,600
119436941.4 ,0.0165 ,600
119627288.2 ,0.0170 ,600
119764947.4 ,0.0175 ,600
119850000 ,0.0180 ,600
122200000 ,0.0373 ,600
135125000 ,0.1377 ,600
120 ,0.1823 ,600
27953703.56 ,0.0000 ,700
31042188.82 ,0.0009 ,700
33554876.97 ,0.0013 ,700
35706429.06 ,0.0017 ,700
37601860.68 ,0.0021 ,700
39301972.26 ,0.0026 ,700
40845752.36 ,0.0030 ,700
42259993.2 ,0.0034 ,700
43564050.99 ,0.0039 ,700
44772450.09 ,0.0043 ,700
45896417.24 ,0.0048 ,700
46944839.18 ,0.0053 ,700
47924888.35 ,0.0057 ,700
48842447.53 ,0.0062 ,700
49702407.18 ,0.0066 ,700
50508879.29 ,0.0071 ,700
51265354.62 ,0.0076 ,700
51974820.84 ,0.0080 ,700
52639852.57 ,0.0085 ,700
53262681.26 ,0.0090 ,700
53845250.03 ,0.0095 ,700
54389257.25 ,0.0099 ,700
54896191.54 ,0.0104 ,700
55367360.11 ,0.0109 ,700
55803911.91 ,0.0114 ,700

56206856.64 ,0.0118 ,700
56577080.51 ,0.0123 ,700
56915359.24 ,0.0128 ,700
57222368.95 ,0.0133 ,700
57498695.19 ,0.0138 ,700
57744840.52 ,0.0143 ,700
57961230.71 ,0.0147 ,700
58148219.94 ,0.0152 ,700
58306095 ,0.0157 ,700
58435078.7 ,0.0162 ,700
58535332.45 ,0.0167 ,700
58606958.25 ,0.0172 ,700
58650000 ,0.0177 ,700
59800000 ,0.0370 ,700
66125000 ,0.1373 ,700
120 ,0.1823 ,700
16463585.41 ,0.0000 ,800
17627330.17 ,0.0011 ,800
18572209.62 ,0.0015 ,800
19380641.25 ,0.0020 ,800
20092618.5 ,0.0024 ,800
20731190.53 ,0.0029 ,800
21311093.97 ,0.0034 ,800
21842434.41 ,0.0038 ,800
22332501.41 ,0.0043 ,800
22786758.28 ,0.0048 ,800
23209423.93 ,0.0053 ,800
23603835.32 ,0.0057 ,800
23972683.99 ,0.0062 ,800
24318176.31 ,0.0067 ,800
24642145.65 ,0.0072 ,800
24946132.93 ,0.0076 ,800
25231445.84 ,0.0081 ,800
25499203.26 ,0.0086 ,800
25750369.14 ,0.0091 ,800
25985778.76 ,0.0096 ,800
26206159.31 ,0.0100 ,800
26412146.29 ,0.0105 ,800
26604296.63 ,0.0110 ,800
26783099.3 ,0.0115 ,800
26948984.05 ,0.0120 ,800
27102328.48 ,0.0125 ,800
27243463.99 ,0.0130 ,800
27372680.62 ,0.0134 ,800
27490231.19 ,0.0139 ,800
27596334.61 ,0.0144 ,800
27691178.76 ,0.0149 ,800
27774922.82 ,0.0154 ,800
27847699.2 ,0.0159 ,800

27909615.1 ,0.0164 ,800
27960753.84 ,0.0169 ,800
28001175.75 ,0.0173 ,800
28030918.99 ,0.0178 ,800
28050000 ,0.0183 ,800
28600000 ,0.0377 ,800
31625000 ,0.1381 ,800
120 ,0.1823 ,800
10948558.82 ,0.0000 ,900
11380730.51 ,0.0012 ,900
11731379.96 ,0.0017 ,900
12031441.16 ,0.0021 ,900
12295831.16 ,0.0026 ,900
12533116.95 ,0.0031 ,900
12748763.49 ,0.0036 ,900
12946512.4 ,0.0041 ,900
13129059.47 ,0.0046 ,900
13298423.29 ,0.0050 ,900
13456161.52 ,0.0055 ,900
13603505.5 ,0.0060 ,900
13741447.89 ,0.0065 ,900
13870802.11 ,0.0070 ,900
13992243.83 ,0.0075 ,900
14106340.76 ,0.0080 ,900
14213574.58 ,0.0085 ,900
14314357.31 ,0.0089 ,900
14409043.85 ,0.0094 ,900
14497941.68 ,0.0099 ,900
14581318.47 ,0.0104 ,900
14659408.07 ,0.0109 ,900
14732415.41 ,0.0114 ,900
14800520.41 ,0.0119 ,900
14863881.16 ,0.0124 ,900
14922636.58 ,0.0129 ,900
14976908.55 ,0.0133 ,900
15026803.78 ,0.0138 ,900
15072415.23 ,0.0143 ,900
15113823.42 ,0.0148 ,900
15151097.46 ,0.0153 ,900
15184295.87 ,0.0158 ,900
15213467.35 ,0.0163 ,900
15238651.34 ,0.0168 ,900
15259878.47 ,0.0173 ,900
15277170.93 ,0.0177 ,900
15290542.75 ,0.0182 ,900
15300000 ,0.0187 ,900
15600000 ,0.0381 ,900
17250000 ,0.1385 ,900
120 ,0.1823 ,900

7299039.211 ,0.0000 ,1000
7587153.676 ,0.0012 ,1000
7820919.976 ,0.0017 ,1000
8020960.773 ,0.0021 ,1000
8197220.773 ,0.0026 ,1000
8355411.299 ,0.0031 ,1000
8499175.657 ,0.0036 ,1000
8631008.265 ,0.0041 ,1000
8752706.315 ,0.0046 ,1000
8865615.527 ,0.0050 ,1000
8970774.349 ,0.0055 ,1000
9069003.664 ,0.0060 ,1000
9160965.257 ,0.0065 ,1000
9247201.405 ,0.0070 ,1000
9328162.552 ,0.0075 ,1000
9404227.176 ,0.0080 ,1000
9475716.387 ,0.0085 ,1000
9542904.871 ,0.0089 ,1000
9606029.232 ,0.0094 ,1000
9665294.456 ,0.0099 ,1000
9720878.978 ,0.0104 ,1000
9772938.711 ,0.0109 ,1000
9821610.273 ,0.0114 ,1000
9867013.606 ,0.0119 ,1000
9909254.107 ,0.0124 ,1000
9948424.384 ,0.0129 ,1000
9984605.701 ,0.0133 ,1000
10017869.18 ,0.0138 ,1000
10048276.82 ,0.0143 ,1000
10075882.28 ,0.0148 ,1000
10100731.64 ,0.0153 ,1000
10122863.91 ,0.0158 ,1000
10142311.57 ,0.0163 ,1000
10159100.9 ,0.0168 ,1000
10173252.31 ,0.0173 ,1000
10184780.62 ,0.0177 ,1000
10193695.17 ,0.0182 ,1000
10200000 ,0.0187 ,1000
10400000 ,0.0381 ,1000
11500000 ,0.1385 ,1000
120 ,0.1823 ,1000
3649519.606 ,0.0000 ,1100
3793576.838 ,0.0012 ,1100
3910459.988 ,0.0017 ,1100
4010480.386 ,0.0021 ,1100
4098610.386 ,0.0026 ,1100
4177705.65 ,0.0031 ,1100
4249587.829 ,0.0036 ,1100
4315504.132 ,0.0041 ,1100

4376353.157 ,0.0046 ,1100
4432807.763 ,0.0050 ,1100
4485387.175 ,0.0055 ,1100
4534501.832 ,0.0060 ,1100
4580482.628 ,0.0065 ,1100
4623600.703 ,0.0070 ,1100
4664081.276 ,0.0075 ,1100
4702113.588 ,0.0080 ,1100
4737858.193 ,0.0085 ,1100
4771452.435 ,0.0089 ,1100
4803014.616 ,0.0094 ,1100
4832647.228 ,0.0099 ,1100
4860439.489 ,0.0104 ,1100
4886469.355 ,0.0109 ,1100
4910805.136 ,0.0114 ,1100
4933506.803 ,0.0119 ,1100
4954627.054 ,0.0124 ,1100
4974212.192 ,0.0129 ,1100
4992302.851 ,0.0133 ,1100
5008934.592 ,0.0138 ,1100
5024138.409 ,0.0143 ,1100
5037941.141 ,0.0148 ,1100
5050365.819 ,0.0153 ,1100
5061431.957 ,0.0158 ,1100
5071155.785 ,0.0163 ,1100
5079550.448 ,0.0168 ,1100
5086626.156 ,0.0173 ,1100
5092390.309 ,0.0177 ,1100
5096847.584 ,0.0182 ,1100
5100000 ,0.0187 ,1100
5200000 ,0.0381 ,1100
5750000 ,0.1385 ,1100
120 ,0.1823 ,1100

Input for Chapter 5

*Material, name=CONCRETE

*Density

2.4e-09,

*Elastic

14000., 0.2, 0.

9500., 0.2, 100.

7000., 0.2, 200.

4958.33, 0.2, 300.
3500., 0.2, 400.
2210.53, 0.2, 500.
1260., 0.2, 600.
750., 0.2, 700.
362.07, 0.2, 800.
186.67, 0.2, 900.
93.33, 0.2,1000.
23.33, 0.2,1100.

***Expansion**

9e-06, 0.
9.7e-06, 100.
1.2e-05, 200.
1.5e-05, 300.
2e-05, 400.
2.6e-05, 500.
3.4e-05, 600.
4.3e-05, 700.
1e-10, 800.
1e-10,1200.
1e-10,2000.

***Concrete Damaged Plasticity**

15., 0.1, 1.16, 0.666, 0.01

***Concrete Compression Hardening**

35., 0., 0.0001, 20.
33.7983, 0.0005, 0.0001, 20.
30.9865, 0.001, 0.0001, 20.
27.5591, 0.0015, 0.0001, 20.
24.1318, 0.002, 0.0001, 20.
21., 0.0025, 0.0001, 20.
18.2638, 0.003, 0.0001, 20.
15.9252, 0.0035, 0.0001, 20.
13.9456, 0.004, 0.0001, 20.
12.2745, 0.0045, 0.0001, 20.
10.8621, 0.005, 0.0001, 20.
9.66406, 0.0055, 0.0001, 20.
8.64323, 0.006, 0.0001, 20.
7.76883, 0.0065, 0.0001, 20.
7.01575, 0.007, 0.0001, 20.
6.36364, 0.0075, 0.0001, 20.
5.79592, 0.008, 0.0001, 20.
5.29914, 0.0085, 0.0001, 20.
4.86229, 0.009, 0.0001, 20.
4.47634, 0.0095, 0.0001, 20.
4.13386, 0.01, 0.0001, 20.
3.82868, 0.0105, 0.0001, 20.
3.55566, 0.011, 0.0001, 20.
3.31051, 0.0115, 0.0001, 20.
3.08961, 0.012, 0.0001, 20.

2.88991, 0.0125, 0.0001, 20.
2.7088, 0.013, 0.0001, 20.
2.54407, 0.0135, 0.0001, 20.
2.39382, 0.014, 0.0001, 20.
2.25641, 0.0145, 0.0001, 20.
2.13043, 0.015, 0.0001, 20.
2.01467, 0.0155, 0.0001, 20.
1.90804, 0.016, 0.0001, 20.
1.80962, 0.0165, 0.0001, 20.
1.7186, 0.017, 0.0001, 20.
1.63424, 0.0175, 0.0001, 20.
1.55593, 0.018, 0.0001, 20.
1.48309, 0.0185, 0.0001, 20.
1.41524, 0.019, 0.0001, 20.
1.35192, 0.0195, 0.0001, 20.
1.29275, 0.02, 0.0001, 20.
1.23737, 0.0205, 0.0001, 20.
1.18547, 0.021, 0.0001, 20.
1.13675, 0.0215, 0.0001, 20.
1.09098, 0.022, 0.0001, 20.
1.0479, 0.0225, 0.0001, 20.
1.00733, 0.023, 0.0001, 20.
0.969061, 0.0235, 0.0001, 20.
0.93293, 0.024, 0.0001, 20.
0.898779, 0.0245, 0.0001, 20.
0.866467, 0.025, 0.0001, 20.
0.835864, 0.0255, 0.0001, 20.
0.806852, 0.026, 0.0001, 20.
0.779322, 0.0265, 0.0001, 20.
0.753177, 0.027, 0.0001, 20.
0.728324, 0.0275, 0.0001, 20.
33.25, 0., 0.0001, 100.
32.6394, 0.0005, 0.0001, 100.
31.0882, 0.001, 0.0001, 100.
28.9902, 0.0015, 0.0001, 100.
26.656, 0.002, 0.0001, 100.
24.297, 0.0025, 0.0001, 100.
22.0398, 0.003, 0.0001, 100.
19.95, 0.0035, 0.0001, 100.
18.0537, 0.004, 0.0001, 100.
16.3538, 0.0045, 0.0001, 100.
14.8405, 0.005, 0.0001, 100.
13.4979, 0.0055, 0.0001, 100.
12.3084, 0.006, 0.0001, 100.
11.2543, 0.0065, 0.0001, 100.
10.319, 0.007, 0.0001, 100.
9.48743, 0.0075, 0.0001, 100.
8.74646, 0.008, 0.0001, 100.
8.08449, 0.0085, 0.0001, 100.

7.49149, 0.009, 0.0001, 100.
6.95879, 0.0095, 0.0001, 100.
6.47893, 0.01, 0.0001, 100.
6.04545, 0.0105, 0.0001, 100.
5.65283, 0.011, 0.0001, 100.
5.29627, 0.0115, 0.0001, 100.
4.97163, 0.012, 0.0001, 100.
4.67532, 0.0125, 0.0001, 100.
4.40422, 0.013, 0.0001, 100.
4.15563, 0.0135, 0.0001, 100.
3.92717, 0.014, 0.0001, 100.
3.71676, 0.0145, 0.0001, 100.
3.5226, 0.015, 0.0001, 100.
3.34307, 0.0155, 0.0001, 100.
3.17677, 0.016, 0.0001, 100.
3.02245, 0.0165, 0.0001, 100.
2.87899, 0.017, 0.0001, 100.
2.74541, 0.0175, 0.0001, 100.
2.62084, 0.018, 0.0001, 100.
2.5045, 0.0185, 0.0001, 100.
2.39567, 0.019, 0.0001, 100.
2.29374, 0.0195, 0.0001, 100.
2.19813, 0.02, 0.0001, 100.
2.10834, 0.0205, 0.0001, 100.
2.02391, 0.021, 0.0001, 100.
1.94443, 0.0215, 0.0001, 100.
1.86951, 0.022, 0.0001, 100.
1.79882, 0.0225, 0.0001, 100.
1.73205, 0.023, 0.0001, 100.
1.66891, 0.0235, 0.0001, 100.
1.60915, 0.024, 0.0001, 100.
1.55253, 0.0245, 0.0001, 100.
1.49883, 0.025, 0.0001, 100.
1.44787, 0.0255, 0.0001, 100.
1.39945, 0.026, 0.0001, 100.
1.35341, 0.0265, 0.0001, 100.
31.5, 0., 0.0001, 200.
31.1412, 0.0005, 0.0001, 200.
30.1899, 0.001, 0.0001, 200.
28.8305, 0.0015, 0.0001, 200.
27.2253, 0.002, 0.0001, 200.
25.5029, 0.0025, 0.0001, 200.
23.757, 0.003, 0.0001, 200.
22.0511, 0.0035, 0.0001, 200.
20.4248, 0.004, 0.0001, 200.
18.9, 0.0045, 0.0001, 200.
17.4865, 0.005, 0.0001, 200.
16.1863, 0.0055, 0.0001, 200.
14.9962, 0.006, 0.0001, 200.

13.9104, 0.0065, 0.0001, 200.
12.9214, 0.007, 0.0001, 200.
12.0212, 0.0075, 0.0001, 200.
11.2019, 0.008, 0.0001, 200.
10.4559, 0.0085, 0.0001, 200.
9.77586, 0.009, 0.0001, 200.
9.15532, 0.0095, 0.0001, 200.
8.58825, 0.01, 0.0001, 200.
8.06926, 0.0105, 0.0001, 200.
7.59351, 0.011, 0.0001, 200.
7.15666, 0.0115, 0.0001, 200.
6.75487, 0.012, 0.0001, 200.
6.3847, 0.0125, 0.0001, 200.
6.04307, 0.013, 0.0001, 200.
5.72727, 0.0135, 0.0001, 200.
5.43487, 0.014, 0.0001, 200.
5.1637, 0.0145, 0.0001, 200.
4.91182, 0.015, 0.0001, 200.
4.6775, 0.0155, 0.0001, 200.
4.45921, 0.016, 0.0001, 200.
4.25554, 0.0165, 0.0001, 200.
4.06526, 0.017, 0.0001, 200.
3.88724, 0.0175, 0.0001, 200.
3.72047, 0.018, 0.0001, 200.
3.56405, 0.0185, 0.0001, 200.
3.41716, 0.019, 0.0001, 200.
3.27904, 0.0195, 0.0001, 200.
3.14902, 0.02, 0.0001, 200.
3.0265, 0.0205, 0.0001, 200.
2.91091, 0.021, 0.0001, 200.
2.80175, 0.0215, 0.0001, 200.
2.69856, 0.022, 0.0001, 200.
2.60092, 0.0225, 0.0001, 200.
2.50843, 0.023, 0.0001, 200.
2.42075, 0.0235, 0.0001, 200.
2.33755, 0.024, 0.0001, 200.
2.25854, 0.0245, 0.0001, 200.
2.18344, 0.025, 0.0001, 200.
2.11199, 0.0255, 0.0001, 200.
29.75, 0., 0.0001, 300.
29.5553, 0.0005, 0.0001, 300.
29.0206, 0.001, 0.0001, 300.
28.2213, 0.0015, 0.0001, 300.
27.2288, 0.002, 0.0001, 300.
26.1063, 0.0025, 0.0001, 300.
24.907, 0.003, 0.0001, 300.
23.6731, 0.0035, 0.0001, 300.
22.4372, 0.004, 0.0001, 300.
21.2229, 0.0045, 0.0001, 300.

20.0471, 0.005, 0.0001, 300.
18.9206, 0.0055, 0.0001, 300.
17.85, 0.006, 0.0001, 300.
16.8387, 0.0065, 0.0001, 300.
15.8878, 0.007, 0.0001, 300.
14.9965, 0.0075, 0.0001, 300.
14.1631, 0.008, 0.0001, 300.
13.3851, 0.0085, 0.0001, 300.
12.6596, 0.009, 0.0001, 300.
11.9834, 0.0095, 0.0001, 300.
11.3534, 0.01, 0.0001, 300.
10.7663, 0.0105, 0.0001, 300.
10.2191, 0.011, 0.0001, 300.
9.70883, 0.0115, 0.0001, 300.
9.23276, 0.012, 0.0001, 300.
8.78826, 0.0125, 0.0001, 300.
8.37293, 0.013, 0.0001, 300.
7.98452, 0.0135, 0.0001, 300.
7.62097, 0.014, 0.0001, 300.
7.28038, 0.0145, 0.0001, 300.
6.961, 0.015, 0.0001, 300.
6.66123, 0.0155, 0.0001, 300.
6.3796, 0.016, 0.0001, 300.
6.11476, 0.0165, 0.0001, 300.
5.86547, 0.017, 0.0001, 300.
5.63059, 0.0175, 0.0001, 300.
5.40909, 0.018, 0.0001, 300.
5.20002, 0.0185, 0.0001, 300.
5.00249, 0.019, 0.0001, 300.
4.81571, 0.0195, 0.0001, 300.
4.63894, 0.02, 0.0001, 300.
4.47149, 0.0205, 0.0001, 300.
4.31275, 0.021, 0.0001, 300.
4.16214, 0.0215, 0.0001, 300.
4.01912, 0.022, 0.0001, 300.
3.88321, 0.0225, 0.0001, 300.
3.75396, 0.023, 0.0001, 300.
3.63094, 0.0235, 0.0001, 300.
3.51378, 0.024, 0.0001, 300.
26.25, 0., 0.0001, 400.
26.1387, 0.0005, 0.0001, 400.
25.8269, 0.001, 0.0001, 400.
25.3487, 0.0015, 0.0001, 400.
24.7378, 0.002, 0.0001, 400.
24.0254, 0.0025, 0.0001, 400.
23.2399, 0.003, 0.0001, 400.
22.4056, 0.0035, 0.0001, 400.
21.5431, 0.004, 0.0001, 400.
20.6693, 0.0045, 0.0001, 400.

19.7975, 0.005, 0.0001, 400.
18.9381, 0.0055, 0.0001, 400.
18.0988, 0.006, 0.0001, 400.
17.2854, 0.0065, 0.0001, 400.
16.5016, 0.007, 0.0001, 400.
15.75, 0.0075, 0.0001, 400.
15.0319, 0.008, 0.0001, 400.
14.3479, 0.0085, 0.0001, 400.
13.6978, 0.009, 0.0001, 400.
13.0811, 0.0095, 0.0001, 400.
12.4969, 0.01, 0.0001, 400.
11.9439, 0.0105, 0.0001, 400.
11.4209, 0.011, 0.0001, 400.
10.9265, 0.0115, 0.0001, 400.
10.4592, 0.012, 0.0001, 400.
10.0177, 0.0125, 0.0001, 400.
9.60036, 0.013, 0.0001, 400.
9.20591, 0.0135, 0.0001, 400.
8.83298, 0.014, 0.0001, 400.
8.48027, 0.0145, 0.0001, 400.
8.14655, 0.015, 0.0001, 400.
7.83066, 0.0155, 0.0001, 400.
7.53151, 0.016, 0.0001, 400.
7.24804, 0.0165, 0.0001, 400.
6.97931, 0.017, 0.0001, 400.
6.72438, 0.0175, 0.0001, 400.
6.48242, 0.018, 0.0001, 400.
6.25263, 0.0185, 0.0001, 400.
6.03426, 0.019, 0.0001, 400.
5.82662, 0.0195, 0.0001, 400.
5.62906, 0.02, 0.0001, 400.
5.44098, 0.0205, 0.0001, 400.
5.26182, 0.021, 0.0001, 400.
5.09104, 0.0215, 0.0001, 400.
4.92816, 0.022, 0.0001, 400.
4.77273, 0.0225, 0.0001, 400.
21., 0., 0.0001, 500.
20.9439, 0.0005, 0.0001, 500.
20.7843, 0.001, 0.0001, 500.
20.5346, 0.0015, 0.0001, 500.
20.2082, 0.002, 0.0001, 500.
19.8182, 0.0025, 0.0001, 500.
19.3769, 0.003, 0.0001, 500.
18.8956, 0.0035, 0.0001, 500.
18.3845, 0.004, 0.0001, 500.
17.8526, 0.0045, 0.0001, 500.
17.3078, 0.005, 0.0001, 500.
16.7565, 0.0055, 0.0001, 500.
16.2043, 0.006, 0.0001, 500.

15.6558, 0.0065, 0.0001, 500.
15.1147, 0.007, 0.0001, 500.
14.5838, 0.0075, 0.0001, 500.
14.0654, 0.008, 0.0001, 500.
13.5613, 0.0085, 0.0001, 500.
13.0725, 0.009, 0.0001, 500.
12.6, 0.0095, 0.0001, 500.
12.1442, 0.01, 0.0001, 500.
11.7054, 0.0105, 0.0001, 500.
11.2836, 0.011, 0.0001, 500.
10.8786, 0.0115, 0.0001, 500.
10.4902, 0.012, 0.0001, 500.
10.118, 0.0125, 0.0001, 500.
9.7616, 0.013, 0.0001, 500.
9.42044, 0.0135, 0.0001, 500.
9.09403, 0.014, 0.0001, 500.
8.78179, 0.0145, 0.0001, 500.
8.48316, 0.015, 0.0001, 500.
8.19757, 0.0155, 0.0001, 500.
7.92444, 0.016, 0.0001, 500.
7.66323, 0.0165, 0.0001, 500.
7.41338, 0.017, 0.0001, 500.
7.17436, 0.0175, 0.0001, 500.
6.94566, 0.018, 0.0001, 500.
6.72678, 0.0185, 0.0001, 500.
6.51724, 0.019, 0.0001, 500.
6.31659, 0.0195, 0.0001, 500.
6.1244, 0.02, 0.0001, 500.
5.94024, 0.0205, 0.0001, 500.
15.75, 0., 0.0001, 600.
15.7255, 0.0005, 0.0001, 600.
15.6548, 0.001, 0.0001, 600.
15.5422, 0.0015, 0.0001, 600.
15.3922, 0.002, 0.0001, 600.
15.2092, 0.0025, 0.0001, 600.
14.9976, 0.003, 0.0001, 600.
14.7615, 0.0035, 0.0001, 600.
14.5048, 0.004, 0.0001, 600.
14.2311, 0.0045, 0.0001, 600.
13.9439, 0.005, 0.0001, 600.
13.6463, 0.0055, 0.0001, 600.
13.3409, 0.006, 0.0001, 600.
13.0302, 0.0065, 0.0001, 600.
12.7165, 0.007, 0.0001, 600.
12.4016, 0.0075, 0.0001, 600.
12.0871, 0.008, 0.0001, 600.
11.7746, 0.0085, 0.0001, 600.
11.4651, 0.009, 0.0001, 600.
11.1598, 0.0095, 0.0001, 600.

10.8593, 0.01, 0.0001, 600.
10.5644, 0.0105, 0.0001, 600.
10.2757, 0.011, 0.0001, 600.
9.99351, 0.0115, 0.0001, 600.
9.71821, 0.012, 0.0001, 600.
9.45, 0.0125, 0.0001, 600.
9.18905, 0.013, 0.0001, 600.
8.93543, 0.0135, 0.0001, 600.
8.68918, 0.014, 0.0001, 600.
8.45029, 0.0145, 0.0001, 600.
8.21869, 0.015, 0.0001, 600.
7.99431, 0.0155, 0.0001, 600.
7.77702, 0.016, 0.0001, 600.
7.5667, 0.0165, 0.0001, 600.
7.36319, 0.017, 0.0001, 600.
7.16633, 0.0175, 0.0001, 600.
10.5, 0., 0.0001, 700.
10.4869, 0.0005, 0.0001, 700.
10.4491, 0.001, 0.0001, 700.
10.3884, 0.0015, 0.0001, 700.
10.3072, 0.002, 0.0001, 700.
10.2074, 0.0025, 0.0001, 700.
10.0911, 0.003, 0.0001, 700.
9.96047, 0.0035, 0.0001, 700.
9.81731, 0.004, 0.0001, 700.
9.6635, 0.0045, 0.0001, 700.
9.50077, 0.005, 0.0001, 700.
9.33071, 0.0055, 0.0001, 700.
9.1548, 0.006, 0.0001, 700.
8.97439, 0.0065, 0.0001, 700.
8.7907, 0.007, 0.0001, 700.
8.60481, 0.0075, 0.0001, 700.
8.4177, 0.008, 0.0001, 700.
8.23023, 0.0085, 0.0001, 700.
8.04316, 0.009, 0.0001, 700.
7.85714, 0.0095, 0.0001, 700.
7.67274, 0.01, 0.0001, 700.
7.49045, 0.0105, 0.0001, 700.
7.31066, 0.011, 0.0001, 700.
7.13373, 0.0115, 0.0001, 700.
6.95994, 0.012, 0.0001, 700.
6.78951, 0.0125, 0.0001, 700.
6.62262, 0.013, 0.0001, 700.
6.45942, 0.0135, 0.0001, 700.
6.3, 0.014, 0.0001, 700.
6.14444, 0.0145, 0.0001, 700.
5.99277, 0.015, 0.0001, 700.
5.84502, 0.0155, 0.0001, 700.
5.70118, 0.016, 0.0001, 700.

5.25, 0., 0.0001, 800.
5.2439, 0.0005, 0.0001, 800.
5.22621, 0.001, 0.0001, 800.
5.19785, 0.0015, 0.0001, 800.
5.15977, 0.002, 0.0001, 800.
5.11291, 0.0025, 0.0001, 800.
5.05822, 0.003, 0.0001, 800.
4.99662, 0.0035, 0.0001, 800.
4.92897, 0.004, 0.0001, 800.
4.85614, 0.0045, 0.0001, 800.
4.7789, 0.005, 0.0001, 800.
4.69799, 0.0055, 0.0001, 800.
4.61411, 0.006, 0.0001, 800.
4.52787, 0.0065, 0.0001, 800.
4.43986, 0.007, 0.0001, 800.
4.35058, 0.0075, 0.0001, 800.
4.26051, 0.008, 0.0001, 800.
4.17006, 0.0085, 0.0001, 800.
4.07959, 0.009, 0.0001, 800.
3.98943, 0.0095, 0.0001, 800.
3.89986, 0.01, 0.0001, 800.
3.81111, 0.0105, 0.0001, 800.
3.7234, 0.011, 0.0001, 800.
3.63691, 0.0115, 0.0001, 800.
3.55177, 0.012, 0.0001, 800.
3.46811, 0.0125, 0.0001, 800.
3.38604, 0.013, 0.0001, 800.
3.30562, 0.0135, 0.0001, 800.
3.22693, 0.014, 0.0001, 800.
3.15, 0.0145, 0.0001, 800.
3.07487, 0.015, 0.0001, 800.
3.00155, 0.0155, 0.0001, 800.
2.8, 0., 0.0001, 900.
2.79696, 0.0005, 0.0001, 900.
2.78812, 0.001, 0.0001, 900.
2.77394, 0.0015, 0.0001, 900.
2.75487, 0.002, 0.0001, 900.
2.73135, 0.0025, 0.0001, 900.
2.70386, 0.003, 0.0001, 900.
2.67283, 0.0035, 0.0001, 900.
2.63869, 0.004, 0.0001, 900.
2.60186, 0.0045, 0.0001, 900.
2.56271, 0.005, 0.0001, 900.
2.52162, 0.0055, 0.0001, 900.
2.47892, 0.006, 0.0001, 900.
2.43493, 0.0065, 0.0001, 900.
2.38993, 0.007, 0.0001, 900.
2.34419, 0.0075, 0.0001, 900.
2.29793, 0.008, 0.0001, 900.

2.25138, 0.0085, 0.0001, 900.
2.20472, 0.009, 0.0001, 900.
2.15813, 0.0095, 0.0001, 900.
2.11173, 0.01, 0.0001, 900.
2.06567, 0.0105, 0.0001, 900.
2.02006, 0.011, 0.0001, 900.
1.97499, 0.0115, 0.0001, 900.
1.93054, 0.012, 0.0001, 900.
1.88678, 0.0125, 0.0001, 900.
1.84377, 0.013, 0.0001, 900.
1.80156, 0.0135, 0.0001, 900.
1.76017, 0.014, 0.0001, 900.
1.71965, 0.0145, 0.0001, 900.
1.68, 0.015, 0.0001, 900.
1.4, 0., 0.0001, 1000.
1.39848, 0.0005, 0.0001, 1000.
1.39406, 0.001, 0.0001, 1000.
1.38697, 0.0015, 0.0001, 1000.
1.37743, 0.002, 0.0001, 1000.
1.36568, 0.0025, 0.0001, 1000.
1.35193, 0.003, 0.0001, 1000.
1.33642, 0.0035, 0.0001, 1000.
1.31935, 0.004, 0.0001, 1000.
1.30093, 0.0045, 0.0001, 1000.
1.28136, 0.005, 0.0001, 1000.
1.26081, 0.0055, 0.0001, 1000.
1.23946, 0.006, 0.0001, 1000.
1.21746, 0.0065, 0.0001, 1000.
1.19496, 0.007, 0.0001, 1000.
1.17209, 0.0075, 0.0001, 1000.
1.14897, 0.008, 0.0001, 1000.
1.12569, 0.0085, 0.0001, 1000.
1.10236, 0.009, 0.0001, 1000.
1.07906, 0.0095, 0.0001, 1000.
1.05587, 0.01, 0.0001, 1000.
1.03284, 0.0105, 0.0001, 1000.
1.01003, 0.011, 0.0001, 1000.
0.987495, 0.0115, 0.0001, 1000.
0.965271, 0.012, 0.0001, 1000.
0.943392, 0.0125, 0.0001, 1000.
0.921887, 0.013, 0.0001, 1000.
0.900779, 0.0135, 0.0001, 1000.
0.880086, 0.014, 0.0001, 1000.
0.859823, 0.0145, 0.0001, 1000.
0.84, 0.015, 0.0001, 1000.
0.35, 0., 0.0001, 1100.
0.34962, 0.0005, 0.0001, 1100.
0.348516, 0.001, 0.0001, 1100.
0.346743, 0.0015, 0.0001, 1100.

0.344358, 0.002, 0.0001, 1100.
0.341419, 0.0025, 0.0001, 1100.
0.337983, 0.003, 0.0001, 1100.
0.334104, 0.0035, 0.0001, 1100.
0.329837, 0.004, 0.0001, 1100.
0.325232, 0.0045, 0.0001, 1100.
0.320339, 0.005, 0.0001, 1100.
0.315202, 0.0055, 0.0001, 1100.
0.309865, 0.006, 0.0001, 1100.
0.304366, 0.0065, 0.0001, 1100.
0.298741, 0.007, 0.0001, 1100.
0.293023, 0.0075, 0.0001, 1100.
0.287242, 0.008, 0.0001, 1100.
0.281423, 0.0085, 0.0001, 1100.
0.275591, 0.009, 0.0001, 1100.
0.269766, 0.0095, 0.0001, 1100.
0.263966, 0.01, 0.0001, 1100.
0.258209, 0.0105, 0.0001, 1100.
0.252508, 0.011, 0.0001, 1100.
0.246874, 0.0115, 0.0001, 1100.
0.241318, 0.012, 0.0001, 1100.
0.235848, 0.0125, 0.0001, 1100.
0.230472, 0.013, 0.0001, 1100.
0.225195, 0.0135, 0.0001, 1100.
0.220022, 0.014, 0.0001, 1100.
0.214956, 0.0145, 0.0001, 1100.
0.21, 0.015, 0.0001, 1100.

*Concrete Tension Stiffening

2., 0., 0.001, 0.
1.8, 0.001, 0.001, 0.
1.4, 0.002, 0.001, 0.
1., 0.003, 0.001, 0.
0.8, 0.004, 0.001, 0.
0.6, 0.005, 0.001, 0.
0.5, 0.006, 0.001, 0.
0.4, 0.007, 0.001, 0.
0.3, 0.008, 0.001, 0.
0.3, 0.009, 0.001, 0.
0.2, 0.01, 0.001, 0.
0.2, 0.011, 0.001, 0.
0.2, 0.012, 0.001, 0.
0.2, 0.013, 0.001, 0.
0.1, 0.014, 0.001, 0.
0.1, 0.015, 0.001, 0.
0.1, 0.016, 0.001, 0.
0.1, 0.017, 0.001, 0.
0.1, 0.018, 0.001, 0.
0.1, 0.019, 0.001, 0.
0.1, 0.02, 0.001, 0.

0.1, 0.021, 0.001, 0.
0.1, 0.022, 0.001, 0.
0.1, 0.023, 0.001, 0.
0.1, 0.024, 0.001, 0.
0.1, 0.025, 0.001, 0.
0.4, 0.2, 0.001, 0.
1.9, 0., 0.001, 100.
1.8, 0.001, 0.001, 100.
1.5, 0.002, 0.001, 100.
1.3, 0.003, 0.001, 100.
1., 0.004, 0.001, 100.
0.8, 0.005, 0.001, 100.
0.7, 0.006, 0.001, 100.
0.6, 0.007, 0.001, 100.
0.5, 0.008, 0.001, 100.
0.4, 0.009, 0.001, 100.
0.4, 0.01, 0.001, 100.
0.3, 0.011, 0.001, 100.
0.3, 0.012, 0.001, 100.
0.3, 0.013, 0.001, 100.
0.2, 0.014, 0.001, 100.
0.2, 0.015, 0.001, 100.
0.2, 0.016, 0.001, 100.
0.2, 0.017, 0.001, 100.
0.1, 0.018, 0.001, 100.
0.1, 0.019, 0.001, 100.
0.1, 0.02, 0.001, 100.
0.1, 0.025, 0.001, 100.
0.4, 0.2, 0.001, 100.
1.8, 0., 0.001, 200.
1.7, 0.001, 0.001, 200.
1.6, 0.002, 0.001, 200.
1.4, 0.003, 0.001, 200.
1.2, 0.004, 0.001, 200.
1., 0.005, 0.001, 200.
0.9, 0.006, 0.001, 200.
0.7, 0.007, 0.001, 200.
0.6, 0.008, 0.001, 200.
0.6, 0.009, 0.001, 200.
0.5, 0.01, 0.001, 200.
0.4, 0.011, 0.001, 200.
0.4, 0.012, 0.001, 200.
0.3, 0.013, 0.001, 200.
0.3, 0.014, 0.001, 200.
0.3, 0.015, 0.001, 200.
0.3, 0.016, 0.001, 200.
0.2, 0.017, 0.001, 200.
0.2, 0.018, 0.001, 200.
0.2, 0.019, 0.001, 200.

0.2, 0.02, 0.001, 200.
0.2, 0.021, 0.001, 200.
0.2, 0.022, 0.001, 200.
0.1, 0.023, 0.001, 200.
0.1, 0.024, 0.001, 200.
0.1, 0.025, 0.001, 200.
0.4, 0.2, 0.001, 200.
1.7, 0., 0.001, 300.
1.7, 0.001, 0.001, 300.
1.6, 0.002, 0.001, 300.
1.4, 0.003, 0.001, 300.
1.3, 0.004, 0.001, 300.
1.1, 0.005, 0.001, 300.
1., 0.006, 0.001, 300.
0.9, 0.007, 0.001, 300.
0.8, 0.008, 0.001, 300.
0.7, 0.009, 0.001, 300.
0.6, 0.01, 0.001, 300.
0.6, 0.011, 0.001, 300.
0.5, 0.012, 0.001, 300.
0.5, 0.013, 0.001, 300.
0.4, 0.014, 0.001, 300.
0.4, 0.015, 0.001, 300.
0.4, 0.016, 0.001, 300.
0.3, 0.017, 0.001, 300.
0.3, 0.018, 0.001, 300.
0.3, 0.019, 0.001, 300.
0.3, 0.02, 0.001, 300.
0.2, 0.021, 0.001, 300.
0.2, 0.022, 0.001, 300.
0.2, 0.023, 0.001, 300.
0.2, 0.025, 0.001, 300.
0.8, 0.2, 0.001, 300.
1.5, 0., 0.001, 400.
1.5, 0.001, 0.001, 400.
1.4, 0.002, 0.001, 400.
1.3, 0.003, 0.001, 400.
1.2, 0.004, 0.001, 400.
1.1, 0.005, 0.001, 400.
1., 0.006, 0.001, 400.
0.9, 0.007, 0.001, 400.
0.9, 0.008, 0.001, 400.
0.8, 0.009, 0.001, 400.
0.7, 0.01, 0.001, 400.
0.7, 0.011, 0.001, 400.
0.6, 0.012, 0.001, 400.
0.5, 0.013, 0.001, 400.
0.5, 0.014, 0.001, 400.
0.5, 0.015, 0.001, 400.

0.4, 0.016, 0.001, 400.
0.4, 0.017, 0.001, 400.
0.4, 0.018, 0.001, 400.
0.3, 0.019, 0.001, 400.
0.3, 0.02, 0.001, 400.
0.3, 0.021, 0.001, 400.
0.3, 0.022, 0.001, 400.
1.2, 0.2, 0.001, 400.
1.2, 0., 0.001, 500.
1.2, 0.001, 0.001, 500.
1.2, 0.002, 0.001, 500.
1.1, 0.003, 0.001, 500.
1.1, 0.004, 0.001, 500.
1., 0.005, 0.001, 500.
0.9, 0.006, 0.001, 500.
0.9, 0.007, 0.001, 500.
0.8, 0.008, 0.001, 500.
0.7, 0.009, 0.001, 500.
0.7, 0.01, 0.001, 500.
0.6, 0.011, 0.001, 500.
0.6, 0.012, 0.001, 500.
0.6, 0.013, 0.001, 500.
0.5, 0.014, 0.001, 500.
0.5, 0.015, 0.001, 500.
0.5, 0.016, 0.001, 500.
0.4, 0.017, 0.001, 500.
0.4, 0.018, 0.001, 500.
0.4, 0.019, 0.001, 500.
0.3, 0.02, 0.001, 500.
1.2, 0.2, 0.001, 500.
0.9, 0., 0.001, 600.
0.9, 0.001, 0.001, 600.
0.9, 0.002, 0.001, 600.
0.9, 0.003, 0.001, 600.
0.8, 0.004, 0.001, 600.
0.8, 0.005, 0.001, 600.
0.8, 0.006, 0.001, 600.
0.7, 0.007, 0.001, 600.
0.7, 0.008, 0.001, 600.
0.7, 0.009, 0.001, 600.
0.6, 0.01, 0.001, 600.
0.6, 0.011, 0.001, 600.
0.6, 0.012, 0.001, 600.
0.5, 0.013, 0.001, 600.
0.5, 0.014, 0.001, 600.
0.5, 0.015, 0.001, 600.
0.4, 0.016, 0.001, 600.
0.4, 0.017, 0.001, 600.
1.6, 0.2, 0.001, 600.

0.6, 0., 0.001, 700.
0.6, 0.001, 0.001, 700.
0.6, 0.002, 0.001, 700.
0.6, 0.003, 0.001, 700.
0.6, 0.004, 0.001, 700.
0.5, 0.005, 0.001, 700.
0.5, 0.006, 0.001, 700.
0.5, 0.007, 0.001, 700.
0.5, 0.008, 0.001, 700.
0.5, 0.009, 0.001, 700.
0.4, 0.01, 0.001, 700.
0.4, 0.011, 0.001, 700.
0.4, 0.012, 0.001, 700.
0.4, 0.013, 0.001, 700.
0.4, 0.014, 0.001, 700.
0.3, 0.015, 0.001, 700.
0.3, 0.025, 0.001, 700.
1.2, 0.2, 0.001, 700.
0.3, 0., 0.001, 800.
0.3, 0.001, 0.001, 800.
0.3, 0.002, 0.001, 800.
0.3, 0.003, 0.001, 800.
0.3, 0.004, 0.001, 800.
0.3, 0.005, 0.001, 800.
0.3, 0.006, 0.001, 800.
0.3, 0.007, 0.001, 800.
0.2, 0.008, 0.001, 800.
0.2, 0.009, 0.001, 800.
0.2, 0.01, 0.001, 800.
0.2, 0.011, 0.001, 800.
0.2, 0.012, 0.001, 800.
0.2, 0.013, 0.001, 800.
0.2, 0.014, 0.001, 800.
0.2, 0.015, 0.001, 800.
0.8, 0.2, 0.001, 800.
0.2, 0., 0.001, 900.
0.2, 0.001, 0.001, 900.
0.2, 0.002, 0.001, 900.
0.2, 0.003, 0.001, 900.
0.2, 0.004, 0.001, 900.
0.1, 0.005, 0.001, 900.
0.1, 0.006, 0.001, 900.
0.1, 0.007, 0.001, 900.
0.1, 0.008, 0.001, 900.
0.1, 0.009, 0.001, 900.
0.1, 0.01, 0.001, 900.
0.1, 0.011, 0.001, 900.
0.1, 0.012, 0.001, 900.
0.1, 0.013, 0.001, 900.

0.1, 0.014, 0.001, 900.
0.1, 0.015, 1., 900.
0.1, 0., 0.001, 1000.
0.1, 0.001, 0.001, 1000.
0.1, 0.002, 0.001, 1000.
0.1, 0.003, 0.001, 1000.
0.1, 0.004, 0.001, 1000.
0.1, 0.005, 0.001, 1000.
0.1, 0.006, 0.001, 1000.
0.1, 0.007, 0.001, 1000.
0.1, 0.008, 0.001, 1000.
0.1, 0.009, 0.001, 1000.
0.1, 0.01, 0.001, 1000.
0.1, 0.011, 0.001, 1000.
0.1, 0.012, 0.001, 1000.
0.1, 0.013, 0.001, 1000.
0.1, 0.014, 0.001, 1000.
0., 0.015, 1., 1000.
0., 0., 0.001, 1100.
0., 0.001, 0.001, 1100.
0., 0.002, 0.001, 1100.
0., 0.003, 0.001, 1100.
0., 0.004, 0.001, 1100.
0., 0.005, 0.001, 1100.
0., 0.006, 0.001, 1100.
0., 0.007, 0.001, 1100.
0., 0.008, 0.001, 1100.
0., 0.009, 0.001, 1100.
0., 0.01, 0.001, 1100.
0., 0.011, 0.001, 1100.
0., 0.012, 0.001, 1100.
0., 0.013, 0.001, 1100.
0., 0.014, 0.001, 1100.
0., 0.015, 1., 1100.

Input for Chapter 7

*Material, name=Concrete
*Density
2400.,
*Elastic
14331200000,0.2,20
10331700000,0.2,100
7838710000,0.2,200
5799420000,0.2,300
4061370000,0.2,400

2590740000,0.2,500
1489230000,0.2,600
882000000,0.2,700
422920000,0.2,800
212951000,0.2,900
104516000,0.2,1000
23267500,0.2,1100
*Expansion
9.03E-006,20
9.69E-006,100
1.18E-005,200
1.52E-005,300
2.00E-005,400
2.63E-005,500
3.38E-005,600
4.28E-005,700
1.00E-010,701
1.00E-010,1200
1.00E-010,2000
*Concrete Damaged Plasticity
7.5,0.1,1.16,1,0.01,20
*Concrete Compression Hardening
28662400,0,0.0001,20
30000000,0.0005,0.0001,20
28970000,0.001,0.0001,20
8283480,0.006,0.0001,20
3836860,0.01,0.0001,20
1400780,0.018,0.0001,20
624277,0.028,0.0001,20
25829200,0,0.0001,100
27868100,0.0005,0.0001,100
28500000,0.001,0.0001,100
27976600,0.0015,0.0001,100
26647000,0.002,0.0001,100
10550100,0.007,0.0001,100
5964680,0.0095,0.0001,100
4539660,0.0125,0.0001,100
2590670,0.0175,0.0001,100
1160070,0.0275,0.0001,100
23516100,0,0.0001,200
25500800,0.00058,0.0001,200
27000000,0.0015,0.0001,200
26692400,0.002,0.0001,200
25877000,0.0025,0.0001,200
10303900,0.009,0.0001,200
5789890,0.0135,0.0001,200
4009290,0.017,0.0001,200
2594140,0.022,0.0001,200
1810280,0.027,0.0001,200

20298000,0,0.0001,300
24721700,0.0015,0.0001,300
25500000,0.0025,0.0001,300
25333100,0.003,0.0001,300
23339000,0.0045,0.0001,300
12854100,0.01,0.0001,300
8759210,0.0135,0.0001,300
6532260,0.0165,0.0001,300
4287850,0.0215,0.0001,300
3011810,0.0265,0.0001,300
18276200,0,0.0001,400
21496800,0.0015,0.0001,400
22395700,0.0025,0.0001,400
22500000,0.003,0.0001,400
22404600,0.0035,0.0001,400
20593200,0.0055,0.0001,400
10711600,0.013,0.0001,400
8586570,0.0155,0.0001,400
5763760,0.0205,0.0001,400
4090910,0.0255,0.0001,400
14249100,0,0.0001,500
17107000,0.002,0.0001,500
18000000,0.004,0.0001,500
16608700,0.007,0.0001,500
10033200,0.0145,0.0001,500
7026490,0.0198,0.0001,500
5091630,0.0245,0.0001,500
10424600,0,0.0001,600
12620100,0.0025,0.0001,600
13291200,0.004,0.0001,600
13500000,0.0055,0.0001,600
13193300,0.0075,0.0001,600
10629900,0.013,0.0001,600
8100000,0.018,0.0001,600
6142570,0.023,0.0001,600
7056000,0,0.0001,700
8536740,0.003,0.0001,700
9000000,0.006,0.0001,700
8537550,0.0095,0.0001,700
7846980,0.012,0.0001,700
6266280,0.017,0.0001,700
4886730,0.022,0.0001,700
3594820,0,0.0001,800
4352640,0.0035,0.0001,800
4500000,0.006,0.0001,800
4026850,0.0115,0.0001,800
3266670,0.0165,0.0001,800
2572760,0.0215,0.0001,800
2023040,0,0.0001,900

2400000,0.0055,0.0001,900
2196610,0.0105,0.0001,900
1810060,0.0155,0.0001,900
1440000,0.0205,0.0001,900
1045160,0,0.0001,1000
1200000,0.005,0.0001,1000
1098310,0.01,0.0001,1000
905028,0.015,0.0001,1000
720000,0.02,0.0001,1000
630000,0,0.0001,1100
650000,0.0025,0.0001,1100
630000,0.0075,0.0001,1100
610000,0.0125,0.0001,1100
600000,0.0175,0.0001,1100
*Concrete Tension Stiffening
2866240,0,0.0001,20
*Material, name="Mild Steel"
*Density
7800.,
*Elastic
2.1e+11, 0.3, 0.
2.1e+11, 0.3, 100.
1.89e+11, 0.3, 200.
1.68e+11, 0.3, 300.
1.47e+11, 0.3, 400.
1.26e+11, 0.3, 500.
6.51e+10, 0.3, 600.
2.73e+10, 0.3, 700.
1.89e+10, 0.3, 800.
1.42e+10, 0.3, 900.
9.45e+09, 0.3,1000.
4.73e+09, 0.3,1100.
4.73e+09, 0.3,1200.
*Expansion
0., 20.
1.25e-05, 100.
1.29e-05, 200.
1.33e-05, 300.
1.37e-05, 400.
1.41e-05, 500.
1.45e-05, 600.
1.49e-05, 700.
1.5e-05, 735.
1.41e-05, 800.
1.34e-05, 900.
1.41e-05,1000.
1.46e-05,1100.
*Plastic
3e+08, 0., 20.

3.00152e+08, 0.0008, 20.
 3.00304e+08, 0.0013, 20.
 3.00447e+08, 0.0018, 20.
 3.00599e+08, 0.00229, 20.
 3.00751e+08, 0.00279, 20.
 3.00902e+08, 0.00329, 20.
 3.01046e+08, 0.00379, 20.
 3.01198e+08, 0.00428, 20.
 3.01349e+08, 0.00478, 20.
 3.01501e+08, 0.00527, 20.
 3.01645e+08, 0.00577, 20.
 3.01796e+08, 0.00626, 20.
 3.01948e+08, 0.00676, 20.
 3.021e+08, 0.00725, 20.
 3.02243e+08, 0.00775, 20.
 3.02395e+08, 0.00824, 20.
 3.02547e+08, 0.00874, 20.
 3.02699e+08, 0.00923, 20.
 3.02842e+08, 0.00972, 20.
 3.02994e+08, 0.01022, 20.
 3.03146e+08, 0.01071, 20.
 3.03298e+08, 0.0112, 20.
 3.03441e+08, 0.0117, 20.
 3.03593e+08, 0.01219, 20.
 3.03745e+08, 0.01268, 20.
 3.03896e+08, 0.01317, 20.
 3.0404e+08, 0.01366, 20.
 3.04192e+08, 0.01416, 20.
 3.04343e+08, 0.01465, 20.
 3.04495e+08, 0.01514, 20.
 3.04639e+08, 0.01563, 20.
 3.0479e+08, 0.01612, 20.
 3.04942e+08, 0.01661, 20.
 3.05094e+08, 0.0171, 20.
 3.05237e+08, 0.01759, 20.
 3.05389e+08, 0.01808, 20.
 3.89222e+08, 0.03702, 20.
 4.30387e+08, 0.13733, 20.
 3e+08, 0., 100.
 3.00152e+08, 0.0008, 100.
 3.00304e+08, 0.0013, 100.
 3.00447e+08, 0.0018, 100.
 3.00599e+08, 0.00229, 100.
 3.00751e+08, 0.00279, 100.
 3.00902e+08, 0.00329, 100.
 3.01046e+08, 0.00379, 100.
 3.01198e+08, 0.00428, 100.
 3.01349e+08, 0.00478, 100.
 3.01501e+08, 0.00527, 100.

3.01645e+08, 0.00577, 100.
3.01796e+08, 0.00626, 100.
3.01948e+08, 0.00676, 100.
3.021e+08, 0.00725, 100.
3.02243e+08, 0.00775, 100.
3.02395e+08, 0.00824, 100.
3.02547e+08, 0.00874, 100.
3.02699e+08, 0.00923, 100.
3.02842e+08, 0.00972, 100.
3.02994e+08, 0.01022, 100.
3.03146e+08, 0.01071, 100.
3.03298e+08, 0.0112, 100.
3.03441e+08, 0.0117, 100.
3.03593e+08, 0.01219, 100.
3.03745e+08, 0.01268, 100.
3.03896e+08, 0.01317, 100.
3.0404e+08, 0.01366, 100.
3.04192e+08, 0.01416, 100.
3.04343e+08, 0.01465, 100.
3.04495e+08, 0.01514, 100.
3.04639e+08, 0.01563, 100.
3.0479e+08, 0.01612, 100.
3.04942e+08, 0.01661, 100.
3.05094e+08, 0.0171, 100.
3.05237e+08, 0.01759, 100.
3.05389e+08, 0.01808, 100.
3.89222e+08, 0.03702, 100.
4.30387e+08, 0.13733, 100.
2.54398e+08, 0., 200.
2.601e+08, 0.00087, 200.
2.64401e+08, 0.00134, 200.
2.67968e+08, 0.00181, 200.
2.71064e+08, 0.00229, 200.
2.73805e+08, 0.00277, 200.
2.76284e+08, 0.00325, 200.
2.78544e+08, 0.00374, 200.
2.80619e+08, 0.00422, 200.
2.8255e+08, 0.00471, 200.
2.84338e+08, 0.00519, 200.
2.86008e+08, 0.00568, 200.
2.87577e+08, 0.00616, 200.
2.89044e+08, 0.00665, 200.
2.90419e+08, 0.00714, 200.
2.91718e+08, 0.00763, 200.
2.92932e+08, 0.00811, 200.
2.94079e+08, 0.0086, 200.
2.95151e+08, 0.00909, 200.
2.96171e+08, 0.00958, 200.
2.97116e+08, 0.01006, 200.

2.9801e+08, 0.01055, 200.
2.98845e+08, 0.01104, 200.
2.99629e+08, 0.01153, 200.
3.00354e+08, 0.01202, 200.
3.01037e+08, 0.01251, 200.
3.01661e+08, 0.013, 200.
3.02243e+08, 0.01349, 200.
3.02775e+08, 0.01397, 200.
3.03255e+08, 0.01446, 200.
3.03694e+08, 0.01495, 200.
3.0409e+08, 0.01544, 200.
3.04436e+08, 0.01593, 200.
3.0474e+08, 0.01642, 200.
3.05001e+08, 0.01691, 200.
3.05221e+08, 0.0174, 200.
3.05389e+08, 0.01789, 200.
3.89222e+08, 0.03678, 200.
4.30387e+08, 0.13706, 200.
1.97014e+08, 0., 300.
2.1185e+08, 0.0005, 300.
2.21717e+08, 0.00093, 300.
2.29561e+08, 0.00138, 300.
2.36206e+08, 0.00183, 300.
2.42017e+08, 0.00228, 300.
2.47204e+08, 0.00275, 300.
2.5191e+08, 0.00321, 300.
2.56203e+08, 0.00368, 300.
2.60159e+08, 0.00415, 300.
2.63819e+08, 0.00462, 300.
2.67226e+08, 0.00509, 300.
2.70397e+08, 0.00556, 300.
2.73358e+08, 0.00604, 300.
2.76132e+08, 0.00652, 300.
2.7873e+08, 0.00699, 300.
2.81159e+08, 0.00747, 300.
2.83444e+08, 0.00795, 300.
2.85578e+08, 0.00843, 300.
2.87585e+08, 0.00891, 300.
2.89458e+08, 0.00939, 300.
2.91212e+08, 0.00987, 300.
2.92848e+08, 0.01036, 300.
2.94375e+08, 0.01084, 300.
2.95792e+08, 0.01132, 300.
2.97099e+08, 0.01181, 300.
2.98305e+08, 0.01229, 300.
2.99418e+08, 0.01278, 300.
3.0043e+08, 0.01326, 300.
3.01341e+08, 0.01375, 300.
3.02167e+08, 0.01423, 300.

3.02893e+08, 0.01472, 300.
3.03534e+08, 0.01521, 300.
3.04082e+08, 0.01569, 300.
3.04546e+08, 0.01618, 300.
3.04917e+08, 0.01667, 300.
3.05195e+08, 0.01716, 300.
3.05389e+08, 0.01765, 300.
3.89222e+08, 0.03647, 300.
4.30387e+08, 0.13672, 300.
1.55815e+08, 0., 400.
1.72742e+08, 0.0006, 400.
1.85654e+08, 0.001, 400.
1.9639e+08, 0.00141, 400.
2.05684e+08, 0.00183, 400.
2.13933e+08, 0.00227, 400.
2.21363e+08, 0.0027, 400.
2.28127e+08, 0.00315, 400.
2.34343e+08, 0.00359, 400.
2.40078e+08, 0.00405, 400.
2.45399e+08, 0.0045, 400.
2.50358e+08, 0.00496, 400.
2.5498e+08, 0.00542, 400.
2.59298e+08, 0.00588, 400.
2.63347e+08, 0.00634, 400.
2.67133e+08, 0.00681, 400.
2.70684e+08, 0.00727, 400.
2.74015e+08, 0.00774, 400.
2.77136e+08, 0.00821, 400.
2.80054e+08, 0.00868, 400.
2.82787e+08, 0.00915, 400.
2.85334e+08, 0.00963, 400.
2.87712e+08, 0.0101, 400.
2.89913e+08, 0.01058, 400.
2.91963e+08, 0.01105, 400.
2.93852e+08, 0.01153, 400.
2.95589e+08, 0.01201, 400.
2.97175e+08, 0.01249, 400.
2.98617e+08, 0.01297, 400.
2.99916e+08, 0.01345, 400.
3.01071e+08, 0.01394, 400.
3.02092e+08, 0.01442, 400.
3.02977e+08, 0.0149, 400.
3.03728e+08, 0.01539, 400.
3.04343e+08, 0.01588, 400.
3.04824e+08, 0.01636, 400.
3.0517e+08, 0.01685, 400.
3.05389e+08, 0.01734, 400.
3.11377e+08, 0.03671, 400.
3.44311e+08, 0.13699, 400.

1.3053e+08, 0., 500.
1.42785e+08, 0.00065, 500.
1.52096e+08, 0.00107, 500.
1.59821e+08, 0.00149, 500.
1.66501e+08, 0.00193, 500.
1.72421e+08, 0.00237, 500.
1.7776e+08, 0.00282, 500.
1.82618e+08, 0.00327, 500.
1.87079e+08, 0.00372, 500.
1.91195e+08, 0.00418, 500.
1.95016e+08, 0.00464, 500.
1.98575e+08, 0.00511, 500.
2.01889e+08, 0.00557, 500.
2.04993e+08, 0.00604, 500.
2.07903e+08, 0.00651, 500.
2.10618e+08, 0.00698, 500.
2.13174e+08, 0.00745, 500.
2.15569e+08, 0.00792, 500.
2.17804e+08, 0.0084, 500.
2.19904e+08, 0.00887, 500.
2.21869e+08, 0.00935, 500.
2.23699e+08, 0.00982, 500.
2.25411e+08, 0.0103, 500.
2.26997e+08, 0.01078, 500.
2.28473e+08, 0.01126, 500.
2.2983e+08, 0.01174, 500.
2.31087e+08, 0.01222, 500.
2.32234e+08, 0.0127, 500.
2.33271e+08, 0.01319, 500.
2.34208e+08, 0.01367, 500.
2.35051e+08, 0.01415, 500.
2.35793e+08, 0.01464, 500.
2.36434e+08, 0.01512, 500.
2.36974e+08, 0.01561, 500.
2.37429e+08, 0.0161, 500.
2.37784e+08, 0.01658, 500.
2.38037e+08, 0.01707, 500.
2.38205e+08, 0.01756, 500.
2.42878e+08, 0.03694, 500.
2.68567e+08, 0.13724, 500.
6.9031e+07, 0., 600.
7.72877e+07, 0.00059, 600.
8.36637e+07, 0.00097, 600.
8.90023e+07, 0.00137, 600.
9.36325e+07, 0.00179, 600.
9.77482e+07, 0.00221, 600.
1.01467e+08, 0.00264, 600.
1.04849e+08, 0.00308, 600.
1.07962e+08, 0.00352, 600.

1.10837e+08, 0.00396, 600.
1.13503e+08, 0.00441, 600.
1.15982e+08, 0.00486, 600.
1.18301e+08, 0.00532, 600.
1.20469e+08, 0.00577, 600.
1.22493e+08, 0.00623, 600.
1.24399e+08, 0.00669, 600.
1.26179e+08, 0.00716, 600.
1.27849e+08, 0.00762, 600.
1.29409e+08, 0.00809, 600.
1.30876e+08, 0.00856, 600.
1.32243e+08, 0.00903, 600.
1.33516e+08, 0.0095, 600.
1.34714e+08, 0.00997, 600.
1.35819e+08, 0.01044, 600.
1.36839e+08, 0.01092, 600.
1.37784e+08, 0.01139, 600.
1.38652e+08, 0.01187, 600.
1.39445e+08, 0.01235, 600.
1.4017e+08, 0.01283, 600.
1.4082e+08, 0.01331, 600.
1.41393e+08, 0.01379, 600.
1.41908e+08, 0.01427, 600.
1.42346e+08, 0.01476, 600.
1.42717e+08, 0.01524, 600.
1.43021e+08, 0.01573, 600.
1.43257e+08, 0.01621, 600.
1.43426e+08, 0.0167, 600.
1.43535e+08, 0.01719, 600.
1.46344e+08, 0.03656, 600.
1.61828e+08, 0.13682, 600.
2.9957e+07, 0., 700.
3.43257e+07, 0.00051, 700.
3.77414e+07, 0.00086, 700.
4.06174e+07, 0.00123, 700.
4.31306e+07, 0.00162, 700.
4.53572e+07, 0.00202, 700.
4.73729e+07, 0.00243, 700.
4.92114e+07, 0.00285, 700.
5.09066e+07, 0.00327, 700.
5.24669e+07, 0.0037, 700.
5.3926e+07, 0.00414, 700.
5.52754e+07, 0.00457, 700.
5.6532e+07, 0.00502, 700.
5.77127e+07, 0.00546, 700.
5.88176e+07, 0.00591, 700.
5.98549e+07, 0.00636, 700.
6.08248e+07, 0.00681, 700.
6.17357e+07, 0.00727, 700.

6.25875e+07, 0.00773, 700.
6.33803e+07, 0.00819, 700.
6.41309e+07, 0.00865, 700.
6.48225e+07, 0.00911, 700.
6.54719e+07, 0.00958, 700.
6.60707e+07, 0.01005, 700.
6.66273e+07, 0.01052, 700.
6.71418e+07, 0.01099, 700.
6.76141e+07, 0.01146, 700.
6.80442e+07, 0.01193, 700.
6.84321e+07, 0.01241, 700.
6.87864e+07, 0.01289, 700.
6.90984e+07, 0.01336, 700.
6.93767e+07, 0.01384, 700.
6.96129e+07, 0.01433, 700.
6.98069e+07, 0.01481, 700.
6.99755e+07, 0.01529, 700.
7.00936e+07, 0.01578, 700.
7.01864e+07, 0.01626, 700.
7.0237e+07, 0.01675, 700.
7.16201e+07, 0.03611, 700.
7.91937e+07, 0.13632, 700.
1.85544e+07, 0., 800.
2.02159e+07, 0.00073, 800.
2.14978e+07, 0.00115, 800.
2.25689e+07, 0.00158, 800.
2.34967e+07, 0.00202, 800.
2.43316e+07, 0.00247, 800.
2.50738e+07, 0.00292, 800.
2.57569e+07, 0.00337, 800.
2.63895e+07, 0.00383, 800.
2.6963e+07, 0.00429, 800.
2.75027e+07, 0.00475, 800.
2.80003e+07, 0.00522, 800.
2.84726e+07, 0.00569, 800.
2.89112e+07, 0.00615, 800.
2.9316e+07, 0.00662, 800.
2.9704e+07, 0.0071, 800.
3.00582e+07, 0.00757, 800.
3.03955e+07, 0.00804, 800.
3.0716e+07, 0.00852, 800.
3.10112e+07, 0.00899, 800.
3.12895e+07, 0.00947, 800.
3.15425e+07, 0.00995, 800.
3.17871e+07, 0.01043, 800.
3.20148e+07, 0.01091, 800.
3.22173e+07, 0.01139, 800.
3.24112e+07, 0.01187, 800.
3.25883e+07, 0.01235, 800.

3.27486e+07, 0.01283, 800.
3.29004e+07, 0.01332, 800.
3.30269e+07, 0.0138, 800.
3.3145e+07, 0.01429, 800.
3.32546e+07, 0.01477, 800.
3.3339e+07, 0.01526, 800.
3.34233e+07, 0.01574, 800.
3.34823e+07, 0.01623, 800.
3.35329e+07, 0.01672, 800.
3.35667e+07, 0.01721, 800.
3.3592e+07, 0.0177, 800.
3.42498e+07, 0.03707, 800.
3.78764e+07, 0.13739, 800.
1.27182e+07, 0., 900.
1.33339e+07, 0.00088, 900.
1.38146e+07, 0.00134, 900.
1.42026e+07, 0.00181, 900.
1.45484e+07, 0.00228, 900.
1.4852e+07, 0.00275, 900.
1.51303e+07, 0.00322, 900.
1.53833e+07, 0.0037, 900.
1.5611e+07, 0.00418, 900.
1.58303e+07, 0.00466, 900.
1.60243e+07, 0.00514, 900.
1.62098e+07, 0.00562, 900.
1.63869e+07, 0.0061, 900.
1.65472e+07, 0.00658, 900.
1.6699e+07, 0.00707, 900.
1.68424e+07, 0.00755, 900.
1.69773e+07, 0.00804, 900.
1.71038e+07, 0.00852, 900.
1.72219e+07, 0.009, 900.
1.73315e+07, 0.00949, 900.
1.74327e+07, 0.00998, 900.
1.75339e+07, 0.01046, 900.
1.76183e+07, 0.01095, 900.
1.77026e+07, 0.01144, 900.
1.7787e+07, 0.01192, 900.
1.78544e+07, 0.01241, 900.
1.79219e+07, 0.0129, 900.
1.79894e+07, 0.01338, 900.
1.804e+07, 0.01387, 900.
1.80906e+07, 0.01436, 900.
1.81412e+07, 0.01485, 900.
1.81834e+07, 0.01534, 900.
1.82171e+07, 0.01582, 900.
1.82508e+07, 0.01631, 900.
1.82761e+07, 0.0168, 900.
1.8293e+07, 0.01729, 900.

1.83099e+07, 0.01778, 900.
1.83267e+07, 0.01827, 900.
1.86809e+07, 0.03766, 900.
2.06629e+07, 0.13803, 900.
8.48444e+06, 0., 1000.
8.88926e+06, 0.00088, 1000.
9.20975e+06, 0.00134, 1000.
9.4712e+06, 0.00181, 1000.
9.69891e+06, 0.00228, 1000.
9.90132e+06, 0.00275, 1000.
1.00869e+07, 0.00322, 1000.
1.02555e+07, 0.0037, 1000.
1.04074e+07, 0.00418, 1000.
1.05507e+07, 0.00466, 1000.
1.06857e+07, 0.00514, 1000.
1.08122e+07, 0.00562, 1000.
1.09218e+07, 0.0061, 1000.
1.10315e+07, 0.00658, 1000.
1.11327e+07, 0.00707, 1000.
1.12254e+07, 0.00755, 1000.
1.13182e+07, 0.00804, 1000.
1.14025e+07, 0.00852, 1000.
1.14785e+07, 0.009, 1000.
1.15544e+07, 0.00949, 1000.
1.16218e+07, 0.00998, 1000.
1.16893e+07, 0.01046, 1000.
1.17483e+07, 0.01095, 1000.
1.18074e+07, 0.01144, 1000.
1.1858e+07, 0.01192, 1000.
1.19086e+07, 0.01241, 1000.
1.19507e+07, 0.0129, 1000.
1.19929e+07, 0.01338, 1000.
1.20267e+07, 0.01387, 1000.
1.20604e+07, 0.01436, 1000.
1.20941e+07, 0.01485, 1000.
1.21194e+07, 0.01534, 1000.
1.21447e+07, 0.01582, 1000.
1.21616e+07, 0.01631, 1000.
1.21869e+07, 0.0168, 1000.
1.21953e+07, 0.01729, 1000.
1.22038e+07, 0.01778, 1000.
1.22122e+07, 0.01827, 1000.
1.24568e+07, 0.03766, 1000.
1.37725e+07, 0.13803, 1000.
4.24222e+06, 0., 1100.
4.44463e+06, 0.00088, 1100.
4.60487e+06, 0.00134, 1100.
4.73138e+06, 0.00181, 1100.
4.84946e+06, 0.00228, 1100.

4.95066e+06, 0.00275, 1100.
5.04343e+06, 0.00322, 1100.
5.12777e+06, 0.0037, 1100.
5.20368e+06, 0.00418, 1100.
5.27958e+06, 0.00466, 1100.
5.33862e+06, 0.00514, 1100.
5.40609e+06, 0.00562, 1100.
5.46513e+06, 0.0061, 1100.
5.51573e+06, 0.00658, 1100.
5.56633e+06, 0.00707, 1100.
5.61694e+06, 0.00755, 1100.
5.6591e+06, 0.00804, 1100.
5.70127e+06, 0.00852, 1100.
5.74344e+06, 0.009, 1100.
5.77718e+06, 0.00949, 1100.
5.81091e+06, 0.00998, 1100.
5.84465e+06, 0.01046, 1100.
5.86995e+06, 0.01095, 1100.
5.90369e+06, 0.01144, 1100.
5.92899e+06, 0.01192, 1100.
5.95429e+06, 0.01241, 1100.
5.97116e+06, 0.0129, 1100.
5.99646e+06, 0.01338, 1100.
6.01333e+06, 0.01387, 1100.
6.03019e+06, 0.01436, 1100.
6.04706e+06, 0.01485, 1100.
6.06393e+06, 0.01534, 1100.
6.07236e+06, 0.01582, 1100.
6.0808e+06, 0.01631, 1100.
6.08923e+06, 0.0168, 1100.
6.09766e+06, 0.01729, 1100.
6.1061e+06, 0.01778, 1100.
6.1061e+06, 0.01827, 1100.
6.22417e+06, 0.03766, 1100.
6.89044e+06, 0.13803, 1100.

Appendix E

Papers included:

Usmani, A., C. Röben, and A. Al-Remal, *A Very Simple Method for Assessing Tall Building Safety in Major Fires*. International Journal of Steel Structures, 2009(9): p. 17-28.

Asif Usmani, Charlotte Röben, Louise Johnston, Graeme Flint and Allan Jowsey, Tall building collapse mechanisms initiated by fire, Proceeding of the 4th Workshop on Structures in Fire (SiF'06), Aveiro, Portugal.

A VERY SIMPLE METHOD FOR ASSESSING TALL BUILDING SAFETY IN MAJOR FIRES

ASIF USMANI¹, CHARLOTTE ROBEN² AND AHMAD AL-REMAL²

ABSTRACT

The collapse of tall buildings in a densely populated urban setting is a scenario too terrible to contemplate. Buildings are routinely designed to resist this limit state under the extreme loading conditions of high winds and earthquakes etc. However the potential of multiple floor fires to cause such a disaster remains unrecognised in the profession as no current building codes require the consideration of this type of extreme loading. Previous work by the author and his students has demonstrated that the collapse of tall buildings in multiple floor fires is a distinct possibility as the mechanisms that can cause this are easily reproduced using a non-linear finite element analysis programme. This work has been extended by the author and his students to develop a simple analytical method for systematically assessing the collapse of exterior columns of tall buildings for any given fire scenarios. This paper considerably simplifies the method developed previously to the extent that the limit state of collapse under multiple floor fires can be checked even without the need to consider any particular “design” fire and with calculations that can be performed in minutes. This is based on the assumption that in major fires that affect multiple floors, it is quite likely that a number of floors will reach a state of deflection and reduced stiffness that the main load carrying mechanism will be that of catenary action leading to destabilising *pull-in* forces to be exerted on exterior columns. The paper will outline all the steps that must be carried out to check if the remaining structure (columns, floors, connections etc.) will remain stable under the action of the pull-in forces. It will also provide theoretical justification and discussion for all the steps and assumptions made in the assessment. Furthermore the method will be applied to a number of examples, including that of the WTC towers to check if those buildings were safe under major fires involving multiple floors.

1. INTRODUCTION

There have been relatively few studies of the collapses of the World Trade Centre buildings (chiefly WTC 1, 2 and 7) following the terrorist attacks on September 11, 2001. This is quite surprising given the continued proliferation of high rise buildings all over the world and in particular in the rapidly industrialising economies of Asia. In Europe and North America the engineering community

¹ Professor, University of Edinburgh, School of Engineering and Electronics, The Kings Buildings, Edinburgh EH16 5AG, UK, email: asif.usmani@ed.ac.uk (corresponding author)

² PhD Student, School of Engineering and Electronics, The Kings Buildings, Edinburgh EH16 5AG, UK

(both academia and industry) have been somewhat shy of seeing these collapses as an engineering problem and have seemingly preferred to see it as chiefly a political problem. The strong linkage of international terrorism to these events and the personally felt shock may explain this attitude of denial in the west, but the absence of any significant investigation in the rest of the world, despite the boom in high rise construction, is less easily explained. What remains undeniable is the imperative of understanding these collapses in the most fundamental structural engineering sense in order to avoid such failures for other existing and future high-rise construction. Considering how difficult it is to actively fight fires in the high floors of tall buildings located in difficult to reach the busy urban settings, sufficient inherent passive fire resistance must be considered essential for tall buildings. This paper will discuss some of the work that has taken place at the University of Edinburgh over the last 5 years.

All the analysis carried out by the lead author and his collaborators at the University of Edinburgh have focussed on understanding the collapse of the WTC towers purely because of fire. The Edinburgh team have had considerable experience in using computational modelling to understand whole structure behaviour in fire, beginning with the modelling of the full-scale fire tests in Cardington carried out in the mid 90s (Edinburgh University 2001). This led naturally to applying the same methodology to understanding the collapse of the WTC towers and first hypothesis based on this work was published in 2003 (Usmani *et al.* 2003), followed by a refinement (Usmani 2005). Further investigation with larger models (Flint 2005 and Flint *et al.* 2007), produced another collapse mechanism, however the two were later identified to be of a similar nature, as will be shown in the following sections. The only other significant piece of research on these collapses has been carried out by the official WTC investigation team at the National Institute of Standards and Technology in Maryland, USA (NIST 2005). The results from the Edinburgh and NIST work are not strictly comparable as the latter is a forensic investigation taking into account the damage caused by the aircraft and the detailed modelling of the moving fires, while the former assumes an undamaged structure subjected to a large range of simplified fires. Therefore the NIST results are very specific to the WTC 1 & 2 structures while Edinburgh work is much more generally applicable to understanding tall building behaviour in multiple floor fires. This work was extended to produce a *simple* methodology for estimating the limit load capacity of tall buildings and to determine whether a particular collapse mechanism may or may not occur given a frame, its loading and fire scenario (see Roben *et al.* 2007 and Lange *et al.* 2007). This will eventually provide a framework for routine assessment of tall building safety in multiple floor fires and hopefully encourage engineers to confront this risk head-on instead of pretending that it doesn't exist. This paper extends the previous work to produce an even simpler method which uses basic structural engineering arguments to show that the safety of tall buildings against the two identified collapse mechanisms may quite reasonably be assessed without reference to a specific fire scenario. This new method allows the calculations to be simplified considerably and be carried out routinely with relative ease by any practicing structural engineer. The following sections provide full details of the collapse mechanisms and the simple method and the supporting structural engineering arguments for it by expanding an original conference proceedings publication (Usmani 2008).

2. WEAK FLOOR COLLAPSE MECHANISM

A finite element model of a typical 2D slice of 12 storeys of the WTC 1 & 2 frames was created (Usmani *et al.* 2003) using the structural information provided in the FEMA report (FEMA 2002), as shown in Figure 1.

from the fire floors to non-fire floors and then from one failing floor to another. Such a sequence would clearly be arrested if any floor is able to sustain the applied compression and flexure loading without buckling, pointing to the need for strong and stiff floors at suitable intervals over the height of the building, which can sustain such loading.

3. STRONG FLOOR COLLAPSE MECHANISM

When Flint (Flint 2005) extended his analyses to study larger models, a new and different failure mechanism was discovered. In this mechanism the floors are strong enough to resist the forces of compression and flexure exerted on them because of the membrane (or catenary) action of the fire floors, thus preventing a run-away progressive collapse indicated by the weak floor mechanism. However collapse can still occur as shown in Figures 3 and 4, obtained from analysing 2D and 3D models respectively of structures similar to the WTC towers. In these models the pull-in forces exerted on the column by the fire floors acting as membranes causes the formation of 3 plastic hinges (column reaches full plastic yield through a combination of axial compression and bending), thus initiating collapse. This collapse is initiated by localised hinge formation, which is not inherently progressive like the weak floor mechanism, however once the three hinges are formed and there are a considerable number of floors above the location of the fire, then the loads from the superstructure will perpetuate the collapse. If there are only a few floors above the fire floors (say the fire is near the top), the collapse may only be local or not occur at all.

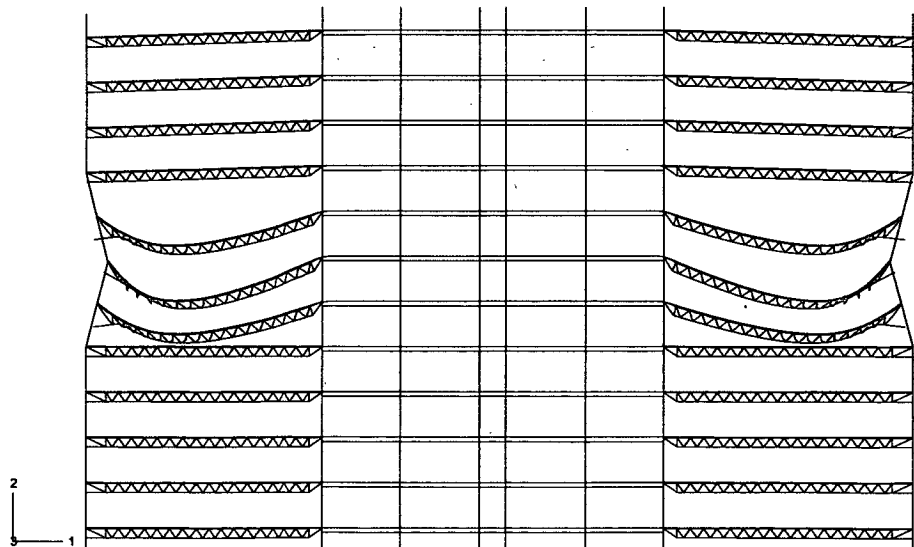


Figure 3: Strong floor localised collapse that will initiate progressive collapse (2D WTC Model)

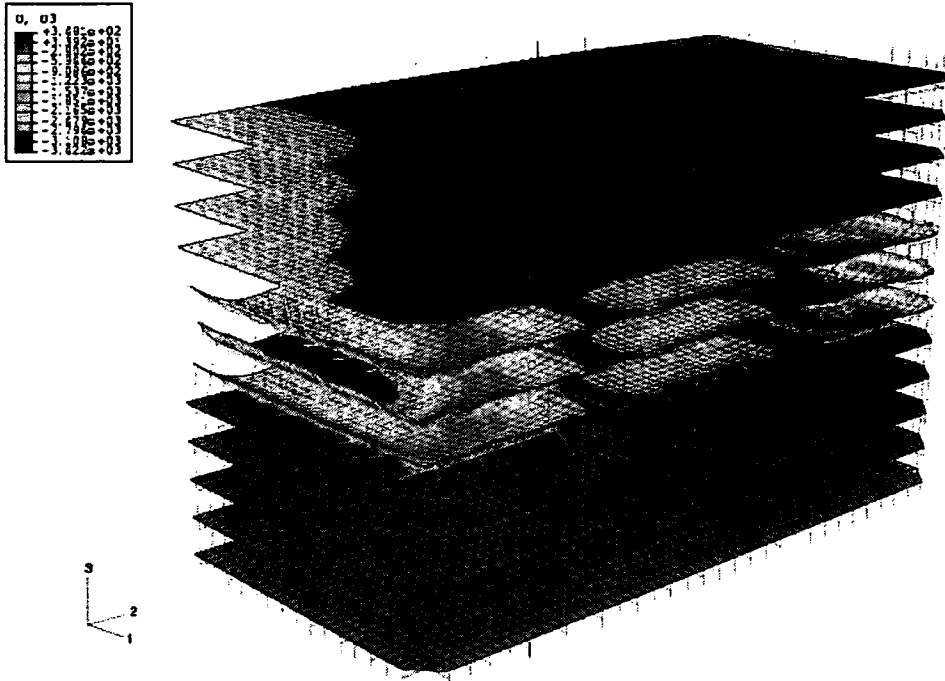


Figure 4: Strong floor localised collapse that will initiate progressive collapse (3D WTC Model)

4. GENERIC TALL BUILDING FRAMES IN MULTIPLE FLOOR FIRES

The two main failure mechanisms established in the previous sections are illustrated in Figure 5. Figure 5(a) shows a mechanism that would occur if a stiff column was supported by a floor system relatively weak in membrane compression and bending (Usmani *et al.* 2003 and Usmani 2005). If however the floors were stiff enough a plastic collapse type mechanism seems to establish (Flint 2005) as a result of the combined compression and bending as in Figure 5(b). These mechanisms are based on analyses that assume that no connection failure occurs. This assumption allows the focus to be on “global” behaviour as it can be reasonably assumed that this would produce a useful upper bound reference collapse scenario.

Local effects such as connection failure, local cracking of concrete, failure shear connectors and their endless permutations could potentially produce a whole range of alternative collapse scenarios, which could reasonably be assumed to produce earlier failures than the reference scenarios (although this is not by any means certain). In a design context local effects can really only be considered properly in a probabilistic rather than deterministic manner.

The previous analyses were carried out using models close to the WTC towers (using tubular column and truss members for the floor support). This work was extended (Usmani *et al.* 2006 and Roben *et al.* 2007) by investigating more “generic” tall building frames made of standard universal beam and column sections to determine whether the same collapse mechanisms are obtained.

A more conventional composite steel frame model using universal beam and column sections respectively was analysed. The beams are laterally restrained by the stiff concrete core but are free

to rotate. They are fully fixed to the column, which in turn is fixed at the bottom but restrained only in the horizontal direction at the top. The concrete slabs are designed to act compositely with the beams and are connected with multiple point constraints. All sections are modelled using 2-D beam elements. The structure is subjected to loading on the beams and the column. Each beam supports a UDL which includes the self weight of the concrete slab as well as the imposed load. The column is subjected to a point load which represents the additional floors above the analysed structure. To compare the behaviour of the models several parameters were changed to obtain a wide variety of results. This includes changing loads, section sizes and spans. The assumed material properties are in accordance with Euro Code 3-1. The fire is assumed to affect three floors (floors 6, 7 and 8). The steel is assumed to be unprotected and thus has a uniform temperature equal to that of the fire. The maximum and ambient temperatures are taken as 800°C and 20°C respectively with an exponential increase and the columns are protected and are restricted to a maximum temperature of 400 °C as in (Usmani *et al.* 2003).

Figure 6 shows the deformed collapsed shapes for two different models, essentially reproducing the two mechanisms shown in Figure 5. The weak floor mechanism shows that the column forces the floor below the fire floors to buckle, thus increasing the loading on the floor below and starting a progressive collapse. The strong floor mechanism shows a clear plastic collapse with three hinges forming at the floors above and below the fire floors and at the centre fire floor. It also shows that only the fire floors deflect and that no lateral movement of the column occurs at locations away from the fire floors. This coincides with the three hinge failure assumption that the collapse is localised

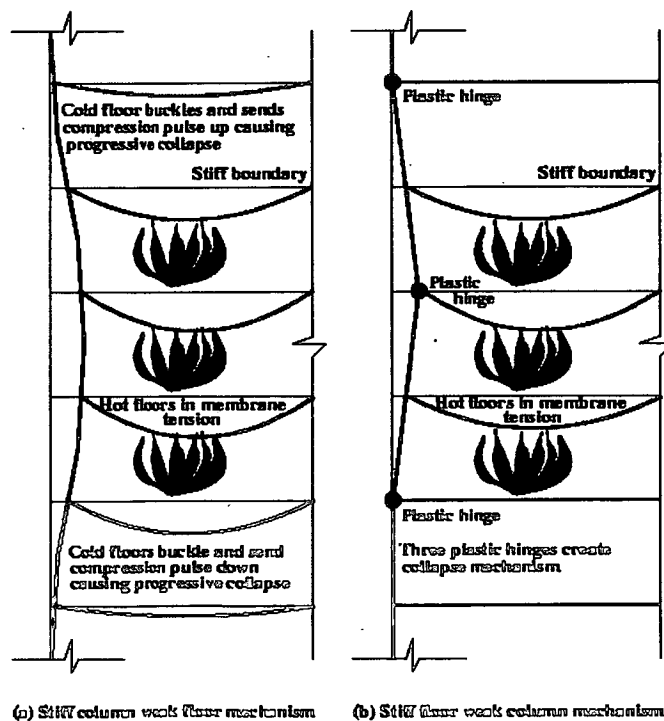
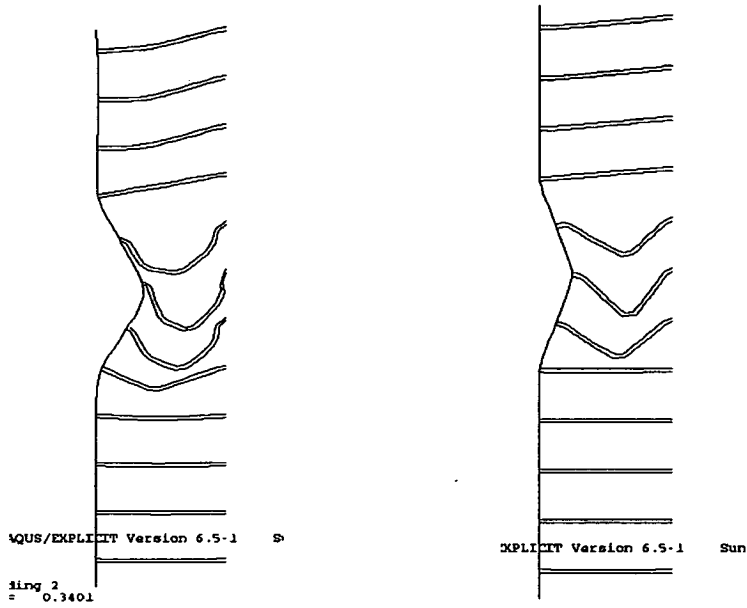


Figure 5: Suggested collapse mechanisms for tall buildings in fire

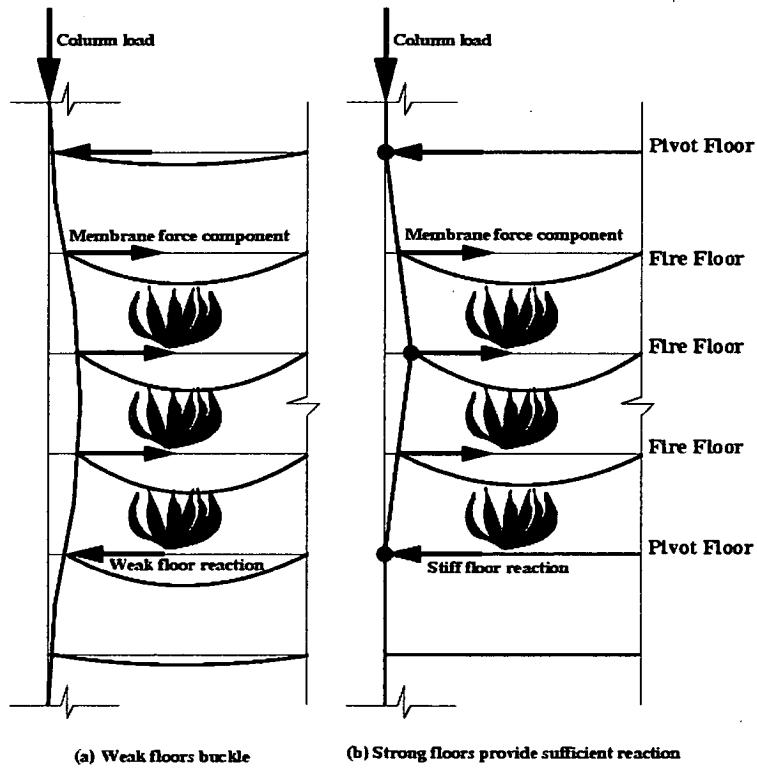


(a) Weak

(b) Strong floor mechanism

floor mechanism

Figure 6: Deflected shapes with a floor buckling and column plastic collapse respectively



(a) Weak floors buckle

(b) Strong floors provide sufficient reaction

Figure 7: Fire induced collapse of tall building frames

5. VERY SIMPLE ASSESSMENT METHOD

The collapse mechanisms discussed above can be used to develop a simple method for assessing the safety of tall building against collapse. Figure 7 illustrates the key idea. A two part paper with full details of the method has been submitted to the Structural Engineer (Roben *et al.* 2007 and Lange *et al.* 2007), which requires relatively simple but detailed calculations of the fire scenarios and thermo-mechanical response of the idealised structural frame. This method however has been further simplified and was first presented at the last SiF'08 conference, Usmani (2008), the details of which are presented in this section.

0. *Start with an adequate model structure & assume number of fire floors involved*

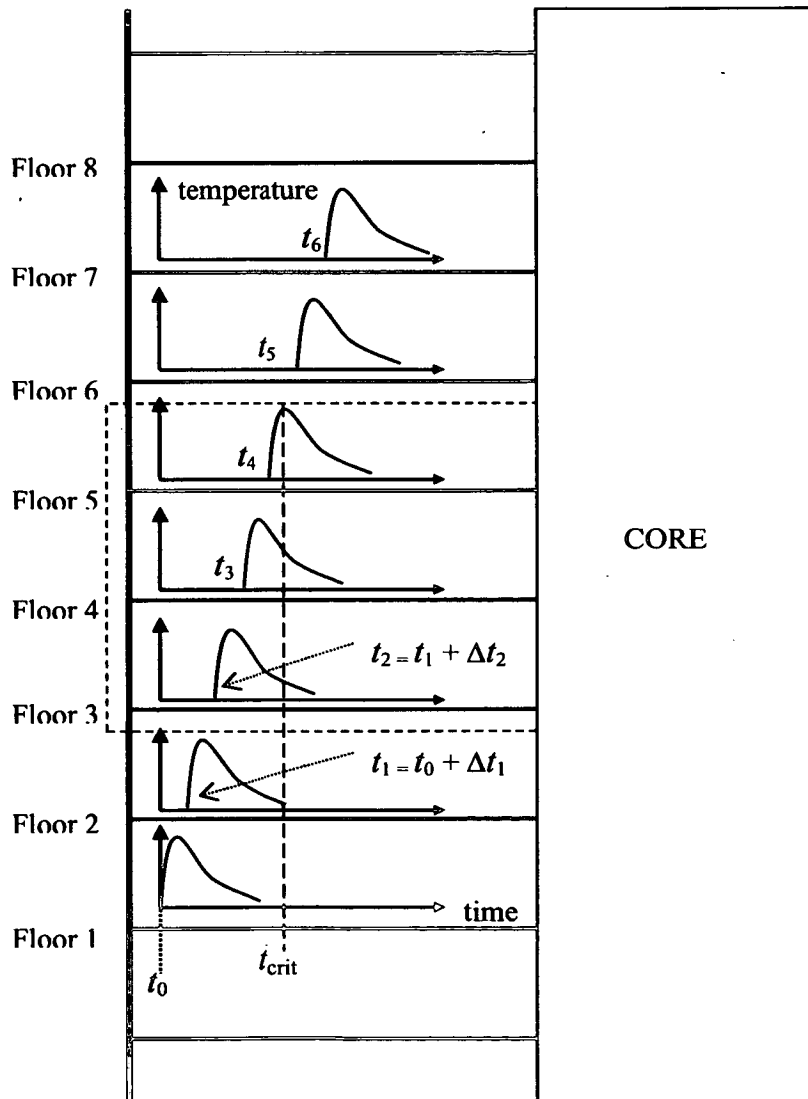


Figure 8: Structural model and number of fire floors involved

Most modern tall buildings are built with a core and a floor plate extending out from the core to a perimeter frame. We can also typically assume that the core is typically a place where large fires are unlikely to occur because of significant barriers to fire spread

(compartmentation) and relatively poor ventilation. Conversely large fires can occur and spread relatively easily in modern open-plan office floors and extensive glazing which could brake and provide sufficient air. Therefore an idealised structural model as shown in Figure 8 is a reasonable assumption, where the fires occur in the outer floor plate and move progressively upward through broken windows. For a given progression scenario one may only consider a limited maximum number of floors will be affected by the fire at the same time. For example the progression scenario in Figure 8 show that one can consider only floors 3, 4 and 5 to be affected by fire at the same time (numbering of floors is assumed here to start from the first floor to ignite). Floors above this have not at this time been ignited while floors below could be considered to have cooled to the point that the structural system has recovered sufficient strength. Clearly the recovery of structural system will depend upon the type of the structural system of the floor (steel framing may cool relatively quickly and recover its stiffness and strength if the connections remain viable), the severity of fire and the extent of residual damage in the structural system. The time at which the largest number of floors are affected, could be considered as a critical time, t_{crit} as shown in Figure 8. A risk analysis should be carried out to determine a reasonable maximum number of floors likely to be affected by fire. Any risk model involving fire effect on structure should incorporate the stochastic time history of the problem at hand. It is reasonable to assume that risk at time, t , is a function of risk at time $t-1$ (previous step). This greatly simplifies risk assessment as each time step can be analysed separately. Fire ignition and subsequent progression can thus be modelled over the following domain of events (for probability of occurrence, please refer to Chapter 7 in Rasbash *et al.* 2004:

- Ignition
- Spread within one floor (initial floor)
- Spread from the initial floor to other floors.

The main components of the risk, probability of occurrence and the associated consequence need to be established. In this case the consequence of interest is spread to other floors.

Probability of spread does not depend on probability of occurrence (ignition). The case of establishing the number of floors affected simultaneously by fire is only relevant after fire has started. Consequently, the probability of ignition should be set to 1.0 for this particular analysis. Fire progression within the initial floor falls under the same argument and its probability can similarly be set to unity.

Fire spread to other floors can be analysed using a fault tree. The possible spread routes (tree branches) are:

1. Compartment failure (structural or thermal). Cracks developing in floor slabs can provide transport route for hot gases that may ignite combustible materials. Floors with relatively high thermal conductivity (thermally thin) cannot impede temperature rise on the cold side. Once the temperature reaches the ignition temperature of any material in the cold floor, fire may start.
2. Surface spread. This is the more likely event as flame and smoke can breach external wall seals or windows more easily than structural floors.

From a physical viewpoint, route 2 is more likely as natural systems pursue the alternative with maximum energy dissipation rate. Observations of past fires support this argument.

Regardless of the spread mechanism, fire spreading beyond the initial floor is most likely to occur after flashover. The lower bound for the time required to initiate spread to further floors, Δt_1 , is the time to flashover, $t_{flashover}$.

$$\Delta t_1 \geq t_{flashover}$$

The most common key event that initiates spread to other floors is the breakage of windows, which is a function of the heat release rate at the initial floor and the structural resistance of the windows. When the heat release rate, $Q''_{f_initial\ floor}$, is sufficient to increase the glass strain to a critical value, glass breaks and fire moves into the next floors.

Depending on the type of wall material the walls themselves may propagate the fire to upper floors which is the worst possible scenario and sets an *upper limit* on the number of floors on fire. Its probability of occurrence depends on the type of wall cladding. While most modern building façades are made of glass, many are finished with external insulation and finish, EIFS, systems which provide superior thermal insulation. However, most insulation boards in EIFS systems are made of combustible materials like expanded or extruded polystyrene or polyisocyanurate (PIR). Some of the insulation materials can even cause *downward* fire movement as they disintegrate and start spalling, thereby igniting lower walls (downward fire spread can also occur from non-fire-resistant openings in floors such as in the case of Windsor Tower fire in Madrid).

Fire spread beyond the next upper floor is less likely to occur as a result of the initial fire. The increase in first upper floor temperature, however, is expected to accelerate time to flashover on that floor and reduce the time required to spread to further floors, i.e.; $\Delta t_2 \leq \Delta t_1$. The maximum number of floors “ N ” involved in fire for determining the upper bound structural fire resistance may be based on the criterion of when the duration of a fire, F_i on floor i (not necessarily the first floor), is *just greater* than the time required for fire to spread to floor $i+N$, i.e. $\Delta t_i + \Delta t_{i+1} + \dots + \Delta t_{i+N}$

The calculation procedure for fire initiation on floor i , can be summarised as follows:

- I. Estimate fire duration for each floor i (from ignition to extinction) F_i
- II. Calculate spread times, $\Delta t_1, \Delta t_2, \Delta t_3, \dots, \Delta t_{n-1}$ for all $n-1$ spreads (n is the total number of floors in the building)
- III. Maximum number of floors N can be obtained for the case of fire initiation on a floor i where:

$$F_i > \Delta t_i + \Delta t_{i+1} + \dots + \Delta t_{i+N}$$

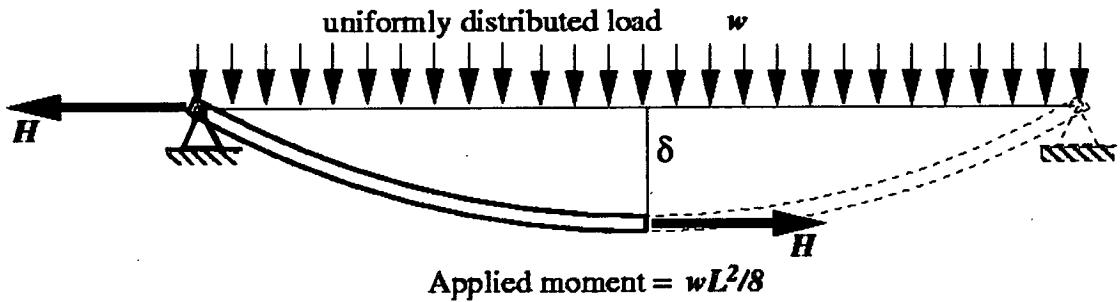
This can be illustrated by the case shown in Figure 8, where,

$$F_2 > \Delta t_2 + \Delta t_3 + \Delta t_4 + \Delta t_5$$

which gives $N=3$ and fires on floors 3, 4 and 5 as the critical case for structural fire resistance.

1. Assume an appropriate deflection to carry to all the load (udl) by tensile membrane action in the floor (T)

Based on the collapse mechanisms discussed above, the key demand on exterior columns arises from pull-in forces exerted by a fire-affected sagging floor in tensile membrane or catenary action. The tensile force for catenary resistance depends upon deflection the deflection δ shown in Figure 9. A beam may continue to retain some bending capacity even under large deflections, so the resistance to the load demand ($wL^2/8$) at high temperatures will typically depend upon a combination of bending and catenary resistance.



Tensile membrane or catenary resistance = $H\delta$

Residual moment capacity = $M_p(T, H)$

Figure 9: Tensile membrane or catenary resistance in a sagging beam

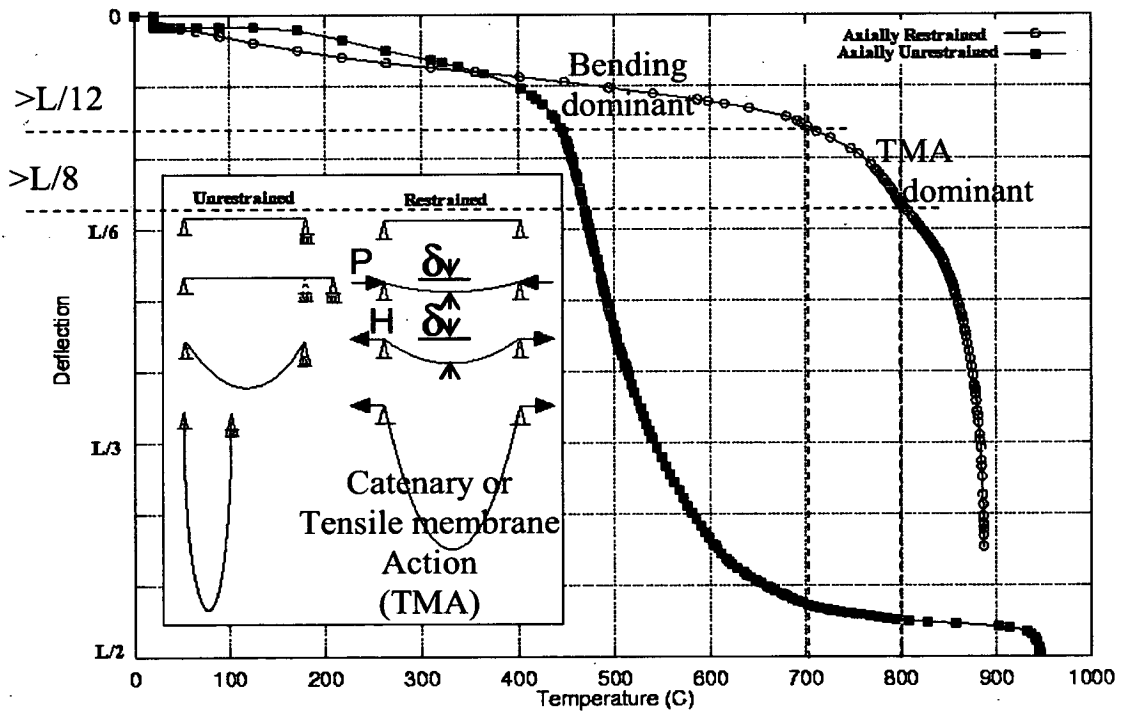


Figure 10: Runaway failure of a steel beam subjected to elevated temperature

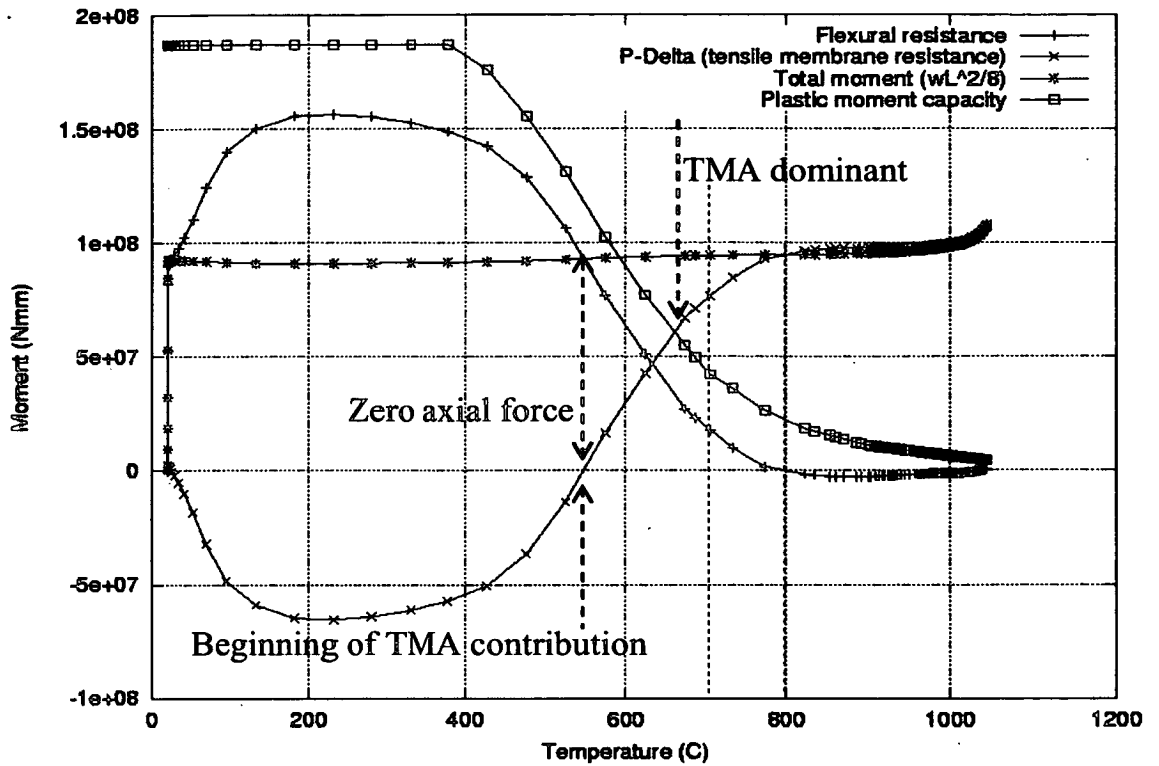


Figure 11: Moment quantities in the restrained beam of Figure 10

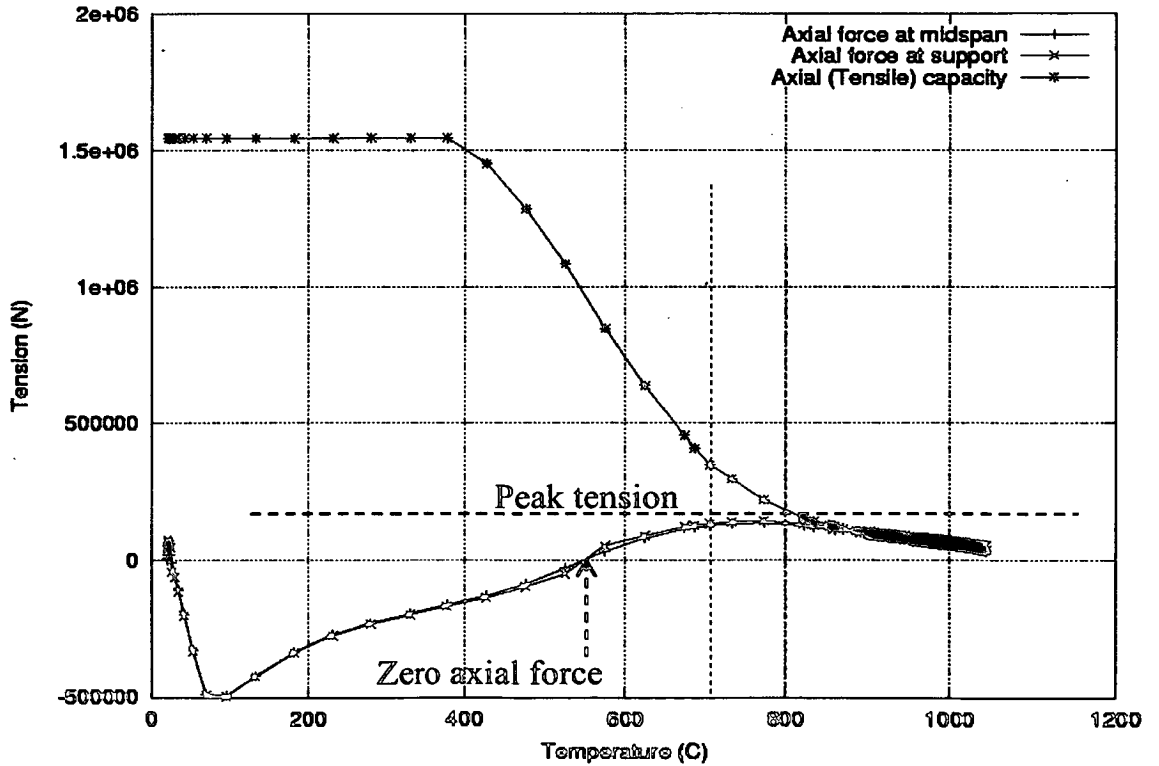


Figure 12: Axial force quantities in the restrained beam of Figure 10

Figure 10 shows the deflections in a bare steel beam loaded with a uniformly distributed load (of half its ultimate capacity) and subjected to heating under unrestrained and restrained end-conditions. The restrained beam clearly shows fire resistance over a longer duration and based on the deflection behaviour it appears that at a temperature of 700°C and a deflection of over $L/12$ the flexural capacity of the beam appears to be exhausted and deflections begin to increase at a much higher rate. This problem was analysed in detail by Lamont *et al.* (2003). The results of this analysis are reproduced in Figures 11 and 12 showing moments and axial forces respectively in the restrained beam. Figure 11 clearly shows that at 700°C the flexural resistance is less than a quarter of the load, the rest being provided by catenary action, which begins at about 550°C. Figure 12 shows that the peak catenary tension occurs between 700°C and 800°C around a deflection of $L/10$ (Figure 10).

Based on the above analysis one may choose a deflection of $L/10$ to determine the pull-in forces on the exterior columns quite conservatively (as practically all the load is being carried by catenary resistance) and apply it simultaneously at all the fire floors determined in step 0 (as described in the application example below). This assumption may be reasonable for large span slender floor systems (such as slabs supported by long-span cellular beams or trusses) where bending resistance may exhaust rather rapidly. The “design pull-in force” can therefore be estimated as:

$$H = (wL^2/8)/(L/10) = 1.25 wL \quad (1)$$

The above assumption may be overly conservative for many real structures, such as in the case of steel frame composite floor systems with relatively smaller spans as considerable moment capacity may remain at the end of the fire. To examine this an analysis of a 9m span and 12m span one-way composite floor is carried out. For the 9m span floor a steel beam (305x165x46) is attached to a 120mm thick slab and is subjected to a 1-hour exponential fire (see Flint *et al.* 2007) reaching a maximum temperature of 800°C at about 1000 seconds.

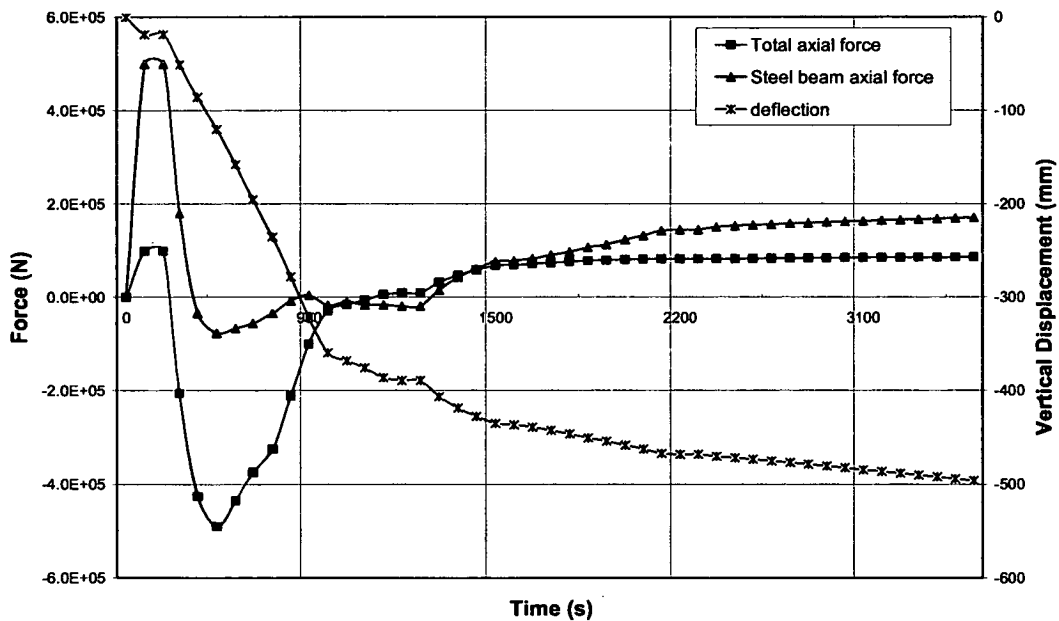


Figure 13: Deflection and axial forces in 9m composite floor.

For a floor panel 3m wide with a live load of 5 kN/m^2 (assuming this to be service load – which can generally be reduced for the fire limit state) the udl on the composite beam formed by the floor system is approximately 24 kN/m . Therefore the applied moment is approximately 229 kNm . The section analysis produces an approximate moment of resistance of approximately 670 kNm at ambient temperature, producing a load ratio (R) of 0.34 . Figure 13 shows the response of the composite beam (restrained at ends) to the load and the fire (applied subsequent to the loading). The maximum deflection is approx. 500 mm and the pull-in force is constant at roughly 85 kN . If the load was being carried entirely by catenary action, at this deflection the pull-in force should have been 486 kN (5.7 times 85), so clearly considerable bending capacity remains in this case and the destabilising forces on the exterior column will be low.

Turning to the 12 m span floor using the same steel beam ($305 \times 165 \times 46$) now attached to a 100 mm thick slab (creating a more slender floor system) and subjected to a 1-hour exponential fire this time reaching a maximum temperature of 1000°C . For a floor panel 3 m wide with a live load of 5 kN/m^2 the udl on the composite beam formed by the floor system is approximately 22.6 kN/m leading to an applied moment of 408 kNm . The moment of resistance now is roughly 615 kNm at ambient producing a load ratio of 0.66 . Figure 14 shows the total axial force evolution in the resulting composite beam over the duration of the fire. The maximum axial force of 236 kN is obtained at 2000 seconds for a deflection of 970 mm . At this deflection full catenary action would produce a force of 420 kN , which is a lot closer to the 236 kN compared to the previous case (only 1.8 times again 5.7 times), which suggests that the higher load ratio in this case causes a greater degradation of bending capacity.

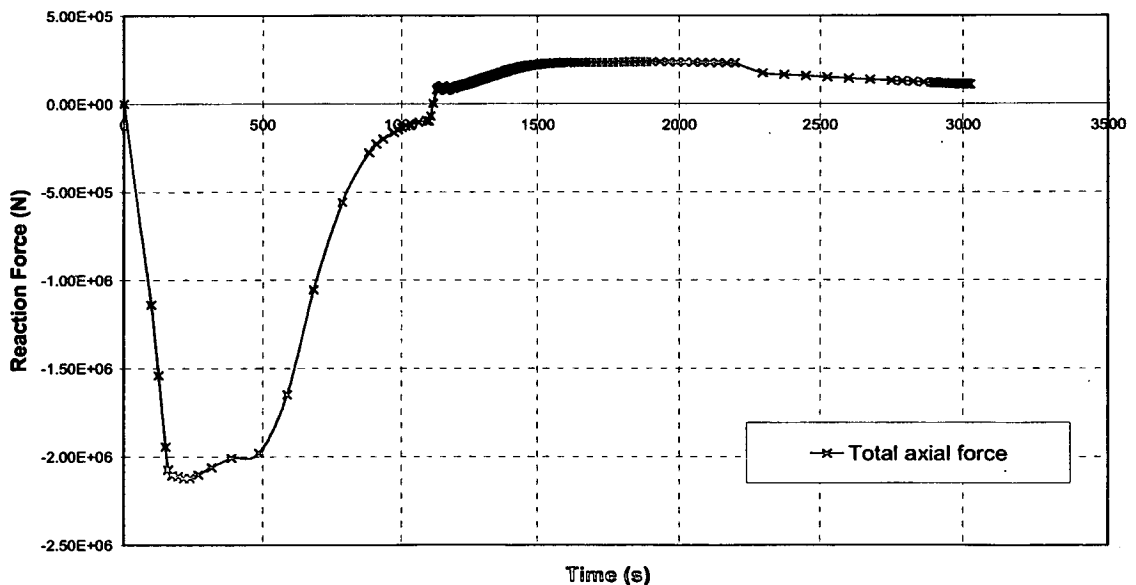


Figure 14: Deflection and axial forces in 9m composite floor.

Based on the above analysis a modified method of calculating the pull-in force is proposed. The previous expression in (1) is simply multiplied by the load ratio.

$$H = 1.25 wLR \quad (2)$$

Applying this to the 9m beam produces 92 kN (which is close to 85 kN obtained from the analysis). For the 12m beam it produces 224kN which is again not far from 236 kN. This sort of estimation may appear crude however it provides a very quick and effective means of ensuring tall building safety in fire and in the author's opinion offers enormous practical value.

2. *Determine if adjacent floors are able to sustain the reaction without instability, if not - WEAK FLOOR COLLAPSE occurs*
3. *If adjacent floors remain stable, check columns using an axial force-moment interaction diagram (function of heating) if the maximum moments and forces remain inside the yeild boundaries, if not - STRONG FLOOR COLLAPSE*

Steps 2. and 3. above are pretty self-explanatory and require ordinary structural analyses to be carried out. These are perhaps best illustrated by the example below.

6. APPLICATION EXAMPLE

Flint *et al.* (2007) published the results of their computational analysis of 2D models of WTC (as shown in Figure 3). This analysis shows a strong floor type collapse mechanism with hinges developing in columns. The method introduced in the previous section is applied to check whether the failure predicted by the finite element model can be reproduced here.

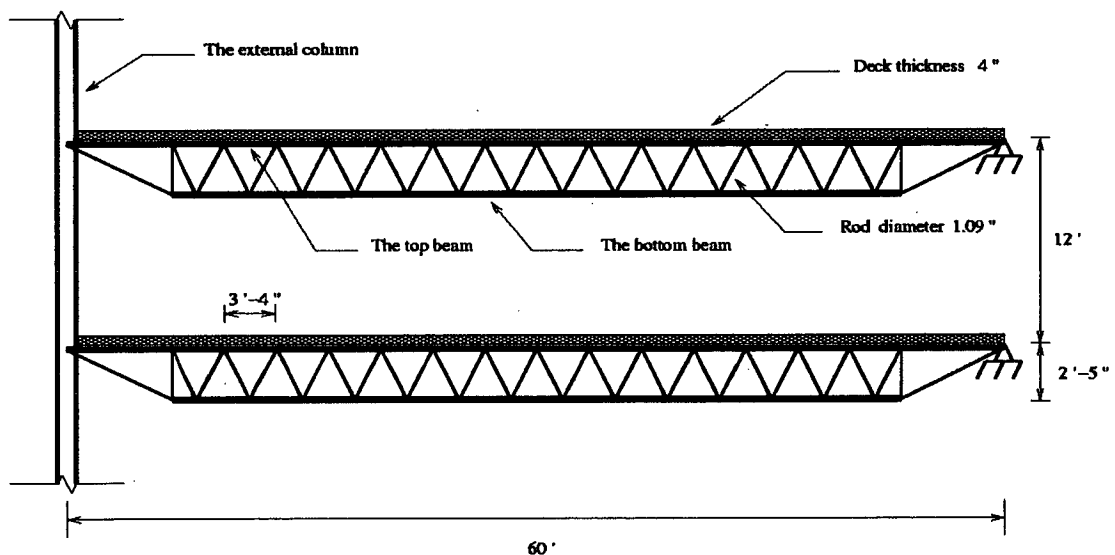


Figure 15: The WTC 1 & 2 floor system.

Figure 15 shows the slender long span floor system (18m) of the WTC towers structure. The udl on the floor is assumed to be 3 kN/m^2 . The column section as modelled is shown in Figure 16. This was necessary as the columns were 1 meter apart and the trusses are two meter apart in the structure. Therefore the udl applied to the member representing the floor was 6 kN/m . Assuming that for this long and slender floor system the bending capacity will be exhausted relatively quickly, the pull-in force H is calculated using Equation (1), or equal to $1.25wL$ or numerically 135 kN . Now the stability of the perimeter column can be assessed for a three

floor fire as discussed below (although it can be argued that a greater number of floors were on fire simultaneously in the WTC 1 & 2 fires – but here we are only concerned with demonstrating the method).

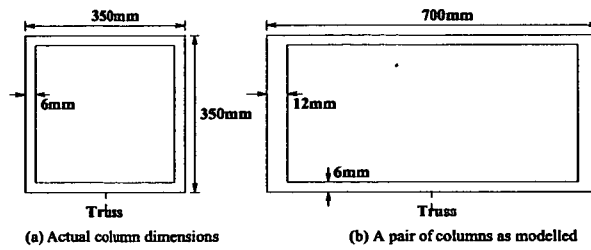


Figure 16: Columns as modelled

Figure 17 shows a simple model of the column, reduced by using symmetry at the point of the middle hinge and truncated at the floor below the lower pivot floor. The symmetry point is assumed to be the 97th floor (WTC tower 1) with 13 floors above that point imposing an estimated load of 700kN at that point.

The model of Figure 17 requires a 2nd order analysis because of the interaction between the axial (representing the load of the superstructure) and lateral loading (representing the tensile pull-in forces from the floor system). This was carried out to obtain results as follows:

1. Lateral displacement at A = 97mm
2. Moment at A = 462.6 kNm
3. Moment at B = 570.4 kNm

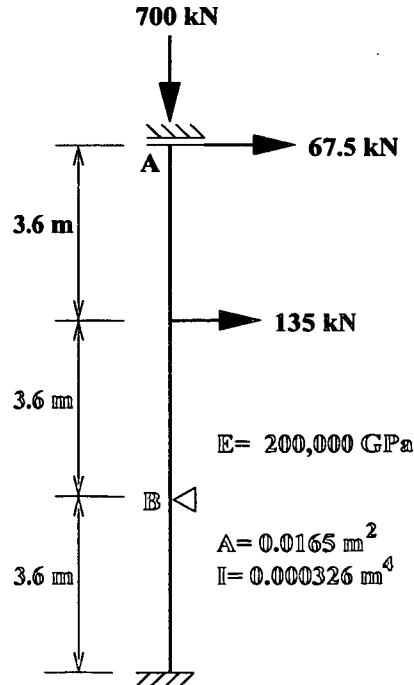


Figure 17: Simple analysis model

Assuming the yield stress of the column to be 300 MPa (the WTC steel ranged from 250 to 690 MPa – with the higher floors using lower grade steel typically) the full plastic moment capacity (M_p) of the column section is 639 kNm and its compressive strength (P_p) is 4954 kN. The linear column interaction formula ($M/M_p + P/P_p < 1.0$) can be used to conservatively estimate whether the column capacity will be sufficient for this, where M is 570.4 kNm and P is 700 kN. This gives a value of 1.03 which is marginally greater than 1.0 however it does clearly suggest that a hinge is very likely to be formed at point B, which will inexorably lead to a hinge at A because of the $P-\delta$ effect, leading to strong floor collapse as discussed earlier. Although the steel yield stress used in this analysis to be on the low side (assuming that the steel on the top level will perhaps be lower strength due to reduced loading), no further reduction is assumed because of the effect of fire and the full ambient value is used. This is not an unreasonable assumption as the perimeter columns has three sides exposed to the atmosphere, however some temperature increase will be expected as fires burn hottest near perimeter openings, i.e. adjacent to the columns.

8. CONCLUSIONS

Buildings are routinely designed to resist the limit state of collapse under the extreme load conditions of high winds and earthquakes etc. however the potential of multiple floor fires to cause such a disaster remains unrecognised in the profession as no current building codes require the consideration of this type of extreme loading. It is clearly demonstrated in this paper that collapse of tall buildings in multiple floor fires is a distinct possibility as the mechanisms that can cause this are easily reproduced using a non-linear finite element analysis programme. The events of September 11, 2001 saw three very tall buildings collapse within hours of each other primarily because of fire and it can be argued that the NIST analyses of these collapses are not the final word as other works such as Usmani *et al.* 2003, Flint 2005 and Flint *et al.* 2007 clearly offer alternative and plausible scenarios in ways more convincing than the NIST analysis as these are based on whole-structure 2D and 3D non-linear analyses that NIST has distinctly failed to produce. The collapse mechanisms produced in these analyses form the basis of the method presented in this paper. The simple analysis based on the method presented also confirms the computational models and points to a significant vulnerability in the design of the WTC structure for large fires, albeit no regulations required this, and still don't, which in the light of recent research such as this seems unfortunate.

This paper clearly shows that the assessment of the collapse potential of a frame in multiple floor fires need not always require rigorous, labour intensive and time consuming finite element analyses. It is possible for frames of relatively regular geometry to be assessed using this simple, cost effective and quick method. Therefore there is no real excuse for ignoring the risk that multiple floor fires pose to tall buildings.

REFERENCES

EDINBURGH UNIVERSITY (2001), "Partners in Technology Report: Behaviour of steel framed structures under fire conditions", *Main Report*, University of Edinburgh.

- FEMA (2002). *World Trade Center Building Performance Study: Data collection, preliminary observations and recommendations*. Technical Report FEMA 403.
- FLINT, G.R. (2005). *Fire Induced Collapse of Tall Buildings*. PhD thesis, University of Edinburgh.
- FLINT, G.R. *et al.* (2007). *Structural response of tall buildings to multiple floor fires*. Journal of Structural Engineering, ASCE J. of Structural Engineering, vol. 133, no. 12, pp 1719-1732.
- LAMONT, S. *et al.* (2003). *Assessment of the fire resistance test with respect to beams in real structures*. AISC Engineering Journal, vol. 40, no. 2, pp 63-75.
- LANGE, D. *et al.* (2007). *Tall building collapse mechanisms initiated by fire – Part II: Design method*. Submitted to the Structural Engineer.
- NIST (2005). *Global Structural Analysis of the Response of the World Trade Center Towers to Impact Damage and Fire*. Technical report NIST NCSTAR 1-6D.
- RASBASH, D.J. *et al.* (2004). *Evaluation of Fire Safety*. John Wiley & Sons Ltd, ISBN 0-471-49382-1
- ROBEN, C. *et al.* (2007). *Tall building collapse mechanisms initiated by fire – Part I: Analysis*. Submitted to the Structural Engineer.
- USMANI, A. *et al.* (2001). *Fundamental principles of structural behaviour under thermal effects*. Fire Safety Journal, vol. 36, pp 721-744.
- USMANI, A. *et al.* (2003) *How did the WTC Towers Collapse? A New Theory*, Fire Safety Journal, vol. 38, pp. 501-533
- USMANI A. (2005). *Stability of the World Trade Center Twin Towers structural frame in multiple floor fires*. Journal of Engineering Mechanics, ASCE, vol. 131, pp. 654-657.
- USMANI, A. *et al.* (2006). *Tall building collapse mechanisms initiated by fire*. Proceedings of the 4th Workshop on Structures in Fire (SiF'06), Aveiro, Portugal.
- USMANI, A. (2008). *A very simple method for assessing tall building safety in major fires*. Proceedings of the 5th Conference on Structures in Fire (SiF'06), Singapore.

TALL BUILDING COLLAPSE MECHANISMS INITIATED BY FIRE

ASIF USMANI¹, CHARLOTTE ROBEN², LOUISE JOHNSTON², GRAEME FLINT¹,
ALLAN JOWSEY³

ABSTRACT

This paper introduces the hypothesis of two possible failure mechanisms for tall buildings in multiple floor fires. This paper extends the previous work done on the WTC towers by investigating more "generic" tall building frames made of standard universal beam and column sections to determine whether the same collapse mechanisms are obtained. The outcome of this paper enables the development of a simple stability assessment method for tall buildings in multiple floor fires.

1. INTRODUCTION

Since the events of September 11, 2001 there has been considerable interest in understanding the collapse of the tall buildings in fire. Whole structure response analyses with the aim of establishing the precise collapse mechanisms for WTC tower like structures were carried out by the research group at University of Edinburgh in collaboration with Arup. The two main failure mechanisms established in this work are illustrated in Figure 1. Figure 1 (a) shows a mechanism that would occur if a stiff column was supported by a relatively weak (in membrane compression) floor system^{1,2}. If however the floors were stiff enough a conventional plastic hinge mechanism seems to establish³ as a result of the moments imposed upon the column by the floors in tension and P- δ moments, shown in Figure 1 (b). These mechanisms are based on analyses that assume that no connection failure occurs. This assumption allows the focus to be on "global" behaviour as it can be reasonably assumed that this would produce a useful upper bound reference collapse scenario. Local effects such as

¹ Doctor, University of Edinburgh, School of Civil and Environmental Engineering,
email: asif.usmani@ed.ac.uk, G.R.Flint@ed.ac.uk

² Undergraduate student, University of Edinburgh, Department of Civil and Environmental Engineering, ,
email: C.C.Roben@sms.ed.ac.uk, L.S.Johnston@sms.ed.ac.uk

³ PhD student, University of Edinburgh, School of Civil and Environmental Engineering, ,
email: A.I.Jowsey@ed.ac.uk

connection failure, local cracking of concrete, failure shear connectors and their endless permutations could potentially produce a whole range of alternative collapse scenarios, which could reasonably be assumed to produce earlier failures than the reference scenarios (although this is not by any means certain). In a design context local effects can really only be considered properly in a probabilistic rather than deterministic manner.

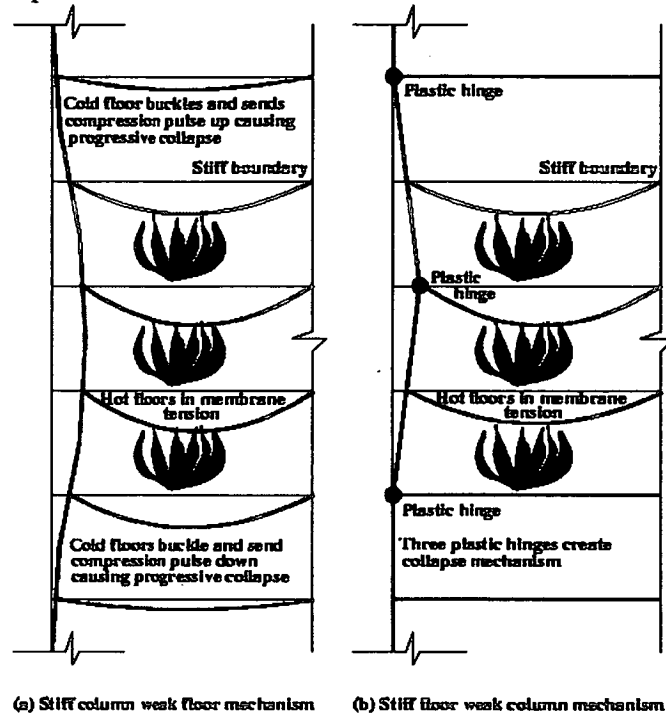


Fig.1 – Suggested collapse mechanisms for WTC towers structure in fire

All previous analyses were carried out using models similar to the WTC towers (using tubular column and truss members for the floor support). This paper extends the previous work by investigating more "generic" tall building frames made of standard universal beam and column sections to determine whether the same collapse mechanisms are obtained. Furthermore, a first attempt is made to develop some generally usable indicator of the propensity of a fire induced collapse in a tall building based on the key parameters of fire severity, number of floors affected and relative column and floor stiffness

2. MULTI-STOREY FRAME MODEL

A more conventional composite steel frame model was constructed to determine that the collapse mechanisms discovered in the context of WTC towers analyses based on the long span truss floor system could be generalised to include more conventional structures. Figure 2 shows the model details.

This is a composite floor system, where the beams and columns are universal beam and column sections respectively. The beams are laterally restrained by the stiff concrete core but are free to rotate. They are fully fixed to the column, which in turn is fixed at the bottom but restrained only in the horizontal direction at the top. The concrete slabs are designed to act compositely with the beams and are connected with multiple point constraints. All sections

are modelled using 2-D beam elements. The structure is subjected to loading on the beams and the column. Each beam supports a UDL which includes the self weight of the concrete slab as well as the imposed load. The column is subjected to a point load which represents the additional floors above the analysed structure. To compare the behaviour of the models several parameters were changed to obtain a wide variety of results. This includes changing loads, section sizes and spans. The assumed material properties are in accordance with Euro Code 3-1.

To model the fire, a generalised exponential curve is chosen to represent the time-temperature relationship and is given by

$$T(t) = T_0 + (T_{\max} - T_0) (1 - e^{-\alpha t}) \quad (1)$$

where, T_{\max} is maximum compartment temperature, T_0 is the initial or ambient temperature, and α is an arbitrary 'rate of heating' parameter. For the purpose of this research the maximum and ambient temperature are taken as 800°C and 20°C respectively, α is taken to be 0.005 and the time t is taken as 3600 seconds.

The fire affects floors 6, 7 and 8. The steel is assumed to be unprotected and thus has a uniform temperature equal to that of the fire, shown in Figure 3. The columns are assumed to be protected and are restricted to a maximum temperature of 400°C at the end of the heating period, which is a conservative estimate. The concrete slabs have a non-uniform temperature distribution and follow the temperatures shown in Figure 4.

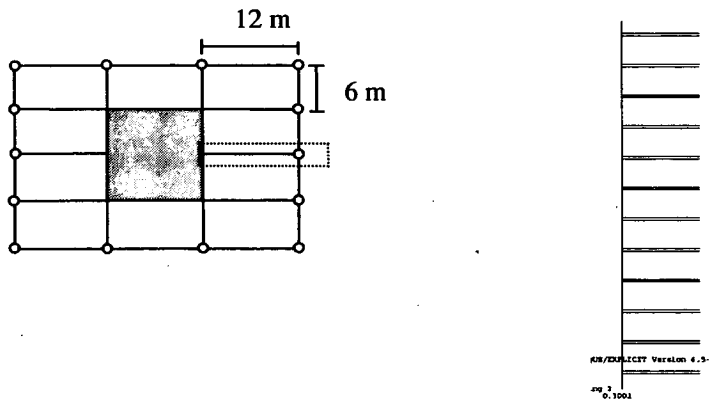


Fig. 2 – Typical plan of a multi-storey frame model and the Finite Element Model cross section adopted

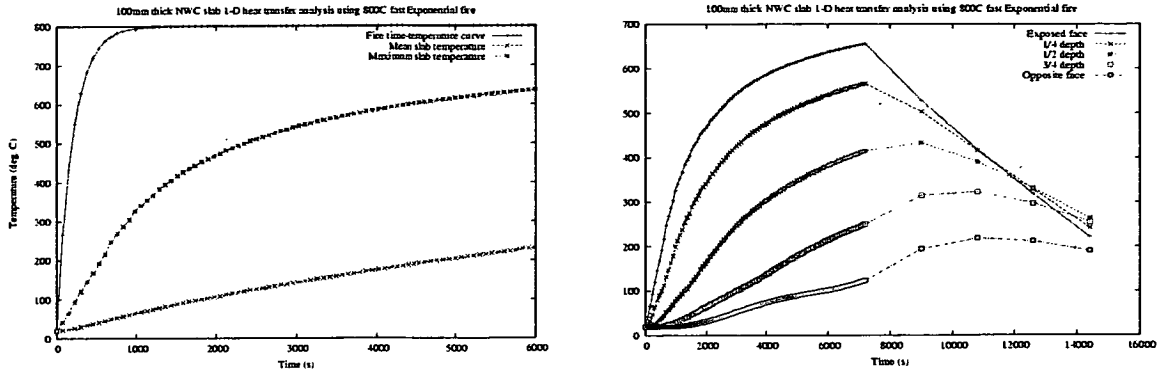


Fig.3 – Generalised fire curve and concrete temperatures through the slab

3. MODELLING RESULTS

Figure 4 shows the deformed collapsed shapes for two different models, essentially reproducing the two mechanisms shown in Figure 1. The weak floor model shows a clear plastic collapse with three hinges forming at the floors above and below the fire floors and at the centre fire floor. The stiff floor model shows that the column forces the floor below the fire floors to buckle, thus increasing the loading on the floor below and starting a progressive collapse.

The horizontal deflection of the column is plotted for both models and can be found in Figure 5. Initially both show a negative displacement, indicating the outward movement of the column due to the thermal expansion of the beams. The weak floor model shows that the fire floors quickly deflect in the positive direction as the beams are pulling it in. As the column increasingly pushes against the floors below the fire these buckle and the column moves inward at these lower floors.

The stiff floor model however, shows that only the fire floors deflect further and that no movement of the column occurs at any other point. This coincides with the three hinge failure assumption that the collapse is localised.

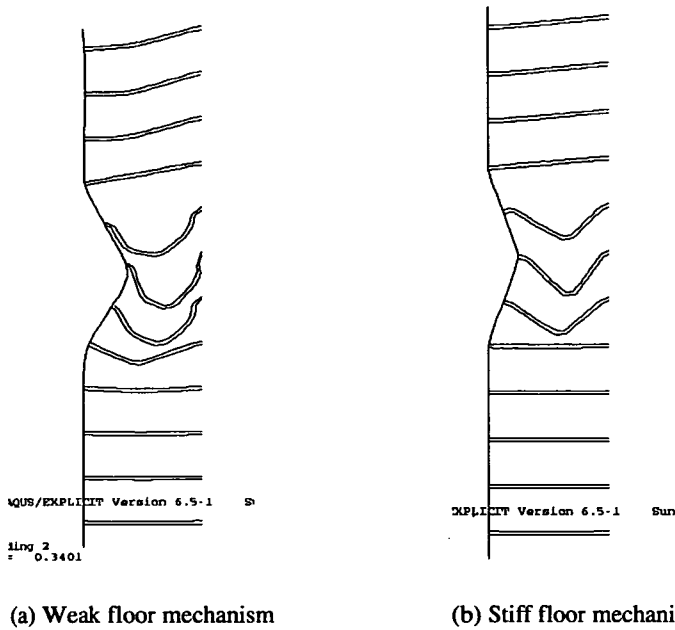
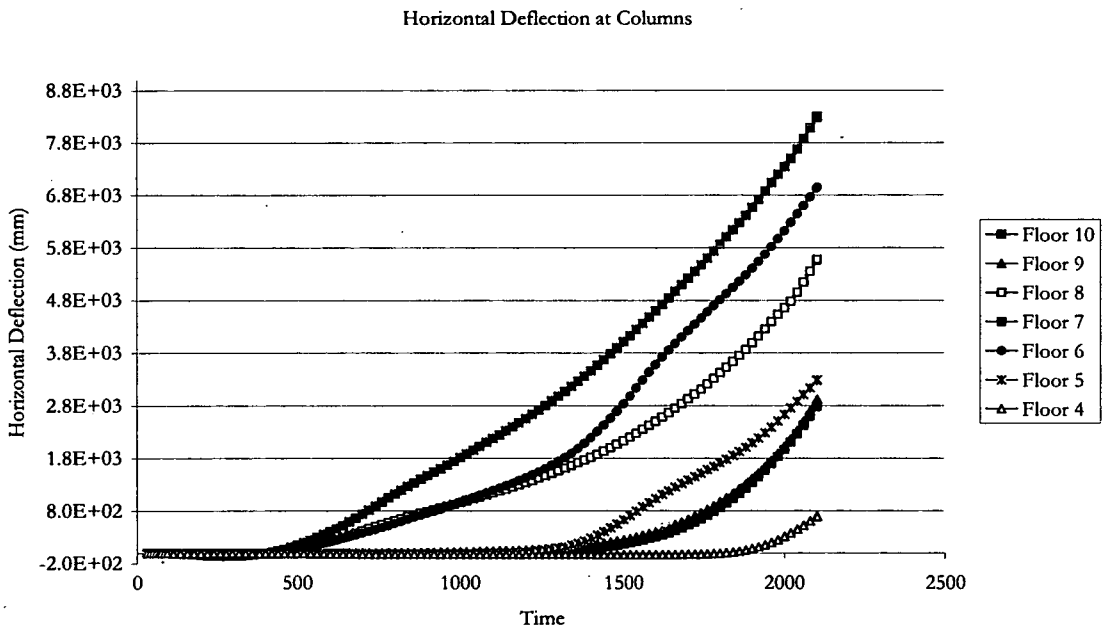
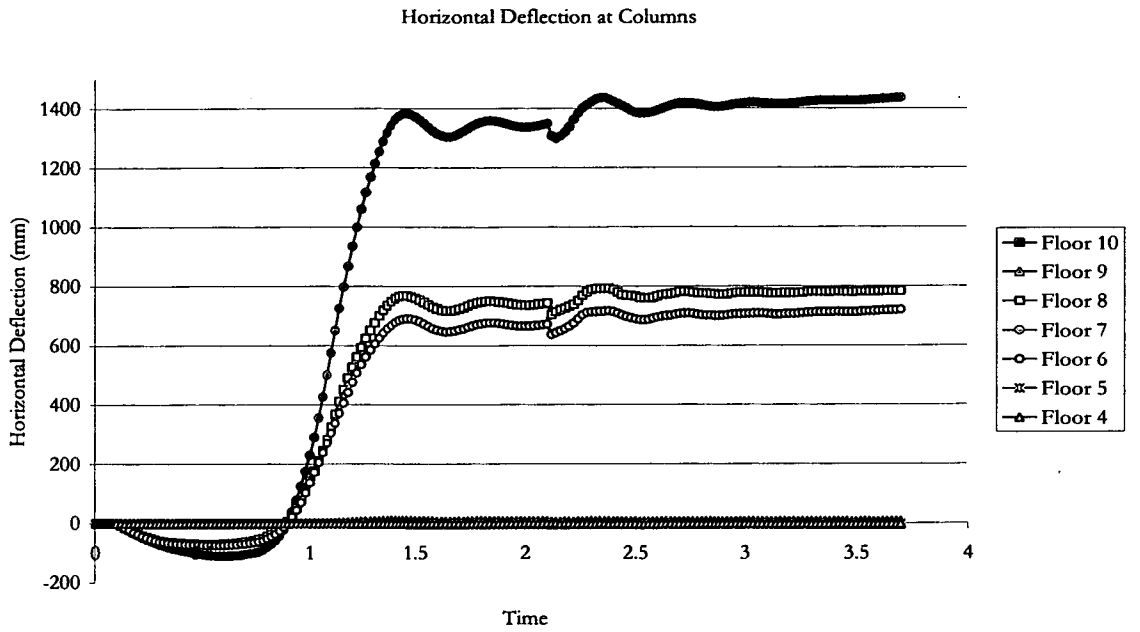


Fig. 4 – Deflected shapes with a buckling and plastic collapse respectively

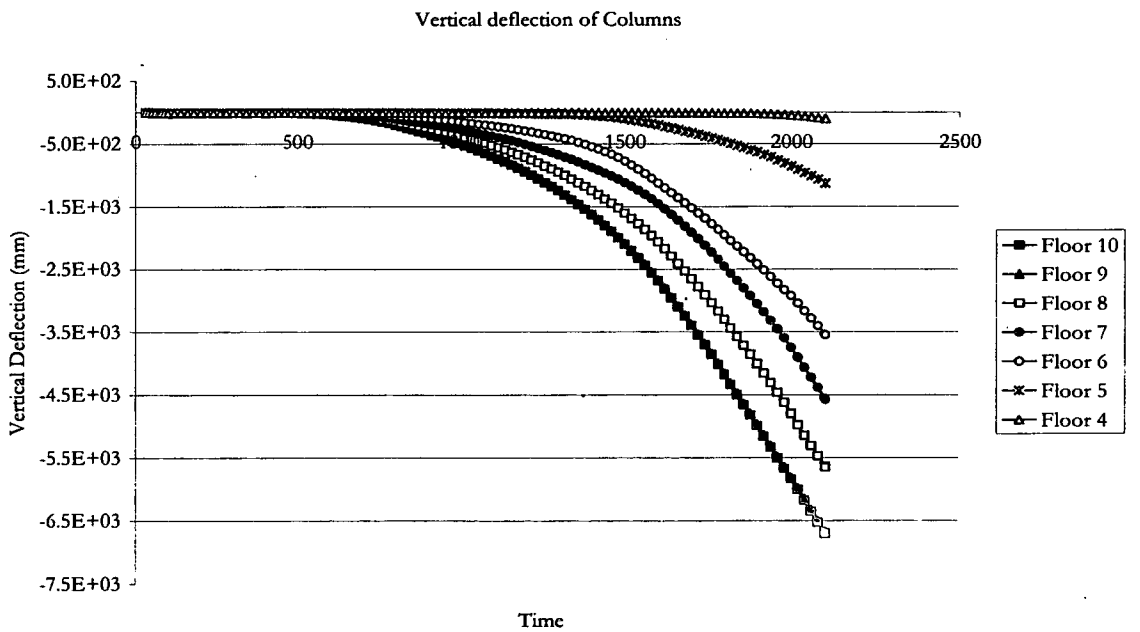
The vertical deflection for the weak beam model shown in Figure 6 indicates that each section of the column deflects downwards starting with all the floors above the fire floors and gradually each consecutive floor follows. The stiff floor model initially has an upward movement due to the thermal expansion of the column. As the column is being pulled in and the collapse movement is initiated there is a sharp increase in vertical deflection for all the fire floors and those above. Floors 4 and below do not encounter any deflection.





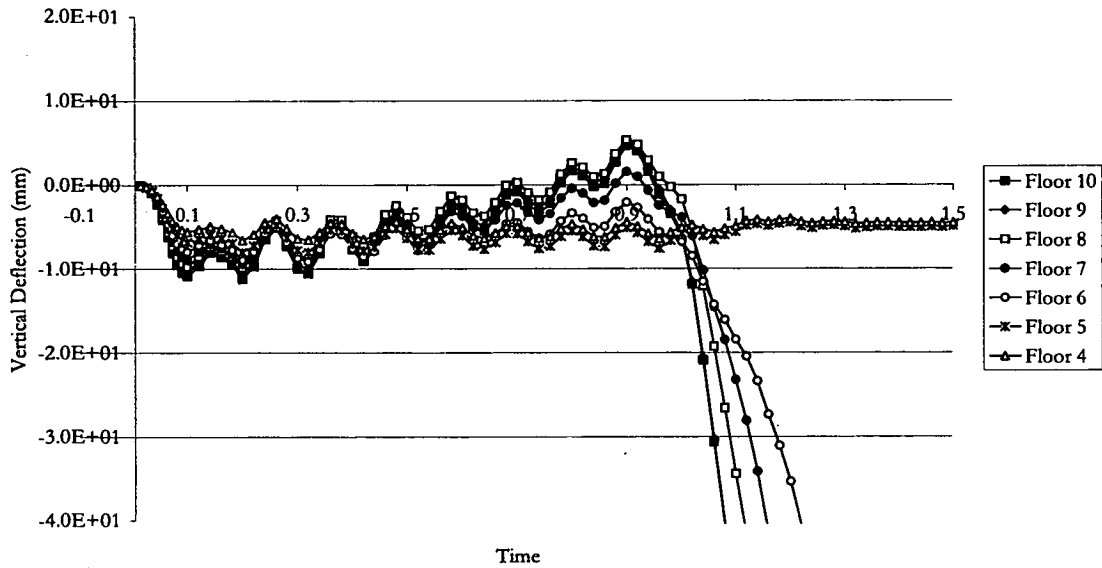
(b) Stiff floor mechanism

Fig.5. – Horizontal deflections of columns



(a) Weak floor mechanism

Vertical Deflection of Columns



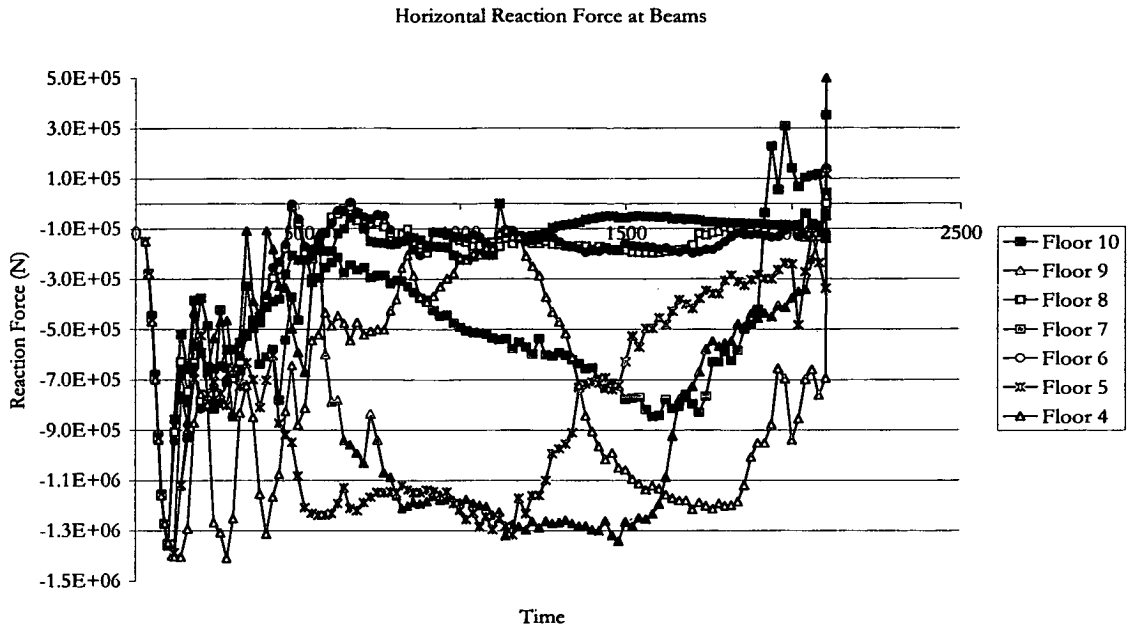
(b) Stiff floor mechanism

Fig.6 – Vertical deflection of columns

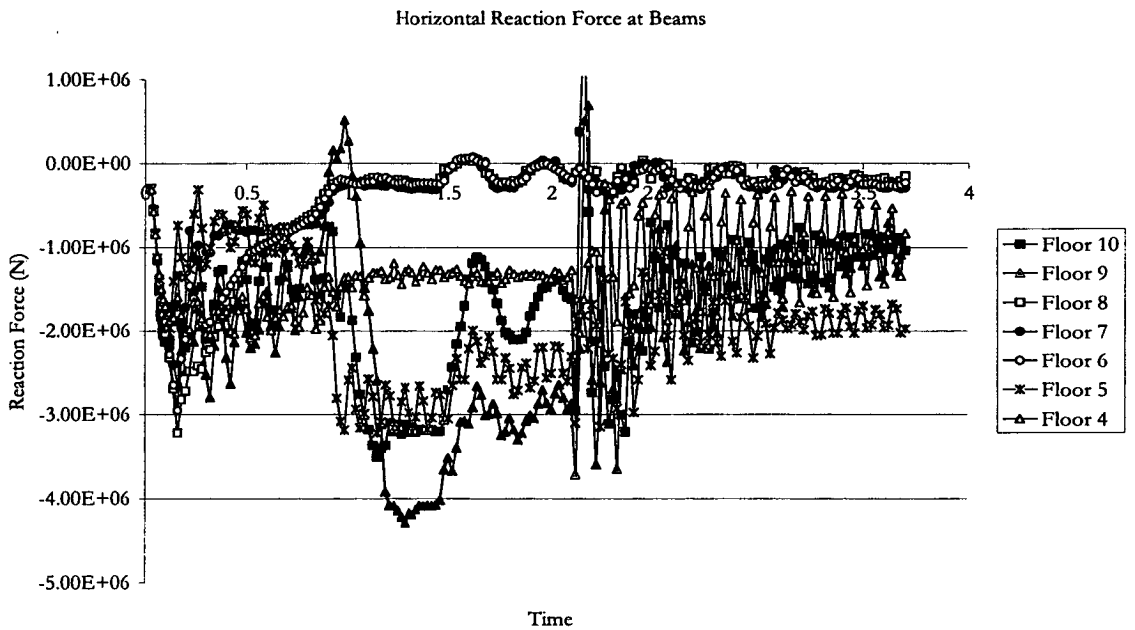
The horizontal reactions at the beam connection to the stiff core show the change in membrane forces over time in Figure 7. The weak floor model indicates that all floors go into an initial state of compression. The three fire floors rapidly reduce in compression until a very small reaction remains. All three floors have buckled at this stage. Floor 5, immediately below the fire floors, experiences an increased reaction as the floors above take a reduced amount. When floor five buckles due to the increased force from the column, the reaction quickly reduces. Now floor 4 sees a rapid increase, until this floor buckles. The progressive failure of floors is thus clearly visible from this graph.

The stiff floor system in Figure 7 (b) also starts off with an immediate compression. The three fire floors buckle and during this process the reaction force reduces. At the same time the force is being redistributed to floors 5 and 9, immediately above and below the fire floors. As these floors are relatively strong no further buckling occurs and the column forms hinges to allow for inward movement of the column due to the deformation of the beams.

Research done by Flint³ shows several floors are in tension rather than compression. The exact reason for why the behaviour seen here is different is yet unknown.



(a) Weak floor mechanism



(b) Stiff floor mechanism

Fig.7 – Horizontal reaction forces at the beams

The section capacity of the column is shown in the interaction diagram of the loading and moments in Figure 8. This relates to the section moment for both models in Figure 9 as it shows when plastic hinges are formed. The weak floor model shows that hinges are formed at floor 5, 7 and 9. Although this is similar to the stiff floor model, the overall behaviour is

significantly different. As the hinge forms at floor 5, the moment at floor 4 increases until that too hinges. This in turn affects the column at floor 3 which also hinges soon after. This clearly indicates the progressive collapse of the floors and column. When comparing the section moments at the column and beam connections with the section capacity of the column, hinges can be seen.

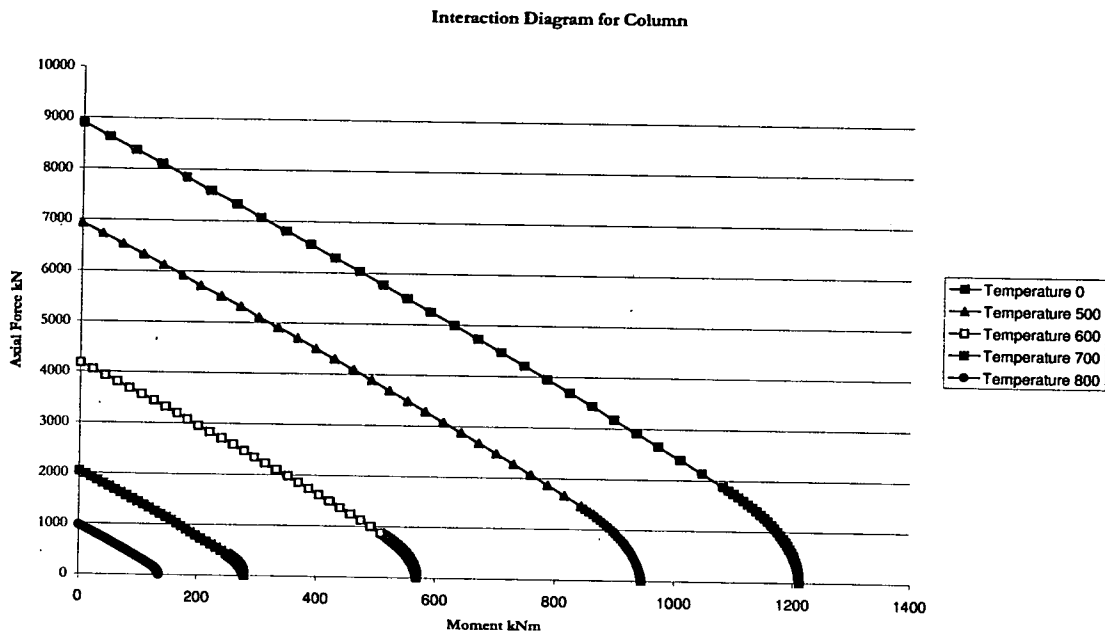
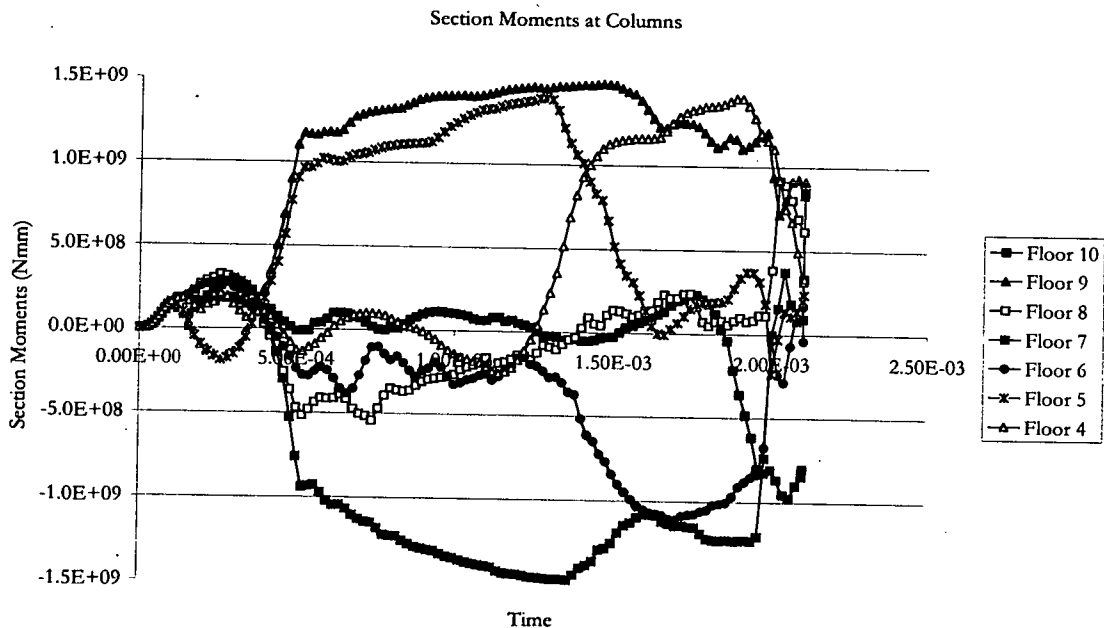
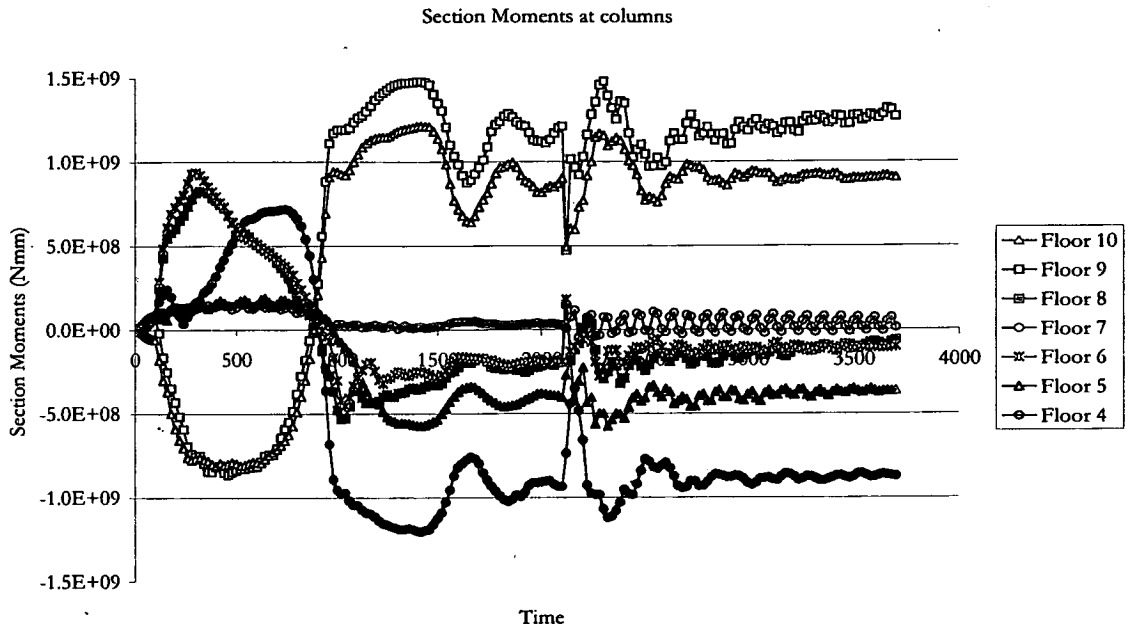


Fig.8 – Interaction Diagram for Column



(a) Weak floor mechanism



(b) Stiff floor mechanism

Fig.9 – Section moments at the column and beam connection

4. A SIMPLE STABILITY ASSESSMENT METHOD FOR TALL BUILDINGS IN MULTIPLE FLOOR FIRE

Figure 10 illustrates a simple method for assessing the stability of columns in tall buildings in multiple (or single) floor fires. The method may be described as follows:

1. Determine the limiting tensile membrane forces in the floors affected by fire. This will involve calculations to obtain the thermally induced displacements and membrane forces in the floor. A detailed description of these can be seen in reference 4.
2. From the membrane forces obtain the moments induced in the columns at the “pivot” floors (adjacent to the fire floors) and the middle fire floor. If an approximation of the column internal displacement can be made, additional P- Δ moments can be calculated.
3. At this point there are two possible mechanisms:
 - a. Calculate the reaction of the pivot floors as shown in Figure 9 (lowest pivot floor is most critical) counteracting the membrane “pull-in” forces (include an appropriate percentage of the column load to this, as the column lateral support requirement is increased due to loss of support at the fire floors). If the floor membrane is unable to provide the reaction calculated, a weak floor failure becomes possible.
 - b. If the floor is able to provide the reaction required, check the temperature dependent moment-force interaction diagram for the column to ensure that the column has not reached the yield surface (and thus formed a plastic hinge). If this is the case then stiff floor failure can occur.

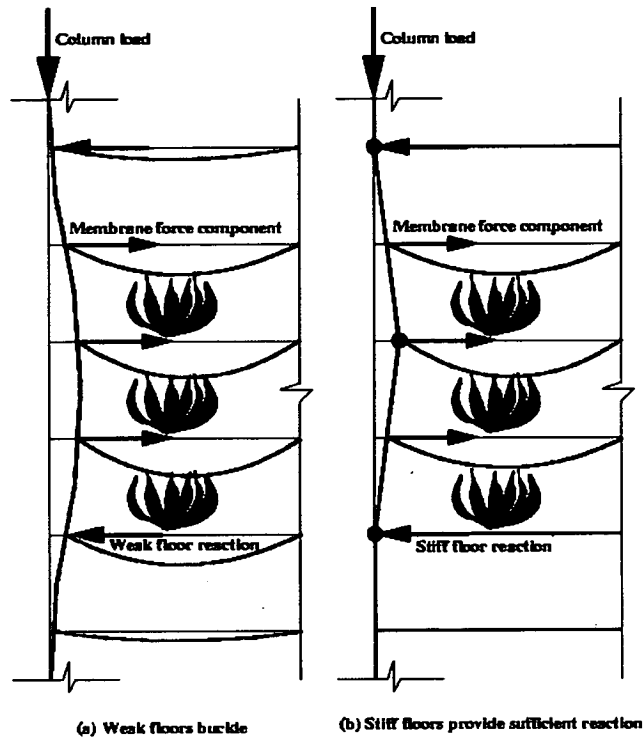


Fig.10 – Mechanics of fire induced collapse in weak and stiff floor buildings

5. CONCLUSION

This paper introduces the hypothesis of two possible failure mechanisms for tall buildings in multiple floor fires. The hypothesis is tested by creating a finite element model of a standard steel frame composite structure. The results of the modelling indicate that the two different failure mechanisms do indeed occur. This conclusion is very important and powerful as it enables the development of a simple stability assessment method for tall buildings in multiple floor fires. A very preliminary exposition of what such a method may entail is also described in the previous section.

6. REFERENCES

- [1]. A.S.Usmani, Y.C.Chung and J.L.Torero. How did the WTC Towers Collapse? A New Theory. *Fire Safety Journal*, 38:501--533, 2003.
- [2]. A.Usmani, Stability of the World Trade Center Twin Towers structural frame in multiple floor fires. *Journal of Engineering Mechanics*, ASCE, 131:654--657, 2005
- [3]. G.R.Flint, *Fire Induced Collapse of Tall Buildings*, PhD thesis, University of Edinburgh, 2005. Available at <http://www.civ.ed.ac.uk/research/fire/thesis.html>
- [4]. N.J.K.Cameron, *The Behaviour and Design of Composite Floor Systems in Fire*, University of Edinburgh, 2004. Available at <http://www.civ.ed.ac.uk/research/fire/thesis.html>